AD NUMBER

AD832218

NEW LIMITATION CHANGE

TO

Approved for public release, distribution unlimited

FROM

Distribution authorized to U.S. Gov't. agencies and their contractors; Critical Technology; APR 1968. Other requests shall be referred to Rome Air Development Command, Griffiss AFB, NY.

AUTHORITY

RADC, USAF ltr, 17 Sep 1971

RADC-TR-68-58
Final Report

LOW NOISE ANTENNA TECHNIQUES

R. W. Martin
C. Rothenberg
L. Zucker

Sperry Gyroscope Company

TECHNICAL REPORT NO. RADC-TR-68-58
April 1968

Rome Air Development Center
Air Force Systems Command
Griffiss Air Force Base, New York

When US Government drawings, specifications, or other data are used for any purpose other than a definitely related government procurement operation, the government thereby incurs no responsibility nor any obligation whatsoever; and the fact that the government may have formulated, furnished, or in any way supplied the said drawings, specifications, or other data is not to be regarded, by implication or otherwise, as in any manner licensing the holder or any other person or corporation, or conveying any rights or permission to manufacturer, use, or sell any patented invention that may in any way be related thereto.

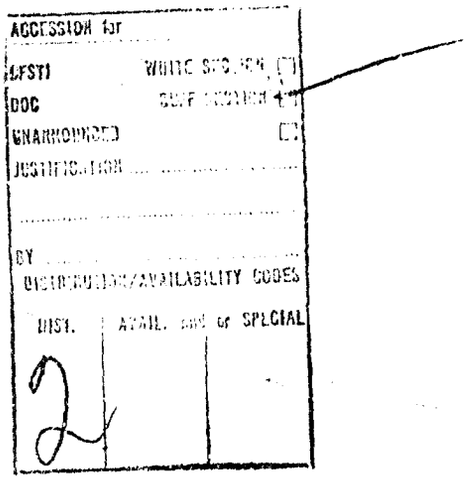

Do not return this copy. Retain or destroy.

LOW NOISE ANTENNA TECHNIQUES

R. W. Martin
C. Rothenberg
L. Zucker

Sperry Gyroscope Company

AFLC, GAFB, N.Y., 7 May 68-113

FOREWORD

This final report was prepared by R.W. Martin, C. Rothenberg and L. Zucker of Sperry Gyroscope Company, Division of Sperry Rand Corporation, Great Neck, New York, under Contract AF30(602)-4325, project number 4506, task number 450604. Secondary report number is SGD-5297-0020; reporting period covered December 1966 to December 1967. RADC project engineer is Martin Jaeger (EMATA).

Distribution of this document is limited because it contains detailed design information on a unique antenna technique.

This report has been reviewed and is approved.

Approved: Martin Jaeger
MARTIN JAEGER
Project Engineer
Antenna & Coherent Optical Section

Approved: Alfred W. Cooke
WILLIAM POPE
Acting Chief
Surveillance & Control Division

FOR THE COMMANDER: Irving J. Gabelman
IRVING J. GABELMAN
Chief, Advanced Studies Group

ABSTRACT

This Final Report describes the progress made in analysis, development and evaluation of a subreflector array illumination control technique. The subreflector array technique is used in conjunction with a parabolic reflector and feed horn to reduce antenna noise temperature while providing increased antenna efficiency. This report includes the results of a model test program which indicates a model efficiency of 68 percent and a noise temperature of 27 degrees kelvin over a 5 percent X-Band frequency range. Discussion also includes a focal fed lens array design and application to conical scanning and monopulse systems.

TABLE OF CONTENTS

TABLE OF CONTENTS (Cont'd)

LIST OF ILLUSTRATIONS

LIST OF ILLUSTRATIONS (Cont'd)

LIST OF TABLES

EVALUATION

An inverse taper producing subreflector array technique used to replace the hyperbolic subreflector in a Cassegrain antenna system was further investigated and developed during this continuation effort to achieve improved antenna efficiency, noise temperature and radiation characteristics. The subreflector array used in the Cassegrain configuration is designed to transform a tapered feed pattern function into a nearly uniform main parabolic reflector aperture illumination function.

The initial X-band breadboard model antenna constructed under a prior study program provided satisfactory radiation pattern characteristics in only one of two principal planes. Large pattern perturbation errors exhibited in the orthogonal plane of the antenna resulted in degradation of the overall model gain and noise temperature performance levels. This was attributed to high surface coupling between adjacent cells in that plane of the subreflector array structure. The model consisted of a 10 ft. main parabolic reflector with a multicellular, polarization independent, subreflector array structure fed by a dual mode conical feed horn. The detailed results of the study program and design parameters are discussed in RADC-TR-65-166, Final Report, entitled, "Low Noise Antenna Techniques", dated July 65.

In the follow-on effort, a linearly polarized subreflector array was fabricated to replace the subreflector used in the existing feasibility antenna model. Corrective design techniques incorporated into the array structure included reduced element spacing and refinement of the shorting surface geometry. Model measurements conducted with the use of either a pencil beam or monopulse feed demonstrated satisfactory antenna performance over a 5% frequency band. Antenna pattern data in terms of beamwidth, side lobe level and null locations indicates that illumination transformation is being achieved in both principal planes of the subreflector array. The 68% antenna efficiency obtained represents a 35% improvement over that provided by the initially constructed model. A significant improvement was achieved in antenna noise temperature performance. Model antenna noise temperatures obtained using the pencil beam and monopulse feeds were 27°K and 32°K, respectively. The antenna noise temperature provided by the initially constructed model was 70°K.

Minimum performance requirements were met with the exception of bandwidth which is 5% rather that the specified 10% at X-band. In addition, H-plane beamwidths are slightly broader than specified. Results of the effort provided design information and performance limitations on a subrflector array technique which can be used with a main parabolic reflector in a Cassegrain geometry to enhance tracking antenna performance.

Martin Jaeger

MARTIN JAEGER
Project Engineer

SECTION 1

INTRODUCTION

This final technical report describes the results obtained in the development and demonstration model test of an inverse taper illumination technique which is applicable to parabolic reflector antenna systems. This technique[1, 2, 3, 4, 5] consists of replacing the Cassegrainian hyperbolic subreflector with a subreflector array structure to provide additional aperture illumination control. The focal fed parabolic reflector version consists of introducing an illumination control lens array between the feed and reflector. These techniques can be used to provide a better compromise for low antenna noise temperature and high antenna efficiency. (See section 8 for all references.)

At the conclusion of the second quarterly program phase [5] a linearly polarized subreflector array structure had been fabricated and was ready for test. Also, a polarization independent subreflector array structure had been designed and calculations had been made to evaluate its performance. An X-band model antenna had been selected to demonstrate performance. Pencil beam feed tests had been completed and a monopulse feed had been designed in preparation for subreflector array model performance evaluation. Also during the second quarterly period, normal incidence surface impedance studies were conducted and model tests, using a simple hyperbolic subreflector, were started.

Progress during this final report period has included the following:

1. Hyperbolic subreflector tests
2. Surface impedance studies and tests for other than a normal oriented reflected wave
3. Linearly polarized subreflector array tests using various shorting surface geometries and various surface matching configurations
4. Tests using both a pencil beam and a monopulse feed
5. Polarization independent subreflector array tests
6. Model antenna gain and noise temperature evaluation
7. Lens-array design studies for a focal fed parabolic reflector

Linearly polarized subreflector array tests with the pencil beam feed have demonstrated a model efficiency of 68 percent over a 5-percent frequency band. This represents a significant improvement as compared to a model efficiency of 51 percent using a simple hyperbolic subreflector. Tests with the monopulse feed have also demonstrated an efficiency of 68 percent. Model antenna noise temperature using the pencil beam and monopulse feeds are 27°K and 32°K, respectively.

The goals established for the test model using the pencil beam and monopulse feeds are as follows:

Parameter	Pencil Beam Minimum	Pencil Beam Objective	Monopulse Objective
Noise temperature	50°K	35°K	50°K
Efficiency	68%	74%	60%
Bandwidth	±5% at X band	±10% at X band	±5% at X band
Gain	46 dB	46 dB	46 dB
VSWR	Less than 1.3	Less than 1.3	Less than 1.5
Half power beamwidth	Less than 0.75°	Less than 0.70°	Less than 0.8°
10-dB beamwidth	Less than 1.3°	Less than 1.2°	Less than 1.4°
20-dB beamwidth	Less than 1.7°	Less than 1.7°	Less than 1.9°
First two sidelobes	Less than -15 dB	Less than -15 dB	Less than -15 dB
Other sidelobes within ±15°	Less than -25 dB	Less than -25 dB	Less than -25 dB
Remaining sidelobes to ±180°	Less than -40 dB	Less than -40 dB	Less than -40 dB
Polarization	Linear	Linear and circular	Linear

With relatively few exceptions the minimum requirements and the objectives have been achieved. The major exception is that the subreflector array bandwidth is found to be 5 percent rather than ±5 percent. Also, but of lesser importance, the beamwidth is somewhat broader than anticipated. The following is a tabulation of the model results achieved:

Parameter	Pencil Beam Performance	Monopulse Performance
Noise temperature	27°K	32°K
Efficiency	68%	68%
Bandwidth	5% at X band	5% at X band
Gain	46.5 dB	46.1 dB
VSWR	Less than 1.3	Less than 1.3
Half power beamwidth	Less than 0.82°	Less than 0.85°
10-dB beamwidth	Less than 1.4°	Less than 1.4°
20-dB beamwidth	Less than 1.8°	Less than 1.9°
First two sidelobes	Less than -15 dB	Less than -15 dB
Other sidelobes within ±15°	Less than -26 dB	Less than -19 dB
Remaining sidelobes to ±180°	Less than -40 dB	Less than -40 dB
Polarization	Linear	Linear

A review of the measured performance indicates that significant gain-noise temperature performance improvements have been achieved over a 5-percent frequency band as compared to a conventional Cassegrain subreflector configuration.

Although the results achieved are encouraging, additional work can be done to improve further the subreflector array performance. Results indicate generally 10 percent broader H-plane beamwidths and lower near-in sidelobes, as compared to the E-plane performance. This results in a somewhat reduced efficiency, as compared to theoretical, and is the result of inherently poorer H-plane element impedance match and element pattern characteristics. Results indicate a significant improvement is possible by applying a shorting surface adjustment to minimize the aperture phase error, but the amplitude error due to element mismatch remains a degrading factor. The subreflector array is found to be highly astigmatic without this control.

Results with the polarization independent subreflector array indicate a model efficiency of 43 percent. This poor performance is due to inadequate element surface impedance description for this dielectrically loaded waveguide configuration.

SECTION 2

PROGRAM DESCRIPTION AND BACKGROUND

The purpose of this program is to develop, demonstrate, and evaluate an inverse taper transformation technique that will reduce reflector antenna noise temperature while providing increased antenna efficiency. The inverse taper technique consists of introducing a structure into the reflector optics, which will operate on the feed illumination pattern, producing a parabolic reflector aperture illumination function that is consistent with low noise temperature and high aperture efficiency requirements. For a Cassegrain antenna, the inverse taper transformation is affected by a subreflector array structure which replaces the hyperbolic subreflector. This provides control of both the parabolic reflector aperture phase and amplitude illumination function. The comparable inverse taper structure for a focal fed parabolic reflector system would be a constrained lens located between the feed and reflector. Transformation of the feed pattern by the inverse taper producing structure permits optimization of the resulting amplitude illumination function. For a high efficiency, low noise temperature design, the illumination function, as viewed from the paraboloid focus, will approach that of uniform illumination within the included angle of the parabolic reflector, and will approach zero in the remaining spillover region.

Within the stated low noise temperature - high efficiency objective, principal areas of investigation included:

- Modification of the inverse taper transformation design equations to include subreflector array surface interaction effects
- Adjustment of the subreflector array shorting surface to achieve optimum inverse taper transformation performance
- Study and implementation of modified subreflector array configurations to minimize surface interaction effects, including reduced intercell spacing techniques
- Additional inverse taper transformation diffraction limitation studies and efficiency-noise temperature tradeoff evaluation and test
- Evaluation and test of the subreflector array as applied to pencil beam, monopulse, and conical scanning feeds

The above program is a continuation of the effort reported under contract AF 30(602)-3382 (1, 2, 3). The analytical investigation initially established the design techniques for utilizing an auxiliary structure to produce a special inverse taper transformation of the feed pattern. This structure was designed to modify a highly tapered feed pattern to provide a nearly uniform main parabolic antenna aperture distribution. The general formulation included generation of the design equations, evaluation of parameter variations, and subsequent optimization of various antenna configurations. This formulation included diffraction pattern limitations and noise temperature evaluation so that efficiency-noise temperature compromise design criteria could be established.

As a check on the established theory, an inverse taper transformation X-band feasibility model antenna was assembled. This unit consisted of three major components:

- A paraboloidal reflector which is 10 feet in diameter, focal length to diameter ratio of 0.4, and surface tolerance of ±1/32 inch
- A subreflector array, which is a multicellular structure (259 cells), approximately 15 inches in diameter, and 10 inches deep to accommodate the adjustable shorts used for the model
- A dual mode (TE_{11}^{o} and TM_{11}^{o}) conical feed horn, selected and designed for low spillover and axially symmetrical pattern performance characteristics

The tests conducted during the above referenced program demonstrated that inverse taper pattern control is possible, and indicated that further development of this technique could be expected to provide improved antenna efficiency-noise temperature performance. The design equations, which were established to produce inverse taper transformation, were found to be satisfactory for only one of the two principal planes of the subreflector array. In this plane of the array, mutual coupling or surface wave effects on the face of the structure were found to be small, and inverse taper transformation was achieved. This was evidenced by a high degree of correlation between measured and calculated beamwidth, sidelobe, and spillover performance characteristics. In the orthogonal plane of the subreflector array, however, the design equations were found to be inadequate to account for the more severe surface wave effects. Subsequent correction of the subreflector array shorting surface improved the pattern characteristics in the region of the main beam. Additional fine correction was suggested to reduce the near-in sidelobe power and spillover power. The difference in surface interaction effects, for the subreflector array structure, was attributed to the difference in effective element spacing in the two planes.

Based on the results of the above program, further development of inverse taper transformation for high efficiency-low noise temperature antenna design was recommended and initiated. The present program is a direct result of the recommended effort and is a continuation of the inverse taper transformation investigations.

During the first quarterly period [4], a computer program was written to simplify the design of a subreflector array. This computer program also provides feed and array pattern performance, aperture illumination efficiency, and back hemisphere spillover loss. This program was used to calculate the performance of the polarization independent, unloaded, square cell array, for which test results had been obtained on a previous phase. [3] The calculations indicated the need for reduced subreflector array element spacing to improve its performance.

Subsequent calculations were made using unloaded rectangular waveguide for use with a single linear polarization design. Substantial improvement was predicted and work was initiated on the design and fabrication of a linearly polarized subreflector array model.

Subreflector array zoning techniques had been evaluated. These could be used to reduce the depth of the subreflector array and to increase the bandwidth of the device. The design technique was extended so that array zoning automatically can be generated and evaluated with a digital computer.

Studies were reported [4] to extend the geometrical optics description for location of the subreflector array shorting surface. These studies indicate that adjustment of the shorting surface could be used to compensate for the array entry surface mismatch effects. The analytical description of the subreflector array was extended to include surface mismatch, and tests were planned for measurement of the necessary parameters.

During the second quarterly period [5] progress was reported with regard to linearly polarized and polarization independent subreflector array techniques, measurement of surface mismatch parameters for normal incidence, and demonstration model subreflector array and feed design configurations.

Fabrication of the linearly polarized subreflector array was completed. This subreflector array consists of 431 aluminum X-band waveguide cells located on a triangular grid. The assembly has a nominal diameter of 15 inches.

Primary pencil beam feed horn pattern tests were completed. Pattern tests were conducted with the upper band and lower band horn phasing sections to determine the optimum shim lengths as a function of frequency.

Tests were conducted on an available C-band reflector array model to determine the normal incidence surface mismatch parameters. The results then were extrapolated to X band. The computer program was then modified to include the normal incidence mismatch parameters in the design of the subreflector array shorting surface.

Polarization independent subreflector array model techniques, using dielectrically loaded square waveguide cells, were established. Pattern and efficiency calculations were made to determine cell spacing and loading for this model.

A spun hyperbolic Cassegrain subreflector, to be used in conjunction with the breadboard paraboloidal reflector and feed, was designed and fabricated. The purpose of this unit was to provide a reference with which to experimentally determine the performance improvement that could be achieved with the subreflector array.

A monopulse feed was being assembled to demonstrate inverse taper transformation with this feed type. The feed has since been completed and consists of two horns which are stacked in the E plane, and fed by a comparator which consists of a folded E-plane hybrid tee. This provides a linearly polarized single-plane monopulse feed with a sum channel and an E-plane difference channel.

SECTION 3

MODEL TEST PROGRAM

3-1 TEST EQUIPMENT AND PROCEDURES

The model antenna consists of a 10-foot diameter aluminum parabolic reflecting dish and supporting structures for feed horn and subreflector combinations. The antenna mount is capable of sufficient elevation motion to peak on the transmitting dish, located 1200 feet away (far field), and allows for positioning the model antenna in any polarization plane.

The platform has a variable speed control and can rotate 360 degrees in azimuth. A synchro in the platform drives a pen recorder which, for most of the patterns illustrated in this report, prints out on the chart paper with a 5 degree per major division scale.

Mode adapters on the feed horns used during tests provide the transition to a coaxial transmission line. The other end of the line connects to a calibrated variable attenuator, crystal mixer, wide-range receiver, and the pen recorder.

A continuous wave test signal at a frequency between 8.2 to 10.0 GHz is generated either by a remotely tuned backward wave oscillator, or by tuning of an X-band klystron at the transmitting site.

Gain measurements are referenced to a gain standard X-band horn. To account for amplitude variations across the aperture of the model antenna, the gain standard horn is moved in elevation across the aperture, and its average signal level is selected for the standard reference level.

The VSWR of the model antenna is measured by means of a slotted line and crystal detector mounted immediately behind the feed horn.

Supports for the feedhorn and subreflector allow for small translations and rotations to optimize antenna performance.

The conical feedhorn used during the test program has two sets of shims to provide proper horn phasing at each test frequency. The monopulse type feed is a pyramidal horn with an H-plane septum and a comparator consisting of a folded E-plane hybrid tee. This permits an E-plane difference channel, as well as sum channels, in both planes. Figure 1 shows the monopulse feed assembly.

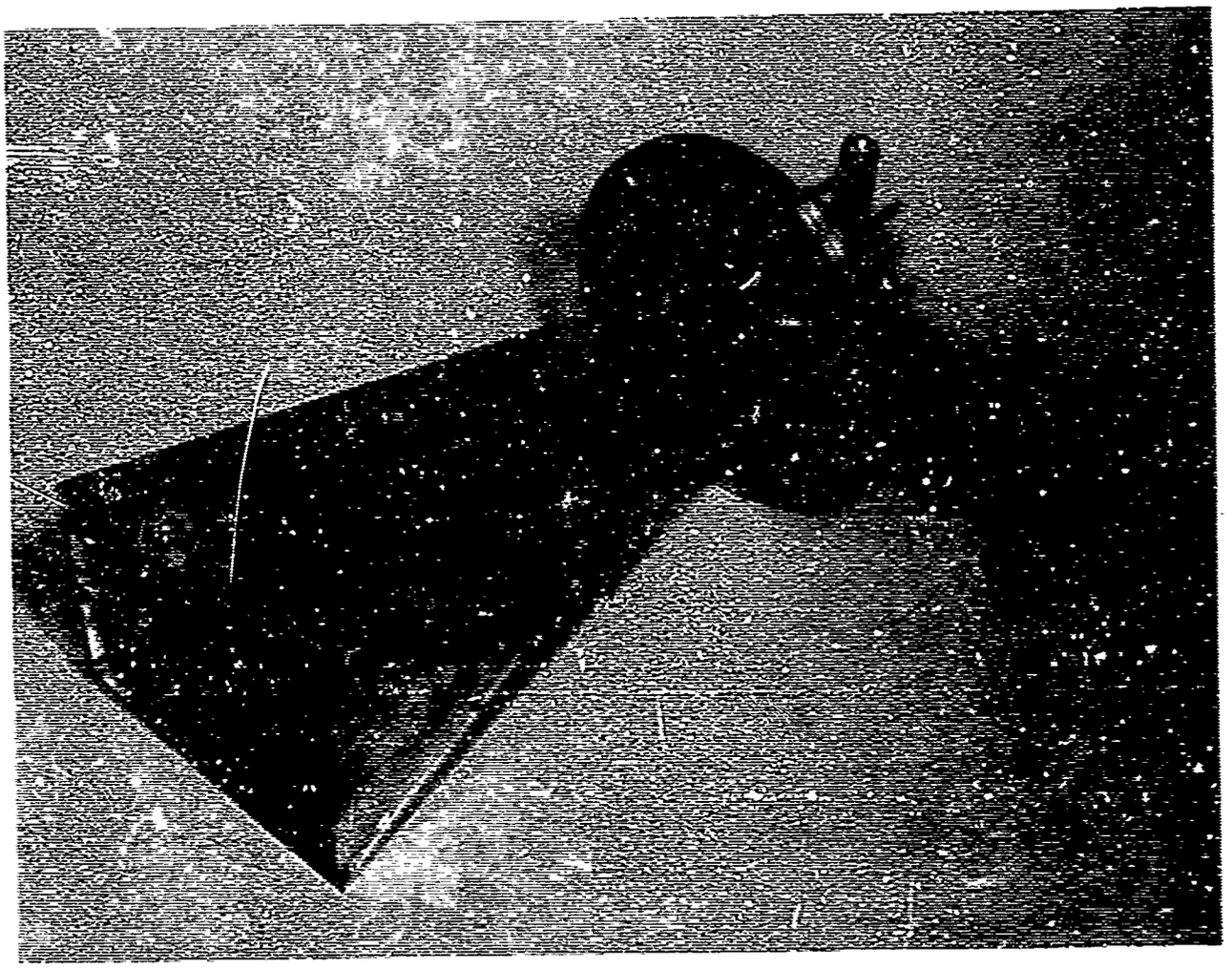

FIGURE 1. MONOPULSE FEED HORN

Three types of subreflectors are used throughout the test program. The first is a spun aluminum hyperbola which permits a basis of comparison for the other two subreflector arrays. One array is linearly polarized and consists of 431 aluminum X-band waveguide cells, located on a triangular grid and having adjustable shorts (see sections 3-2 and 3-3 of reference 5). The other subreflector array is polarization independent and consists of approximately 425 square waveguide cells on a triangular grid, also with adjustable shorts (see section 3-7 of reference 5).

The patterns illustrated and summarized generally represent the best compromise between E- and H-plane patterns for the particular feed-subreflector combination in test. This compromise position of the subreflector is arrived at, first, by finding the optimum E- and H-plane positions for the subreflector; a different setting for each plane sometimes is necessary because of astigmatic effects. The subreflector is then set midway between these optimum points and all patterns are taken for that particular short-setting at all frequencies. The maximum antenna gain has generally been found to occur at these compromise positions, thus justifying this procedure.

3-2 MODEL ANTENNA PERFORMANCE WITH SPUN HYPERBOLIC SUBREFLECTOR

Figure 2 shows the entire model antenna with conical feed assembly and the spun aluminum hyperbolic subreflector. Alignment was carried out, first, by adjusting the element spacings to the calculated theoretical values. Patterns were then taken in both E and H planes, and fine adjustments were made for best focus. Figures 3 and 4 illustrate the results at the best adjustment of elements, and shows the following performance characteristics:

Frequency (GHz)	Pattern Plane	Gain (dB)	Half Power Beamwidth (deg)	10-dB Beamwidth (deg)	20-dB Beamwidth (deg)	First Two Sidelobes (dB)
9.1	H	46.2	0.75	1.30	1.65	20
	E	--	0.80	1.35	1.70	22

The efficiency of this configuration is 51.3 percent, well within the expected value range. A more optimum feed illumination and less aperture blockage would raise this figure, but the measured value is representative for the systems being compared.

FIGURE 2. ANTENNA MODEL WITH HYPERBOLIC SUBREFLECTOR

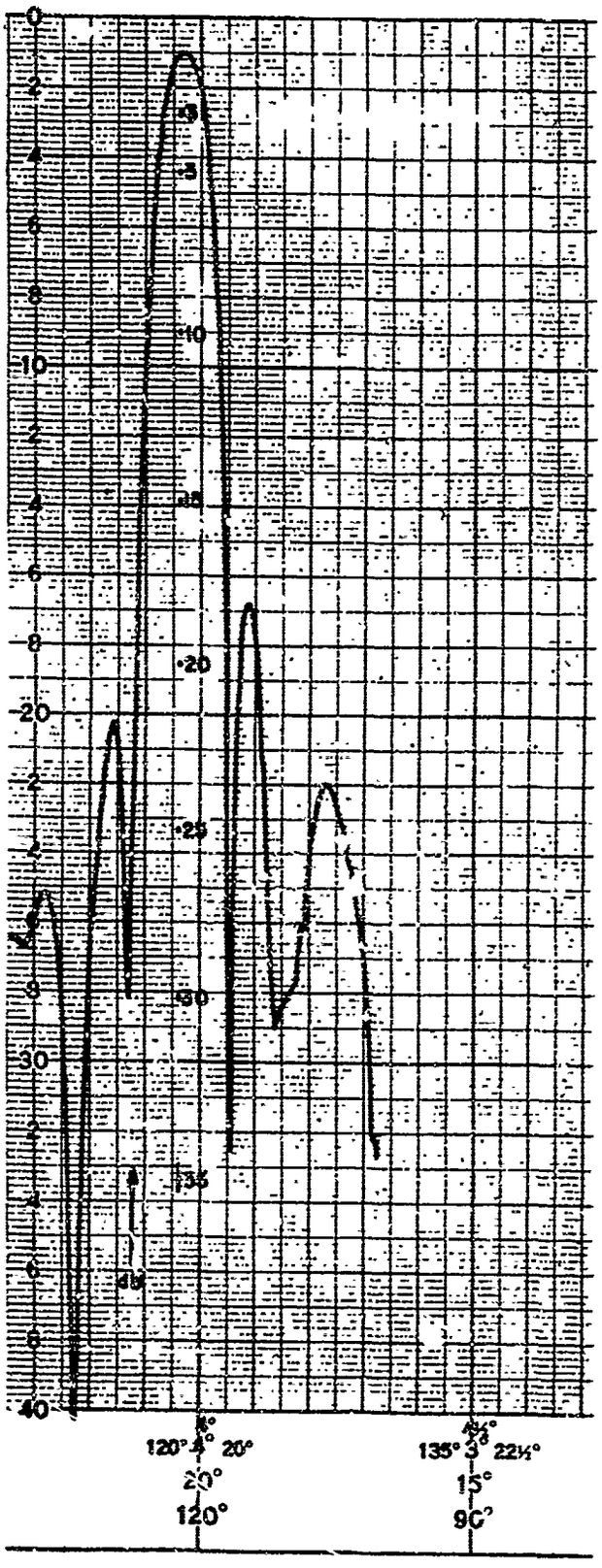

FIGURE 3. HYPERBOLIC SUBREFLECTOR, H-PLANE PATTERN

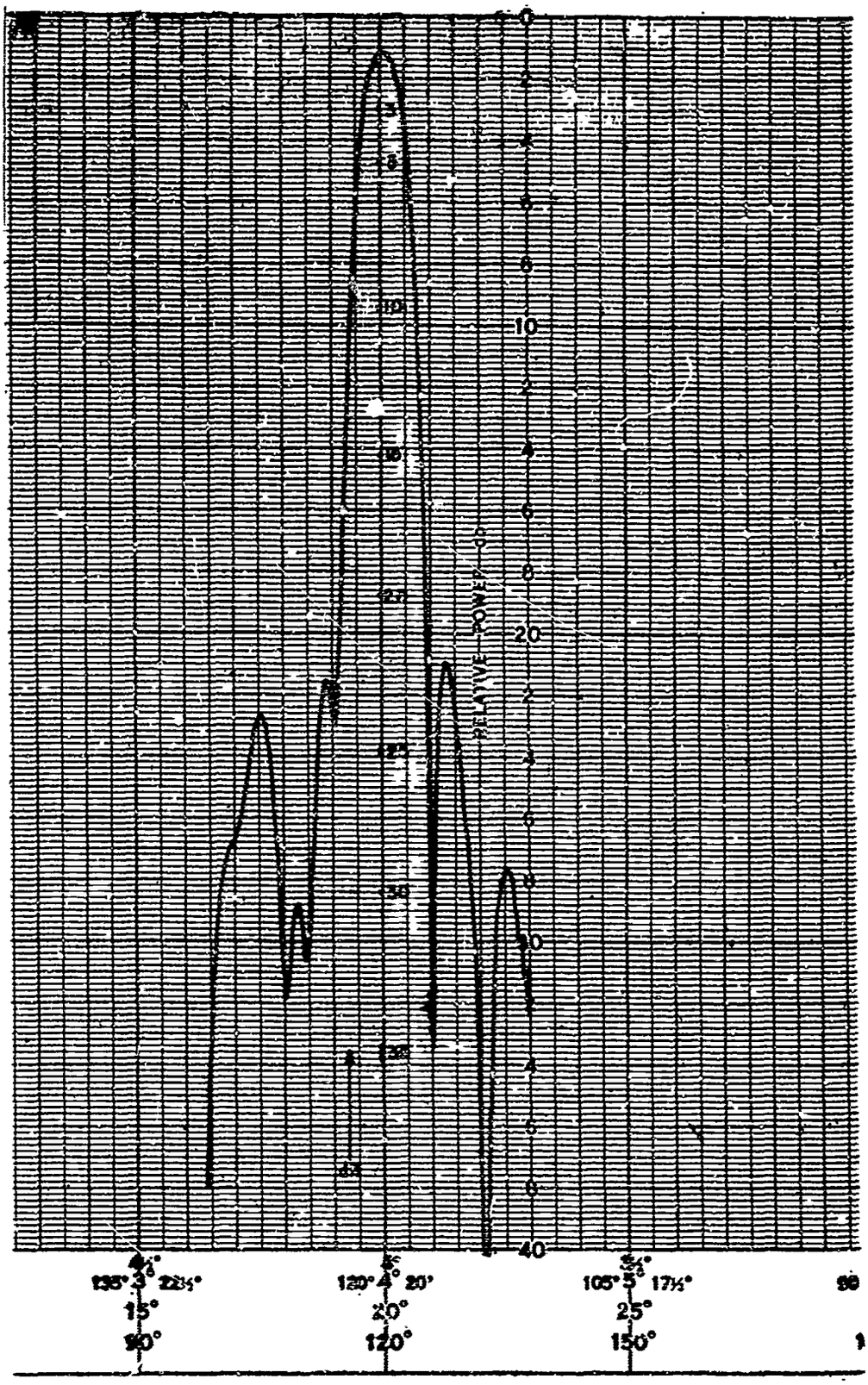

FIGURE 4. HYPERBOLIC SUBREFLECTOR, E-PLANE PATTERN

3-3 SUBREFLECTOR ARRAY, FIRST SHORT SETTING

Figure 5 shows the subreflector array composed of rectangular aluminum X-band waveguide cells in place on the model antenna. Figure 6 is a view of the subreflector array showing the entry surface contour. The first short setting in the subreflector array was based on a constant entry surface susceptance as a function of scan angle, $\beta_S = 0.384$, and a normalized tangential impedance of the surface equal to unity, $Z_{ti}/\eta = 1$. All short settings are derived from the equation:

$$d = \frac{\lambda g}{2\pi} \cot^{-1}\left[R_{01}\left(\frac{\cot(\Delta\varphi/2)}{Z_{ti}/\eta} - \beta_s\right)(\theta,\varphi)\right] \qquad (1)$$

where d is the short depth from the entry surface, λ_g is the guide wavelength, R_{01} is the normalized guide impedance (0.764), and $\Delta\varphi$ is the required phase difference between input and output field vectors.

Figure 7 is the subreflector array geometry. Mechanical adjustment for best focused patterns in the H plane and E plane indicate a degree of astigmatism. A best compromise spacing was obtained by placing the subreflector array midway between the E- and H-plane focus positions. The following results were obtained for the optimum H, E, and compromise positions for the first short setting:

Feedhorn to Subreflector Array Distance (in.)	Frequency (GHz)	Pattern Plane	Half Power Beamwidth (deg)	Gain (dB)	First Sidelobes with Respect to Peak (dB)
19.85 (optimum H)	9.1	H	0.74	46.0	-20
19.85	9.1	E	0.76	--	-15
19.1 (optimum E)	9.1	H	0.75	44.9	-12.5
19.1	9.1	E	0.72	--	-17

Results at the compromise position are shown below:

FIGURE 5. ANTENNA MODEL WITH LINEARLY POLARIZED SUBREFLECTOR ARRAY

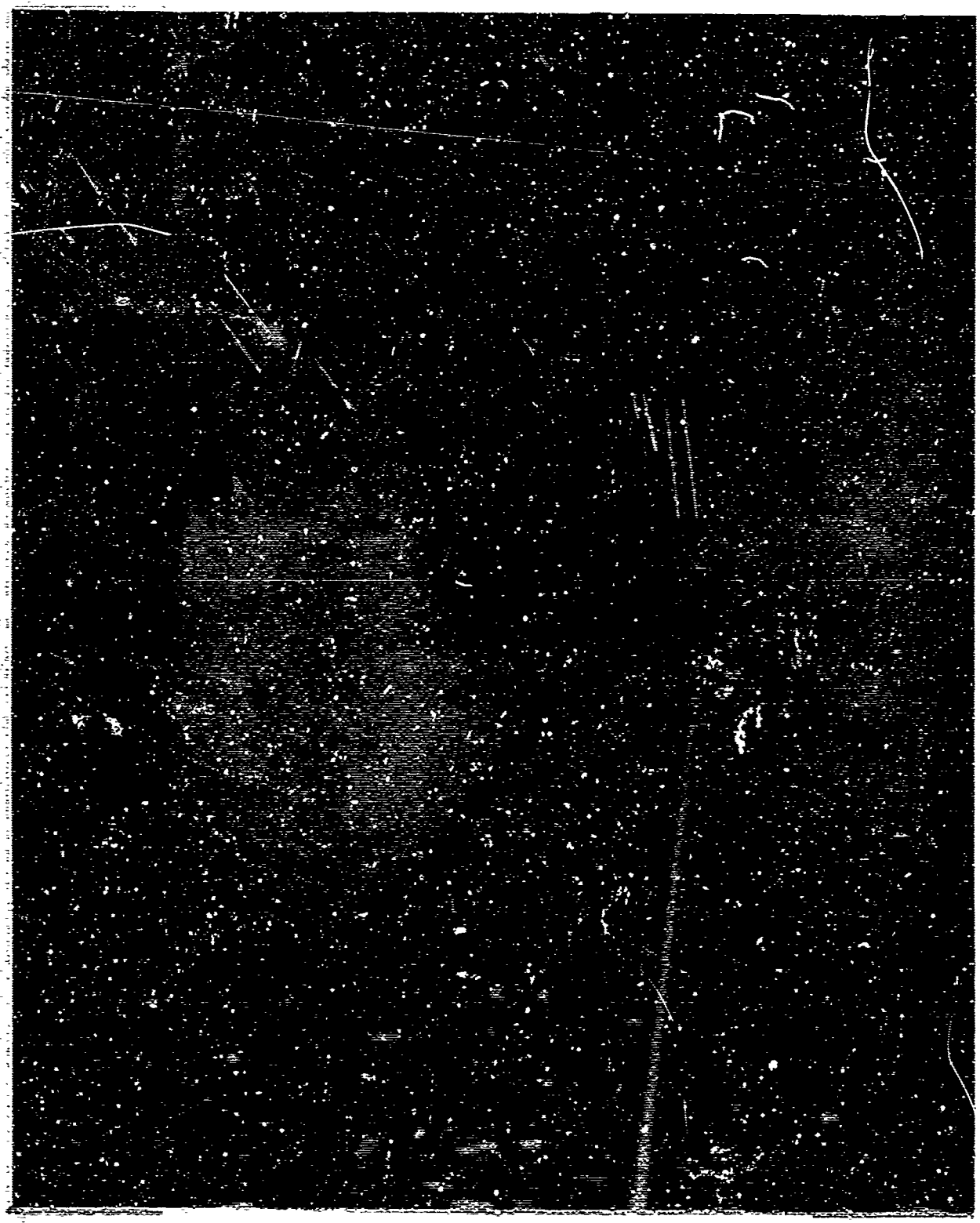

FIGURE 6. LINEARLY POLARIZED SUBREFLECTOR ARRAY

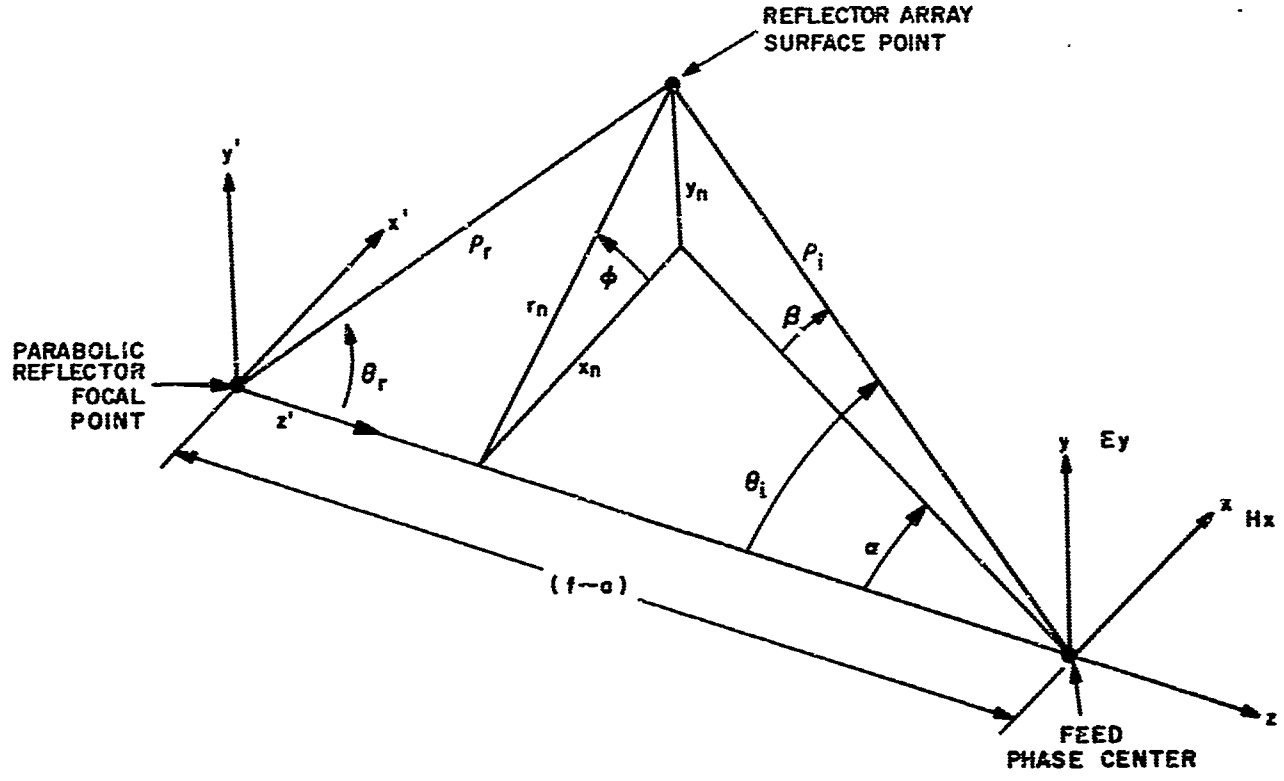

FIGURE 7. SUBREFLECTOR ARRAY GEOMETRY

Frequency (GHz)	Pattern Plane	Gain (dB)	Half Power Beamwidth (deg)	10-dB Beamwidth (deg)	20-dB Beamwidth	First Two Sidelobes (dB)	Other Sidelobes (dB)
9.1	H	46.0	0.78	1.35	--	17	24
	E	--	0.71	1.20	--	17.5	25
	45°	--	0.73	1.35	--	15	24
9.4	H	45.1	0.78	1.45	--	15	24
	E	--	0.71	1.20	--	18	25
	45°	--	0.74	1.30	--	14	22
9.7	H	46.1	0.77	1.50	--	17	21
	E	--	1.20	2.75	--	10	22

Figures 8 through 19 show the patterns obtained after the alignments. They are representative of the performance achieved for various settings and frequencies tested.

No significant gain improvement over a standard hyperbolic subreflector can be detected at the design frequency of 9.1 GHz. However, it is reasonable to assume that correction of the measured astigmatism would provide a gain improvement.

To expedite the resetting of the shorts in over 400 waveguide cells, a new tool was developed, with a dial indicator mounted on the shaft of the short setting probe. This tool, figure 20, allowed the short setting time to be cut roughly in half.

3-4 SUBREFLECTOR ARRAY, SECOND SHORT SETTING

Tests were run using a second shorting surface based on a more exact representation for the tangential surface impedance. The parameter Z_{ti}/η, in equation 1, is not held constant at unity but becomes a function of scan angle.

$$\frac{Z_{ti}}{\eta} = \frac{1 - \sin^2 \theta_i \sin^2 \varphi_i + (\rho\theta_i/\rho)^2 \cos^2 \varphi_i}{(1 - \sin^2 \theta_i \sin^2 \varphi_i)\sqrt{1 + (\rho\theta_i/\rho)^2}} \qquad (2)$$

where

$$\rho\vartheta_i = \frac{\partial\rho}{\partial\theta_i}$$

and θ_i, φ_i are the incidence angles. (See reference 2.)

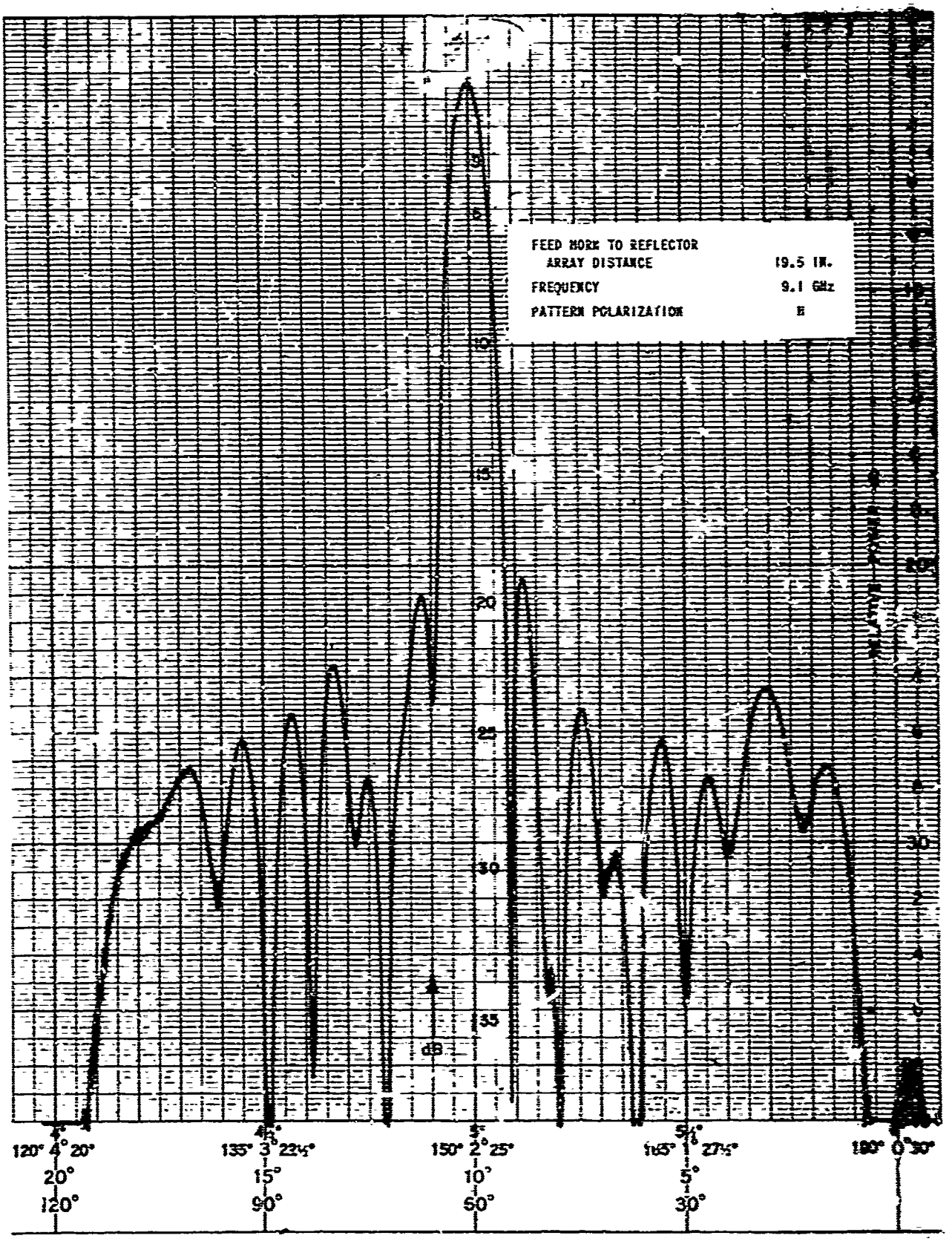

FIGURE 8. ANTENNA PATTERN PERFORMANCE WITH FIRST SHORT SURFACE ADJUSTMENT

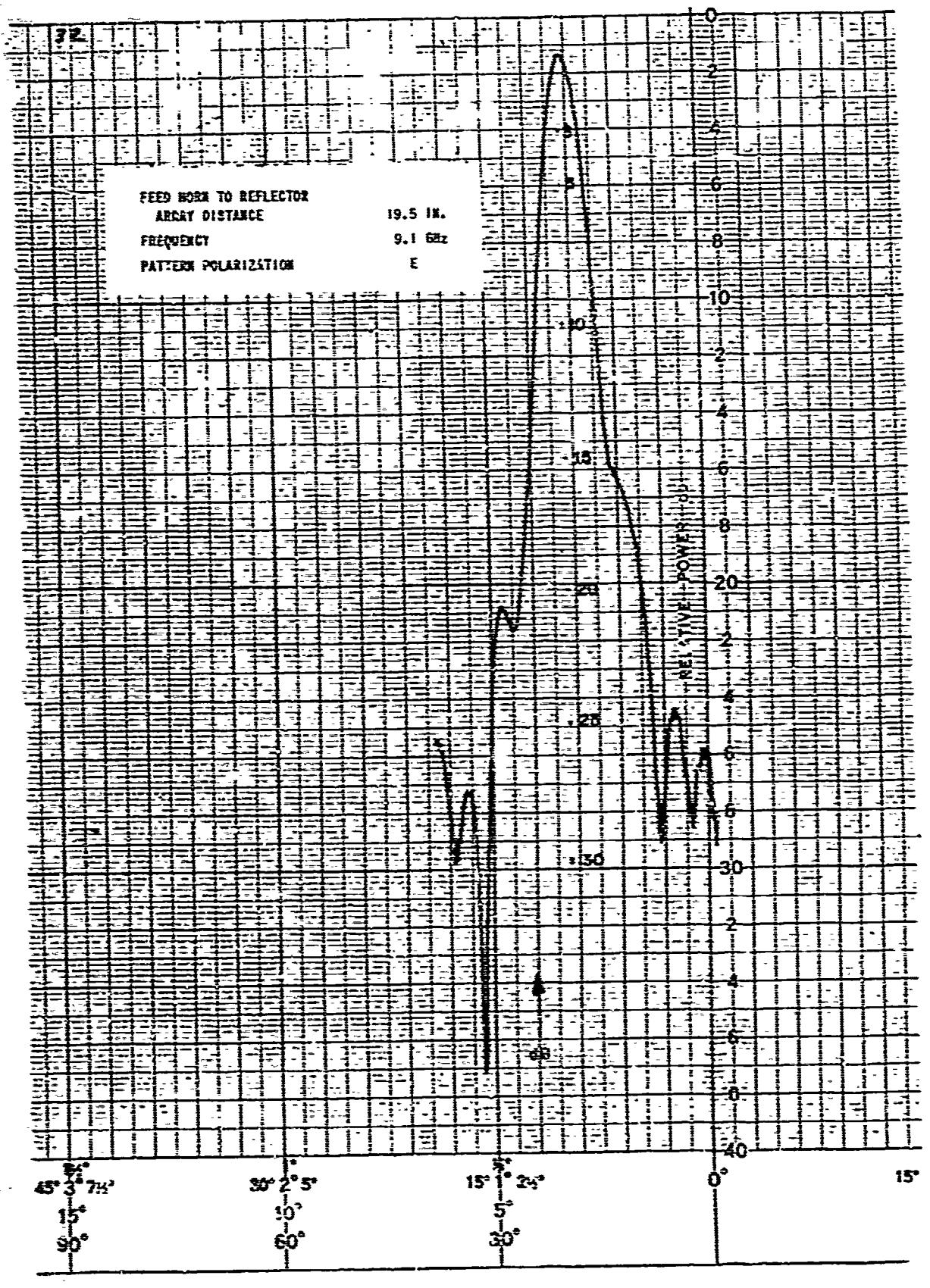

FIGURE 9. ANTENNA PATTERN PERFORMANCE WITH FIRST SHORT SURFACE ADJUSTMENT

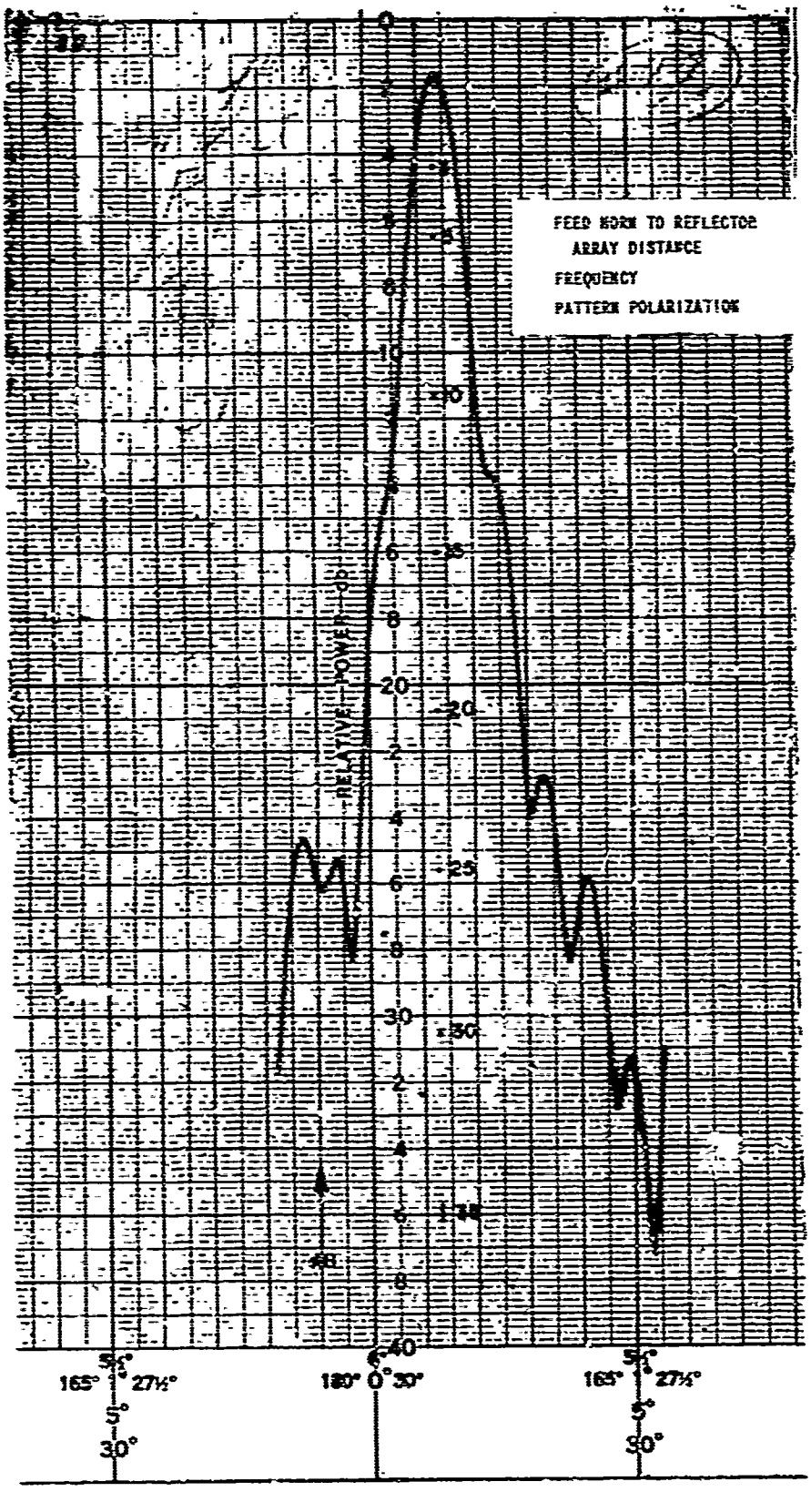

FIGURE 10. ANTENNA PATTERN PERFORMANCE WITH FIRST SHORT SURFACE ADJUSTMENT

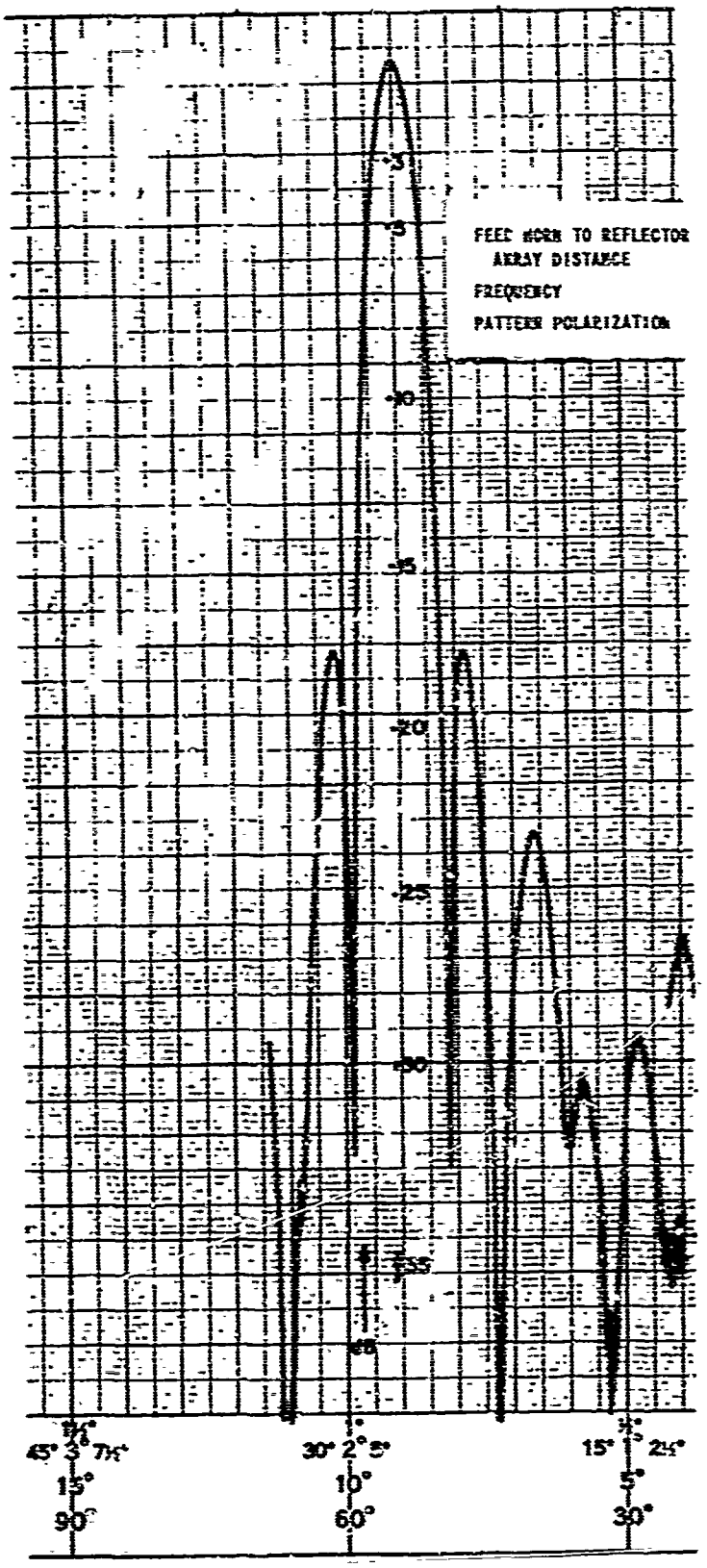

FIGURE 11. ANTENNA PATTERN PERFORMANCE WITH FIRST SHORT SURFACE ADJUSTMENT

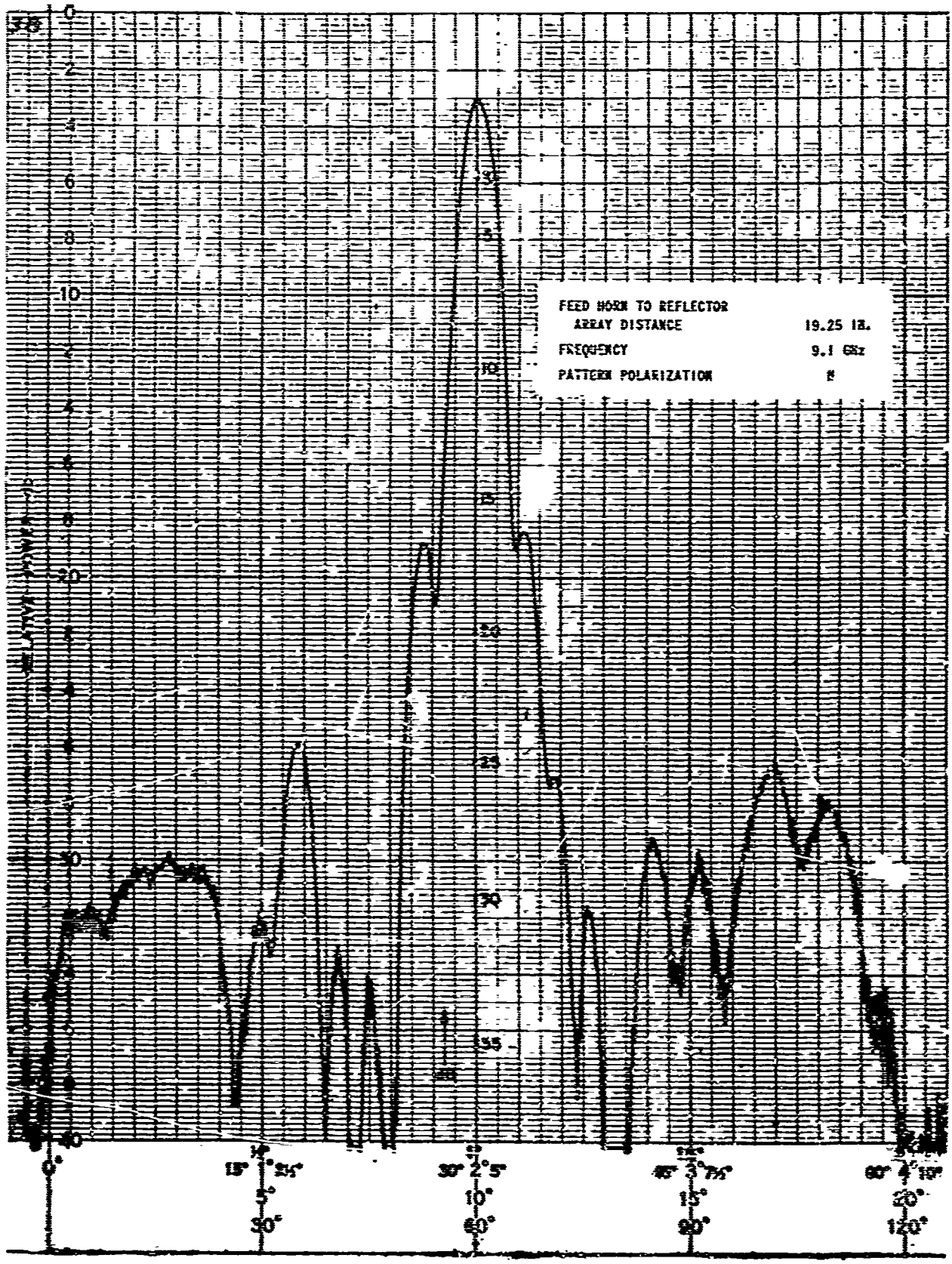

FIGURE 12. ANTENNA PATTERN PERFORMANCE WITH FIRST SHORT SURFACE ADJUSTMENT

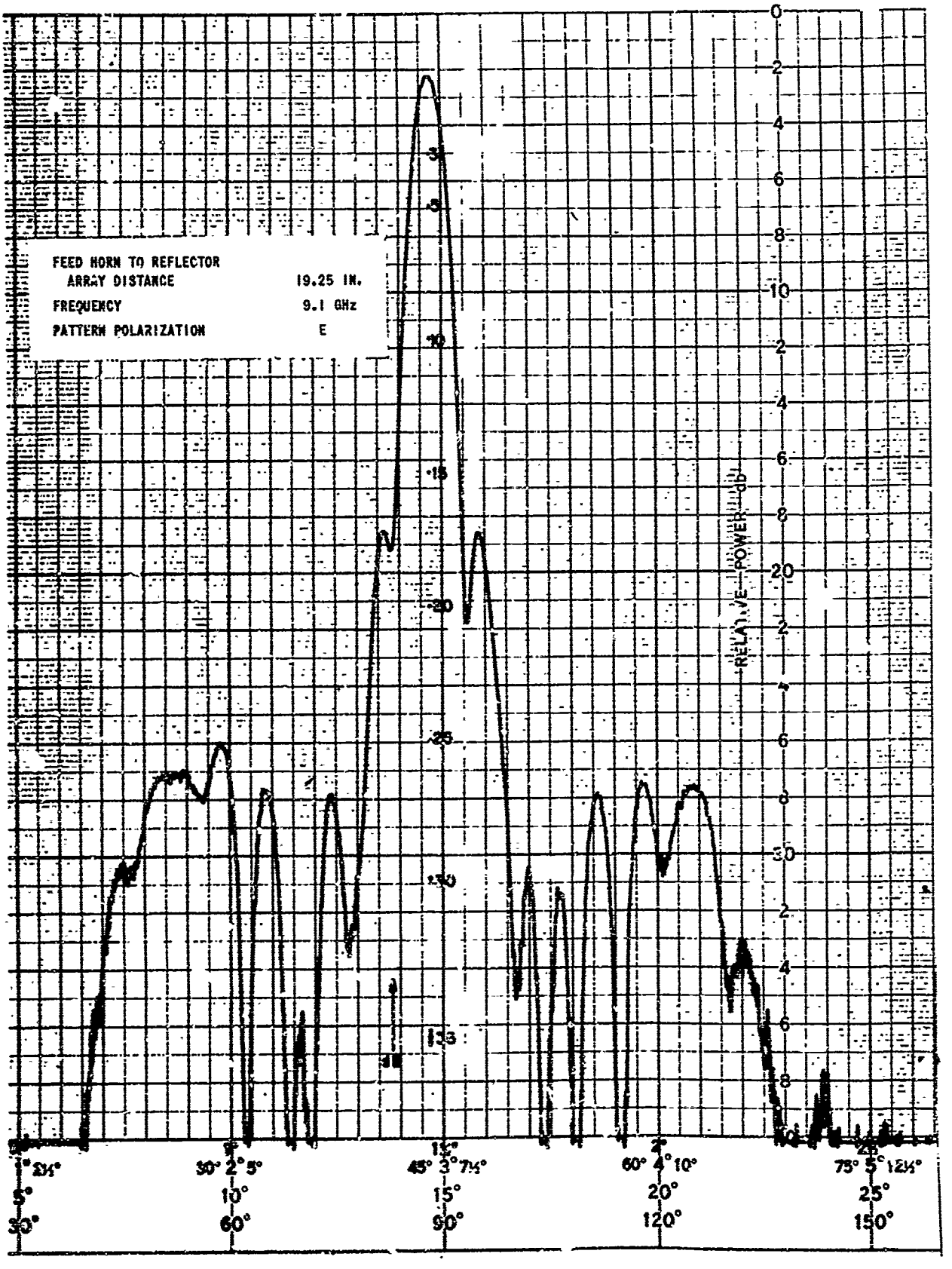

FIGURE 13. ANTENNA PATTERN PERFORMANCE WITH FIRST SHORT SURFACE ADJUSTMENT

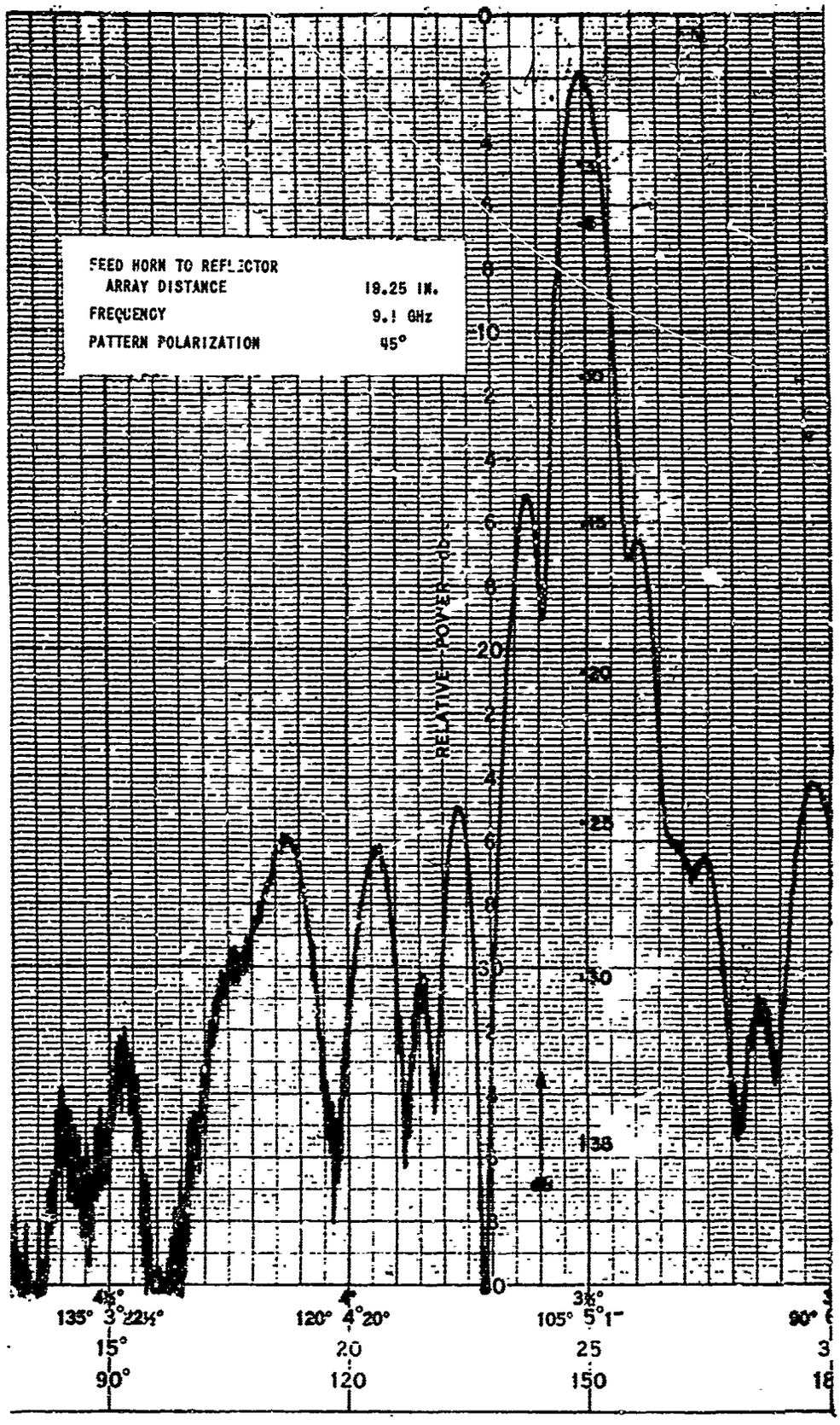

FIGURE 14. ANTENNA PATTERN PERFORMANCE WITH FIRST SHORT SURFACE ADJUSTMENT

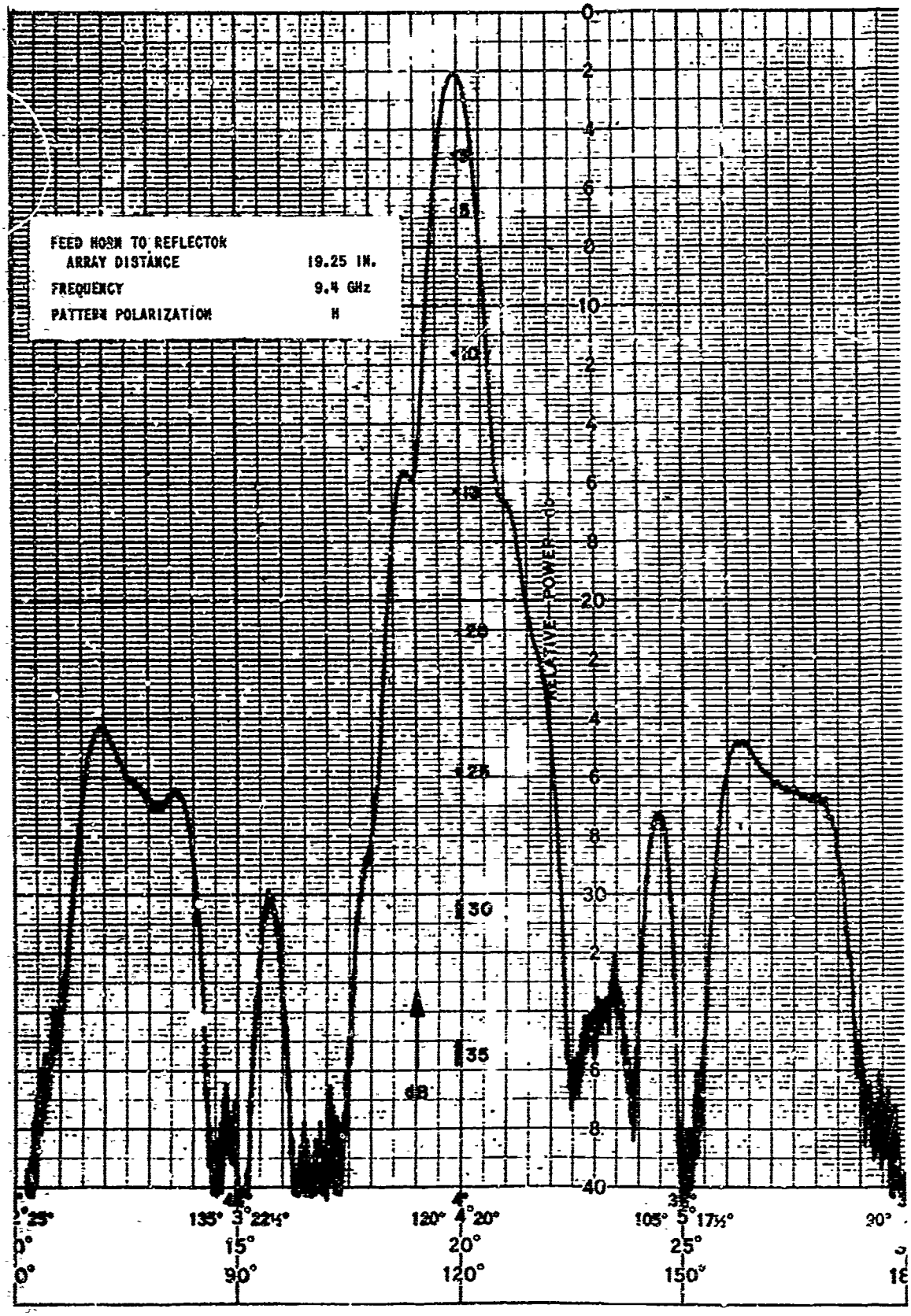

FIGURE 15. ANTENNA PATTERN PERFORMANCE WITH FIRST SHORT SURFACE ADJUSTMENT

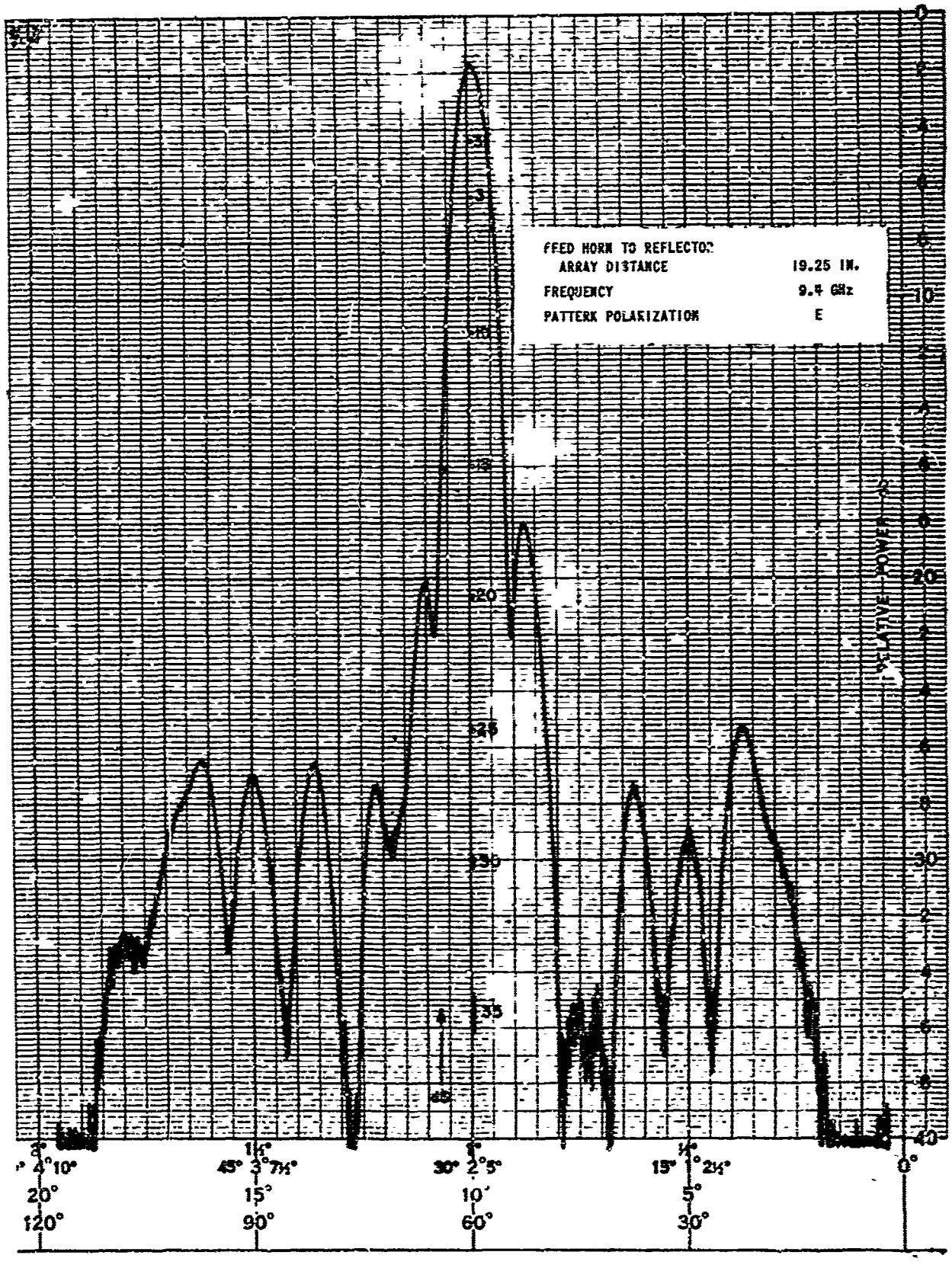

FIGURE 16. ANTENNA PATTERN PERFORMANCE WITH FIRST SHORT SURFACE ADJUSTMENT

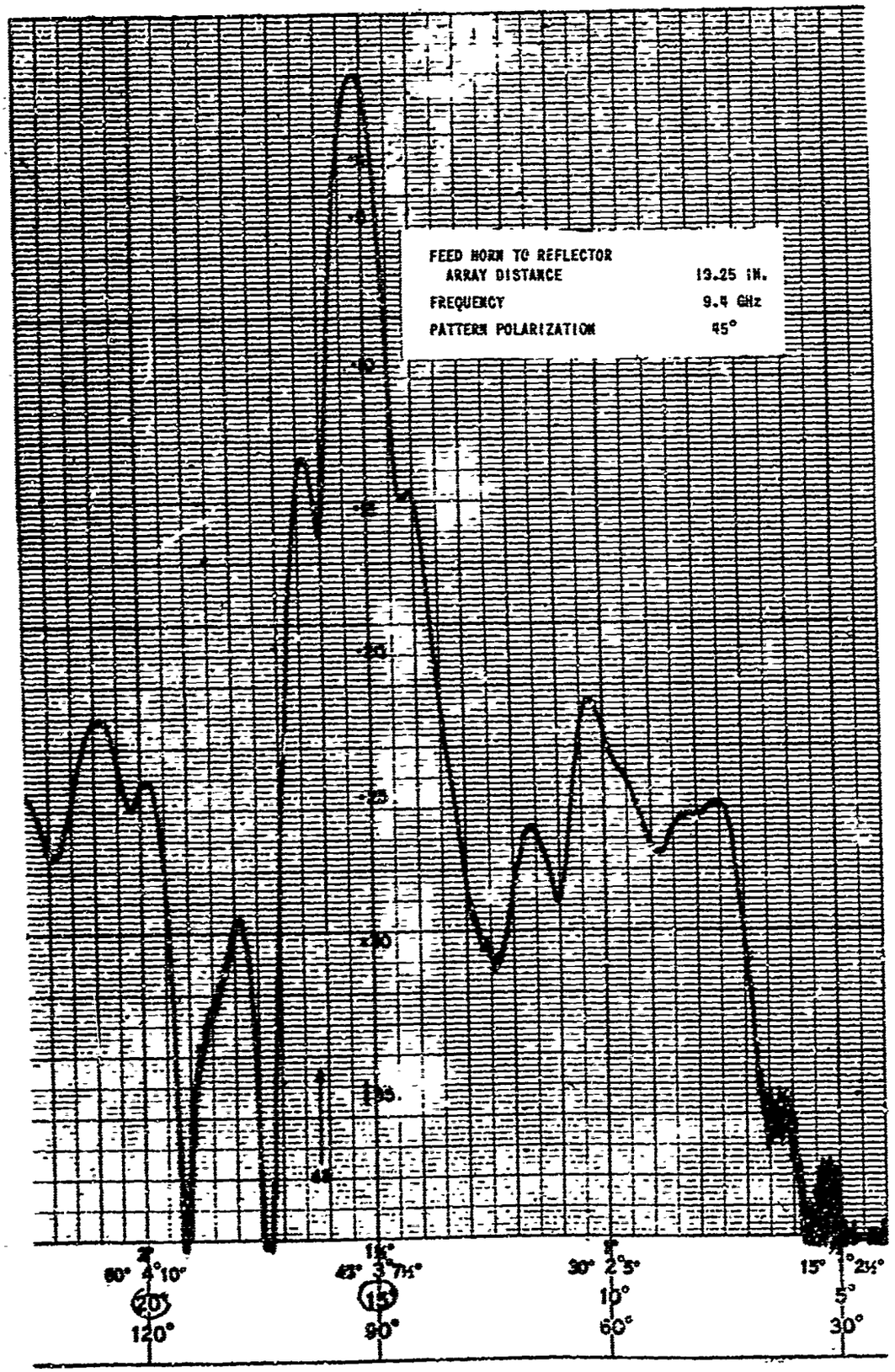

FIGURE 17. ANTENNA PATTERN PERFORMANCE WITH FIRST SHORT SURFACE ADJUSTMENT

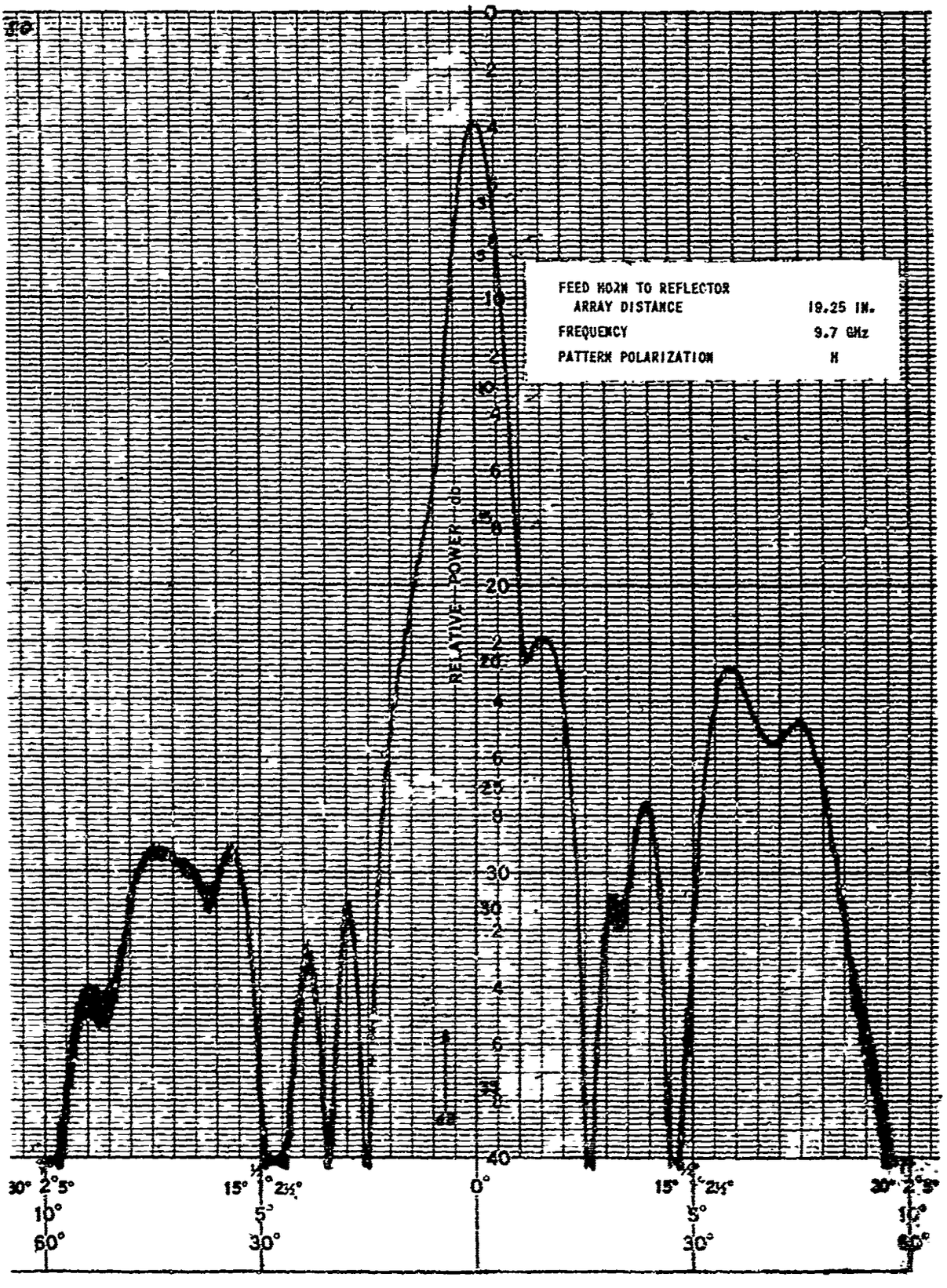

FIGURE 18. ANTENNA PATTERN PERFORMANCE WITH FIRST SHORT SURFACE ADJUSTMENT

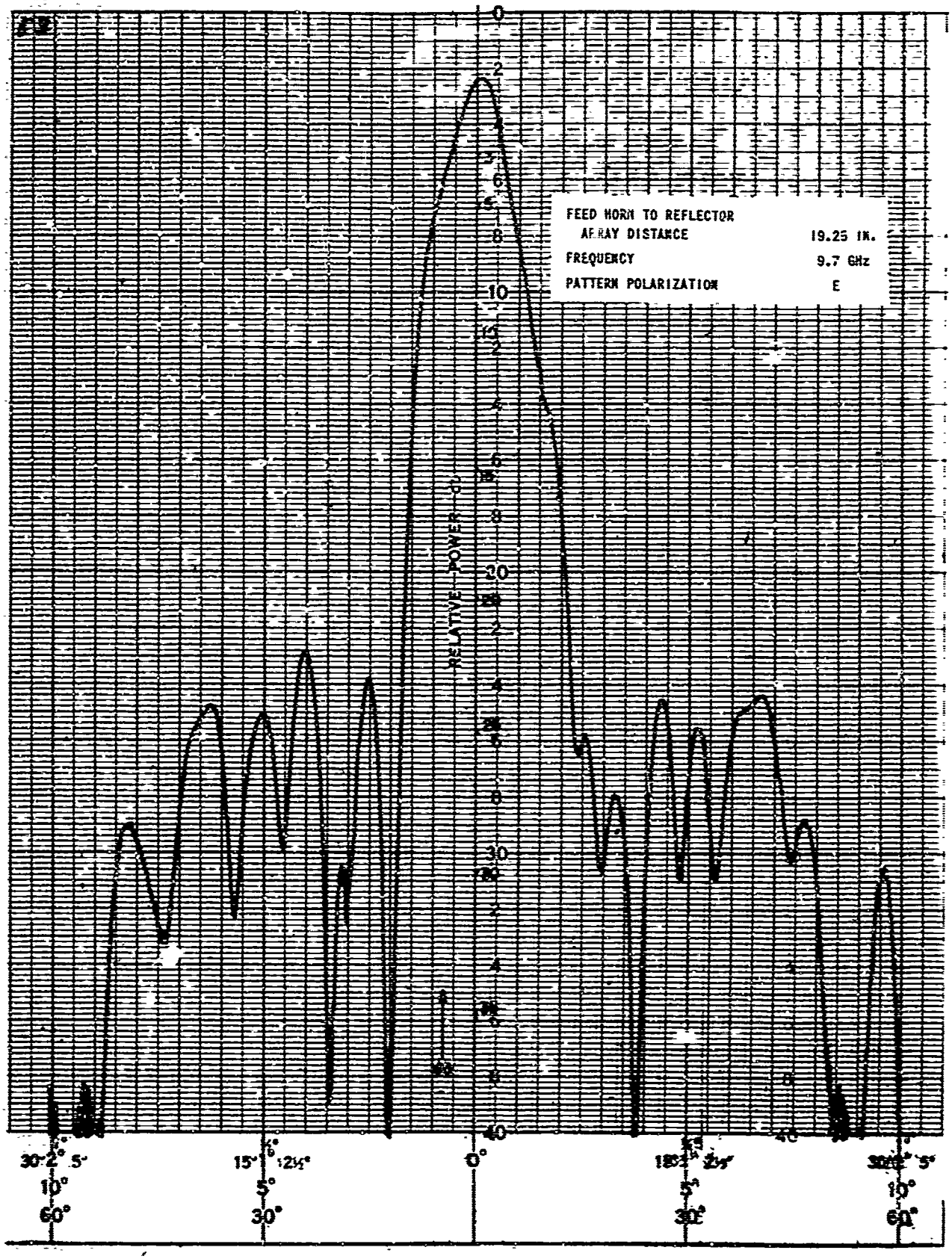

FIGURE 19. ANTENNA PATTERN PERFORMANCE WITH FIRST SHORT SURFACE ADJUSTMENT

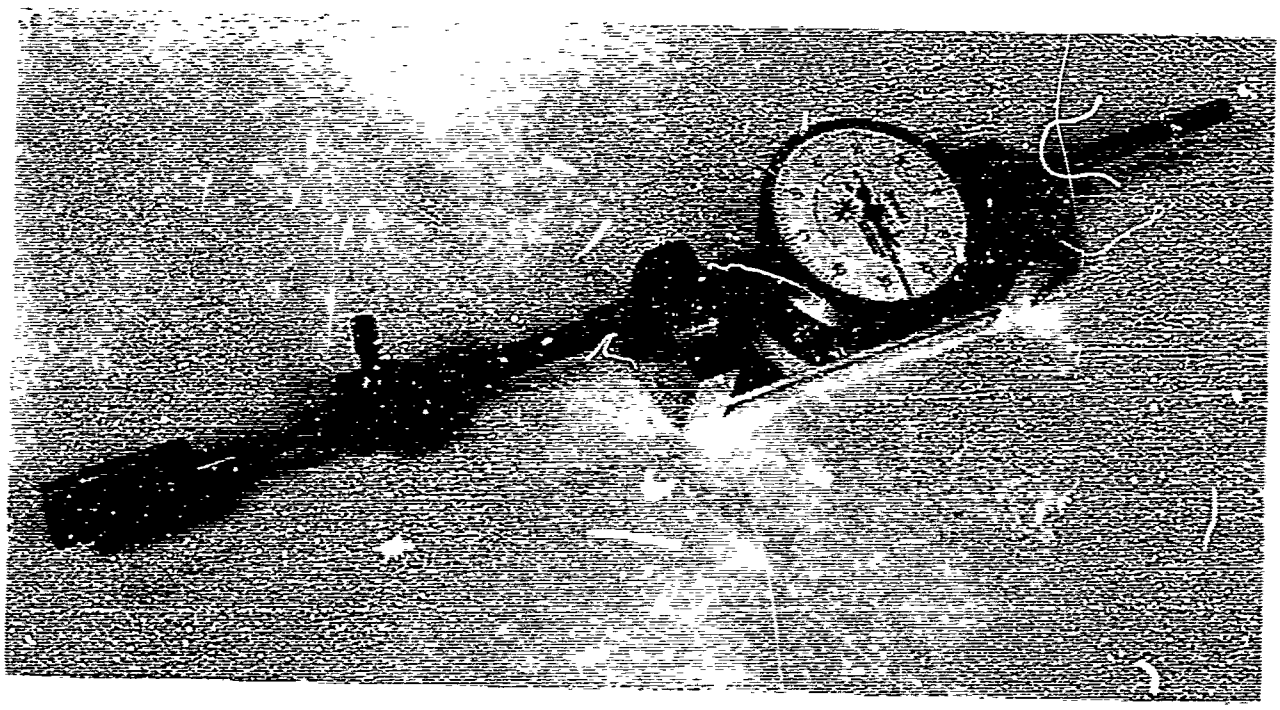

FIGURE 20. SHORT ADJUSTMENT TOOL

Again, a degree of astigmatism was noted. The following list tabulates the measured parameters for the second short setting with optimum H- and E-plane positions, and shows substantially the same performance as the first short setting.

Feed Horn to Subreflector Array Distance (in.)	Frequency (GHz)	Pattern Plane	Half Power Beamwidth (deg)	First Sidelobes with Respect to Peak (dB)
20.25 (optimum H)	9.1	H	0.70	-18
	9.1	E	0.80	-16
19.25 (optimum E)	9.1	H	0.79	-10
	9.1	E	0.70	-19

Results at the compromise position are shown below for the second short setting with 19.75-inch spacing from feed to subreflector array:

Frequency (GHz)	Pattern Plane	Gain (dB)	Half Power Beamwidth (deg)	10-dB Beamwidth (deg)	First Two Sidelobes (dB)	Other Sidelobes (dB)
9.1	H	45.6	0.75	1.30	14	24
	E	--	0.70	1.30	15	23
	45°	--	0.75	1.30	13	27
9.4	H	46.5	0.79	1.40	13	22

Figures 21 through 28 are the second short setting patterns. The results achieved are very similar to those for the first short setting.

3-5 SUBREFLECTOR ARRAY, THIRD SHORT SETTING

The series of experiments, undertaken on a C-band reflector array to obtain a better formulation for the surface susceptance variations with scan angle, were incorporated into the third short setting. Figures 29 through 33 are the measured results showing standing wave ratio as a function of assumed susceptance values. The estimated susceptance values, including the previously measured value for normal incidence and reflection, are listed below.

B_S (0, 0) = 0.384
B_S (41°24', 0) = -0.025 (H plane)
B_S (61°51', 0) = -0.660 (H plane)
B_S (41°24', 90°) = 0.192 (E plane)
B_S (61°51', 90°) = 0.100 (E plane)
B_S (38°34', 45°) = 0.133 (diagonal plane)

Figure 34 shows the apparatus used.

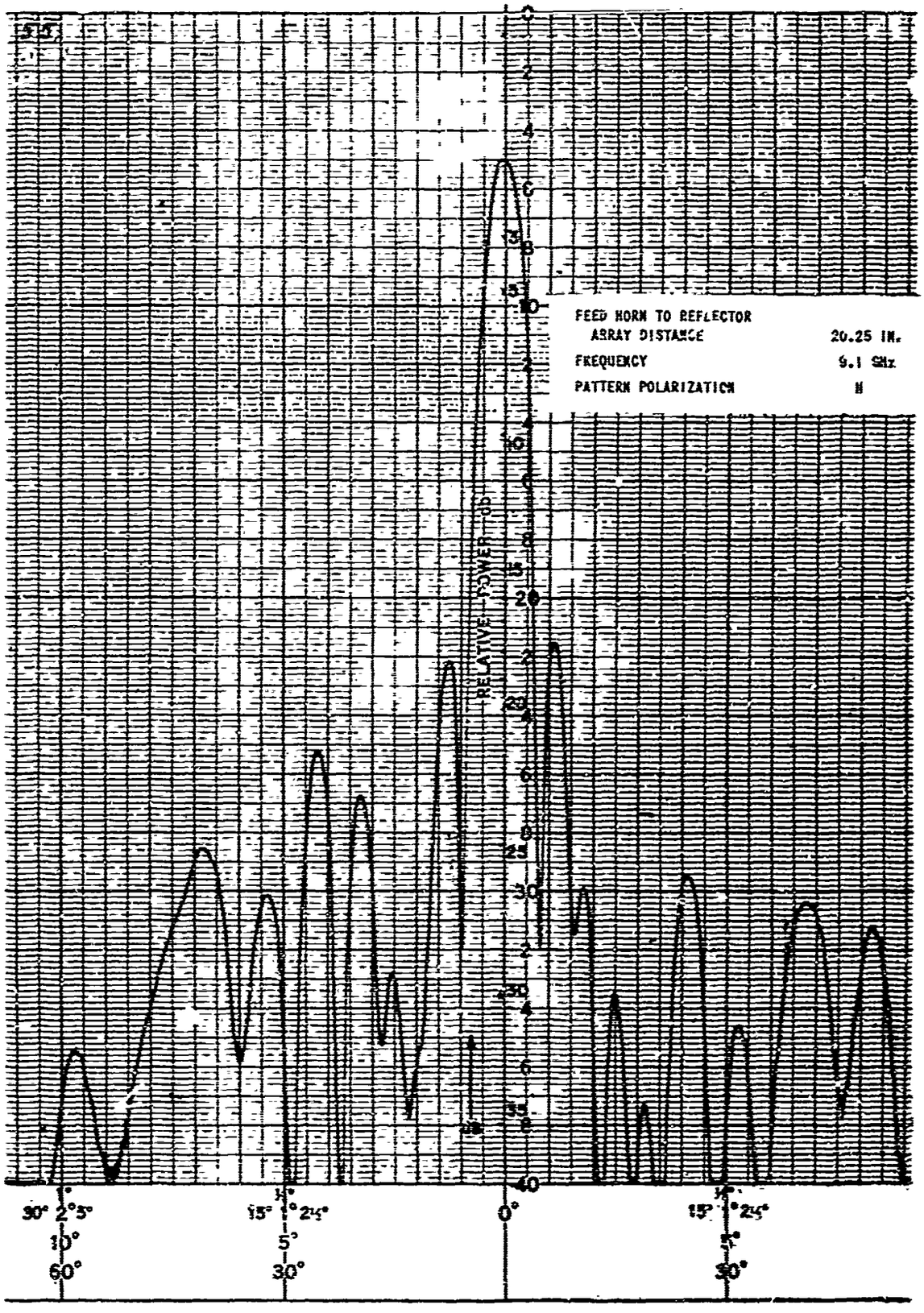

FIGURE 21. ANTENNA PATTERN PERFORMANCE WITH SECOND SHORT SURFACE ADJUSTMENT

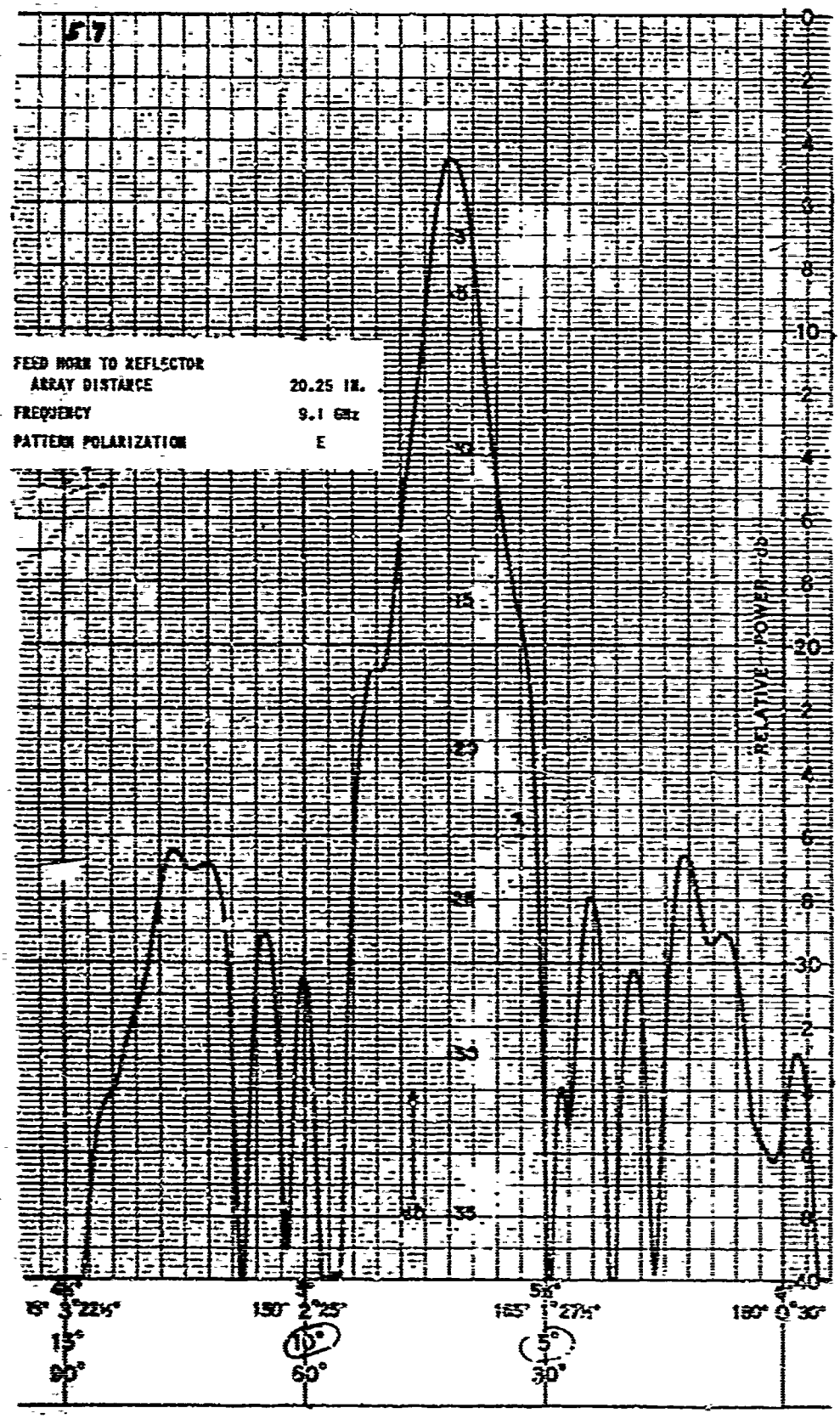

FIGURE 22. ANTENNA PATTERN PERFORMANCE WITH SECOND SHORT SURFACE ADJUSTMENT

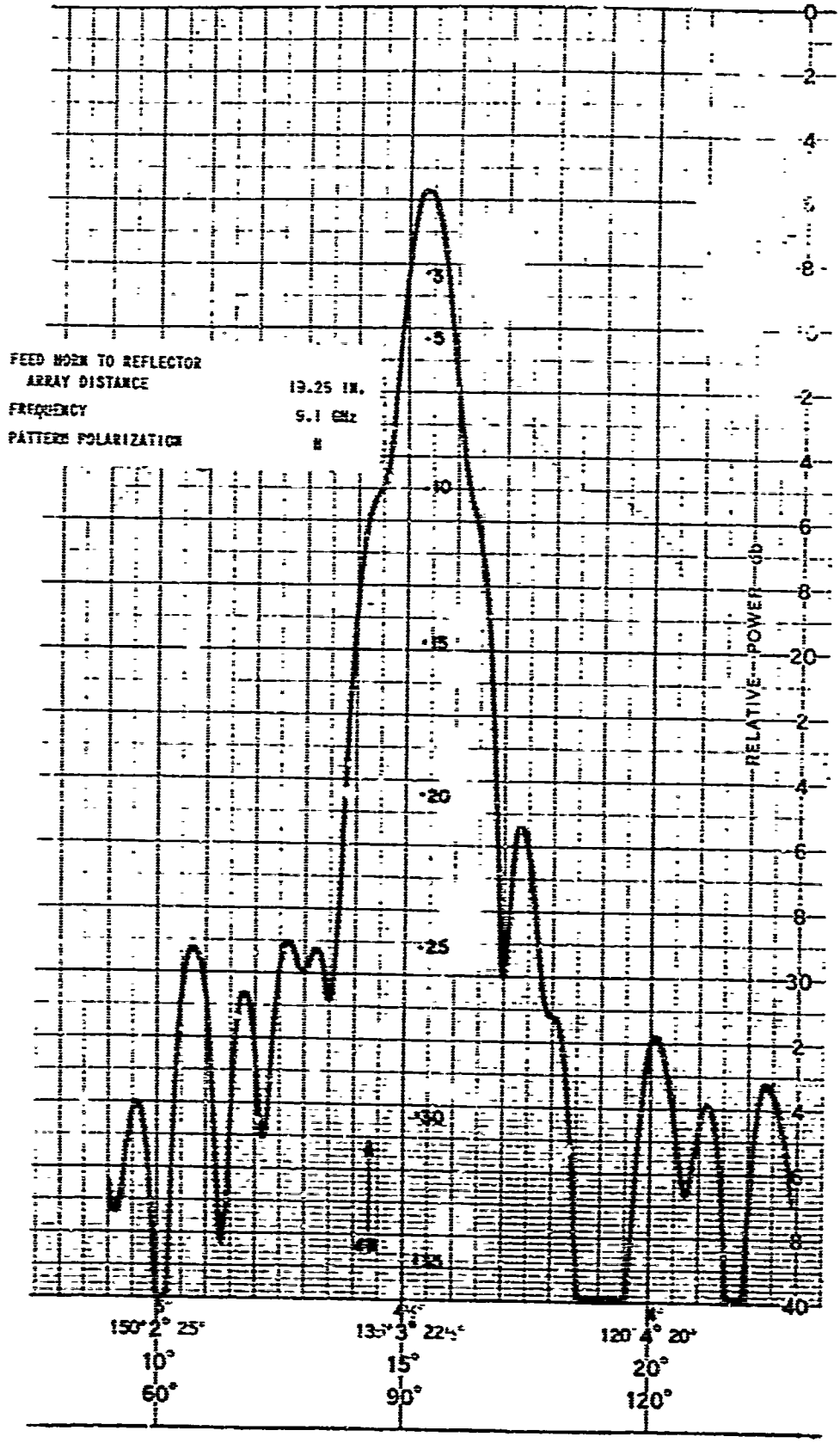

FIGURE 23. ANTENNA PATTERN PERFORMANCE WITH SECOND SHORT SURFACE ADJUSTMENT

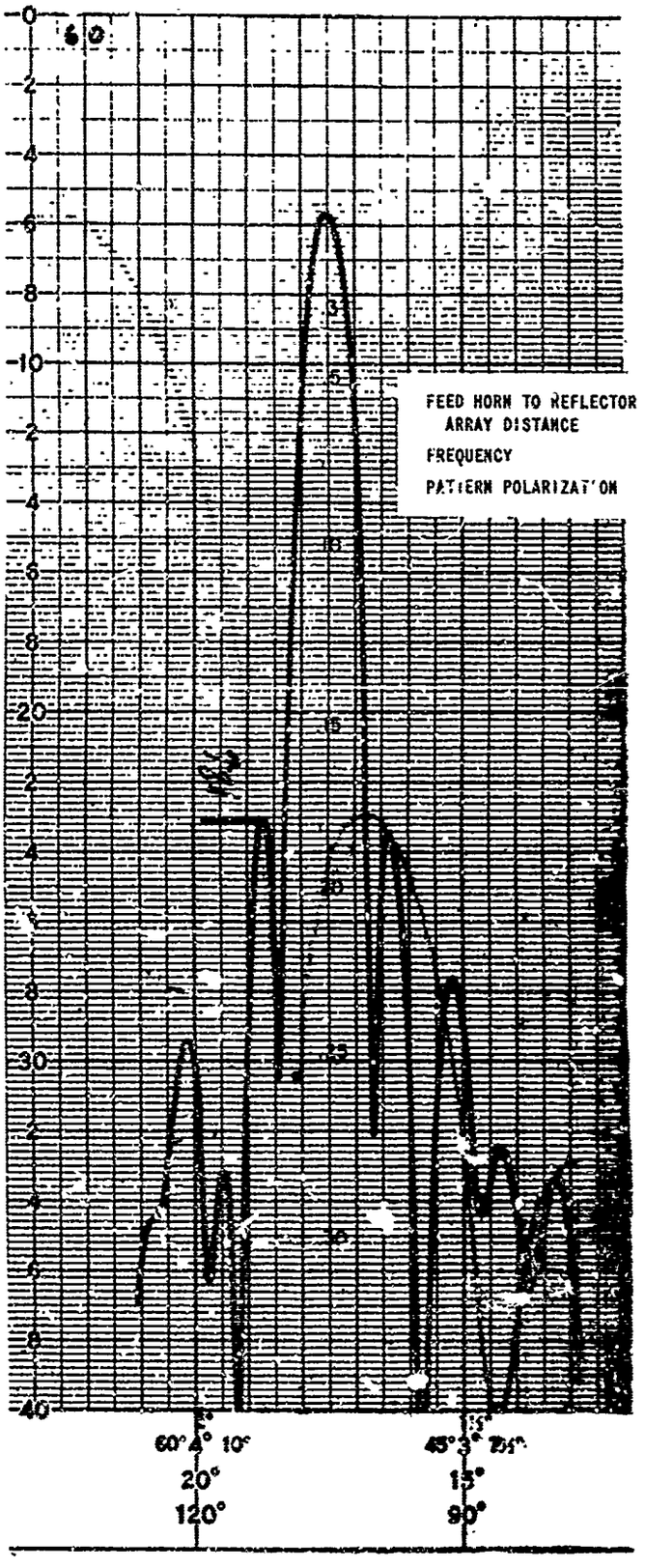

FIGURE 24. ANTENNA PATTERN PERFORMANCE WITH SECOND SHORT SURFACE ADJUSTMENT

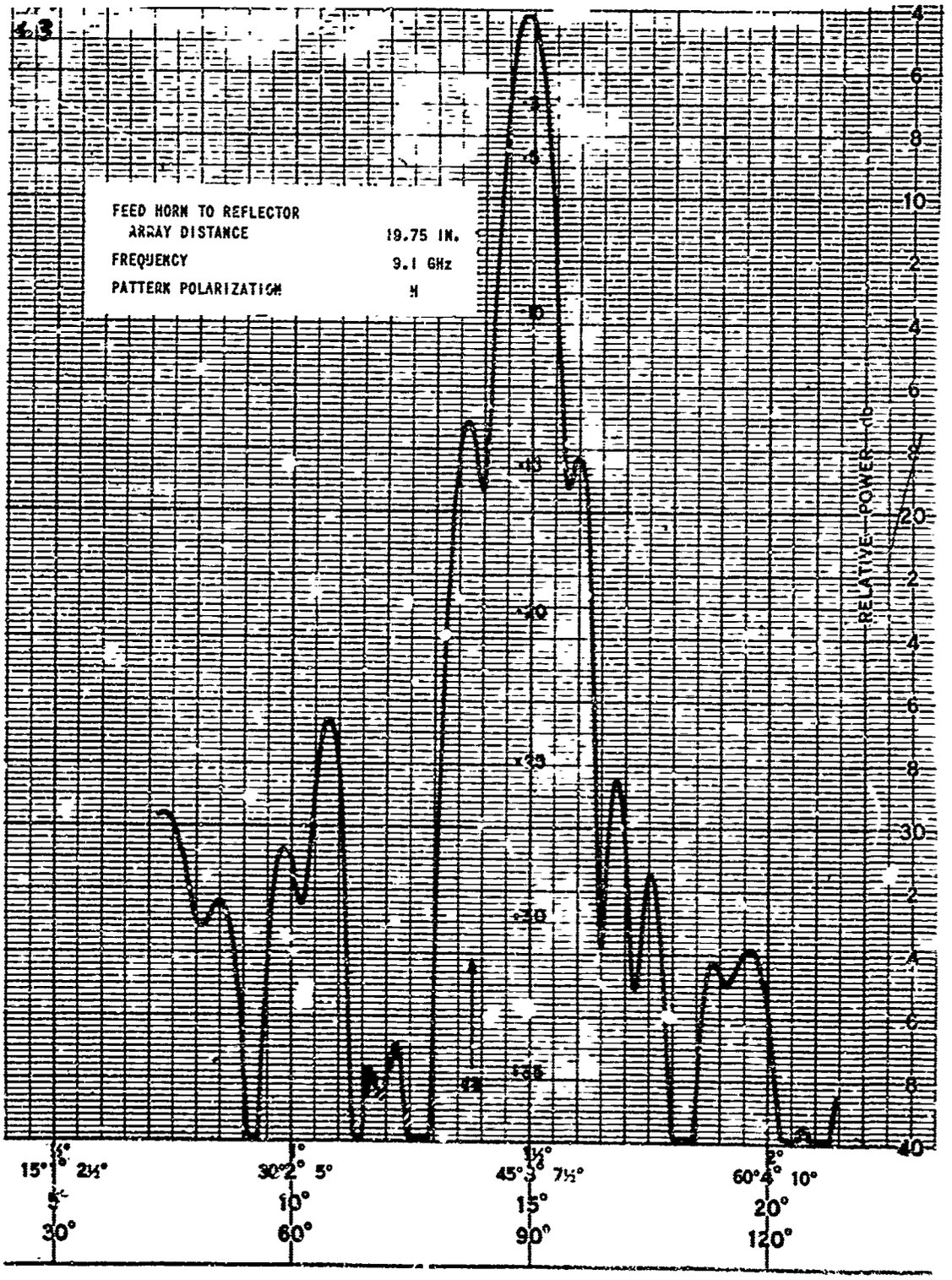

FIGURE 25. ANTENNA PATTERN PERFORMANCE WITH SECOND SHORT SURFACE ADJUSTMENT

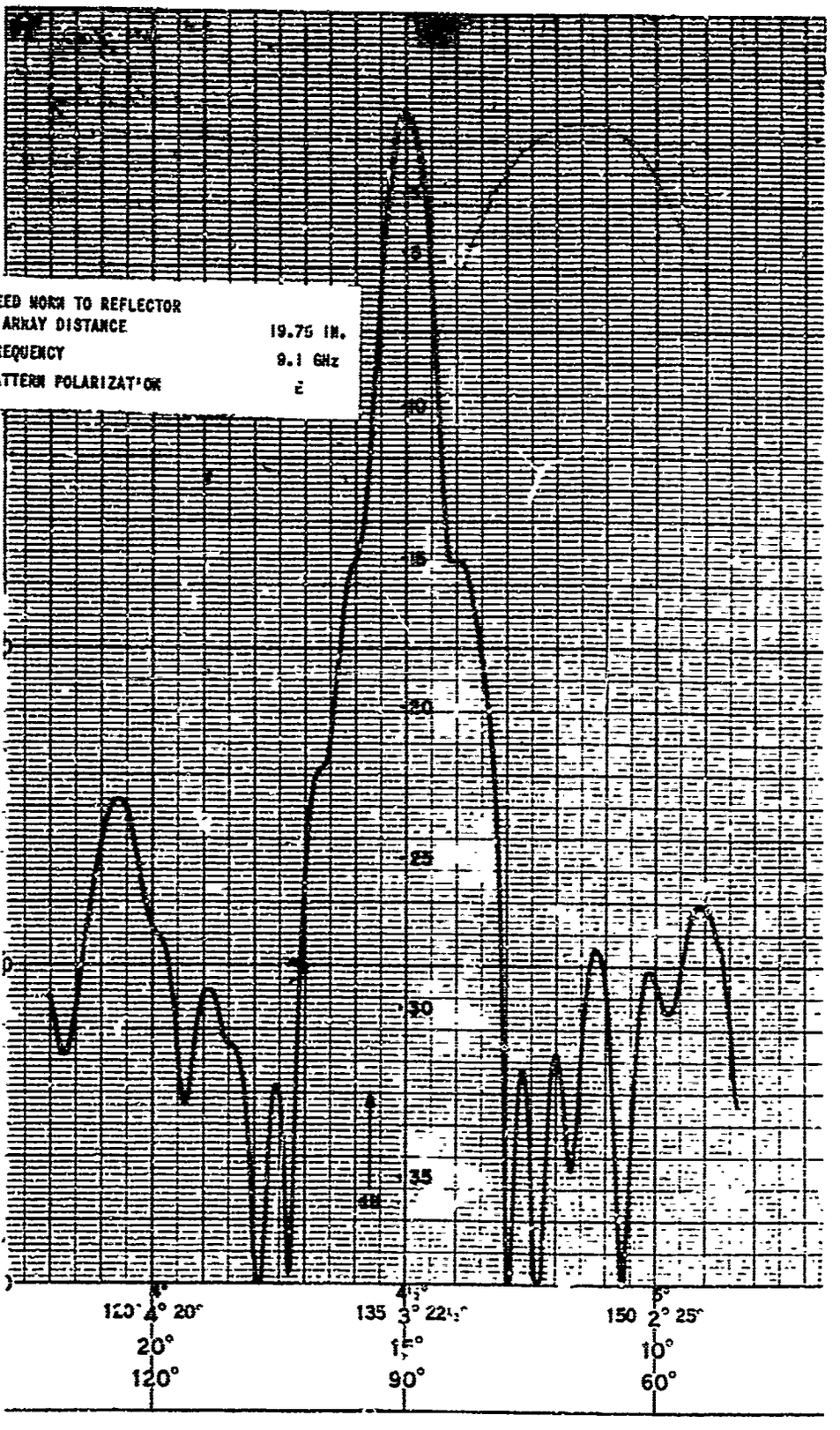

FIGURE 26. ANTENNA PATTERN PERFORMANCE WITH SECOND SHORT SURFACE ADJUSTMENT

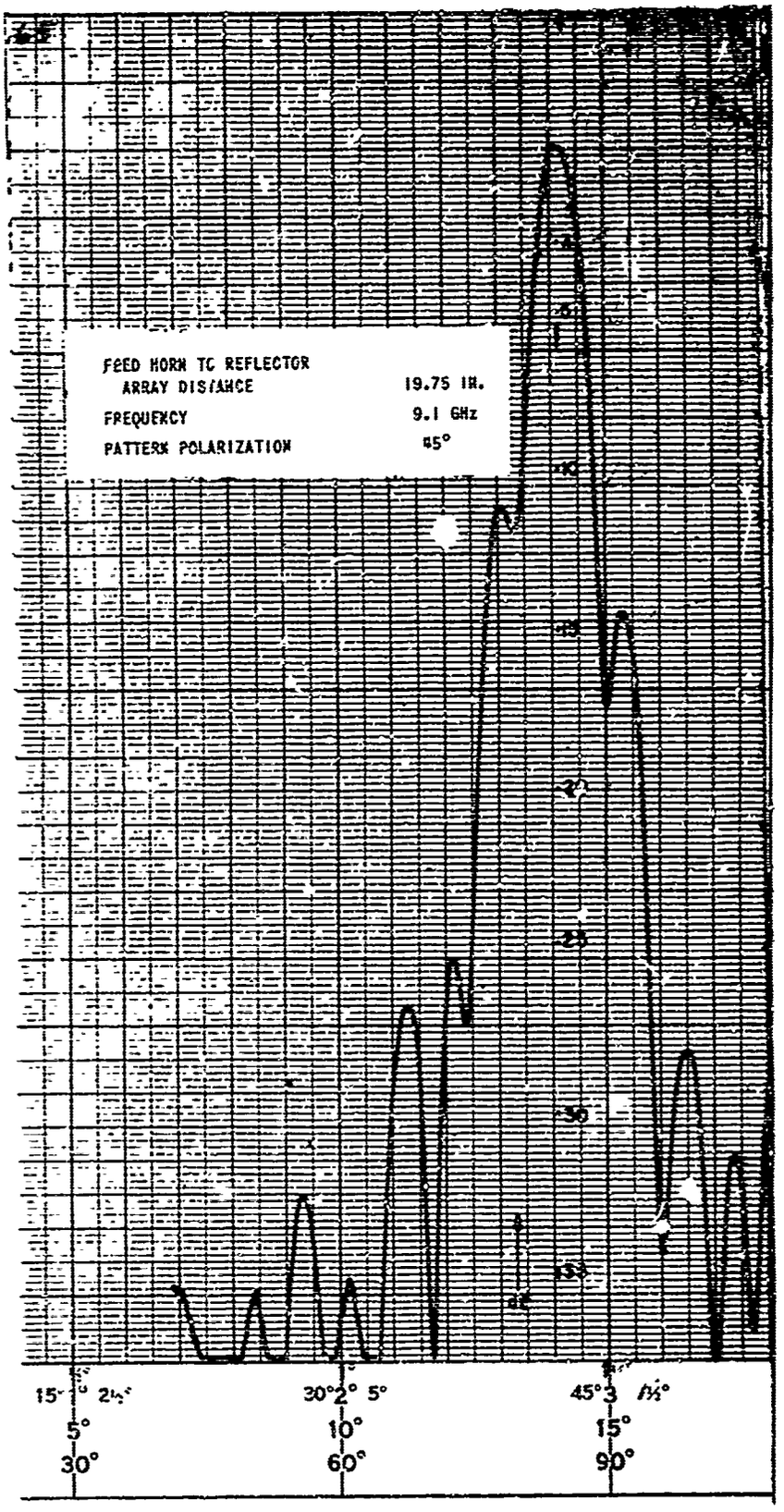

FIGURE 27. ANTENNA PATTERN PERFORMANCE WITH SECOND SHORT SURFACE ADJUSTMENT

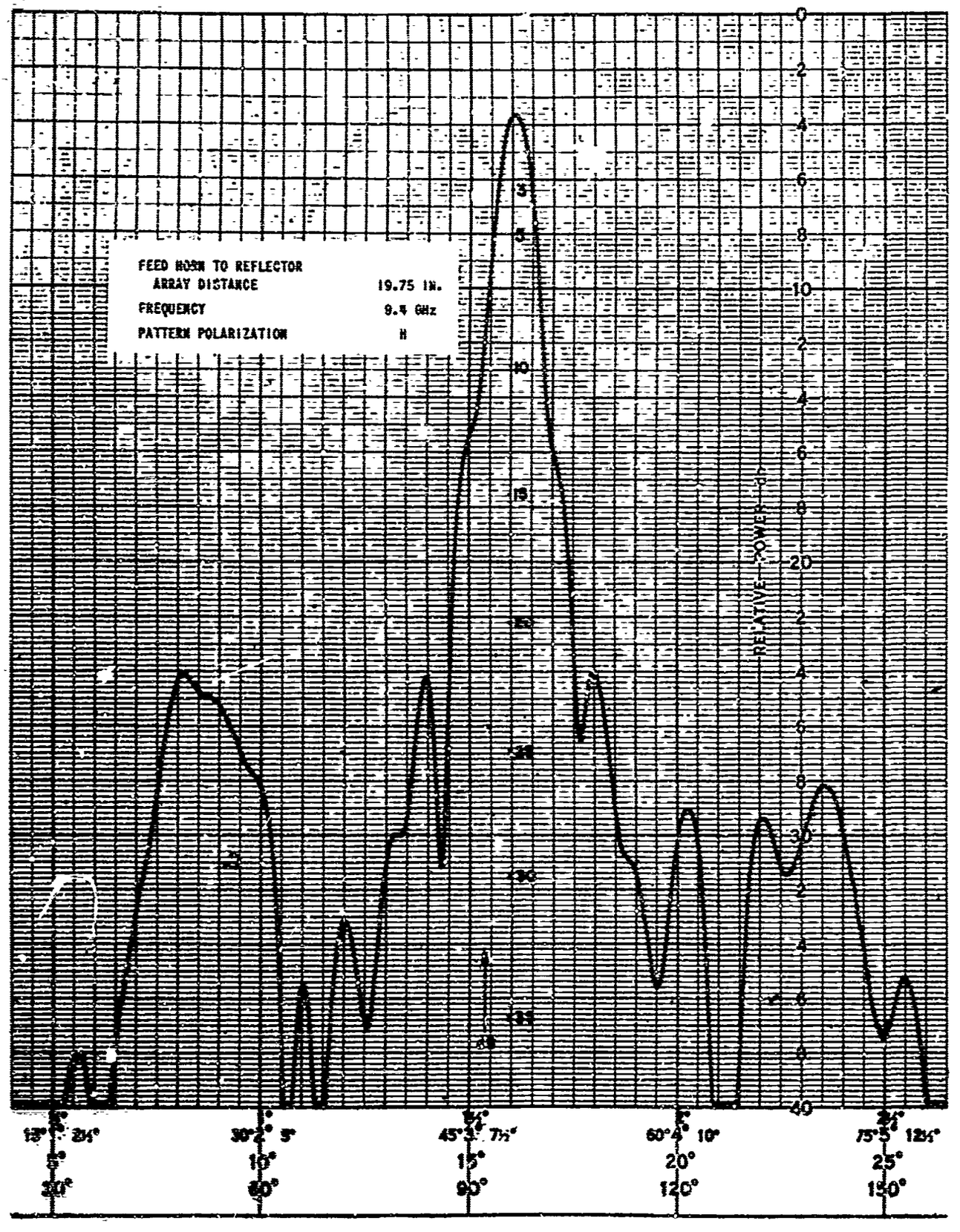

FIGURE 28. ANTENNA PATTERN PERFORMANCE WITH SECOND SHORT SURFACE ADJUSTMENT

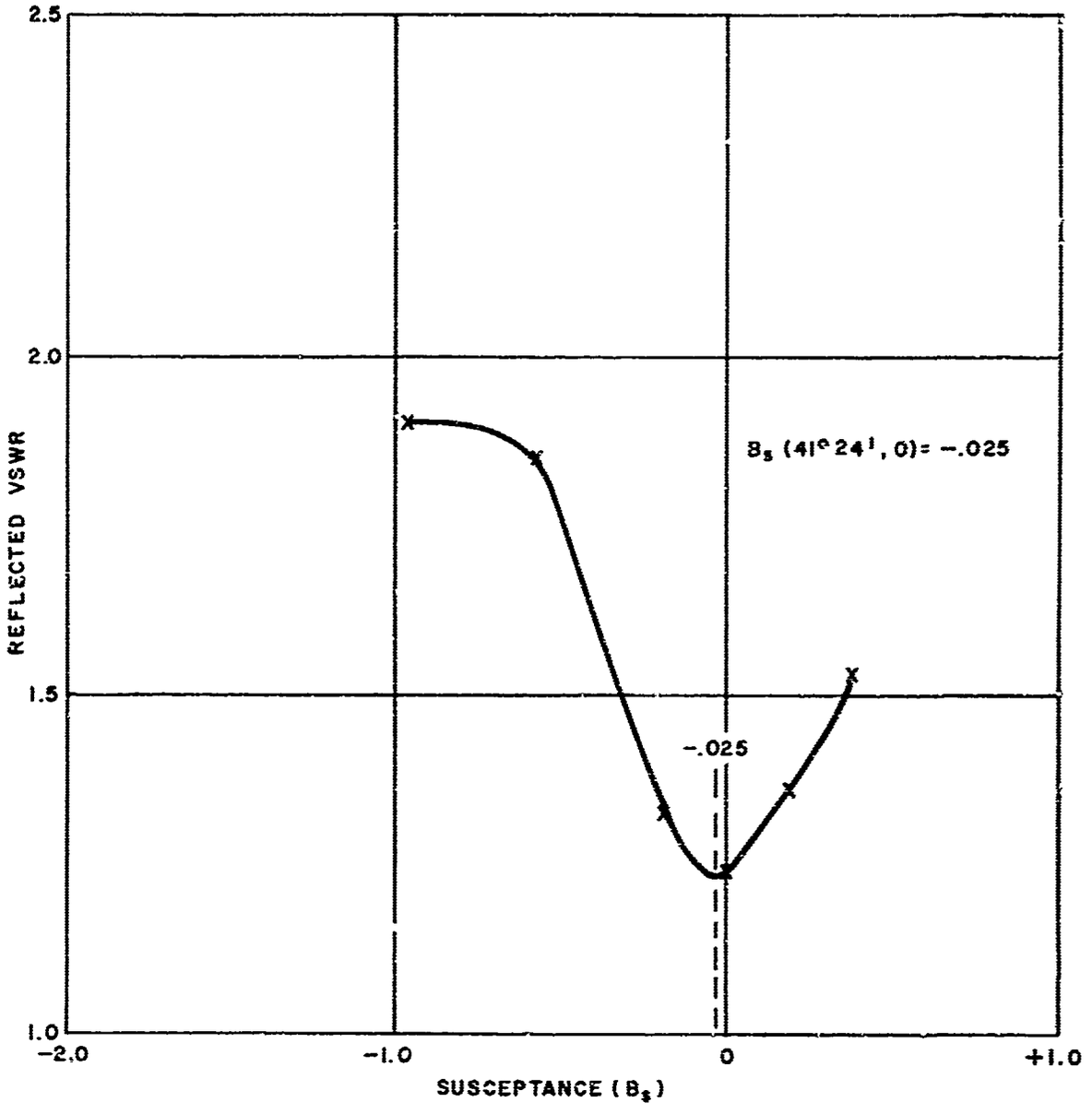

FIGURE 29. VSWR VERSUS ASSUMED SUSCEPTANCE

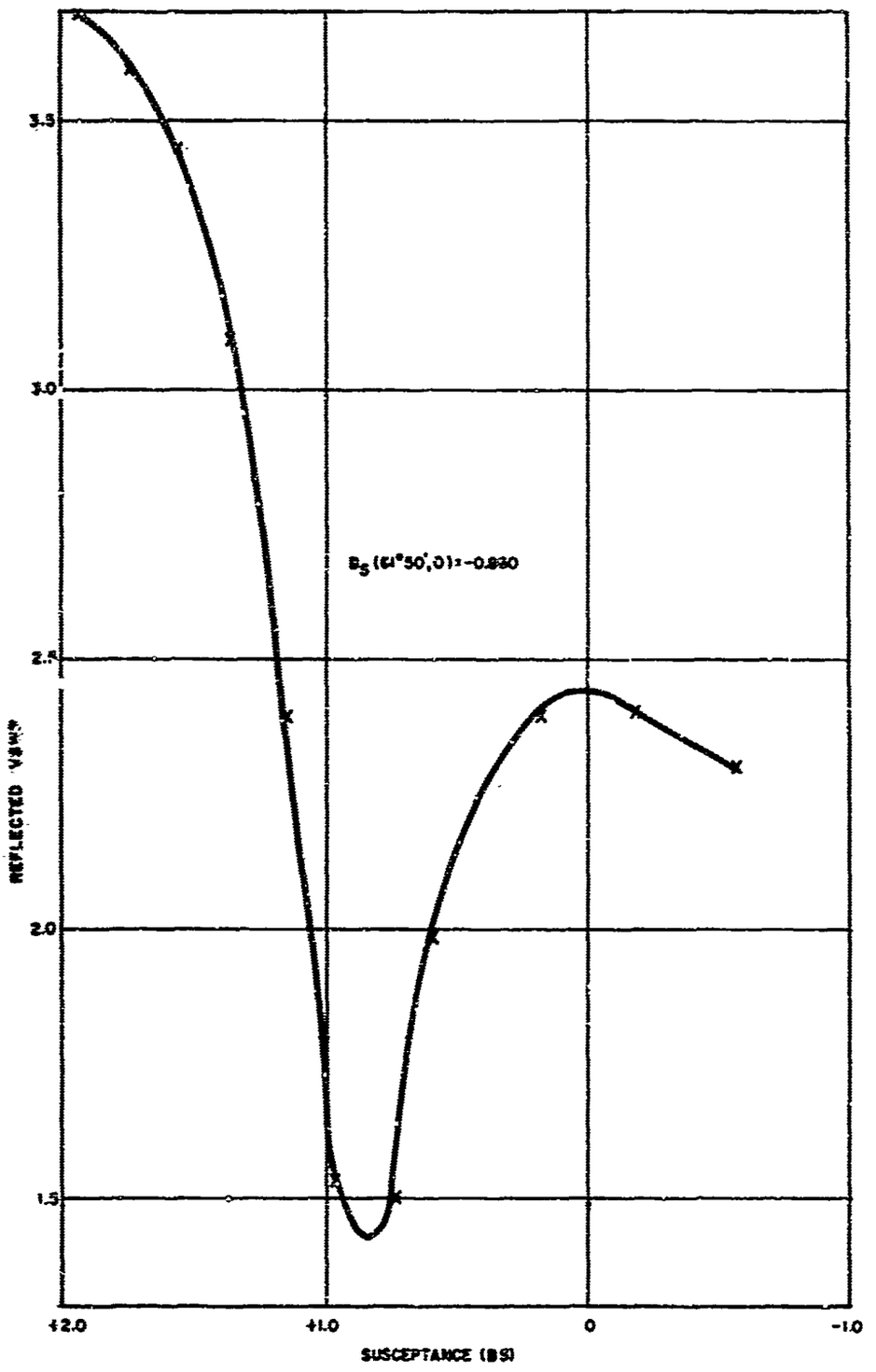

FIGURE 30. VSWR VERSUS ASSUMED SUSCEPTANCE

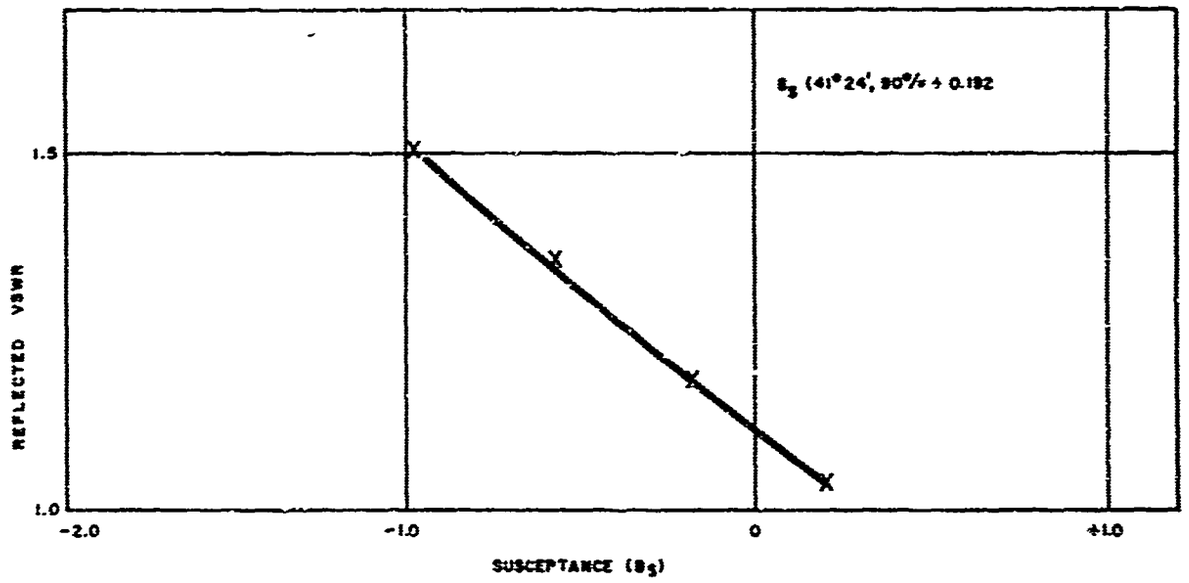

FIGURE 31. VSWR VERSUS ASSUMED SUSCEPTANCE

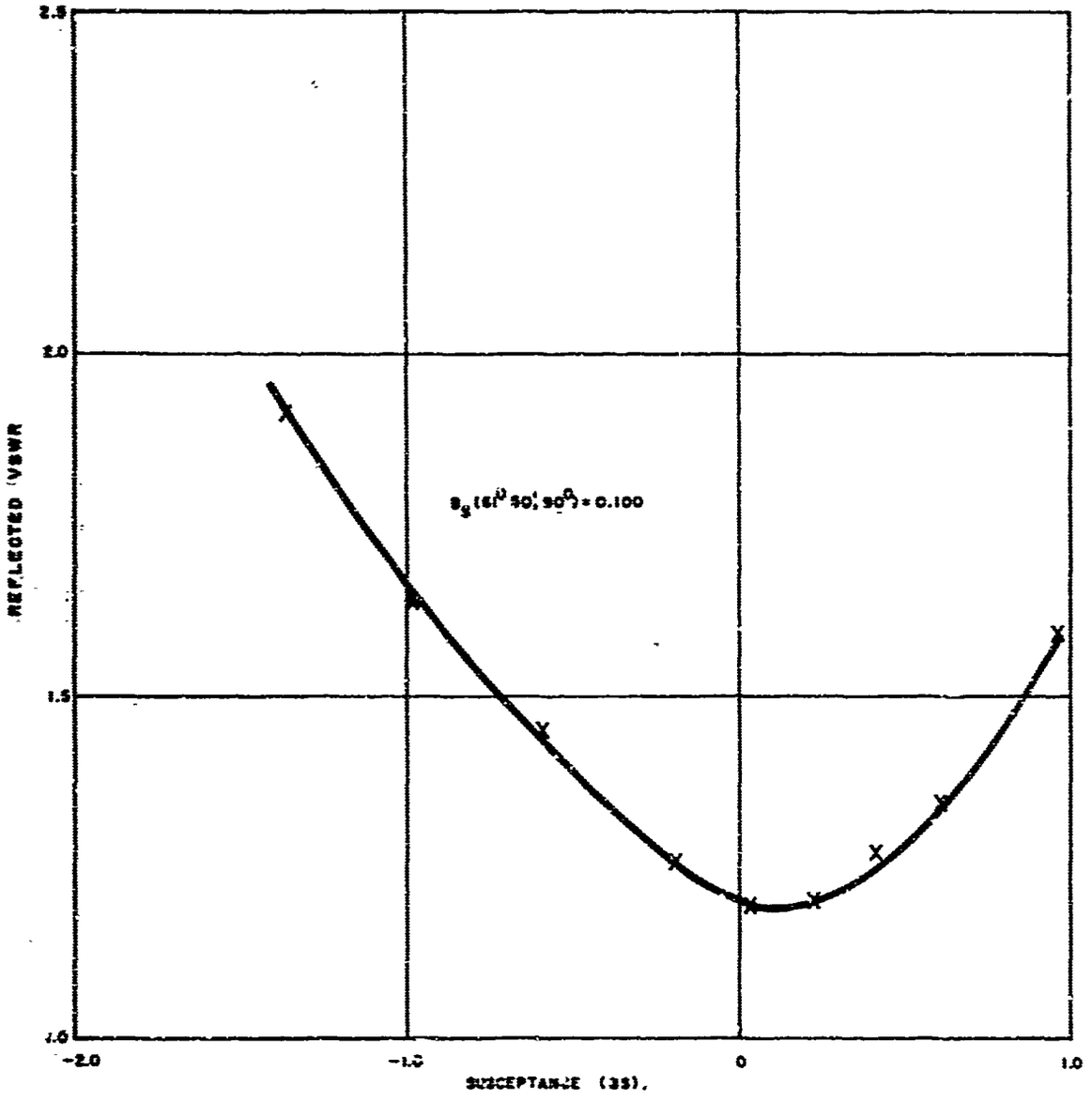

FIGURE 32. VSWR VERSUS ASSUMED SUSCEPTANCE

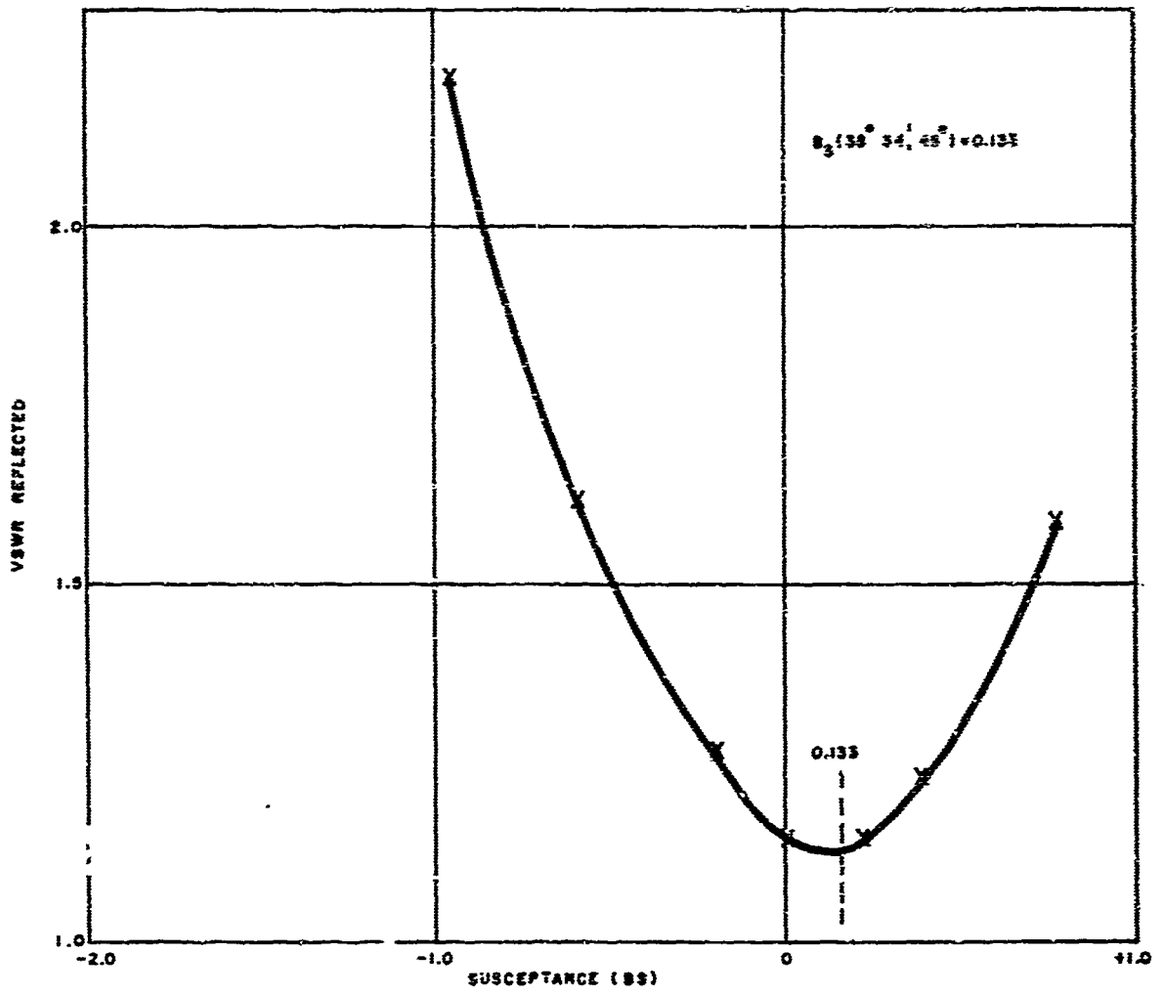

FIGURE 33. VSWR VERSUS ASSUMED SUSCEPTANCE

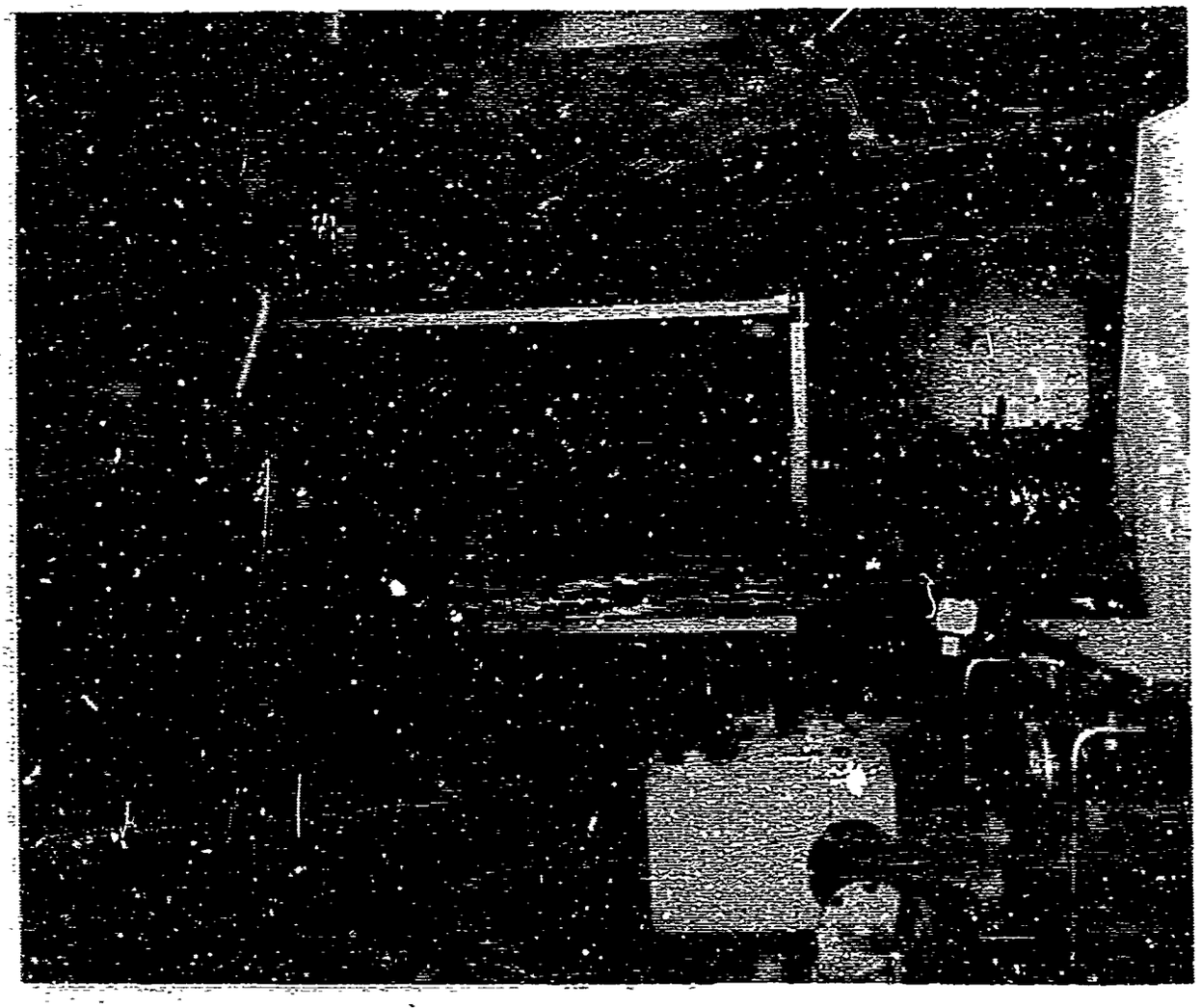

FIGURE 34. C-BAND PLANAR REFLECTOR ARRAY AND PARABOLIC REFLECTOR ILLUMINATOR

These data can be approximated by the expression:

$$B_s(\theta,\varphi) = 0.384 - 0.337 \sin^{1.362} \theta_r \sin^2 \varphi_r - 2.025 \sin^{3.871} \theta_r \cos^2 \varphi_r \quad (3)$$

This expression was used in equation 1 to set the third shorting surface for the X-band, linearly polarized, subreflector array. Since the astigmatism was found to be negligible with this third short setting, only patterns taken at the best gain position are shown in figures 35 to 52. All shorts were also translated a fixed amount so that the center short was half a guide wavelength from the entry surface. Following is a summary of the pattern results for the third short setting with 19.5-inch spacing from feed to subreflector array:

Frequency (GHz)	Pattern Plane	Gain (dB)	Half Power Beamwidth (deg)	10-dB Beamwidth (deg)	20-dB Beamwidth (deg)	First Two Sidelobes (dB)	Other Sidelobes (dB)
9.1	H	46.8	0.80	1.40	1.83	17.5	27
	E	--	0.72	1.20	1.58	18	23
	45°	--	0.74	1.28	1.67	17	32
9.4	H	46.6	0.82	1.38	1.78	15	25
	E	--	0.68	1.18	--	15.5	28
	45°	--	0.80	1.30	1.62	14	26
9.7	H	45.3	0.85	1.48	--	15	20
	E	--	0.68	1.15	1.53	15	27
	45°	--	0.70	1.20	1.48	16	30
10.0	H	47.2	0.85	1.46	1.95	15	23
	E	--	0.69	1.20	--	14	25
	45°	--	0.70	1.20	1.52	14	27
8.2	H	45.2	0.79	1.37	1.68	18	21
	E	--	0.77	1.35	1.80	15	25
	45°	--	0.81	1.36	1.80	18	22
8.6	H	--	0.72	1.31	1.72	18	23
	E	--	0.76	1.25	1.62	16	25
	45°	--	0.73	1.28	1.65	17	20

The center frequency gain of 46.8 dB corresponds to an efficiency of 59 percent. The gain has substantially improved over previous short settings. Having eliminated the problem of astigmatism with the subreflector array, it is assumed that any remaining loss of gain was due to the broad H-plane beamwidth (0.80°).

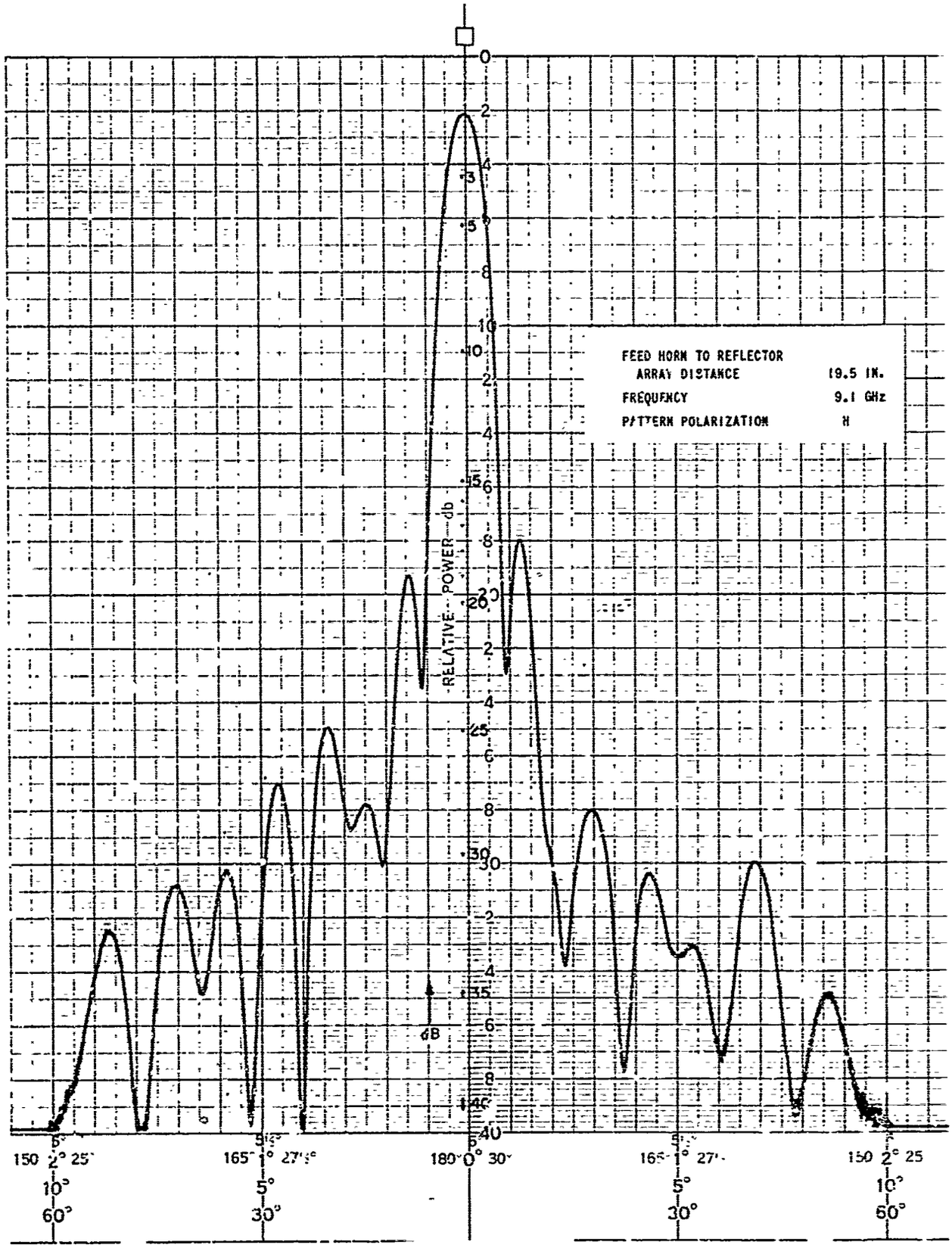

FIGURE 35. ANTENNA PATTERN PERFORMANCE WITH THIRD SHORT SURFACE ADJUSTMENT

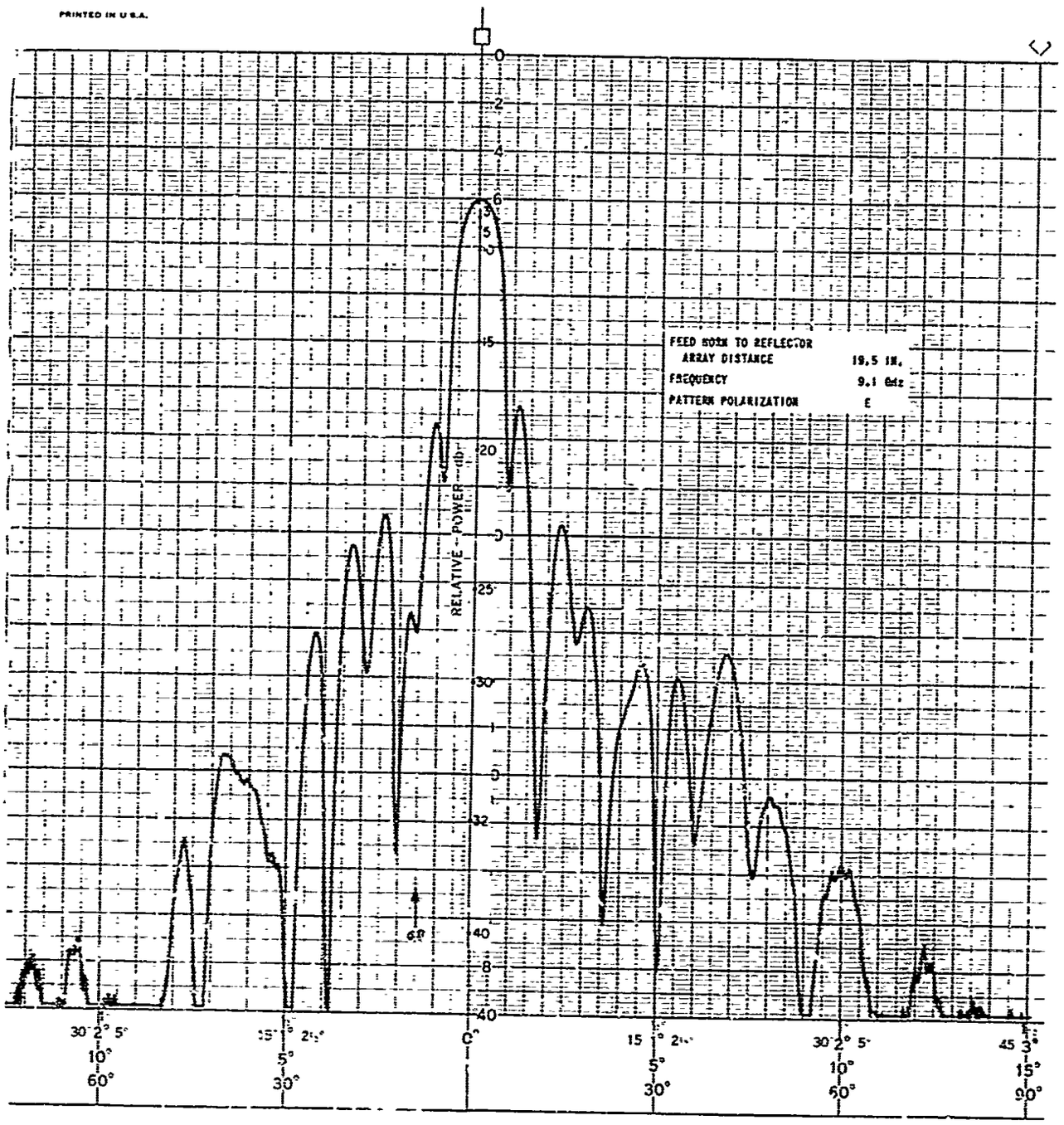

FIGURE 36. ANTENNA PATTERN PERFORMANCE WITH THIRD SHORT SURFACE ADJUSTMENT

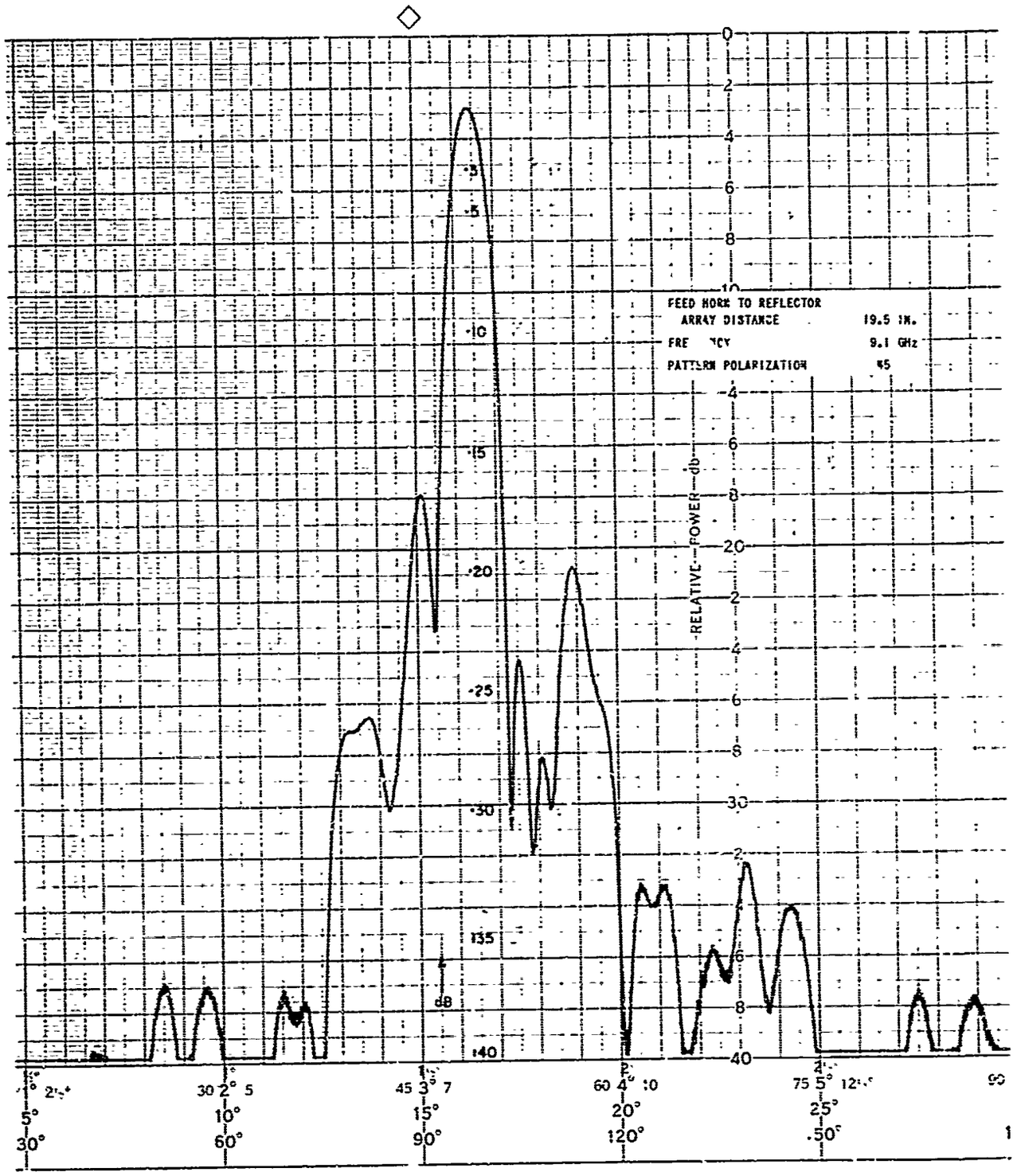

FIGURE 37. ANTENNA PATTERN PERFORMANCE WITH THIRD SHORT SURFACE ADJUSTMENT

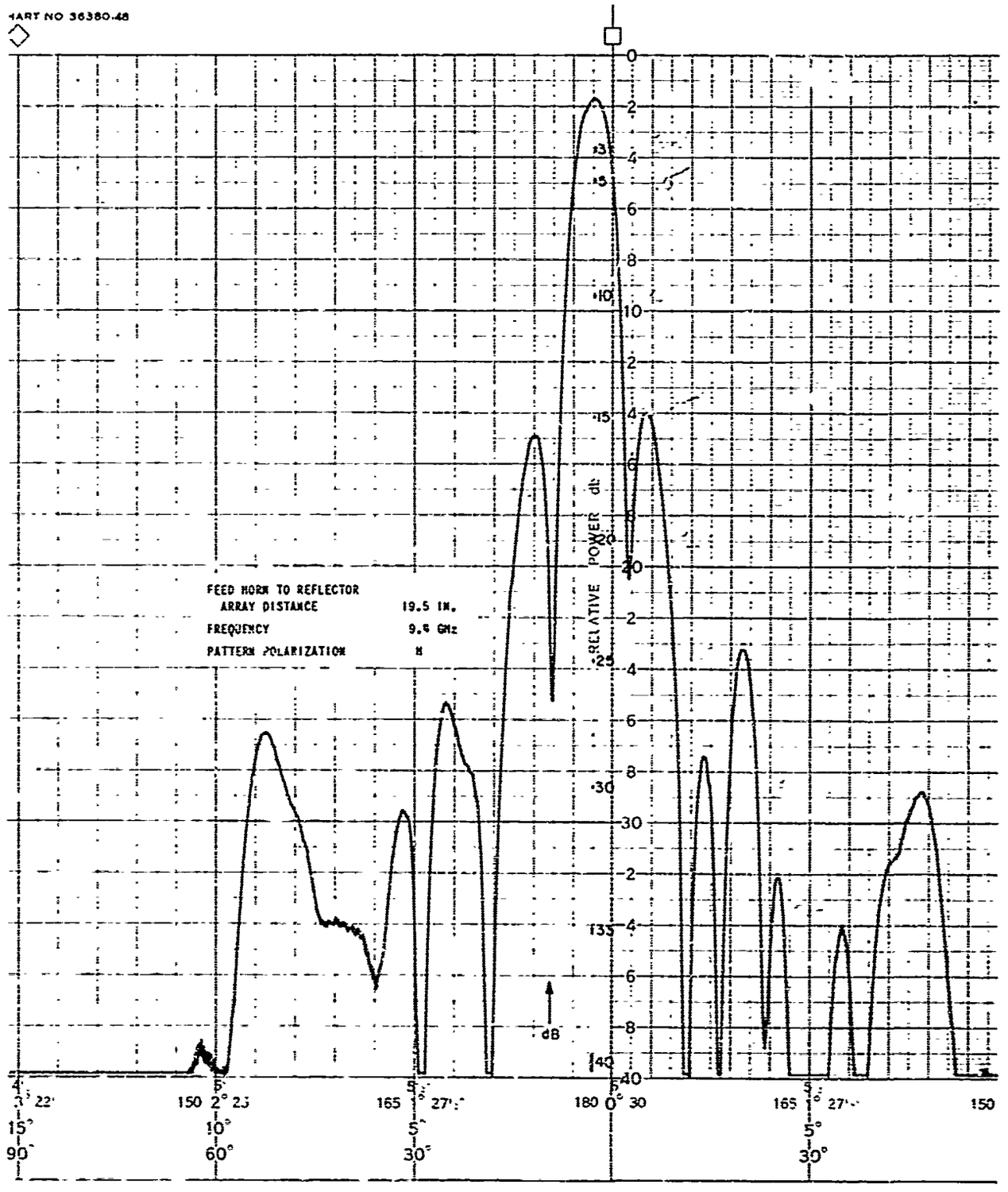

FIGURE 38. ANTENNA PATTERN PERFORMANCE WITH THIRD SHORT SURFACE ADJUSTMENT

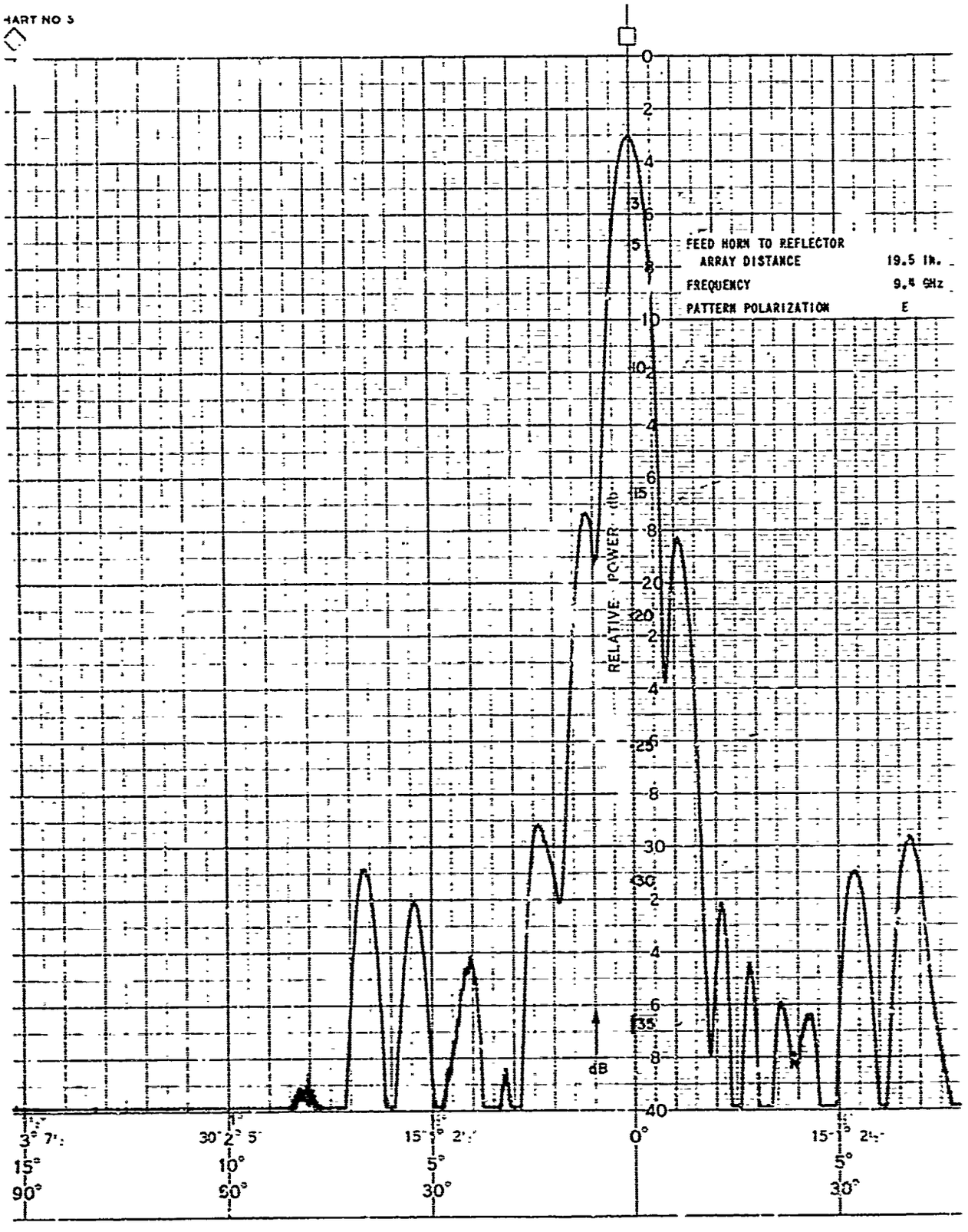

FIGURE 39. ANTENNA PATTERN PERFORMANCE WITH THIRD SHORT SURFACE ADJUSTMENT

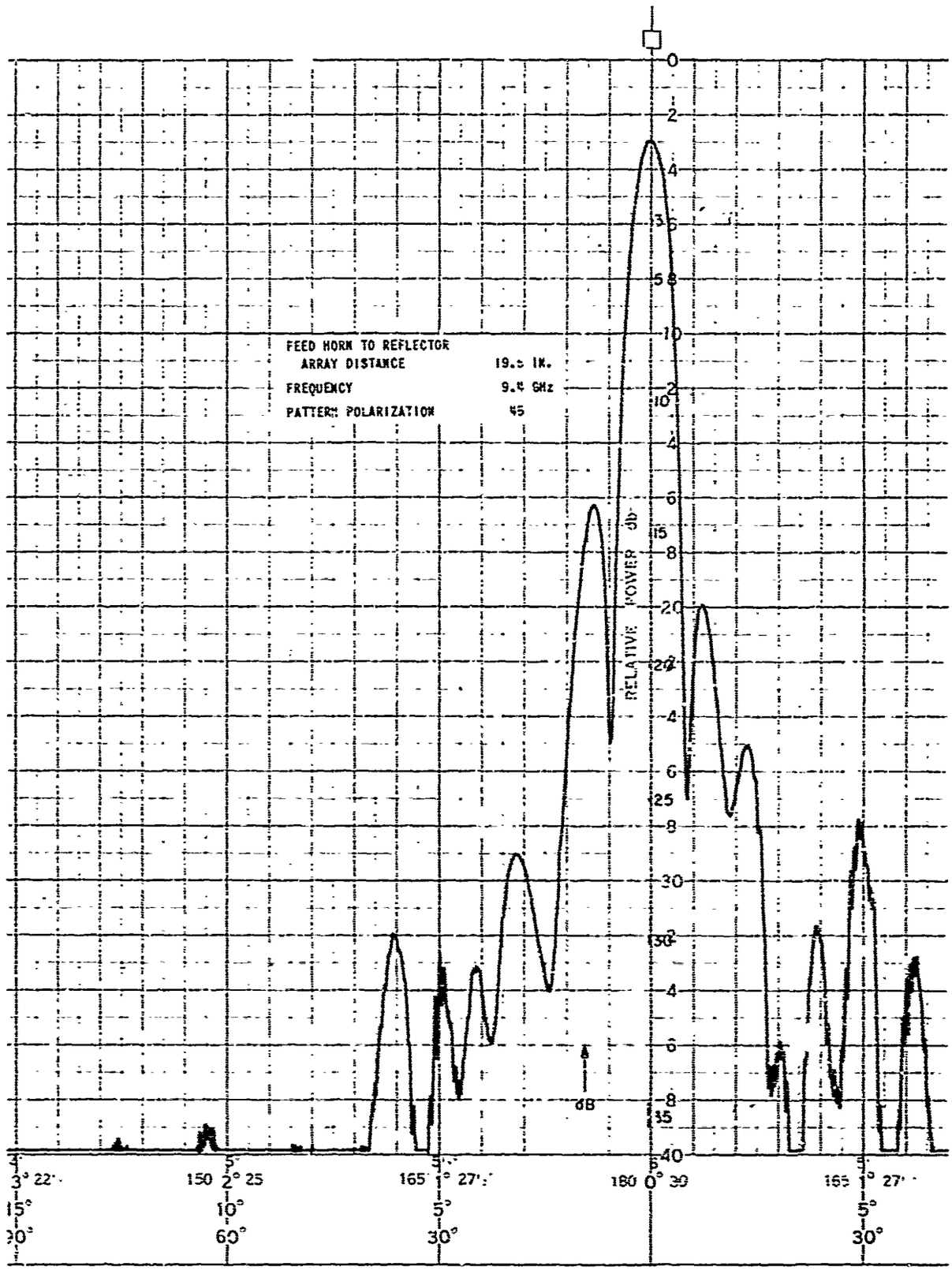

FIGURE 40. ANTENNA PATTERN PERFORMANCE WITH THIRD SHORT SURFACE ADJUSTMENT

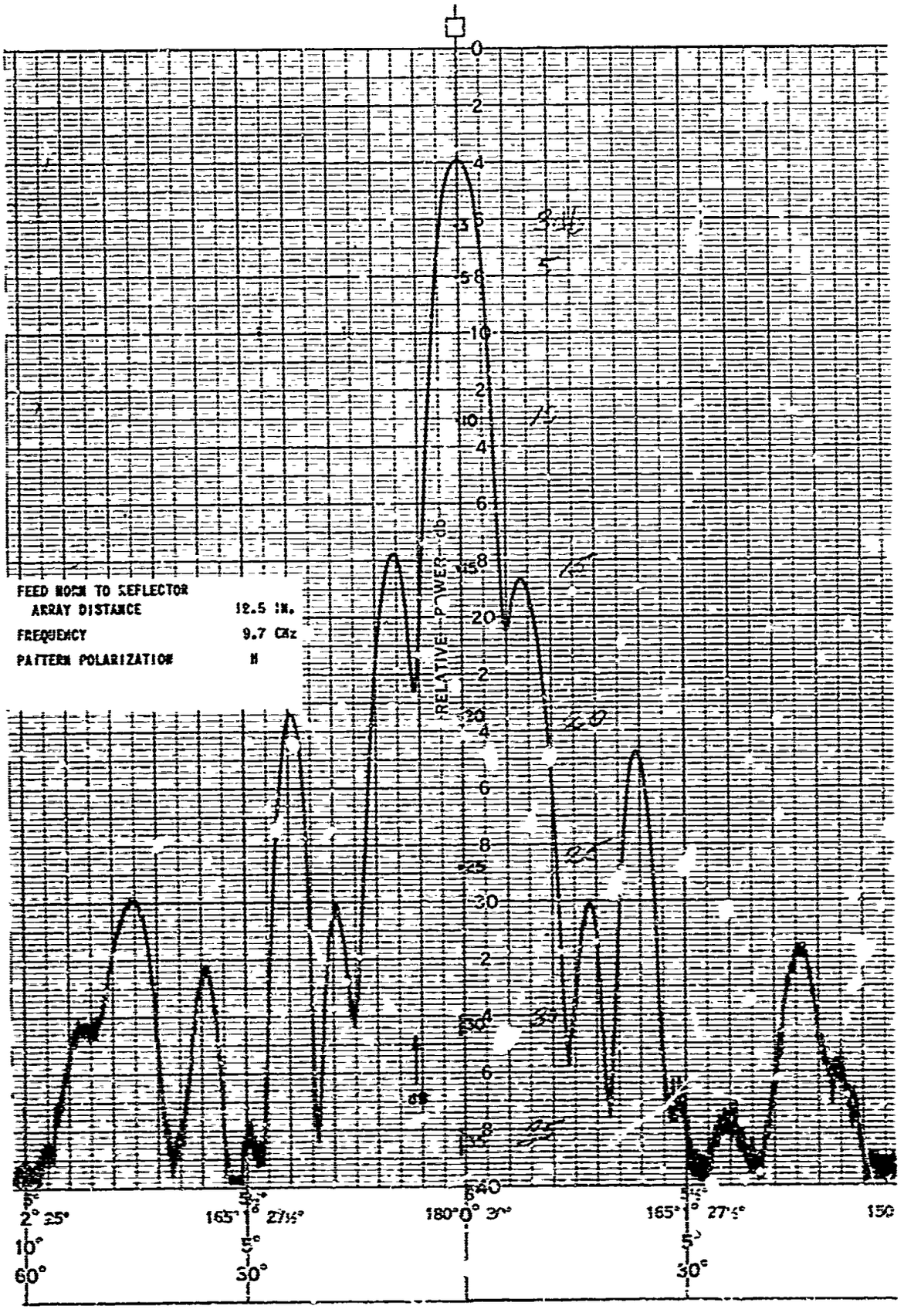

FIGURE 41. ANTENNA PATTERN PERFORMANCE WITH THIRD SHORT SURFACE ADJUSTMENT

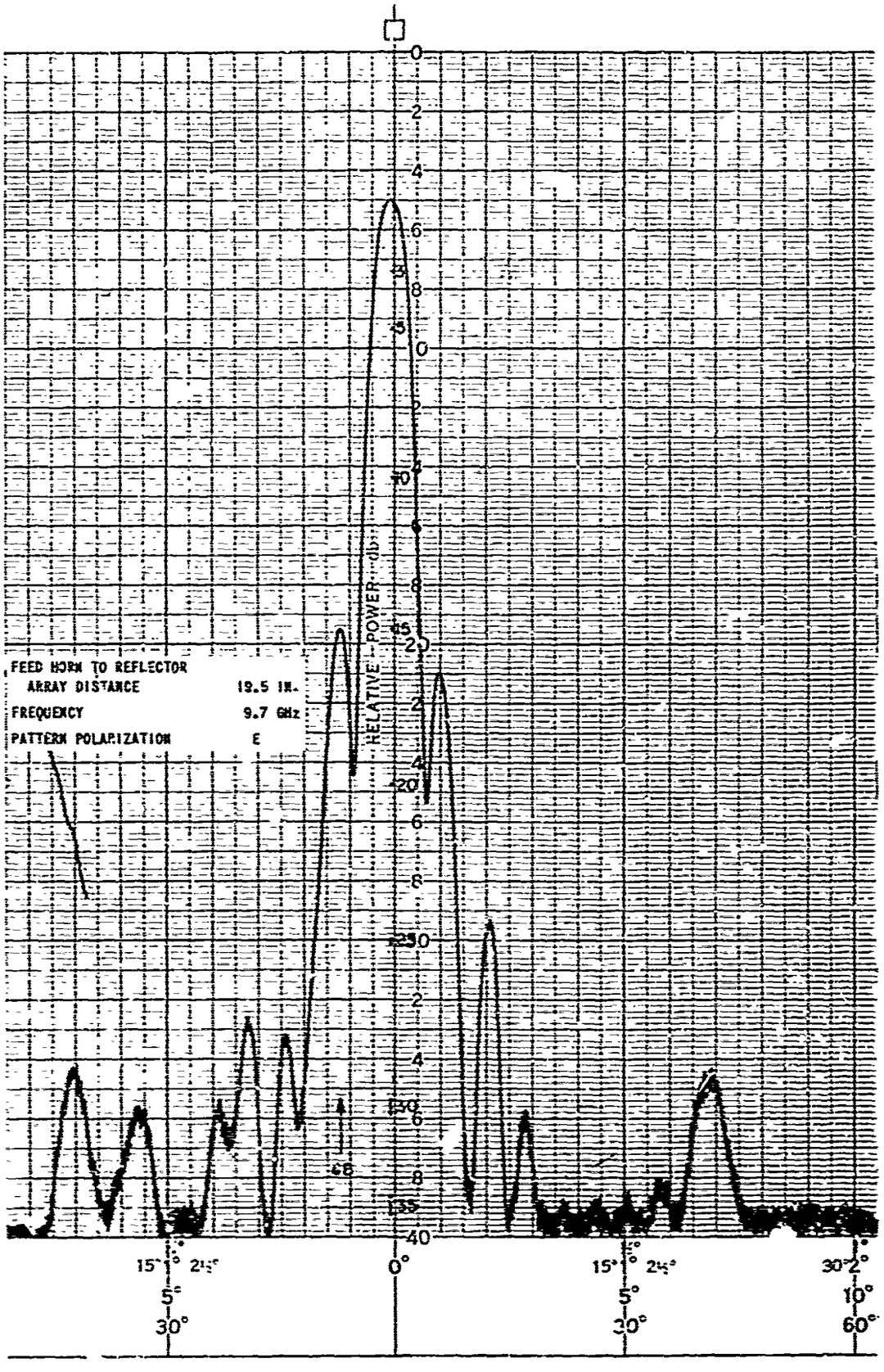

FIGURE 42. ANTENNA PATTERN PERFORMANCE WITH THIRD SHORT SURFACE ADJUSTMENT

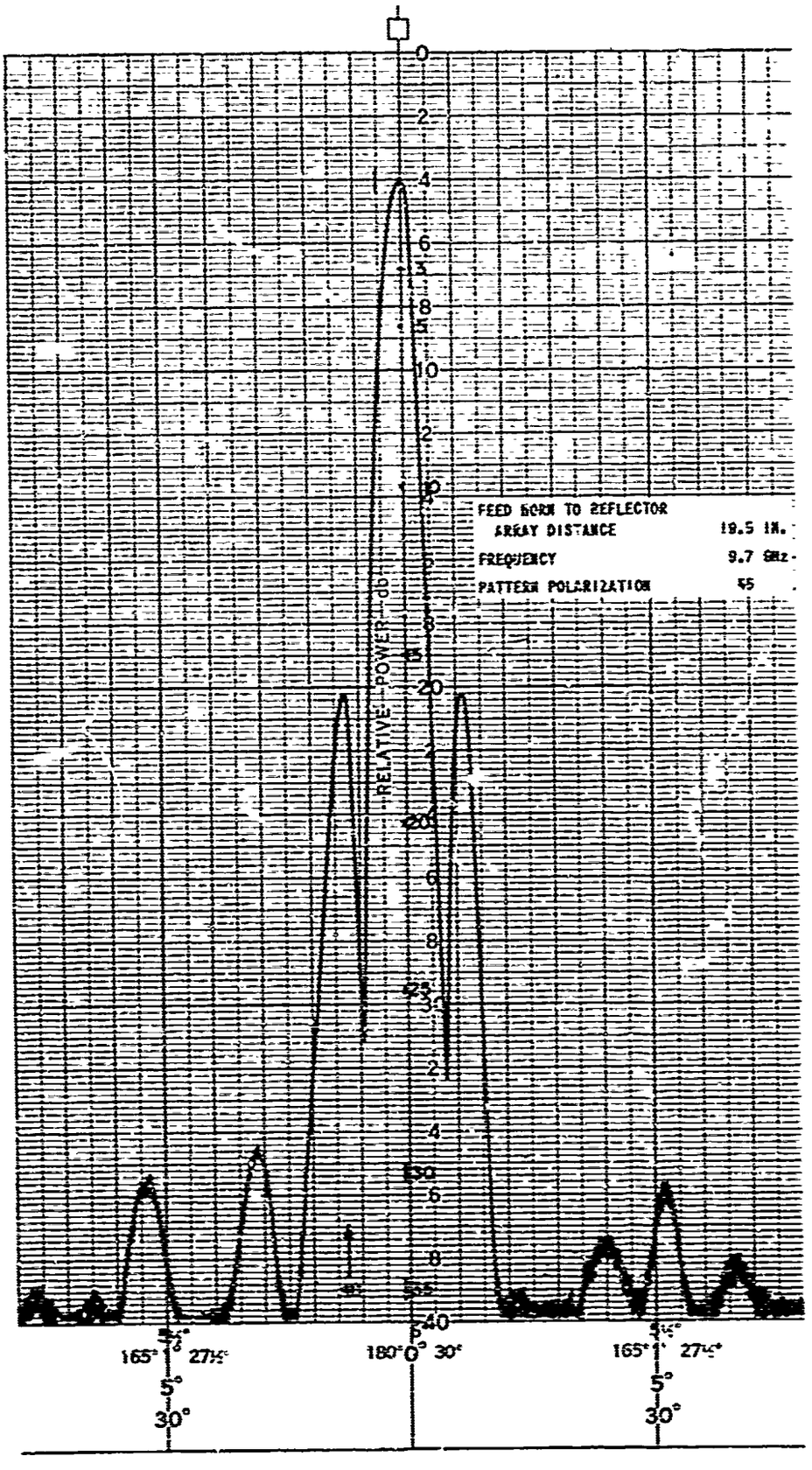

FIGURE 43. ANTENNA PATTERN PERFORMANCE WITH THIRD SHORT SURFACE ADJUSTMENT

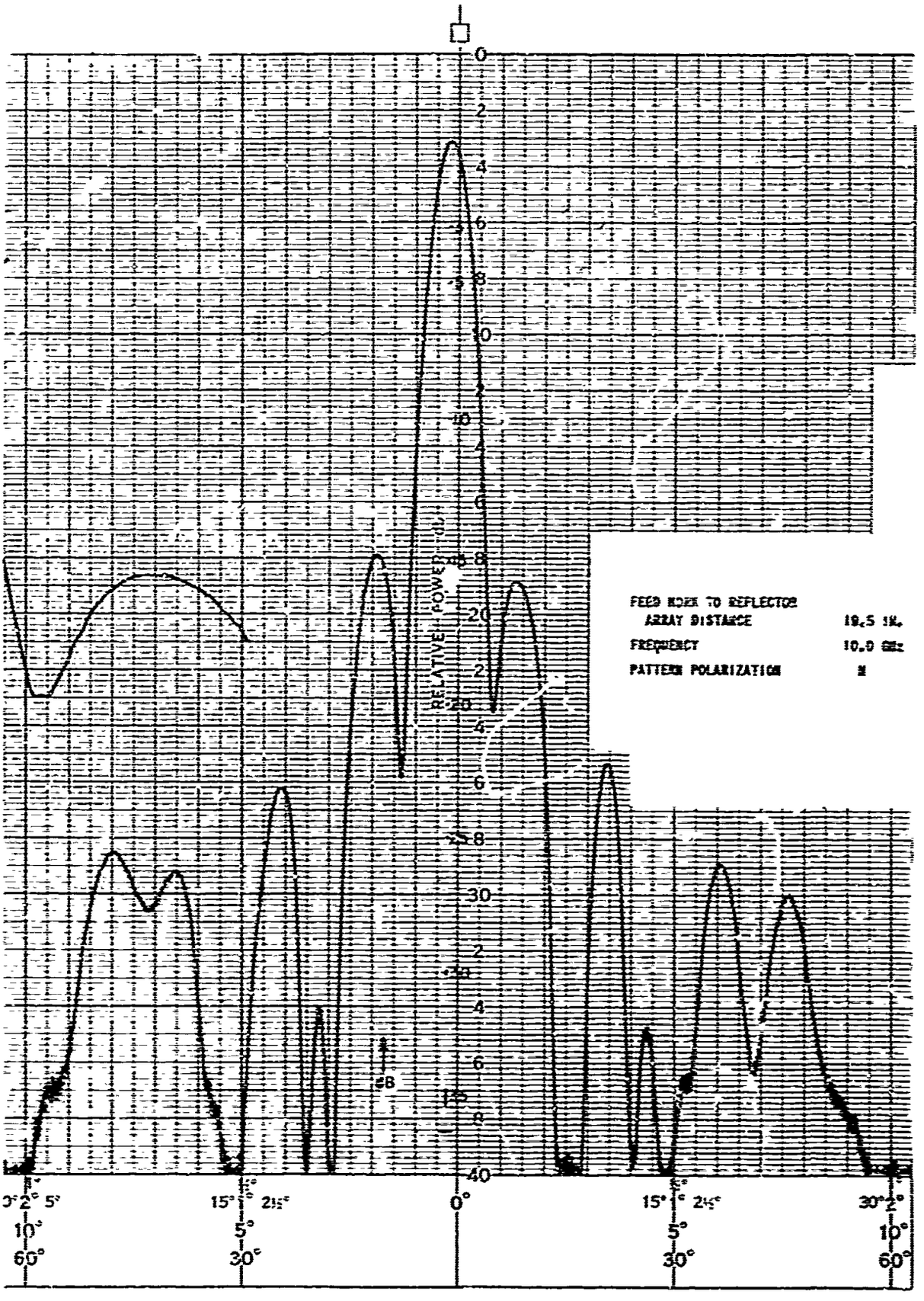

FIGURE 44. ANTENNA PATTERN PERFORMANCE WITH THIRD SHORT SURFACE ADJUSTMENT

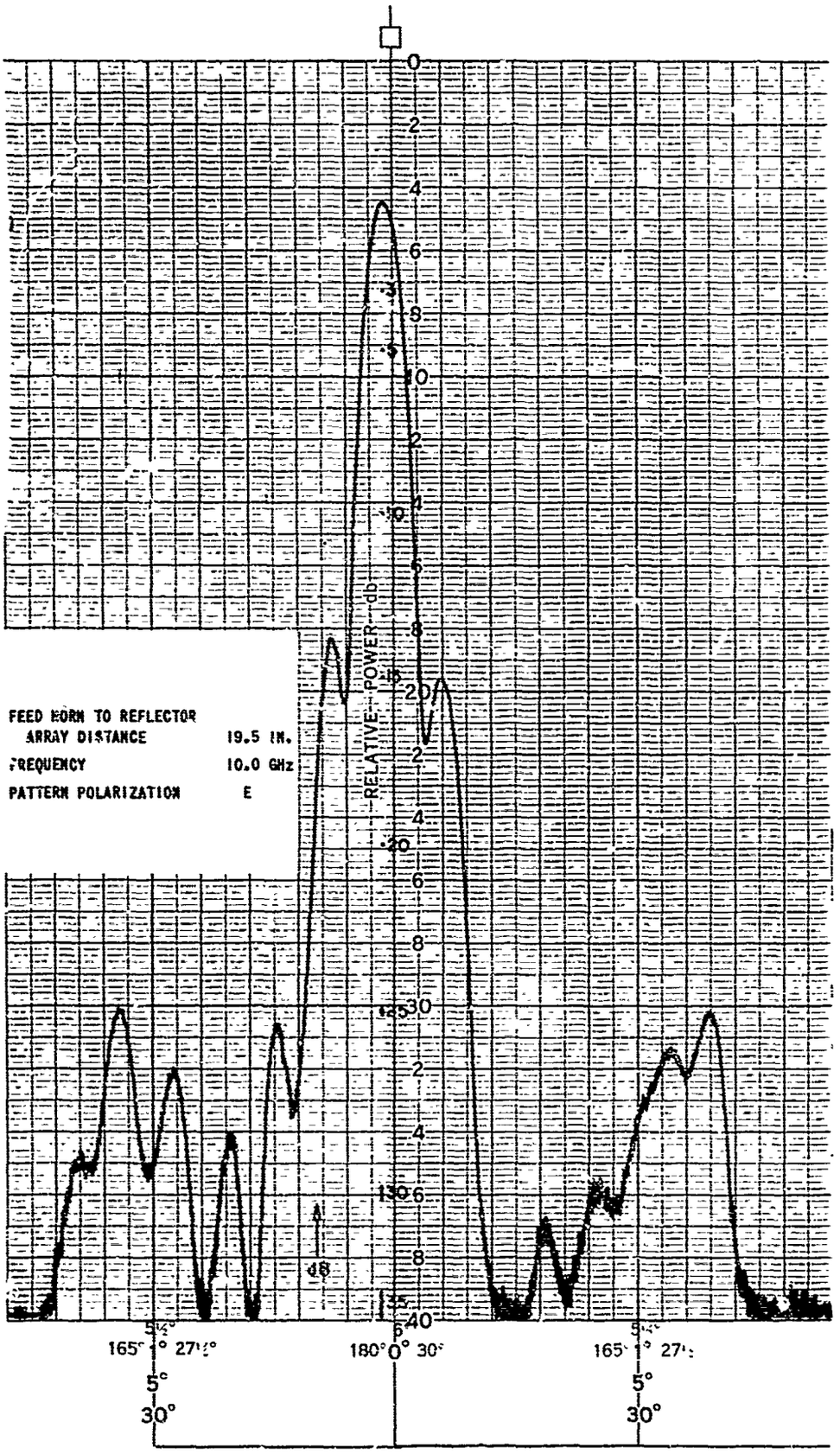

FIGURE 45. ANTENNA PATTERN PERFORMANCE WITH THIRD SHORT SURFACE ADJUSTMENT

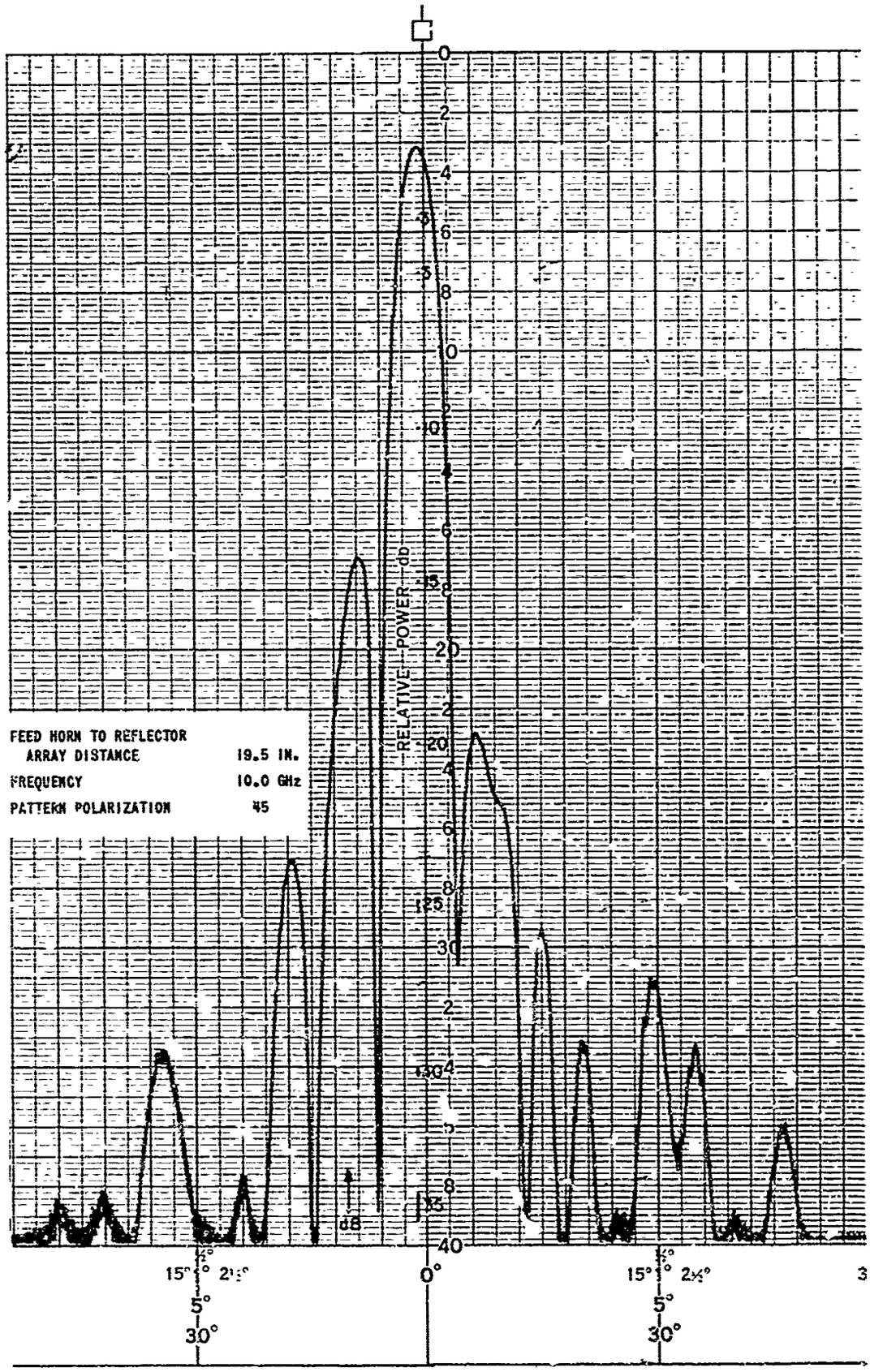

FIGURE 46. ANTENNA PATTERN PERFORMANCE WITH THIRD SHORT SURFACE ADJUSTMENT

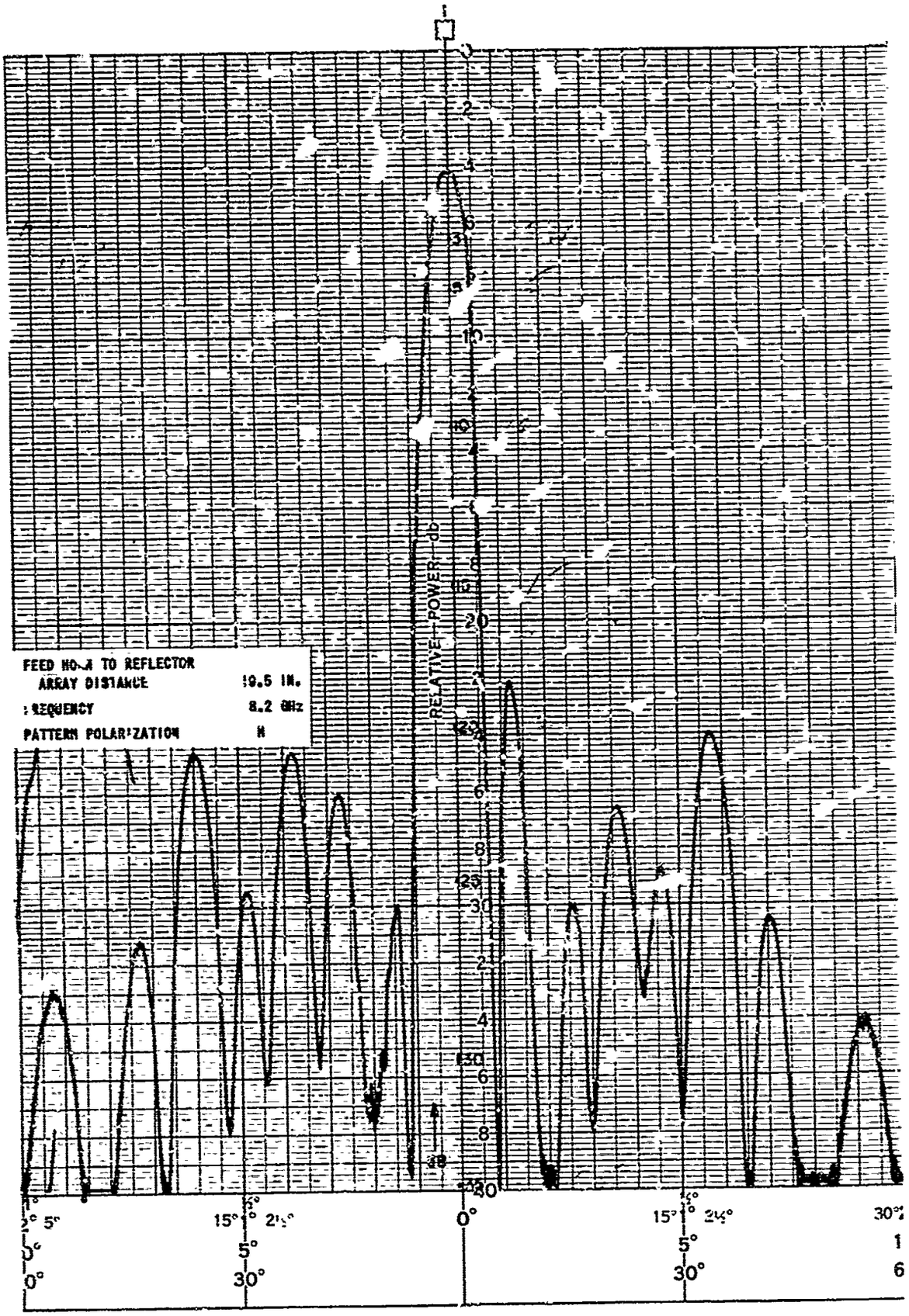

FIGURE 47. ANTENNA PATTERN PERFORMANCE WITH THIRD SHORT SURFACE ADJUSTMENT

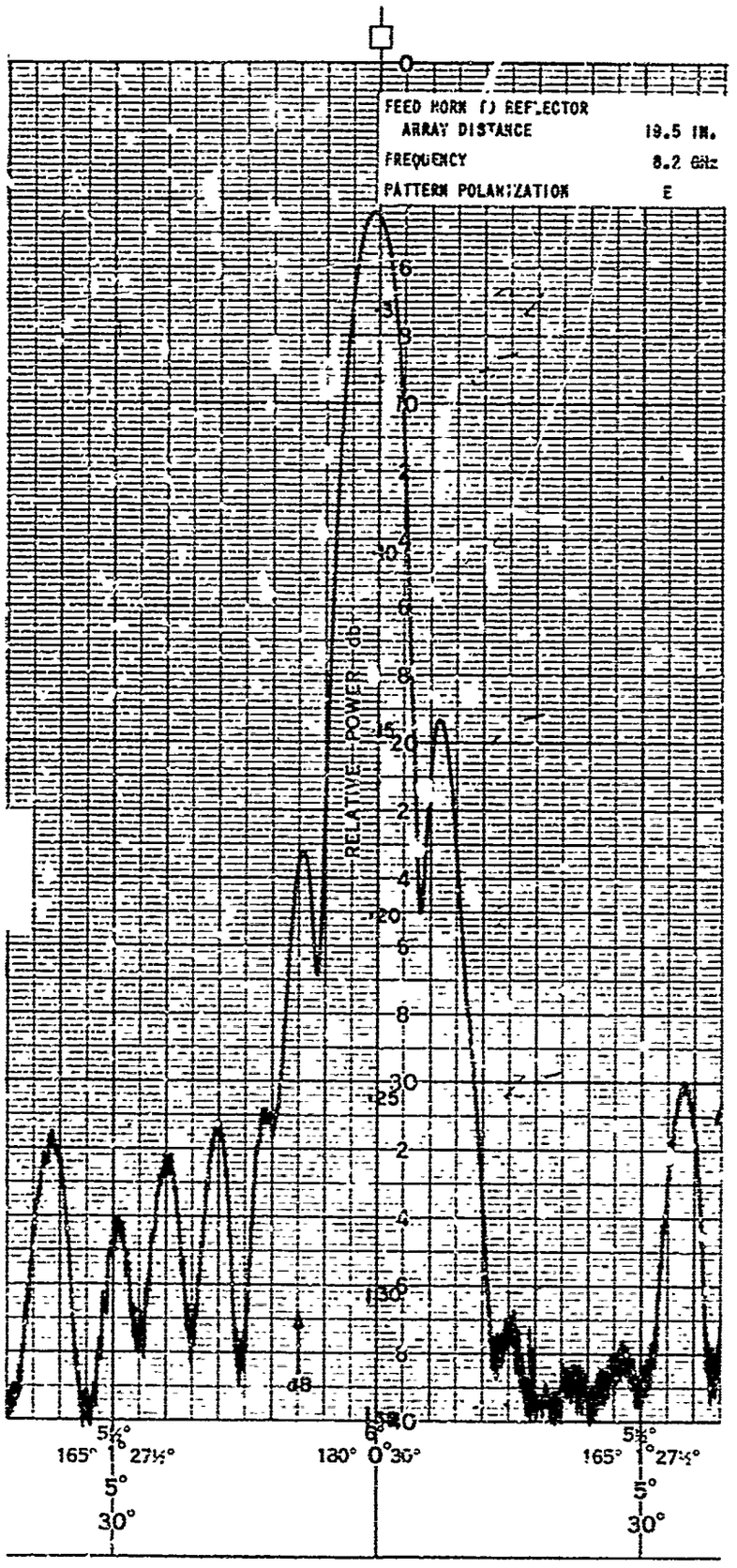

FIGURE 48. ANTENNA PATTERN PERFORMANCE WITH THIRD SHORT SURFACE ADJUSTMENT

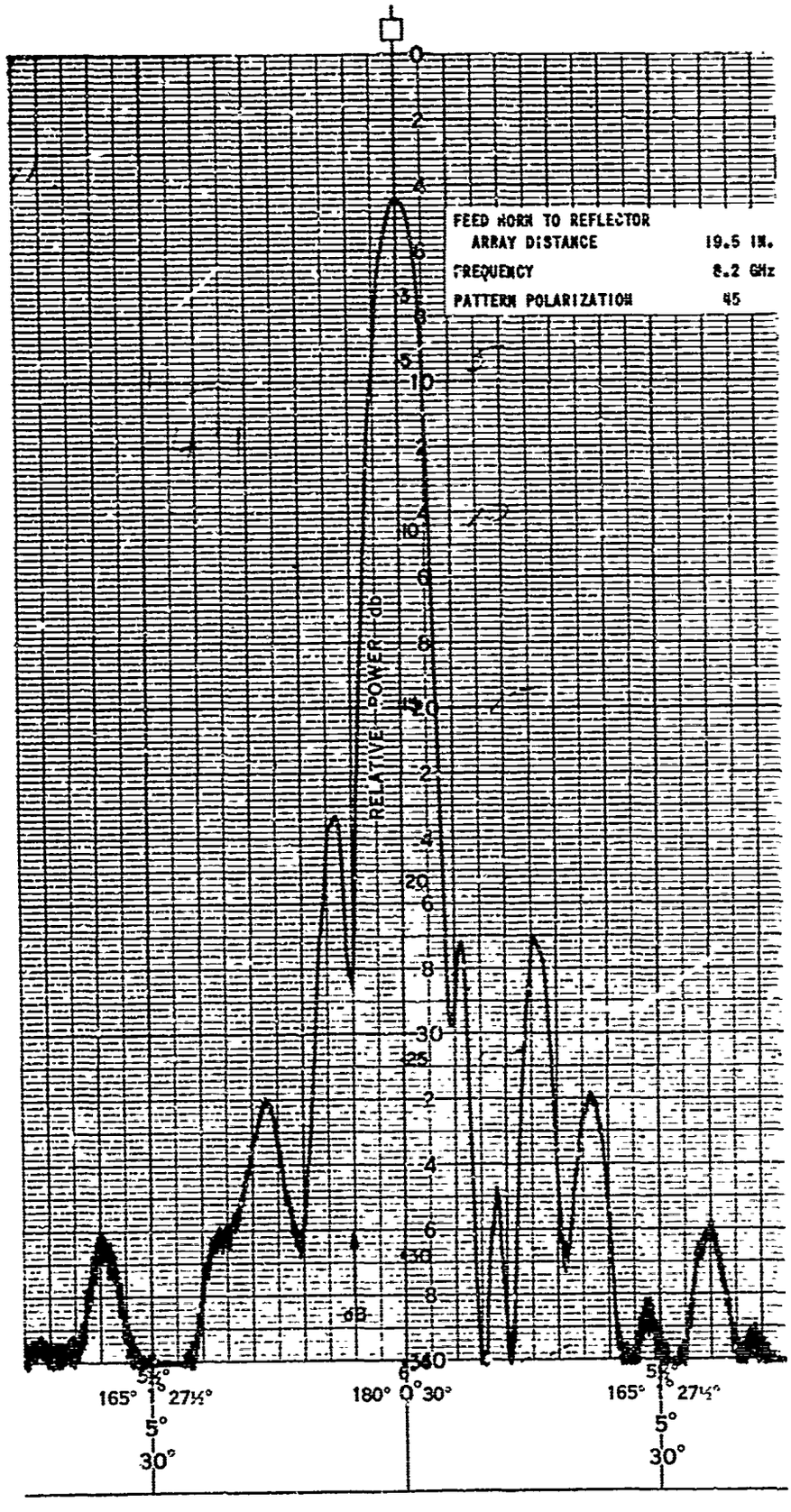

FIGURE 49. ANTENNA PATTERN PERFORMANCE WITH THIRD SHORT SURFACE ADJUSTMENT

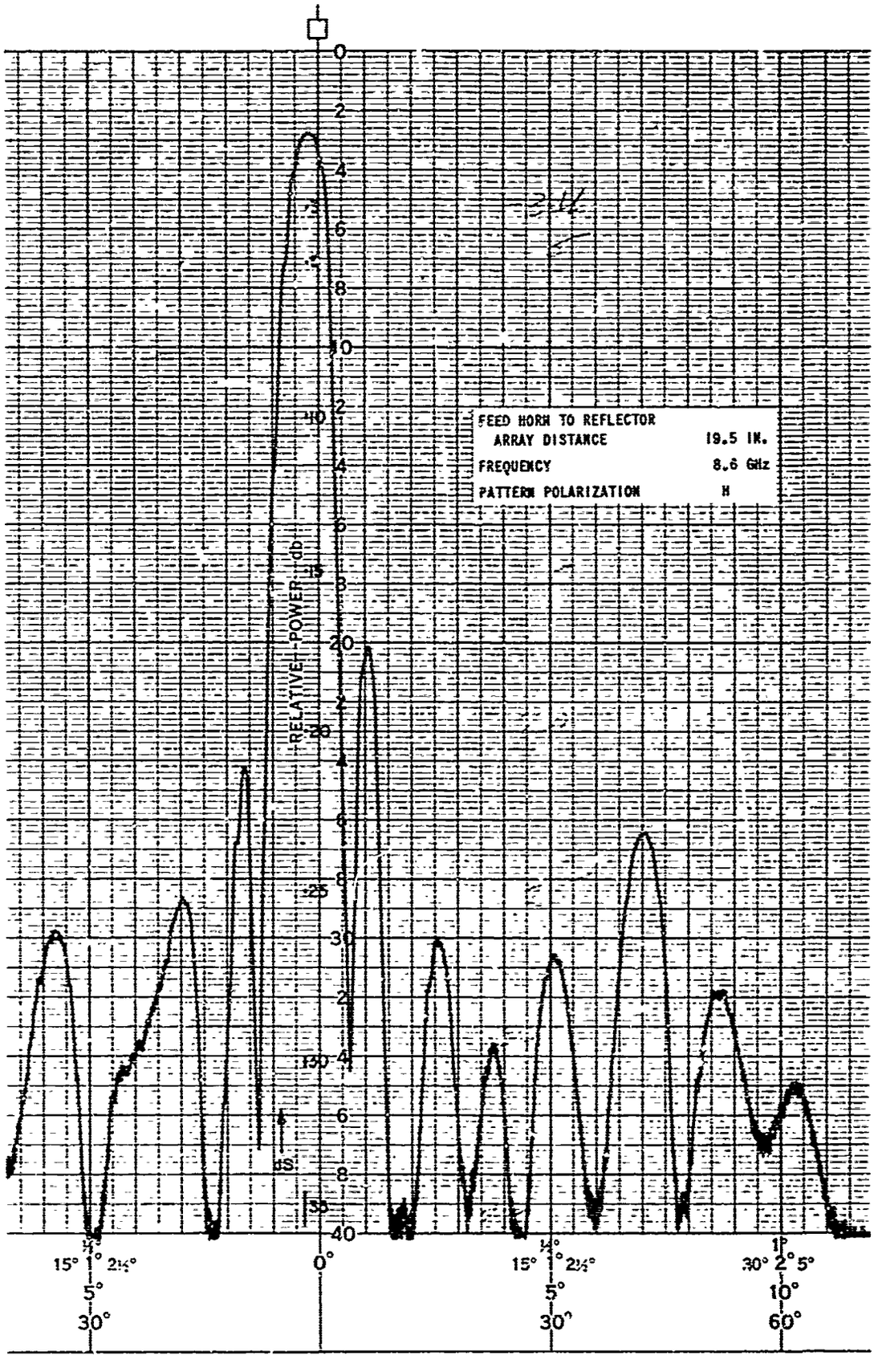

FIGURE 50. ANTENNA PATTERN PERFORMANCE WITH THIRD SHORT SURFACE ADJUSTMENT

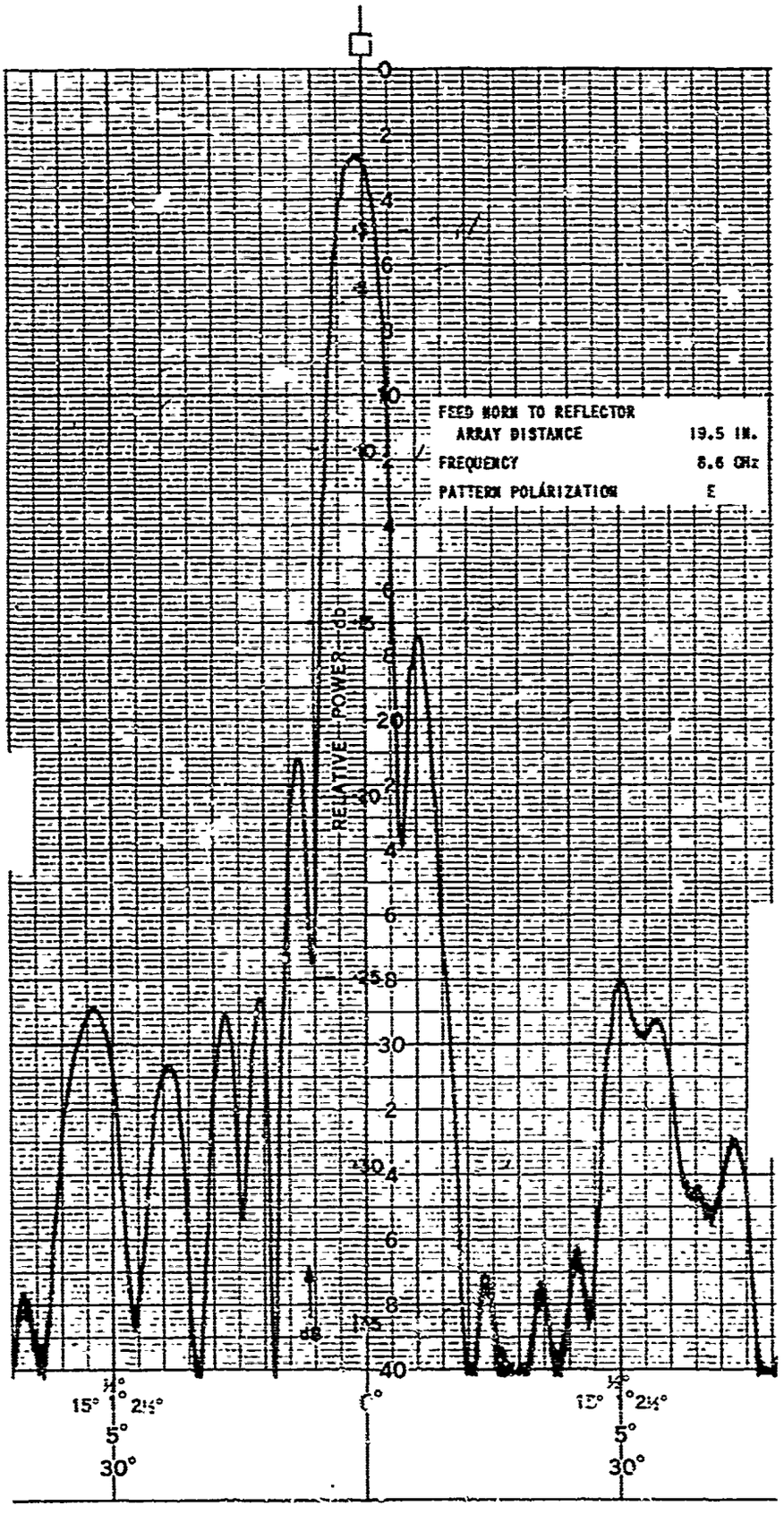

FIGURE 51. ANTENNA PATTERN PERFORMANCE WITH THIRD SCORY SURFACE ADJUSTMENT

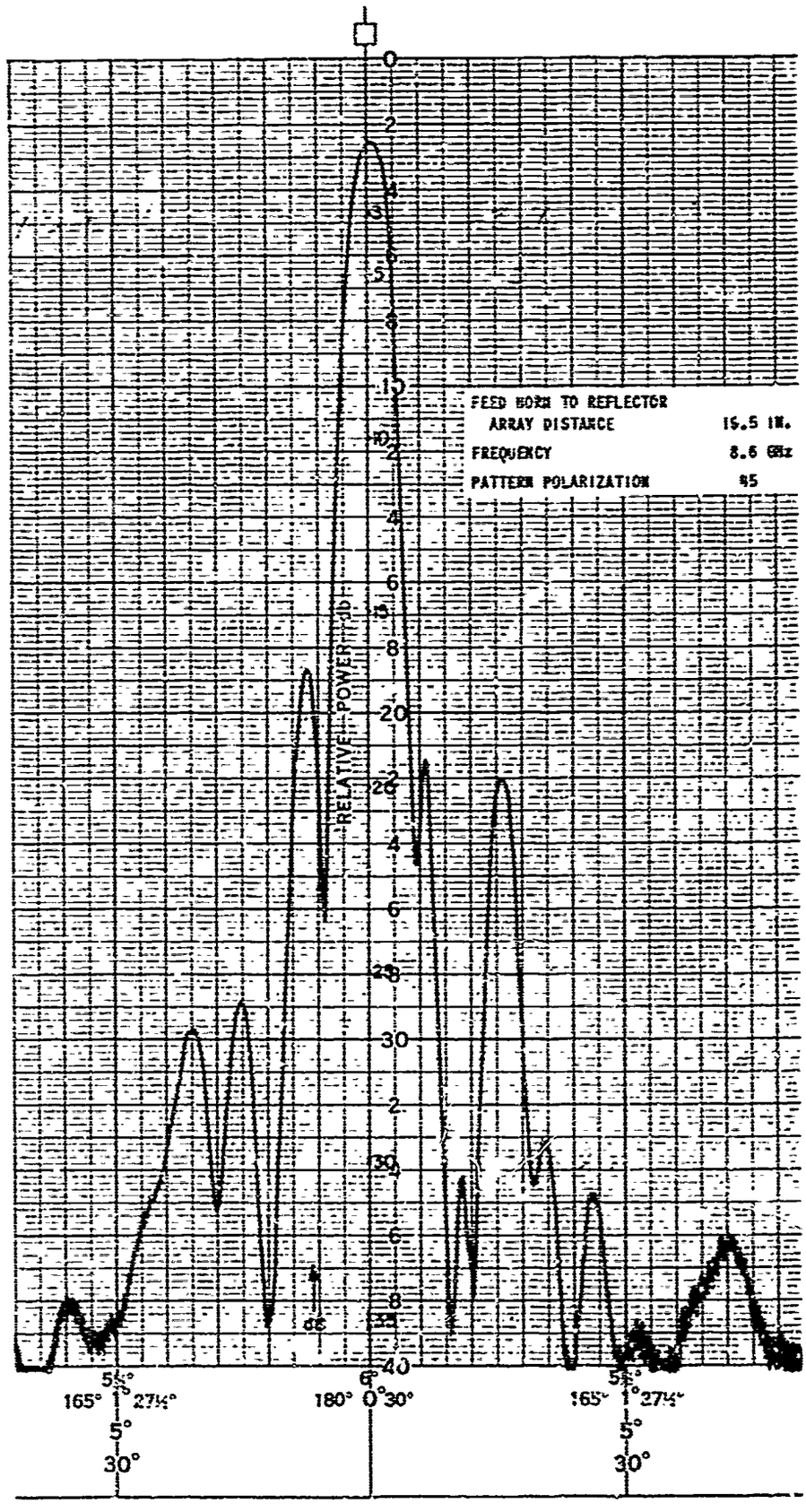

FIGURE 52. ANTENNA PATTERN PERFORMANCE WITH THIRD SHORT SURFACE ADJUSTMENT

3-6 SUBREFLECTOR ARRAY, FOURTH SHORT SETTING

The fourth short setting assumes a surface susceptance variation of

$$B_s = 0.384 - 0.337 \sin^{1.362} \theta_r \sin^2 \varphi_r - 1.724 \sin^{2.590} \theta_r \cos^2 \varphi_r \qquad (4)$$

This differs from the third shorting surface by a modification of the third term on the right side of equation 3. This term predominates for the H-plane subreflector array cells, and the basis for modification was the astigmatism noted for the first and second shorting surface adjustments. This expression is consistant with the measurement accuracy associated with the C-band surface impedance tests.

Figures 53 through 55 are the patterns corresponding to the fourth short setting, taken at the maximum gain position. A gain of 47.1 dB and efficiency of 63 percent at 9.1 GHz occur at this position, and the astigmatism remains negligible.

The model parameters for the fourth short setting with 19.5-inch spacing from feed to subreflector array are as follows:

Frequency (GHz)	Pattern Plane	Gain (dB)	Half Power Beamwidth (deg)	10-dB Beamwidth (deg)	20-dB Beamwidth (deg)	First Two Sidelobes (dB)	Other Sidelobes (dB)
9.1	H	47.1	0.78	1.34	1.73	17	28
	E	--	0.68	1.18	1.52	17	25
	45°	--	0.75	1.30	--	16	27

To insure that the feed-subreflector spacing was indeed at a maximum gain point, small axial movements of the subreflector array were evaluated and the gain measured at each point. At 0.125 inch toward or away from the feed, the measured gain dropped rapidly from 47.1 dB to 46.3 dB at 9.1 GHz.

3-7 SUBREFLECTOR ARRAY, FIFTH SHORT SETTING

For the fifth shorting surface adjustment, another modification of the third term of equation 3 was evaluated.

$$B_s = 0.384 - 0.337 \sin^{1.362} \theta_r \sin^2 \varphi_r - 1.563 \sin^{1.691} \theta_r \cos^2 \varphi_r \qquad (5)$$

Again, the basis of modification was the astigmatism previously noted, and the goal was a narrower H-plane beamwidth within the estimated measurement accuracy of the surface impedance tests.

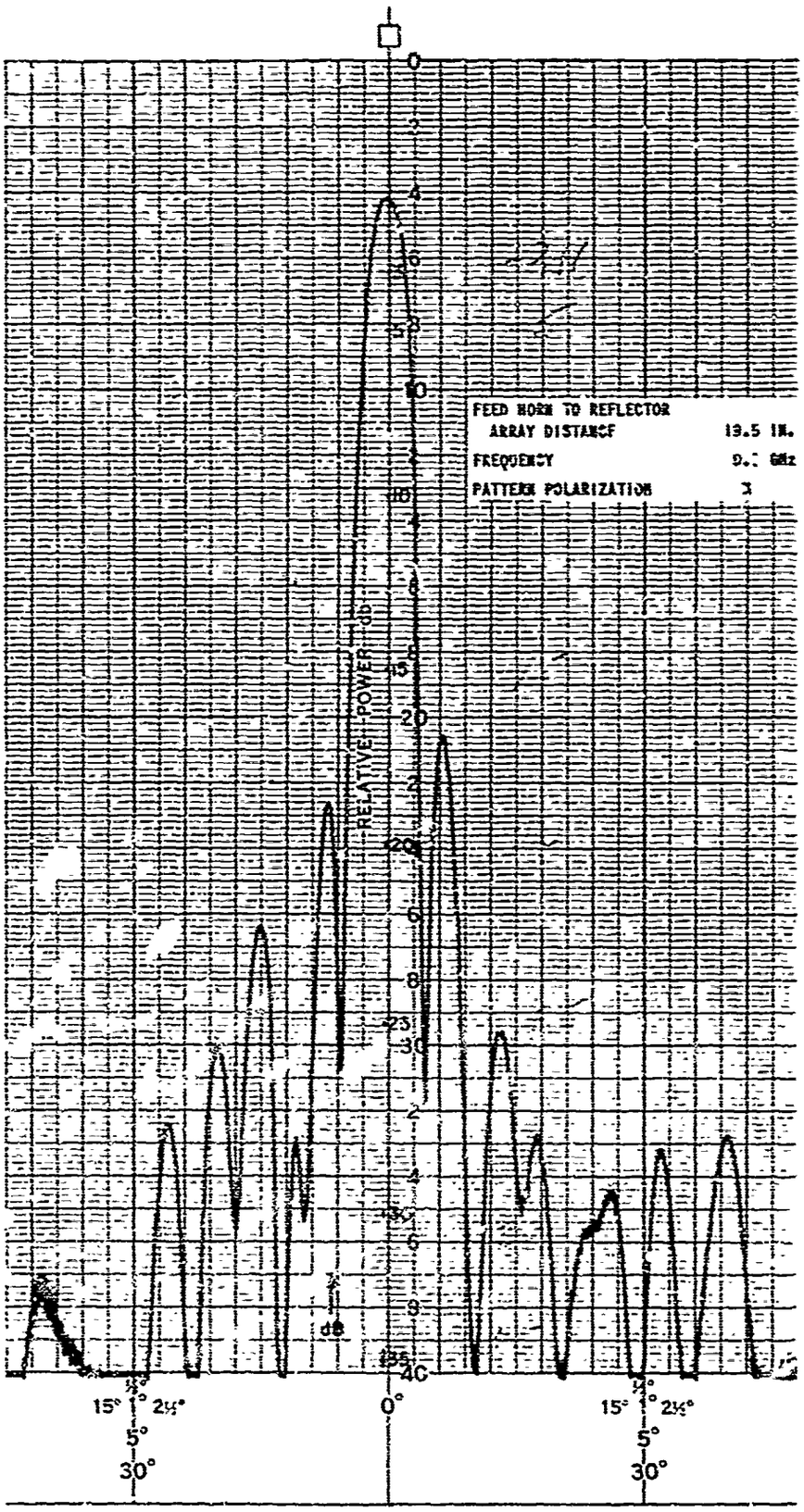

FIGURE 53. ANTENNA PATTERN PERFORMANCE WITH FOURTH SHORT SURFACE ADJUSTMENT

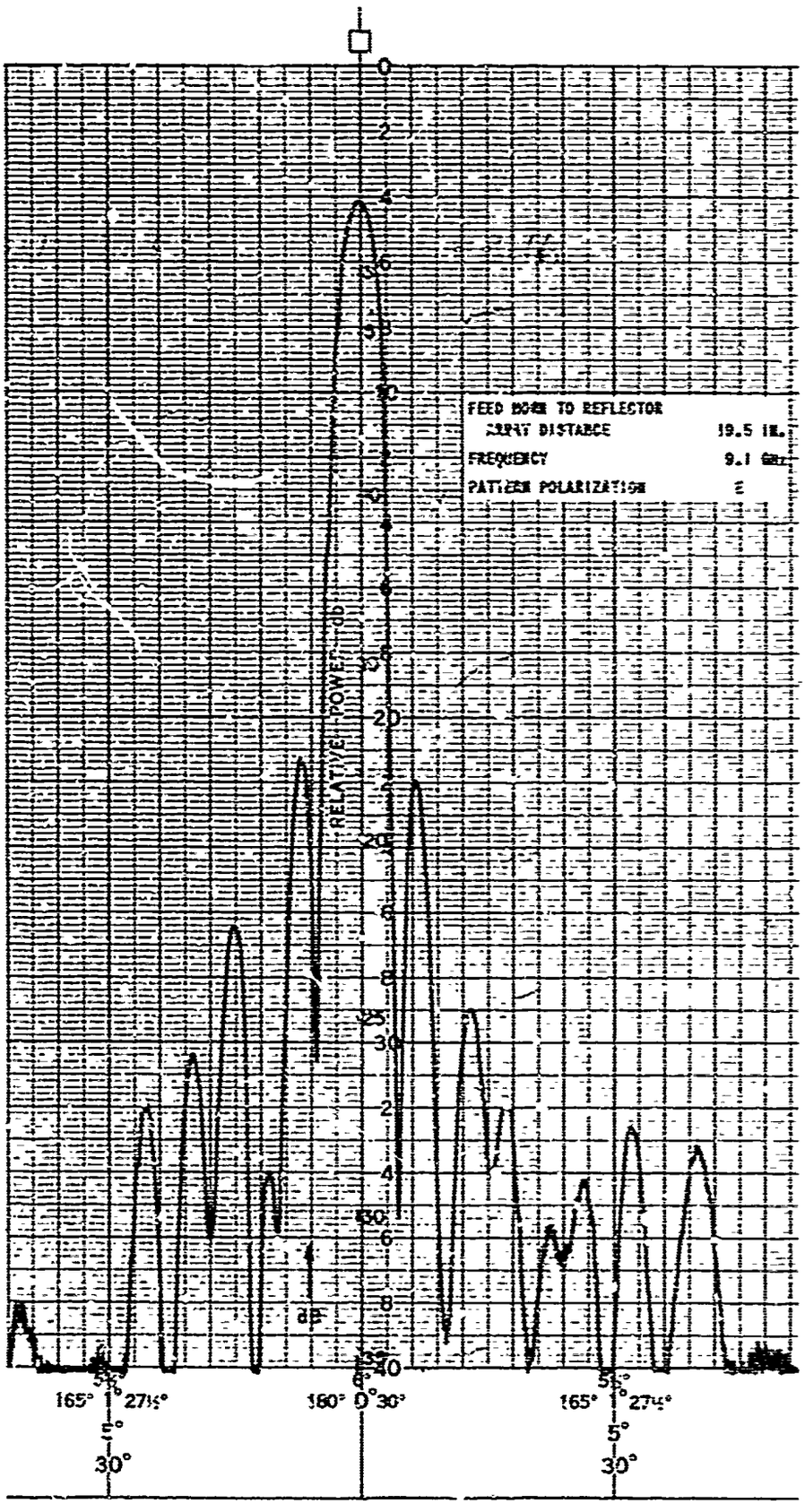

FIGURE 54. ANTENNA PATTERN PERFORMANCE WITH FOURTH SHORT SURFACE ADJUSTMENT

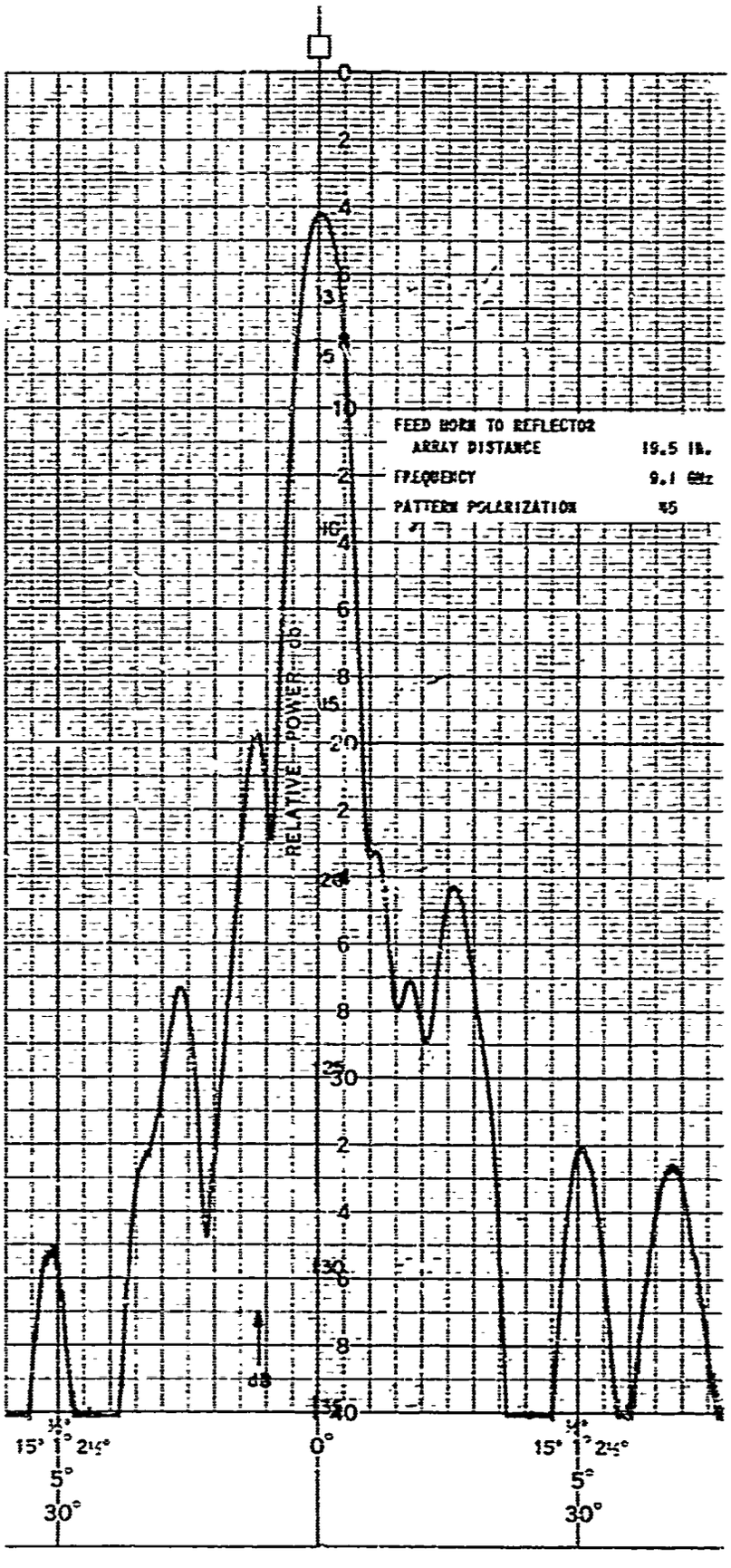

FIGURE 55. ANTENNA PATTERN PERFORMANCE WITH FOURTH SHORT SURFACE ADJUSTMENT

Figures 56 through 64 are the patterns taken at the fifth short setting for the maximum gain position. The gain of 47.1 dB is the same as that obtained with the fourth short setting, except the beamwidths at 9.1 GHz are somewhat larger.

The fifth short setting performance within a ±5-percent band about 9.1 GHz for 19.4-inch spacing from feed to subreflector array is as follows:

Frequency (GHz)	Pattern Plane	Gain (dB)	Half Power Beamwidth (deg)	10-dB Beamwidth (deg)	20-dB Beamwidth (deg)	First Two Sidelobes (dB)	Other Sidelobes (±15°)(dB)
8.6	H	46.7	0.72	1.18	1.60	18	21
	E	--	0.65	1.10	1.60	17	24
	45°	--	0.68	1.30	1.75	16	21
9.1	H	47.1	0.82	1.40	1.90	21.5	26.5
	E	--	0.69	1.12	1.37	15	26
	45°	--	0.76	1.31	--	17.5	30
9.6	H	46.5	0.80	1.37	--	17.5	28
	E	--	0.60	0.95	1.26	14	29
	45°	--	0.82	1.37	--	16	27

3-8 SINGLE ELEMENT PATTERN PERFORMANCE

While the subreflector array astigmatism has been essentially eliminated, the problem which is subsequently found to result from an H-plane array mismatch, is evidenced by larger H-plane beamwidth. To investigate the match into the waveguide cells concerned, the subreflector array was removed from the model antenna and element (waveguide cell) patterns in the array environment were taken. The center cell, and other cells along the center lines of the entry surface, were probed at the rear by means of a specially fabricated spring finger coupling, figure 65. The short was removed from the element under test during measurement of its pattern performance in the array.

The patterns for various waveguide elements throughout the subreflector array are shown in figures 66 through 75. These exhibit a nearly uniform amplitude function throughout the desired scan angle for all elements tested in the E plane, which is desired. Element patterns in the H plane show one or more nulls and more rapid pattern drop-off with scan angle, thus accounting for the larger H-plane beamwidth in the secondary patterns.

In order to improve the H-plane element match, various configurations of capacitive and inductive irises were placed at the entry, and element pattern performance was investigated. Best results were obtained with inductive irises which occupied only one side of the cell. This placement seemed to show best results in obtaining a more uniform element amplitude function in the H plane.

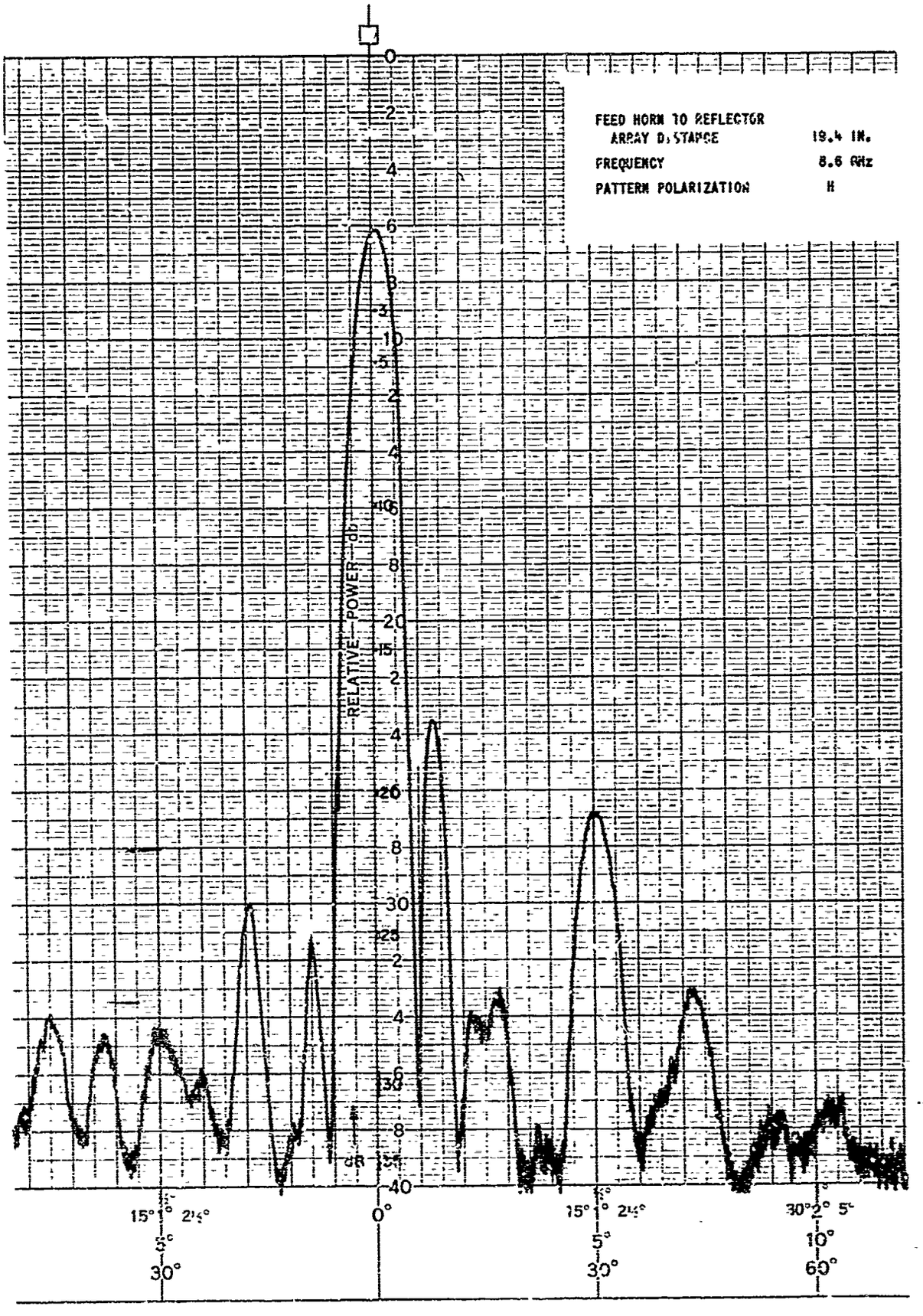

FIGURE 56. ANTENNA PATTERN PERFORMANCE WITH FIFTH SHORT SURFACE ADJUSTMENT

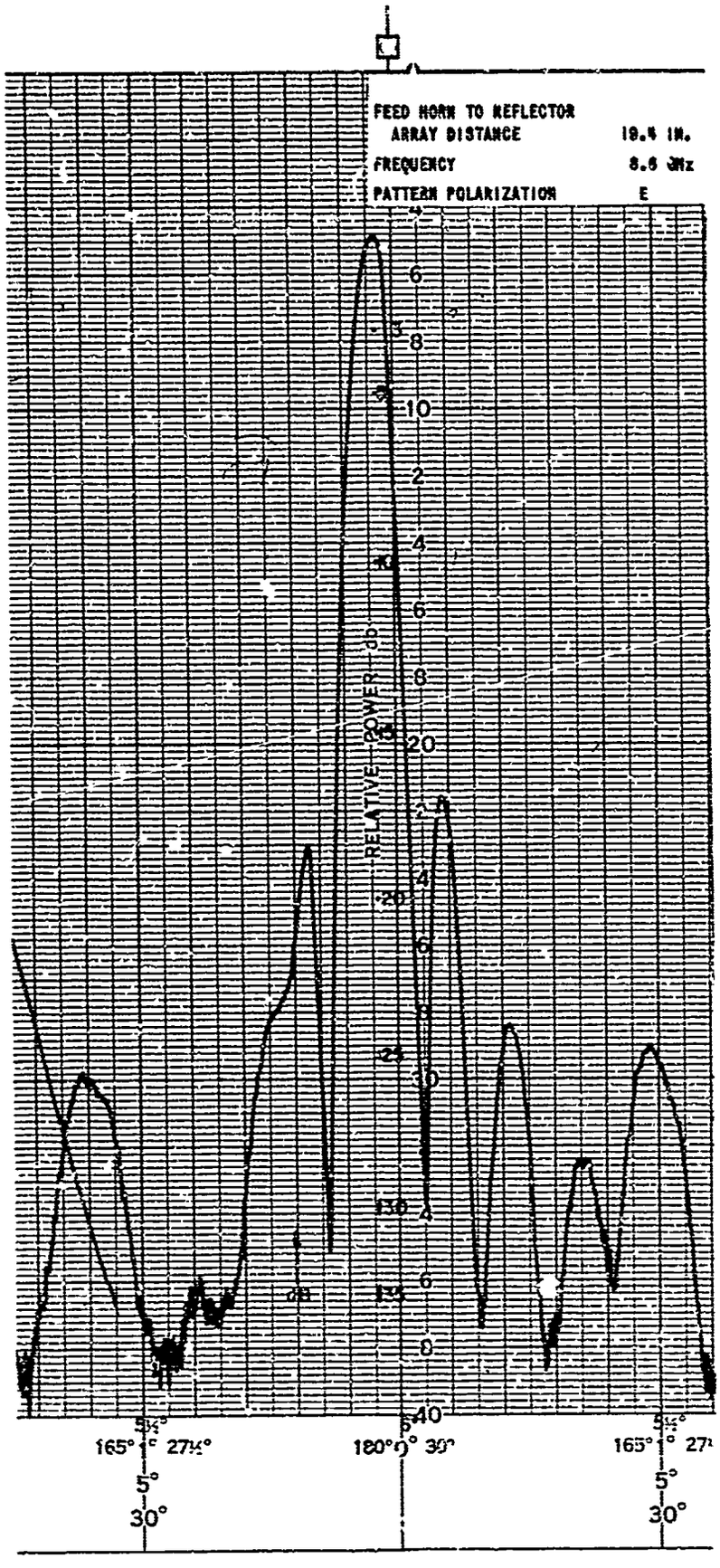

FIGURE 57. ANTENNA PATTERN PERFORMANCE WITH FIFTH SHORT SURFACE ADJUSTMENT

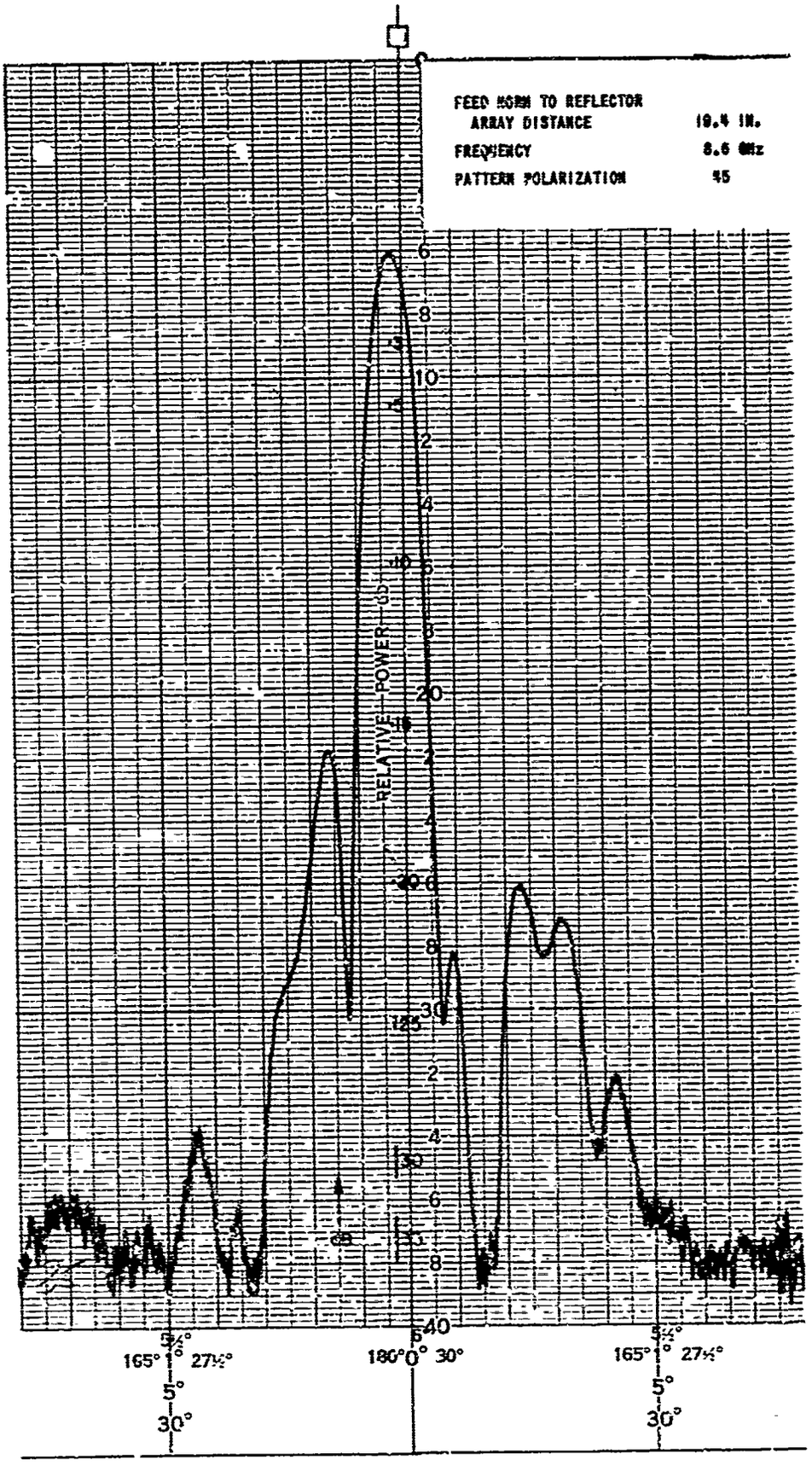

FIGURE 58. ANTENNA PATTERN PERFORMANCE WITH FIFTH SHORT SURFACE ADJUSTMENT

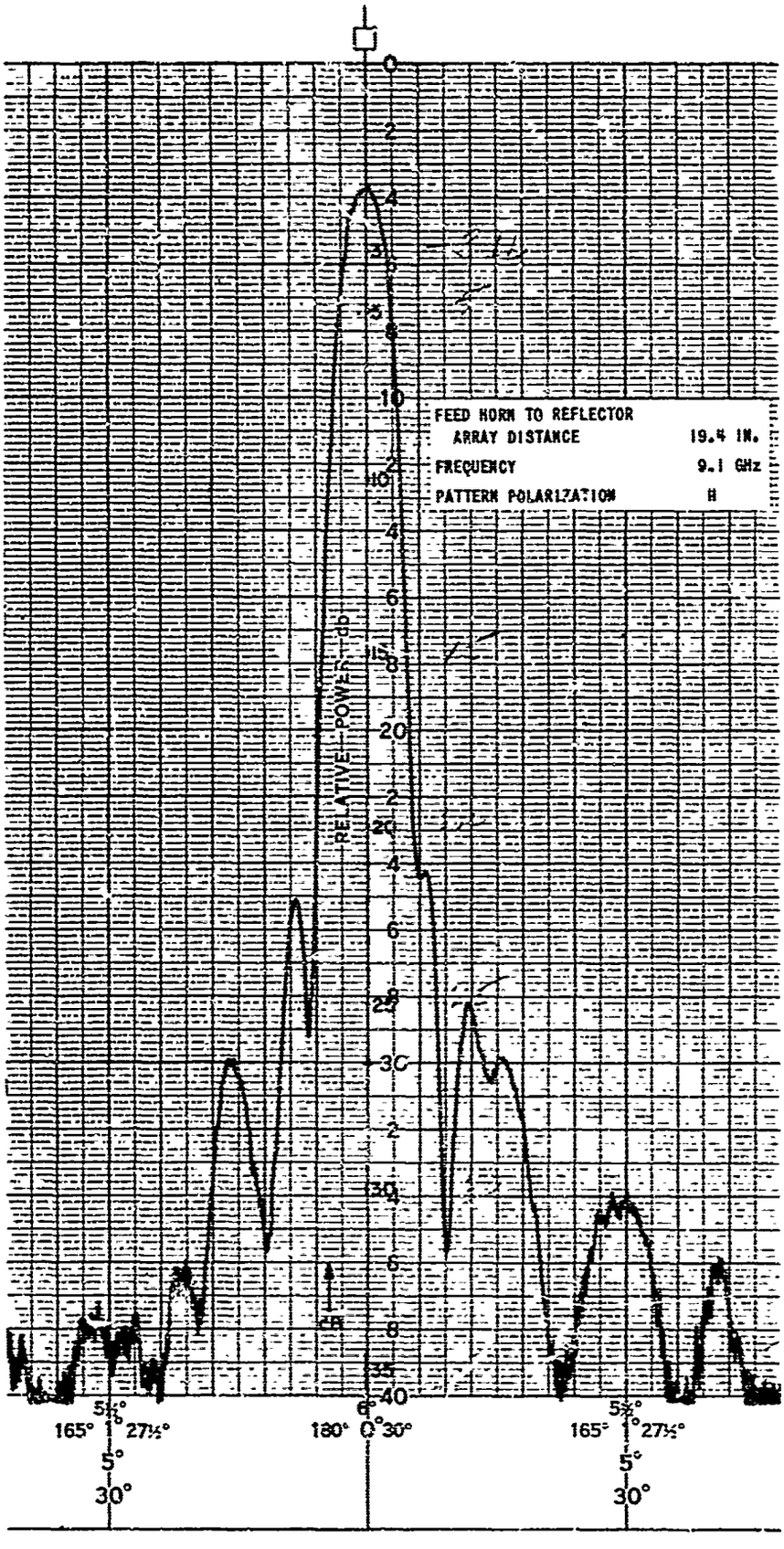

FIGURE 59. ANTENNA PATTERN PERFORMANCE WITH FIFTH SHORT SURFACE ADJUSTMENT

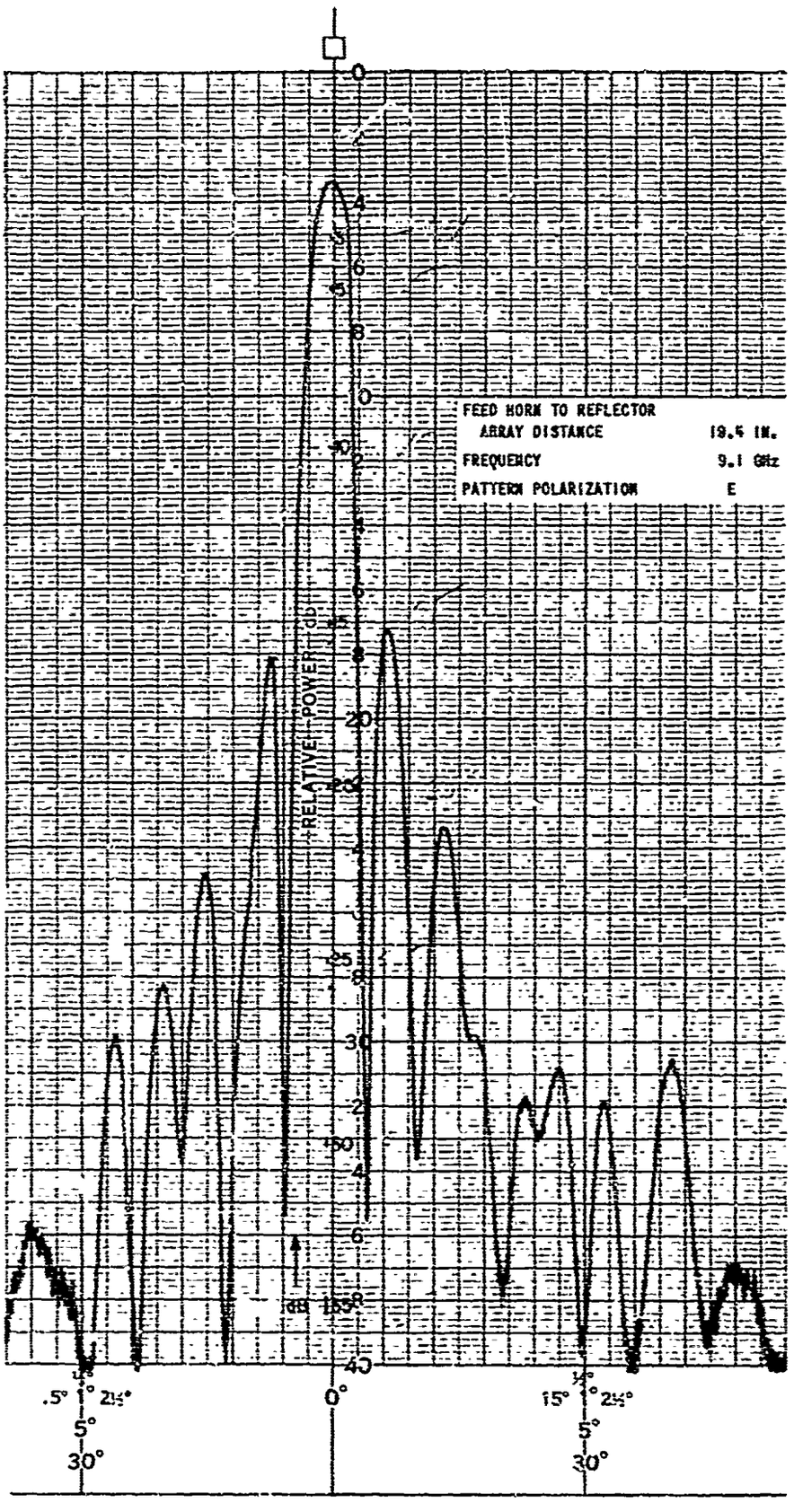

FIGURE 60. ANTENNA PATTERN PERFORMANCE WITH FIFTH SHORT SURFACE ADJUSTMENT

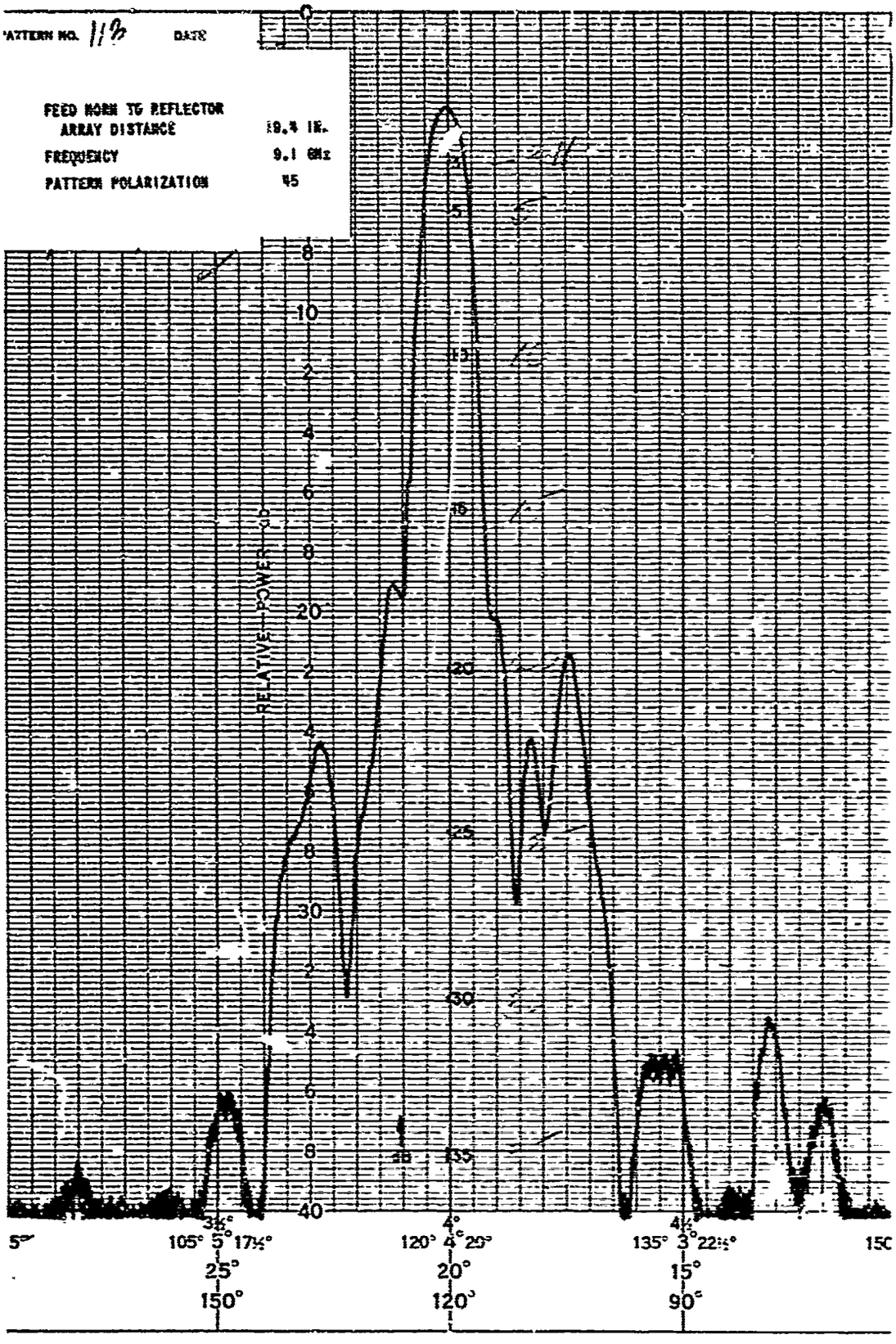

FIGURE 61. ANTENNA PATTERN PERFORMANCE WITH FIFTH SHORT SURFACE ADJUSTMENT

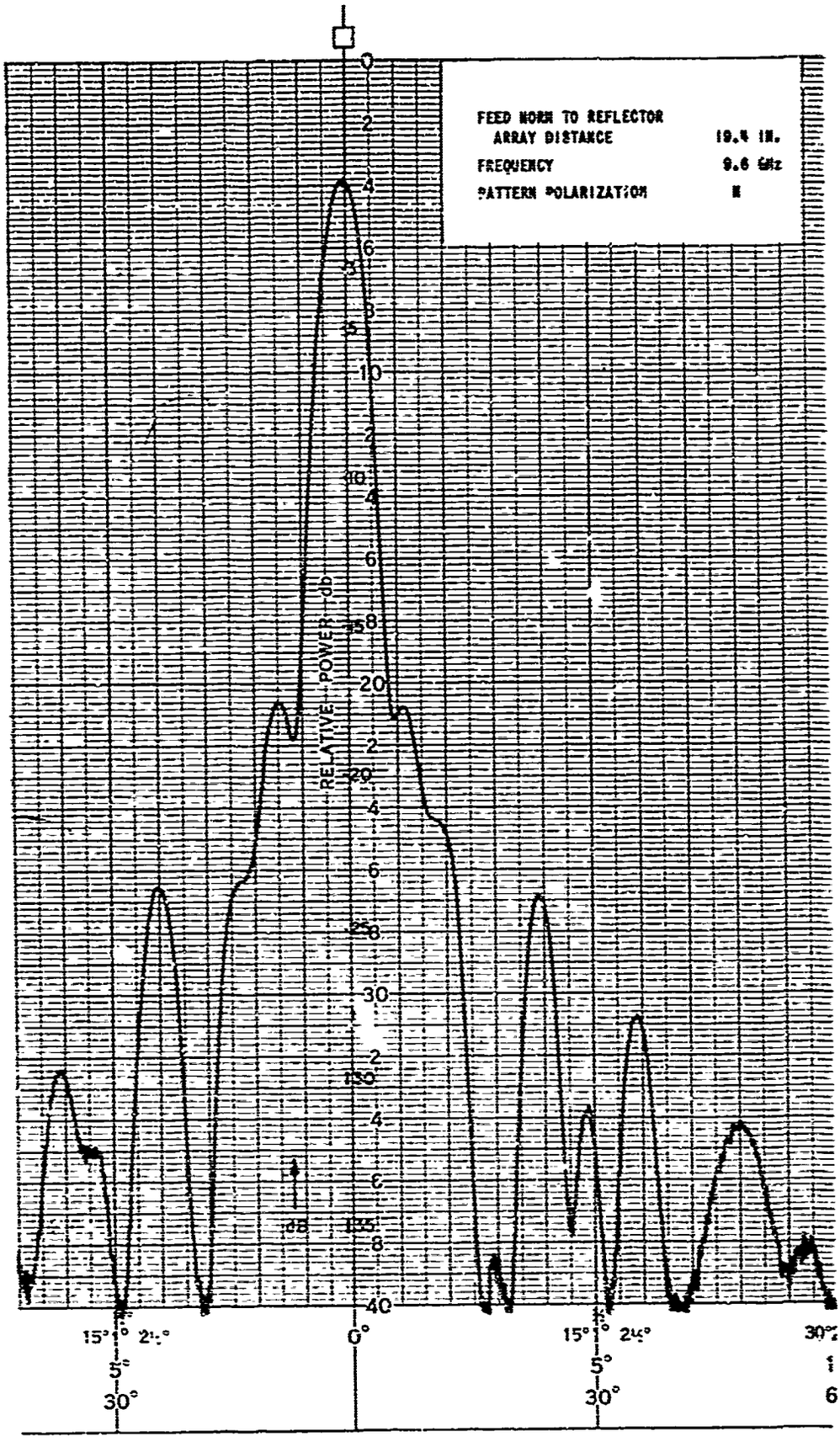

FIGURE 62. ANTENNA PATTERN PERFORMANCE WITH FIFTH SHORT SURFACE ADJUSTMENT

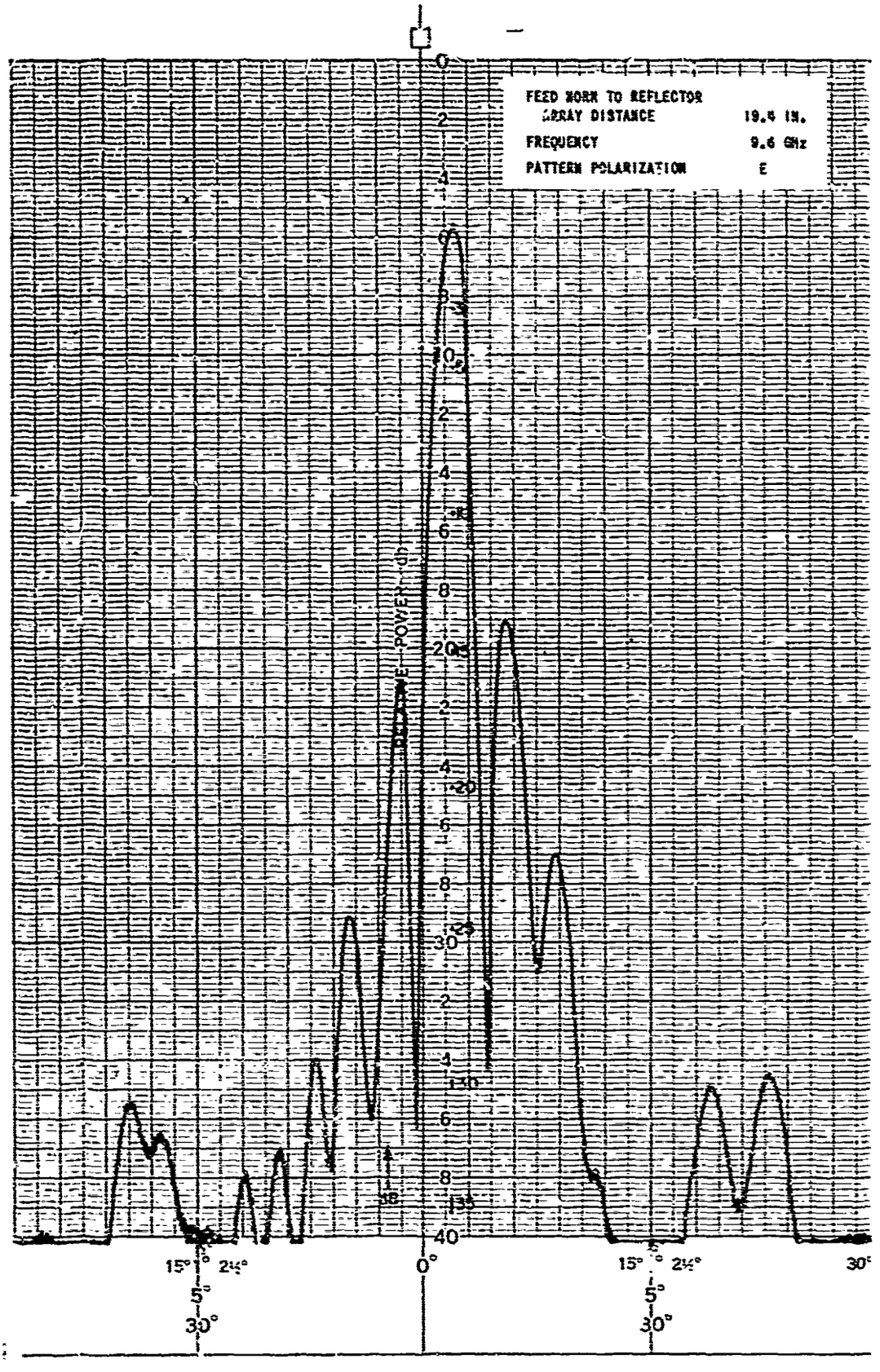

FIGURE 63. ANTENNA PATTERN PERFORMANCE WITH FIFTH SHORT SURFACE ADJUSTMENT

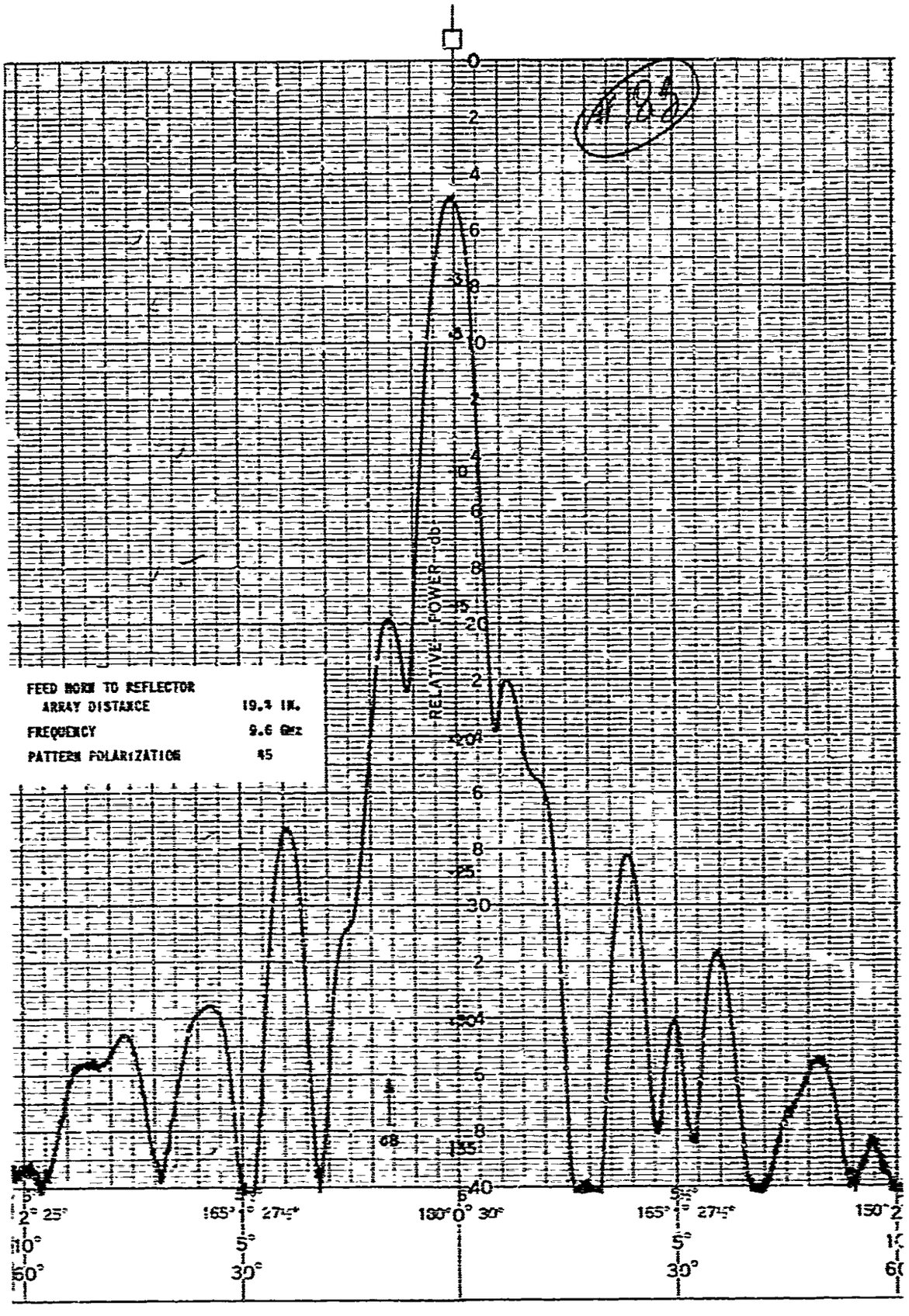

FIGURE 64. ANTENNA PATTERN PERFORMANCE WITH FIFTH SHORT SURFACE ADJUSTMENT

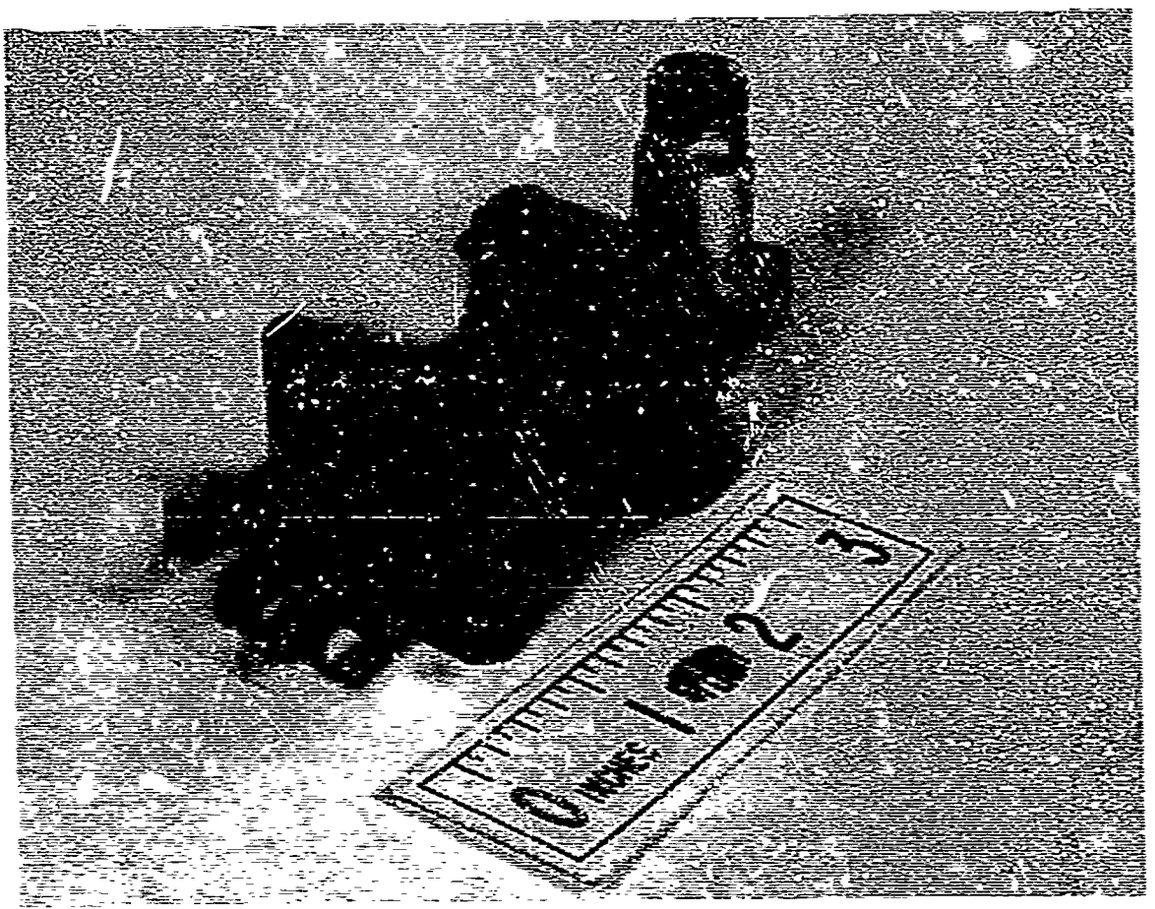

FIGURE 65. SUBREFLECTOR ARRAY COUPLING ADAPTOR

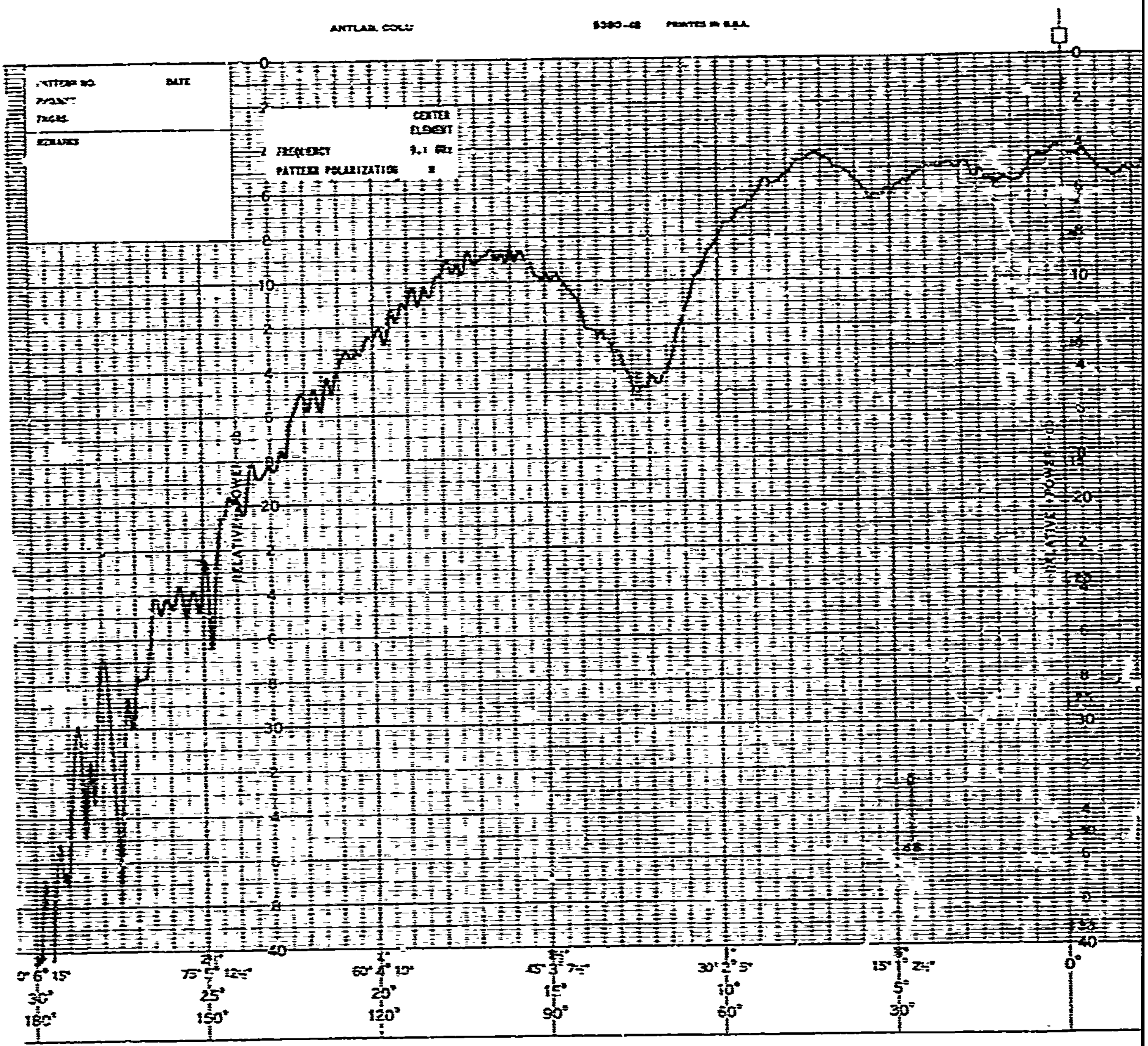

DATE
REMARKS
CENTER
ELEMENT
FREQUENCY
PATTERN POLARIZATION
RELATIVE POWER - dB

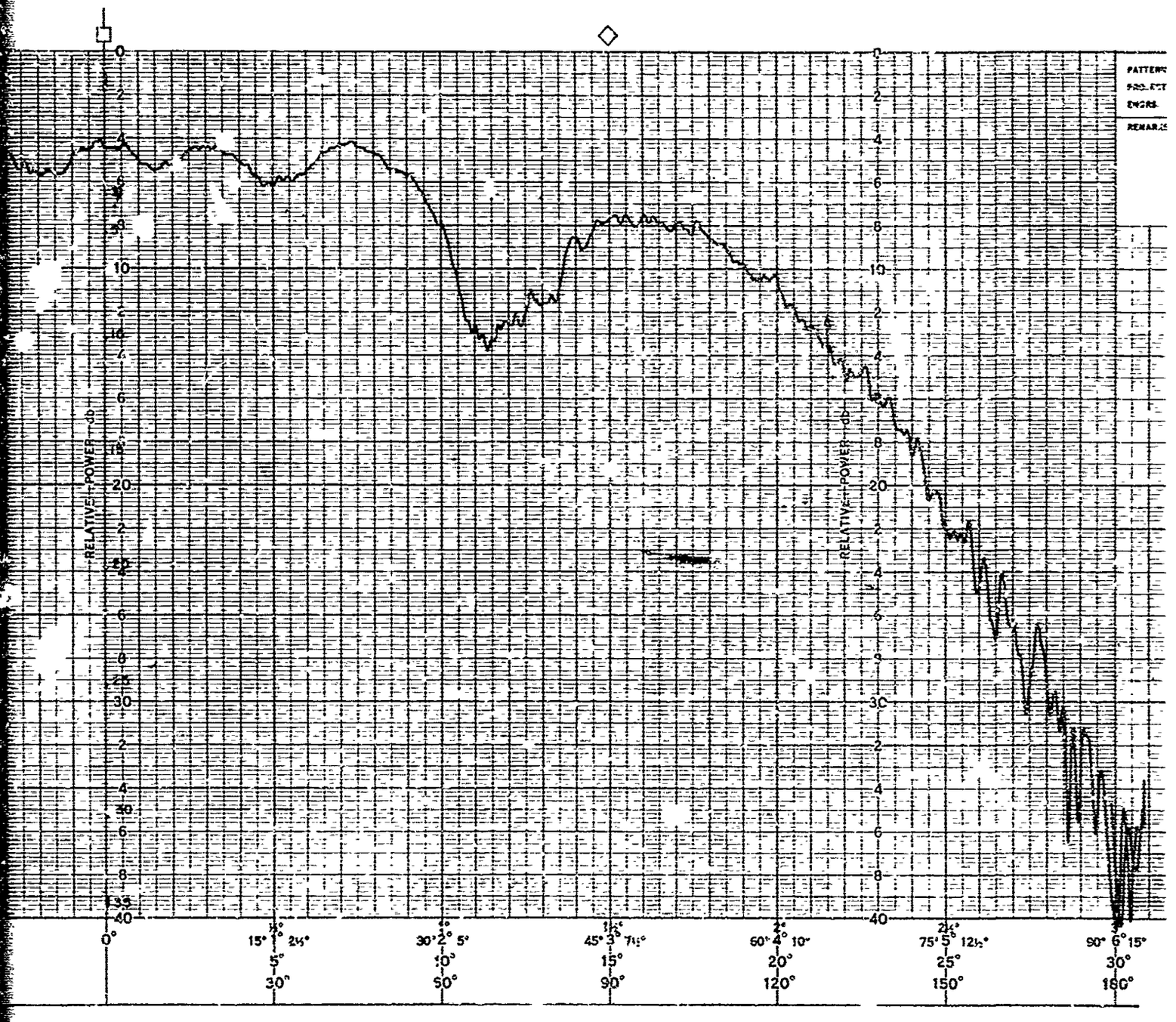

FIGURE 66. SUBREFLECTOR ARRAY SINGLE ELEMENT

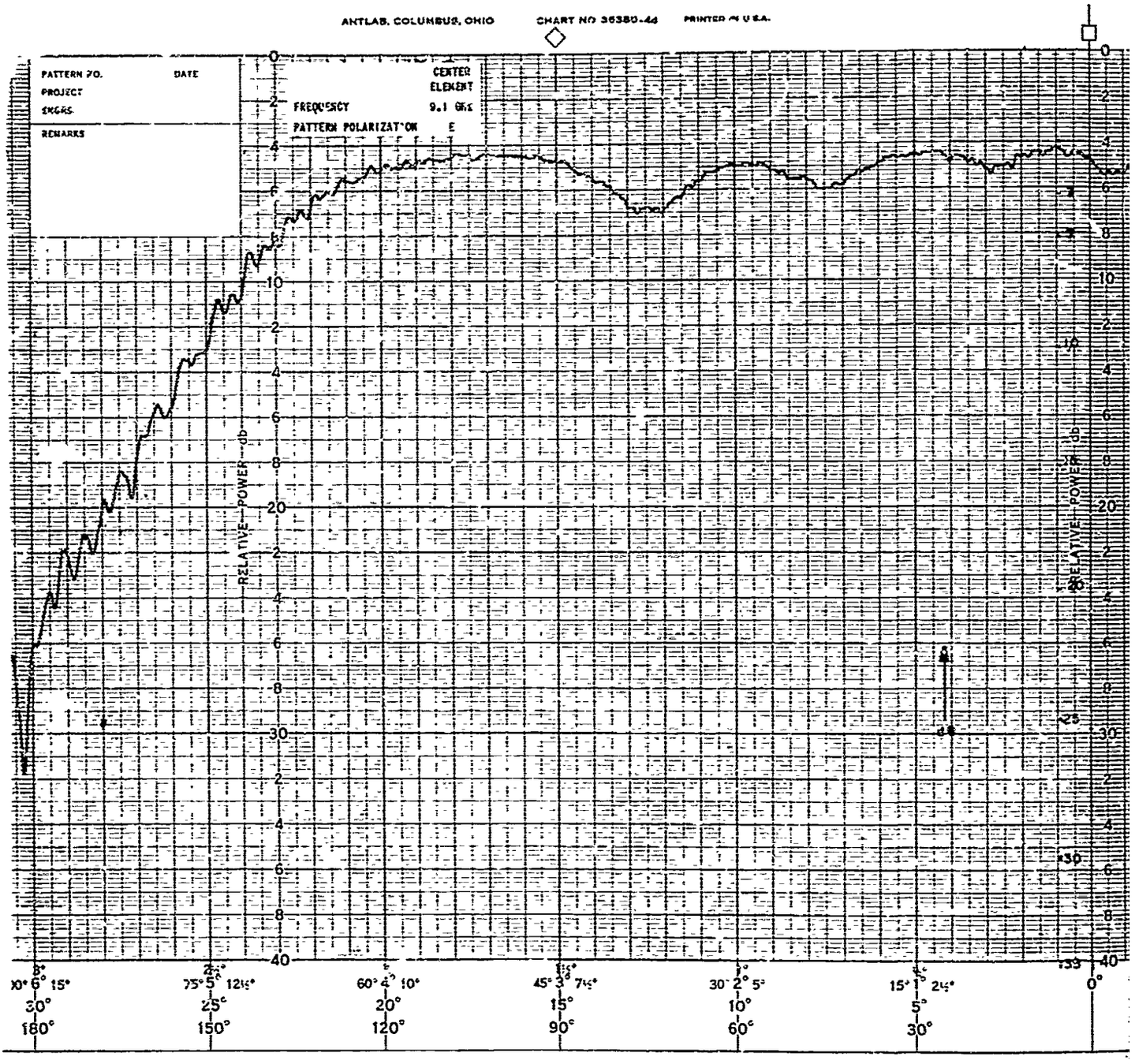

FIGURE 67. SUBREFLECTOR ARRAY SINGLE ELEMENT

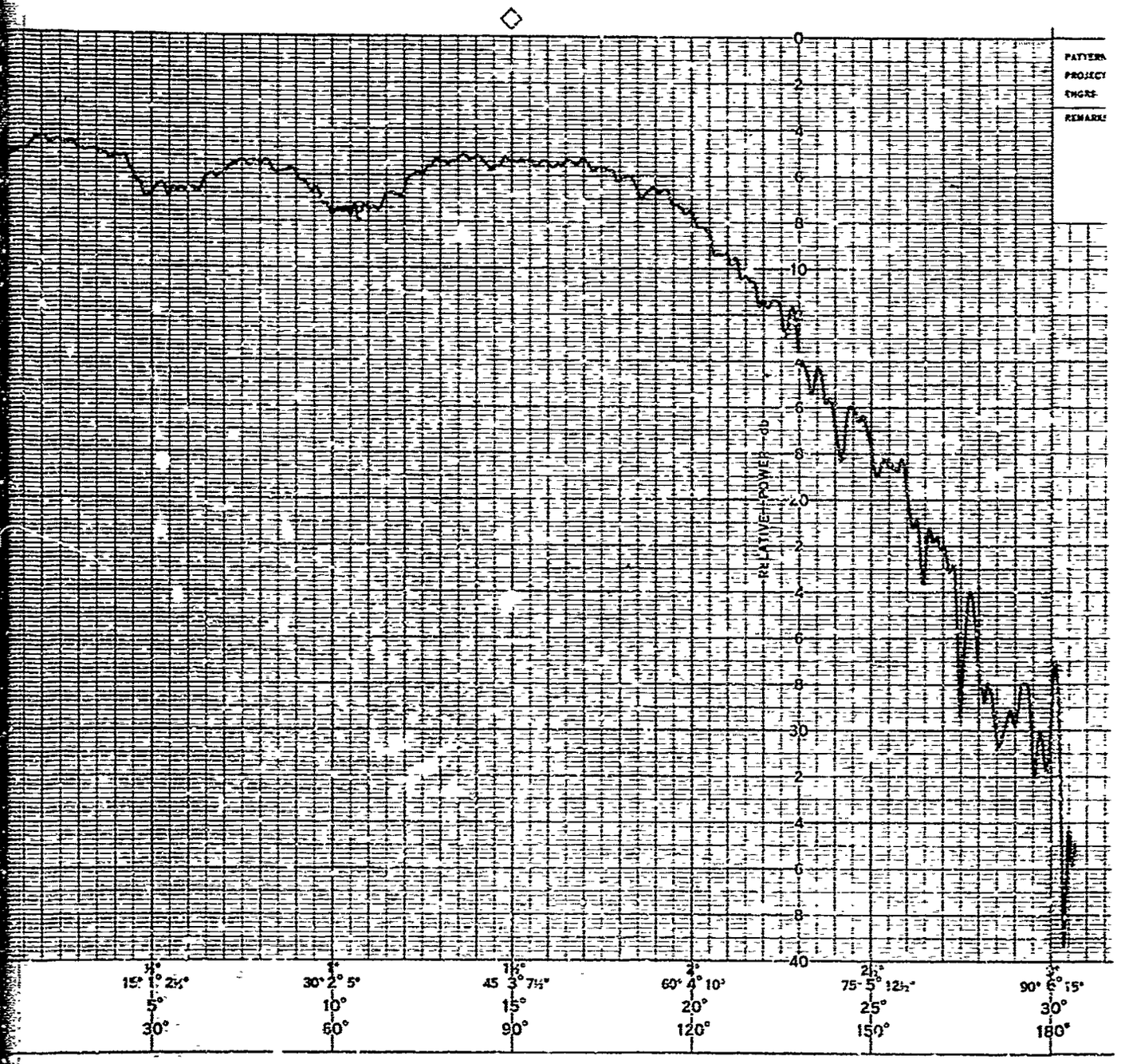
PATTERN
PROJECT
ENGR.
REMARKS
RELATIVE POWER—db
0
2
4
6
8
10
20
30
40
½° 1° 2½° 5° 10° 15° 20° 25° 30°
1° 2° 5° 10° 30° 60° 90° 120° 150° 180°
1½° 3° 7½° 15° 45 90°
2° 4° 10°
2½° 5° 12½°
3° 6° 15°

B

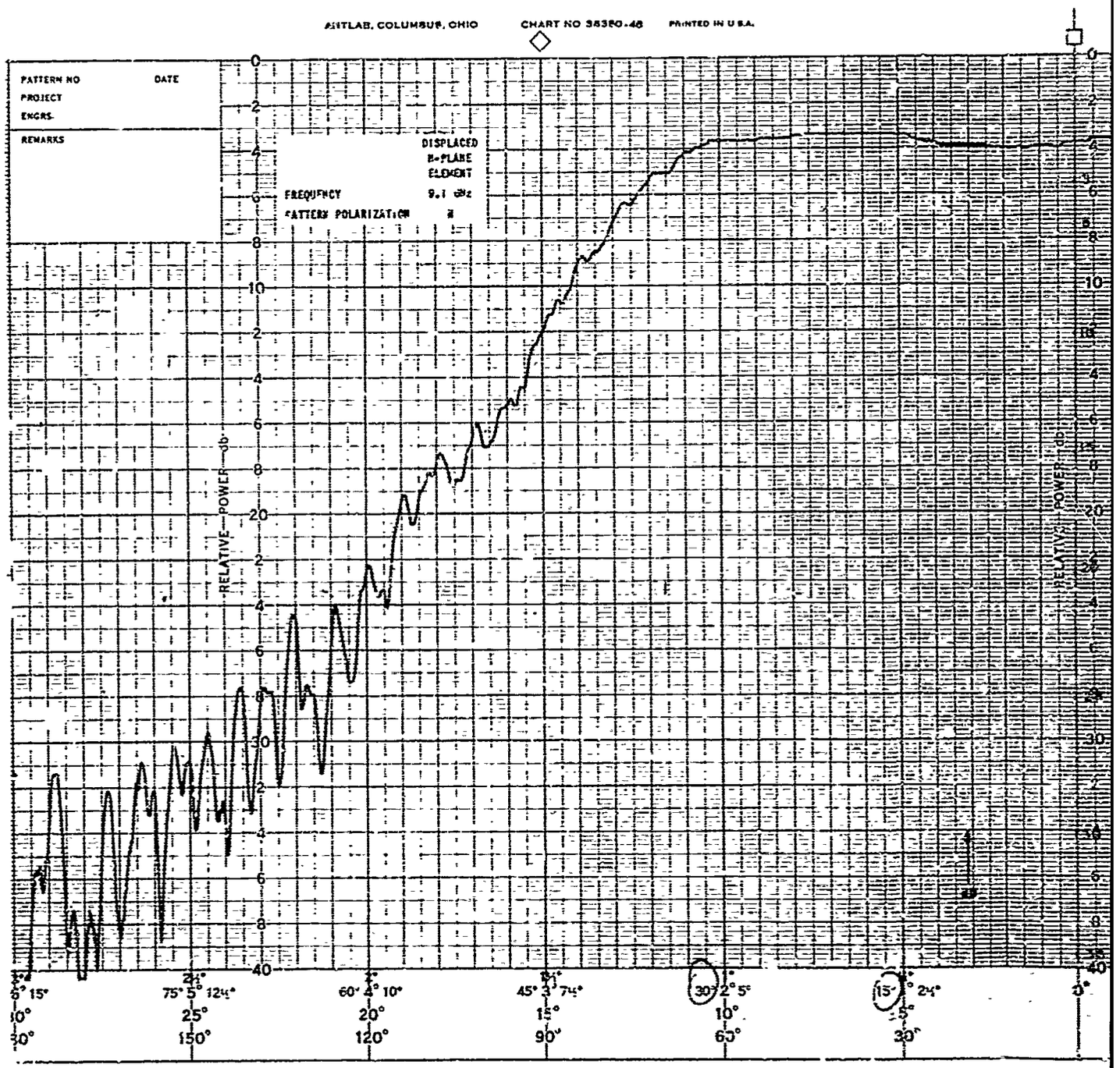
ASTLAB, COLUMBUS, OHIO
CHART NO 36360-46
PRINTED IN U.S.A.
PATTERN NO
DATE
PROJECT
ENGRS.
REMARKS
DISPLACED
H-PLANE
ELEMENT
FREQUENCY
9.1 GHz
PATTERN POLARIZATION
H
RELATIVE POWER db
RELATIVE POWER db
0
2
4
6
8
10
20
30
40
75° 5° 12½°
25°
150°
60° 4° 10°
20°
120°
45° 3° 7½°
15°
90°
30° 2° 5°
10°
60°
15° 1° 2½°
5°
30°
0°

A

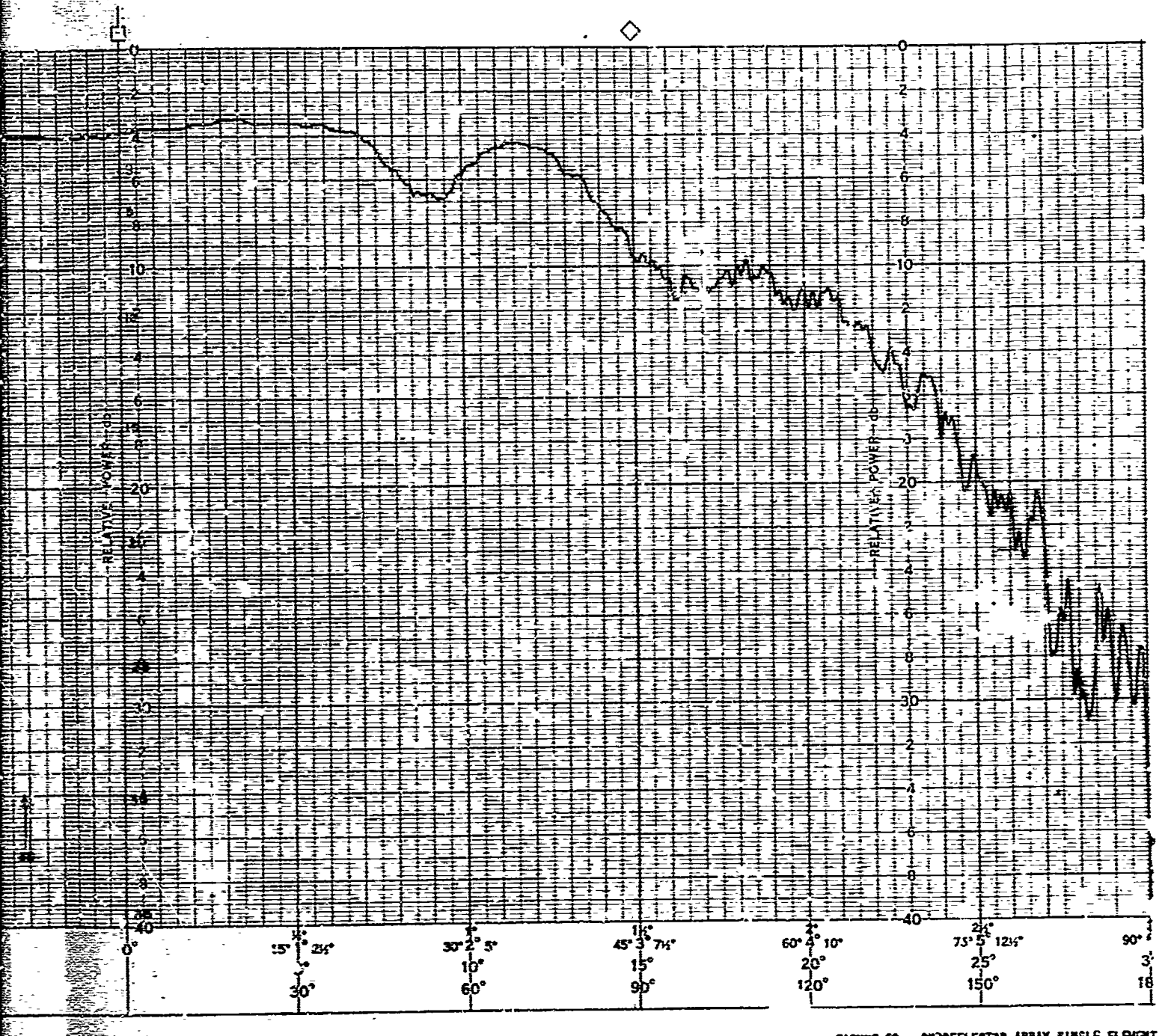

FIGURE 68. SUBREFLECTOR ARRAY SINGLE ELEMENT

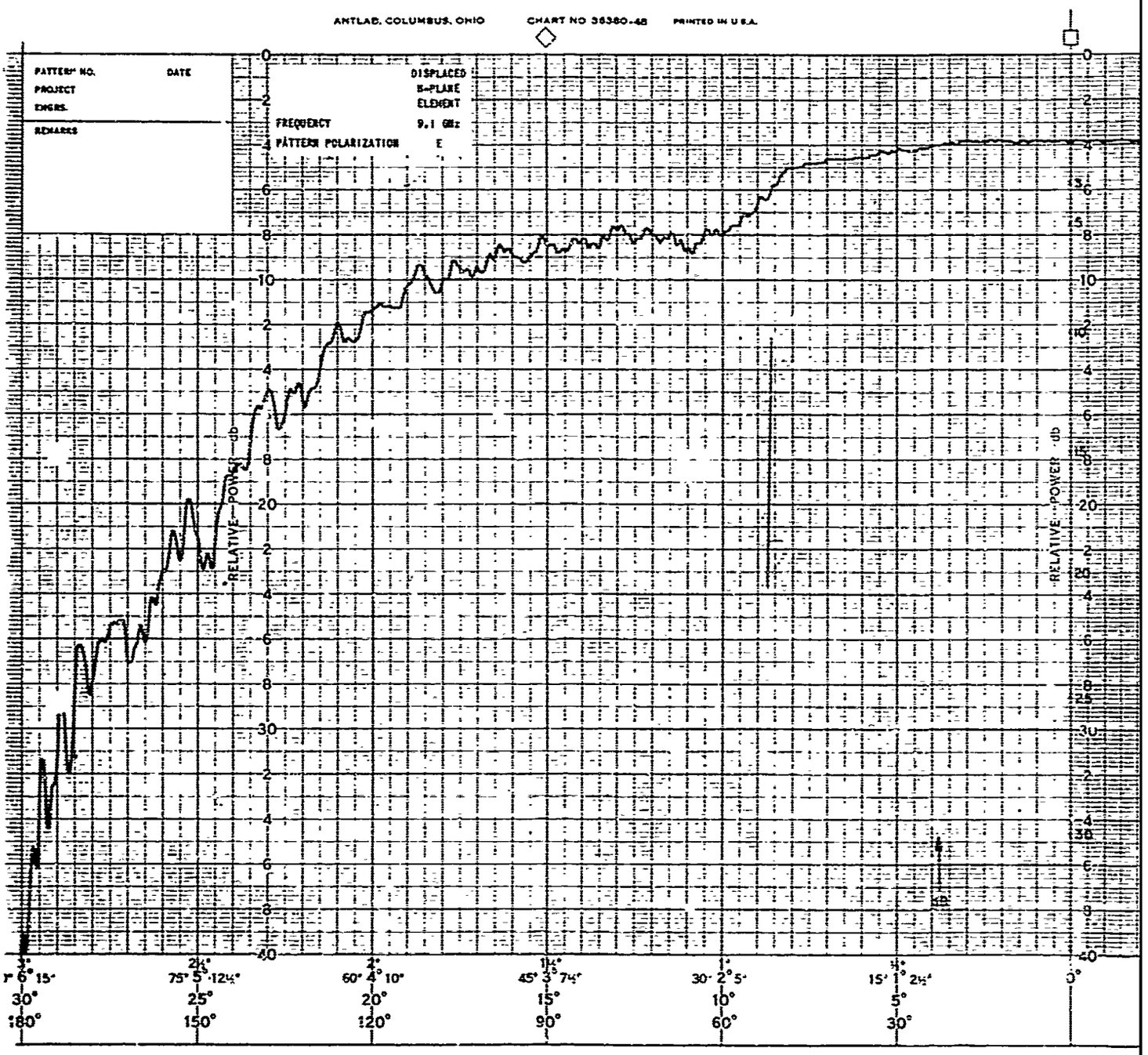

FIGURE 69. SUBREFLECTOR ARRAY SINGLE ELEMENT

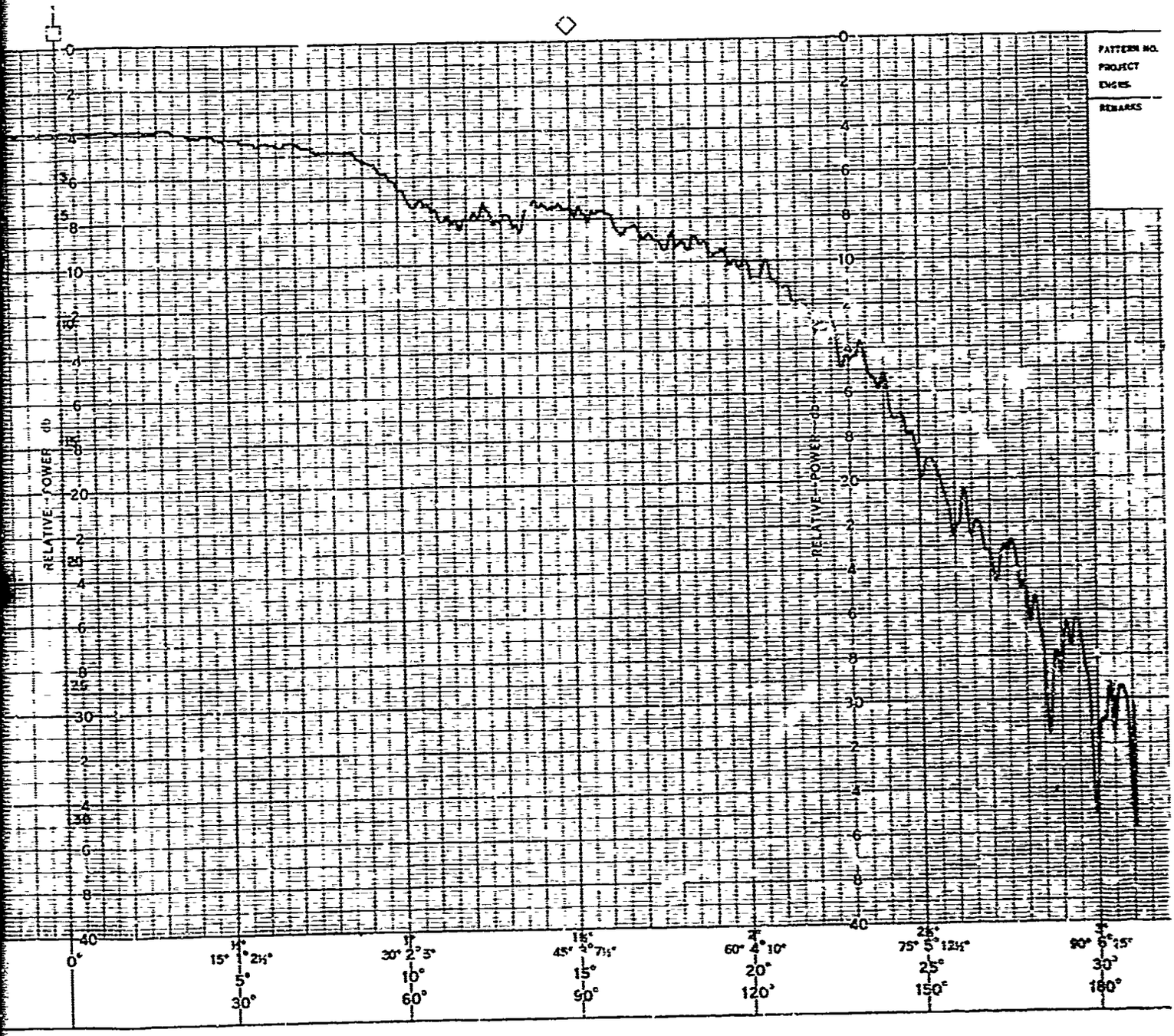
PATTERN NO.
PROJECT
ENGRS.
REMARKS
RELATIVE POWER db
RELATIVE POWER db
0°
15° 1° 2½°
5°
30°
30° 2° 3°
10°
60°
45° 3° 7½°
15°
90°
60° 4° 10°
20°
120°
75° 5° 12½°
25°
150°
90° 6° 15°
30°
180°

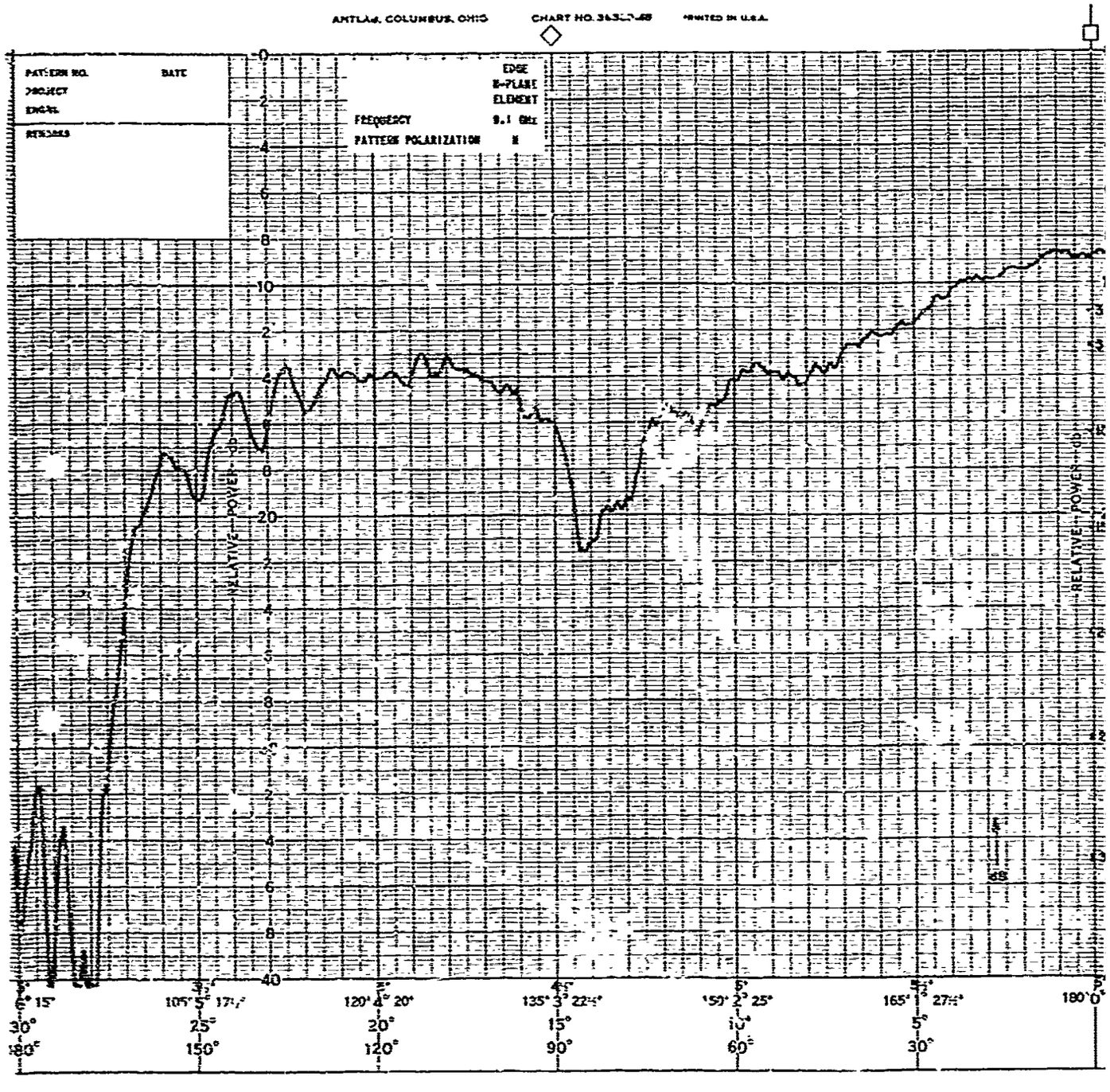
ANTLAB, COLUMBUS, OHIO
CHART NO. 363L7-65
PRINTED IN U.S.A.
PATTERN NO.
DATE
PROJECT
ENGR.
REMARKS
EDGE
H-PLANE
ELEMENT
FREQUENCY
9.1 GHz
PATTERN POLARIZATION
H
RELATIVE POWER - db
RELATIVE POWER - db
3dB
0
2
4
6
8
10
20
30
40
6° 15'
105° 5' 17½'
120° 4' 20'
135° 3' 22½'
150° 2' 25'
165° 1' 27½'
180° 0'
30°
25°
20°
15°
10°
5°
180°
150°
120°
90°
60°
30°

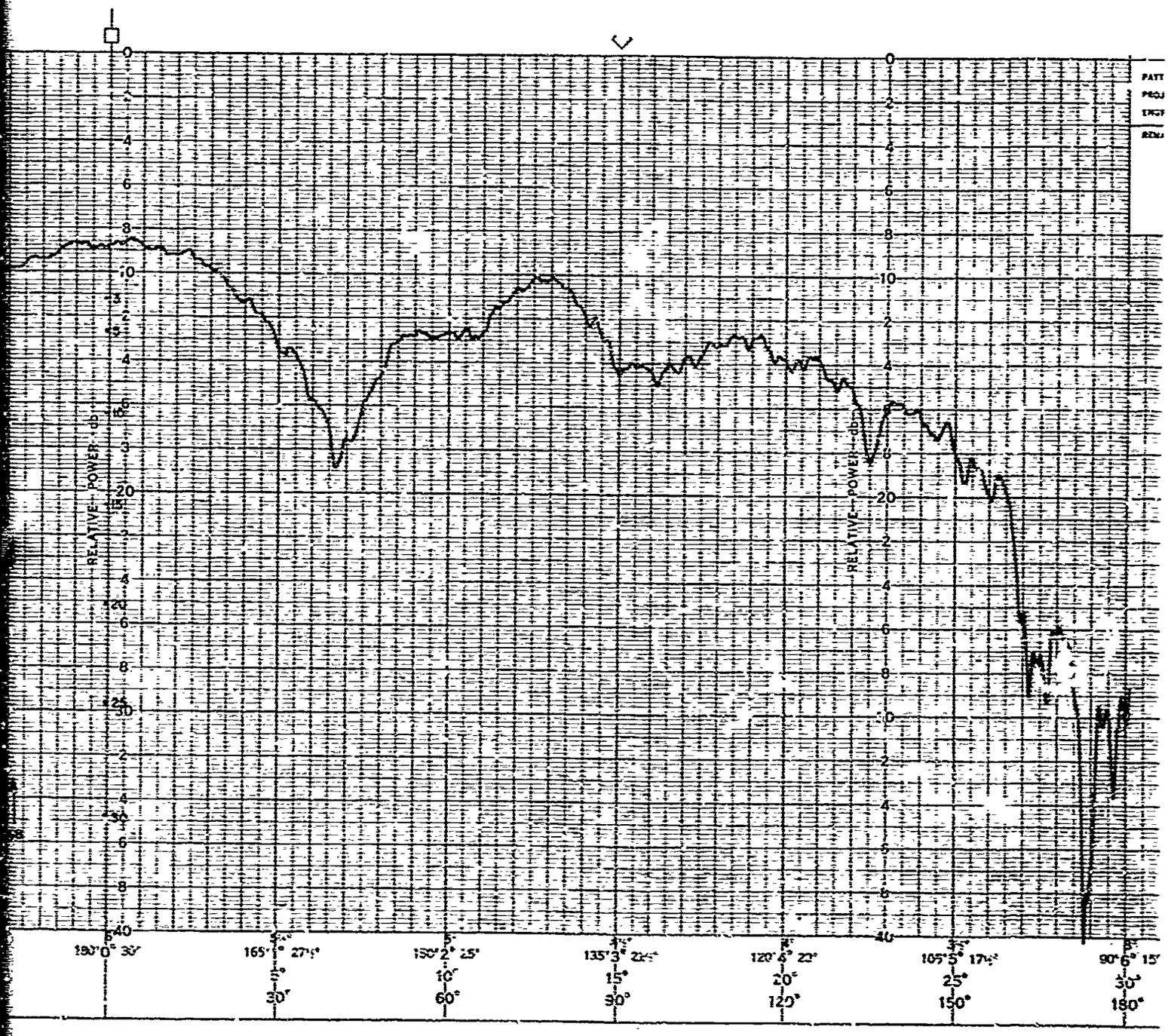

FIGURE 70. SUBREFLECTOR ARRAY SINGLE ELEMENT

B

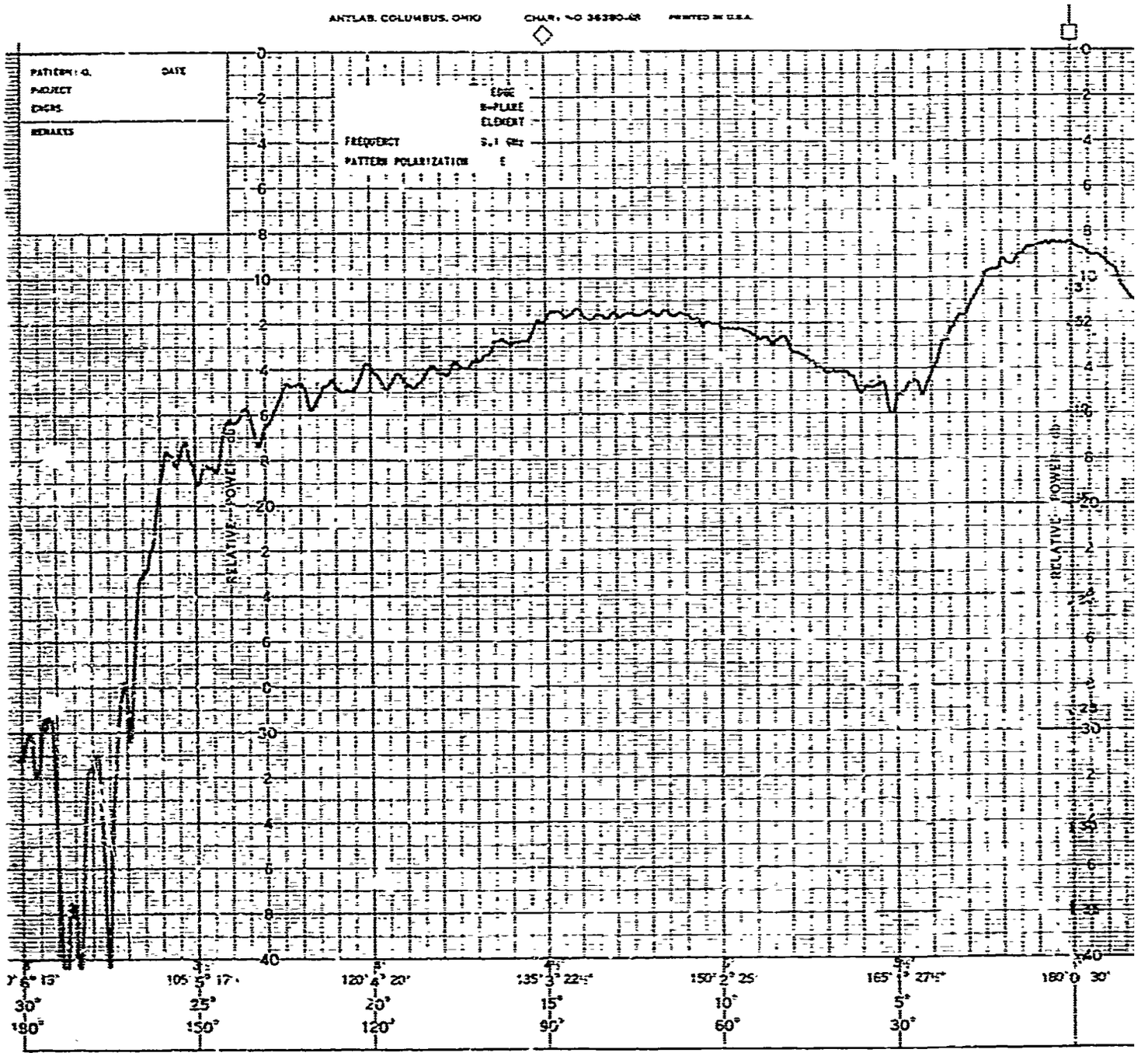

FIGURE 7.. SUBREFLECTOR ARRAY SINGLE ELEMENT

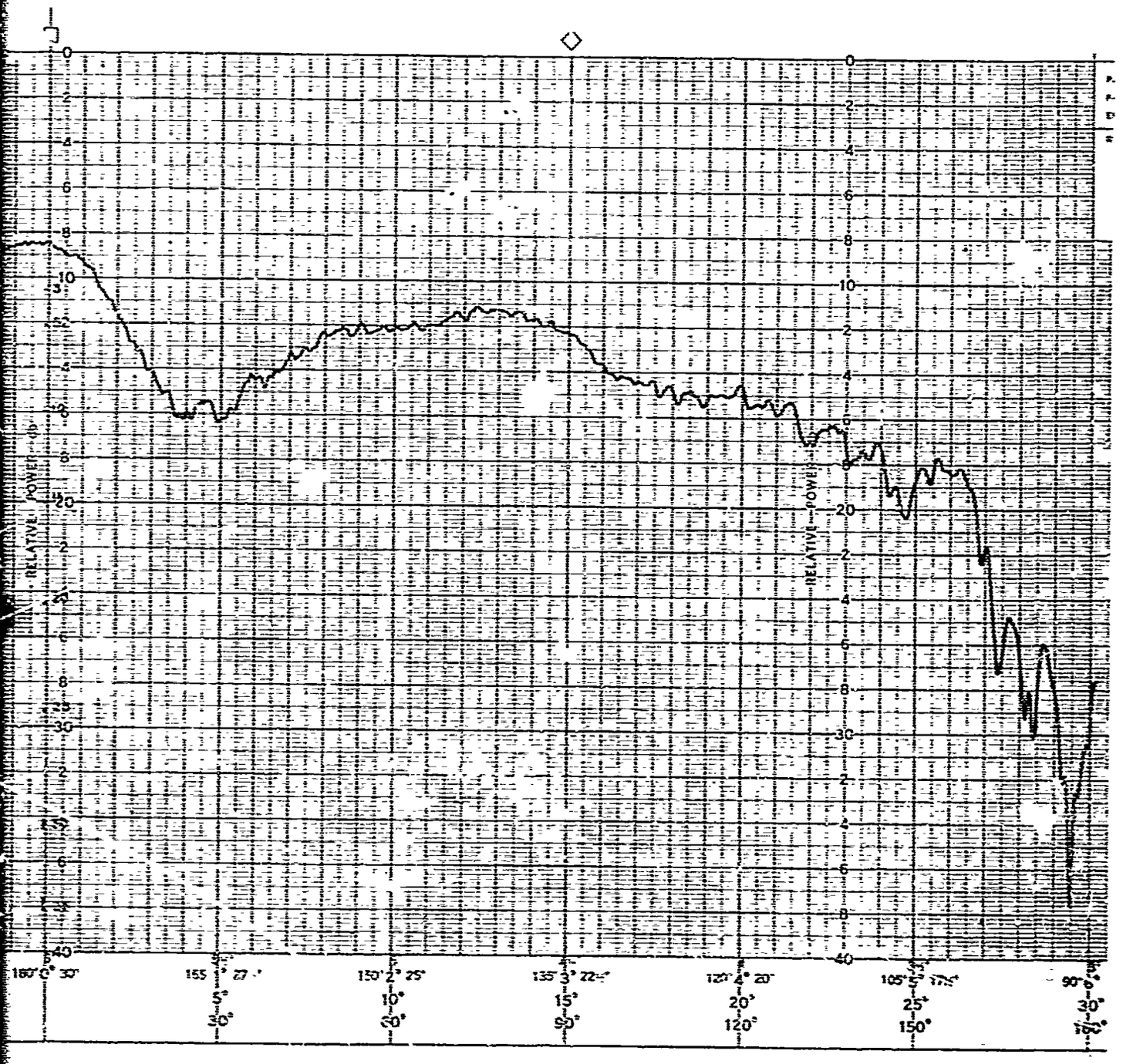
RELATIVE POWER (dB)
0
2
4
6
8
10
20
30
40
180° 0° 30°
155° 27°
150° 25°
135° 22½°
120° 20°
105° 17½°
90°
5°
10°
15°
20°
25°
30°
30°
60°
90°
120°
150°
180°

B

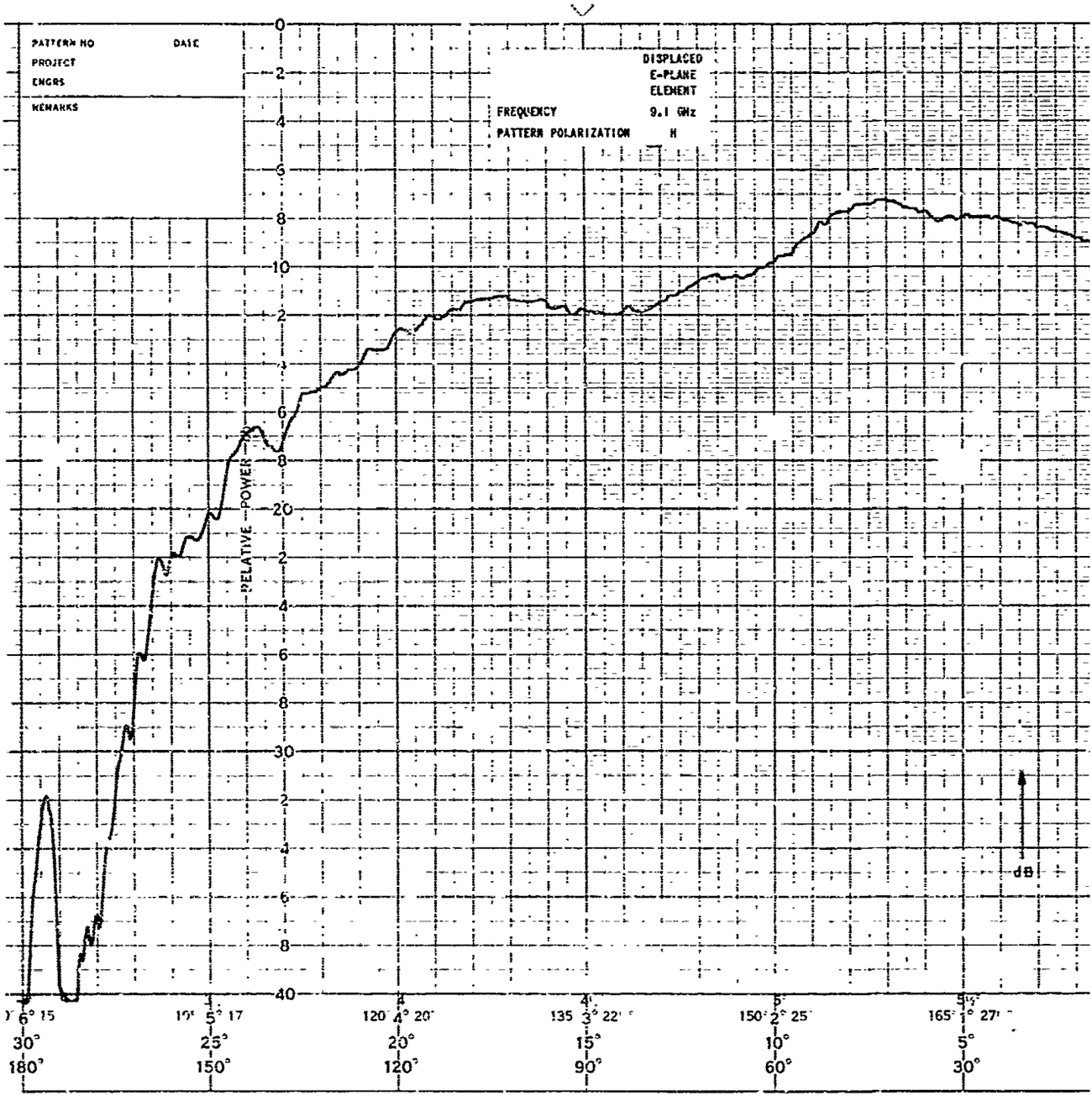
PATTERN NO
DATE
PROJECT
ENGRS
REMARKS
DISPLACED
E-PLANE
ELEMENT
FREQUENCY
9.1 GHz
PATTERN POLARIZATION
H
RELATIVE POWER
dB
0
2
4
6
8
10
2
6
8
20
2
4
6
8
30
2
4
6
8
40
6° 15
5° 17
4° 20
3° 22
2° 25
1° 27
30°
25°
20°
15°
10°
5°
180°
150°
120°
90°
60°
30°

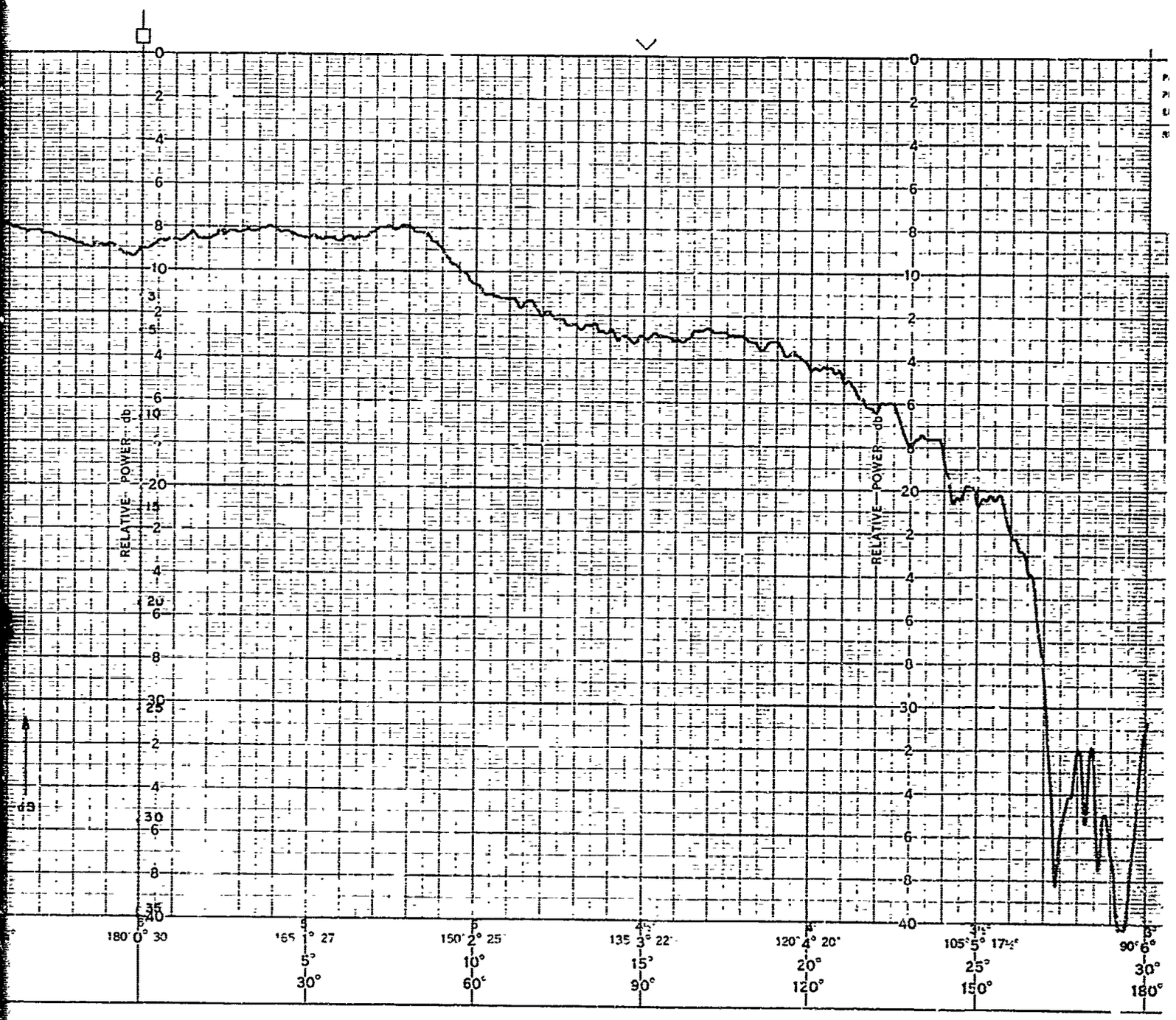

FIGURE 72. SUBREFLECTOR ARRAY SINGLE ELEMENT

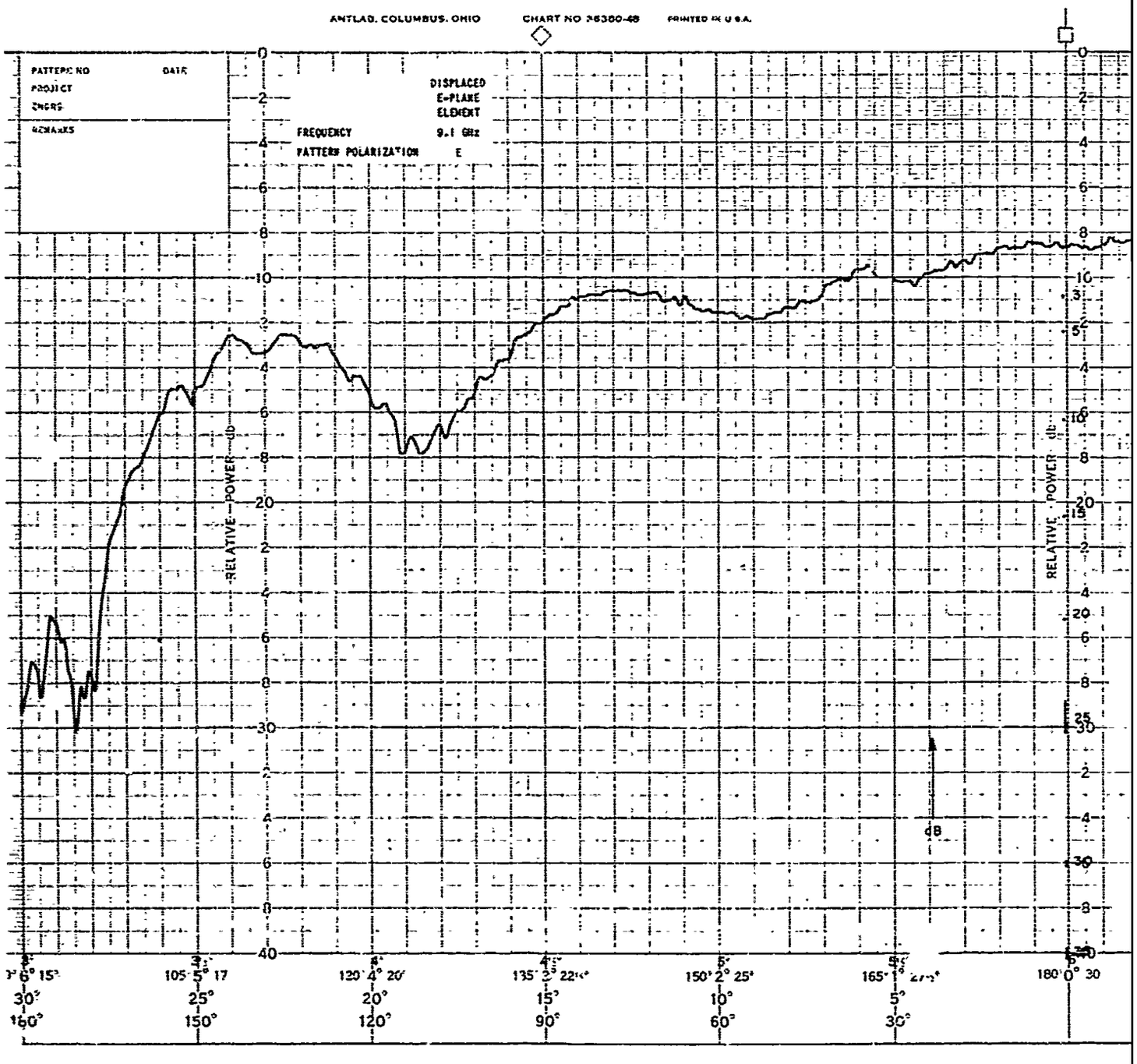

FIGURE 73. SUBREFLECTOR ARRAY SINGLE ELEMENT

A

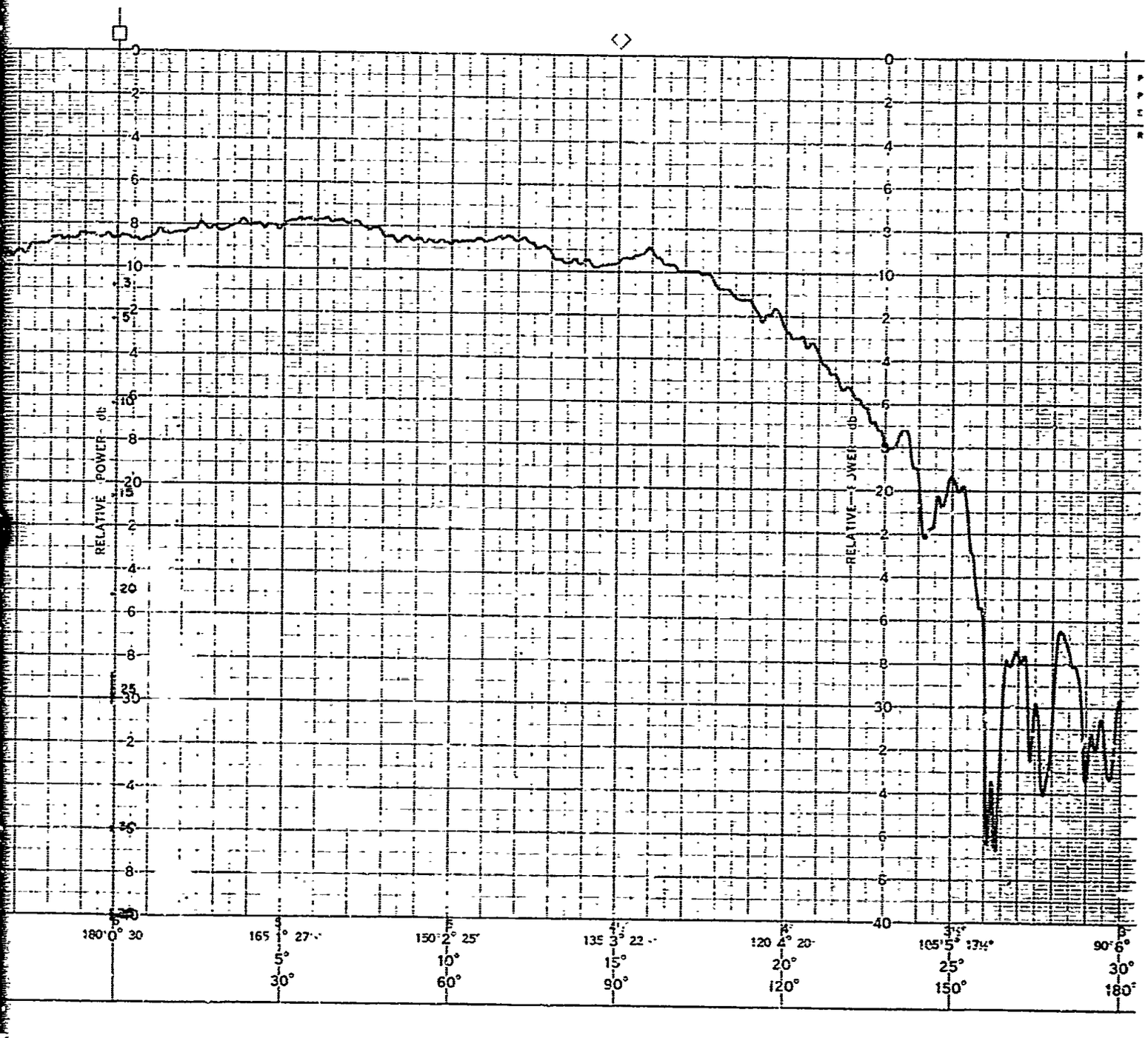
RELATIVE POWER db
RELATIVE POWER db
180° 0° 30
165° 1° 27°
150° 2° 25°
135° 3° 22°
120° 4° 20°
105° 5° 17½°
90° 6°
5°
10°
15°
20°
25°
30°
30°
60°
90°
120°
150°
180°

B

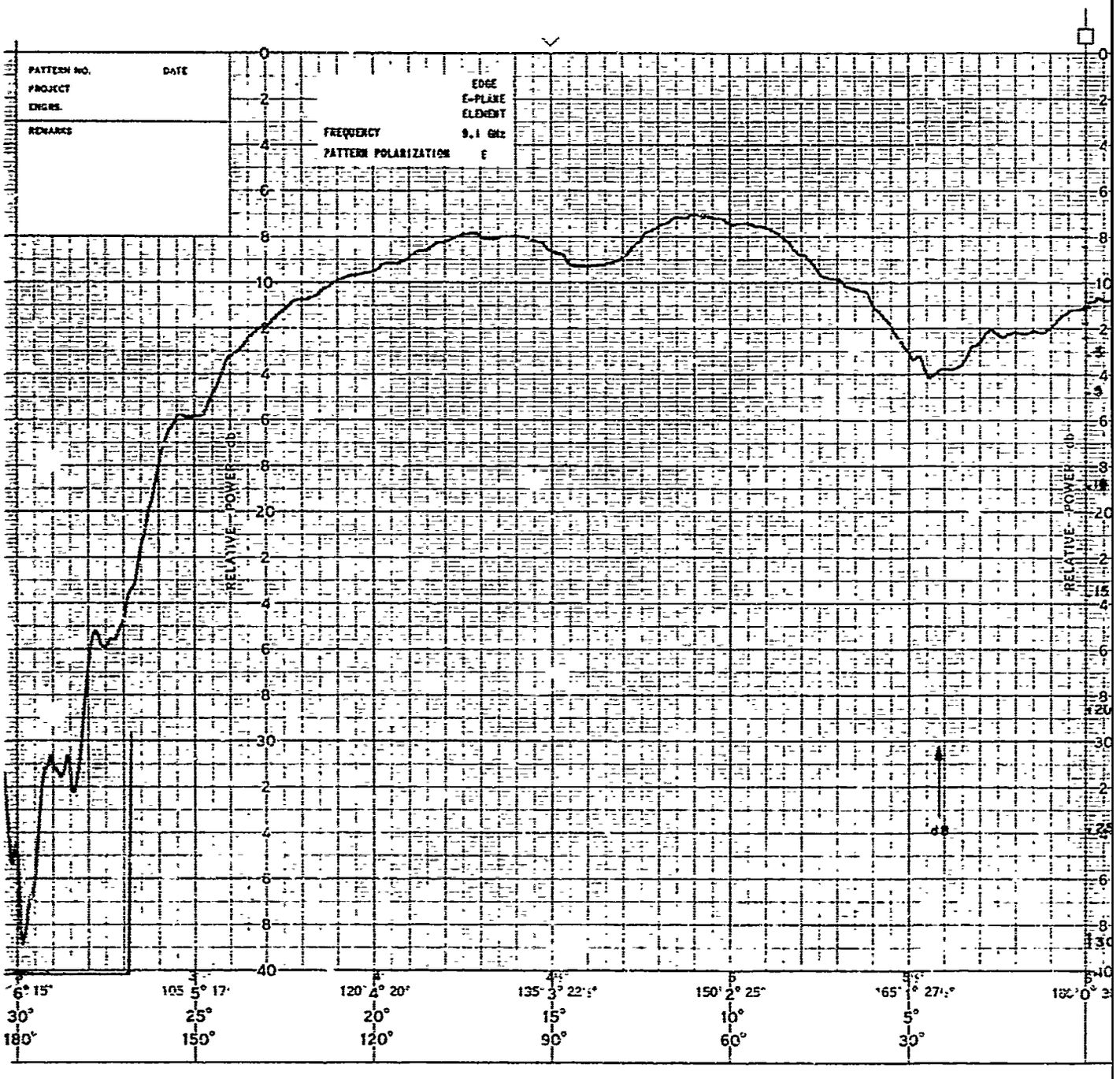
PATTERN NO.
DATE
PROJECT
ENGRS.
REMARKS
EDGE
E-PLANE
ELEMENT
FREQUENCY
9.1 GHz
PATTERN POLARIZATION
E
RELATIVE POWER, db
RELATIVE POWER, db
6° 15'
105 5° 17'
120 4° 20'
135 3° 22.5°
150 2° 25'
165 1° 27.5°
180 0° 30'
30°
25°
20°
15°
10°
5°
180°
150°
120°
90°
60°
30°

A

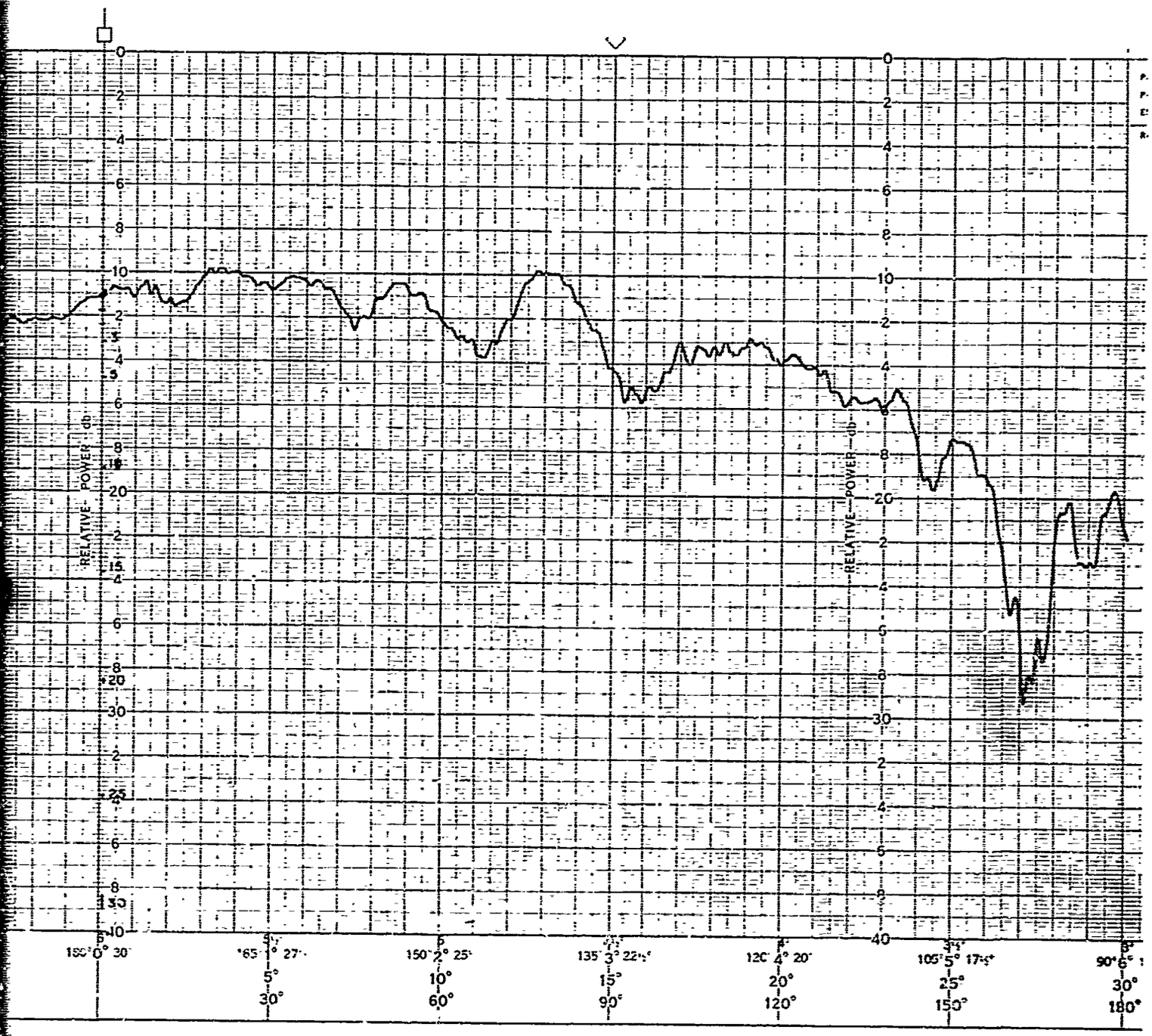

FIGURE 76. SUBREFLECTOR ARRAY SINGLE ELEMENT

B

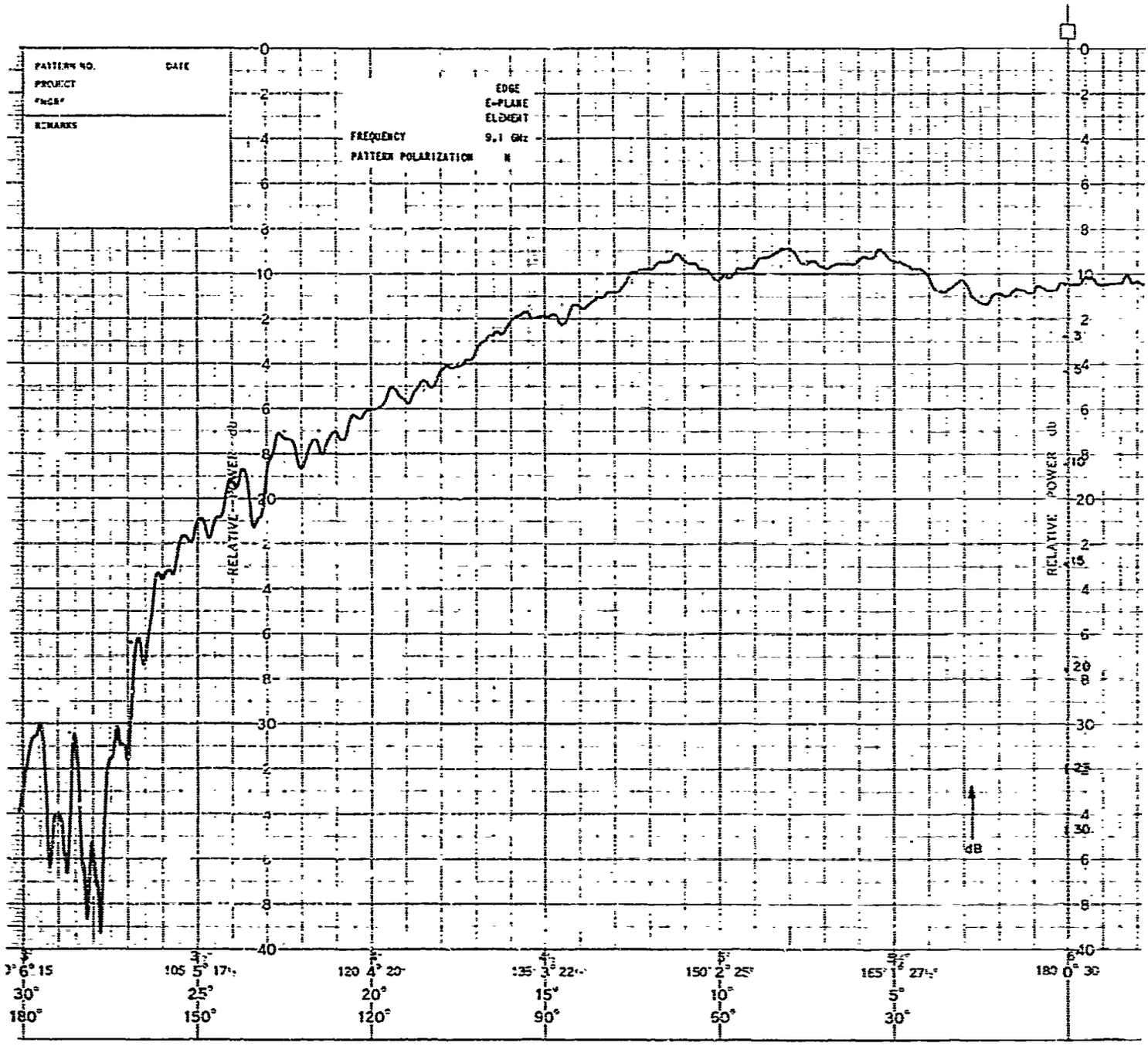

FIGURE 75. SUBREFLECTOR ARRAY SINGLE ELEMENT

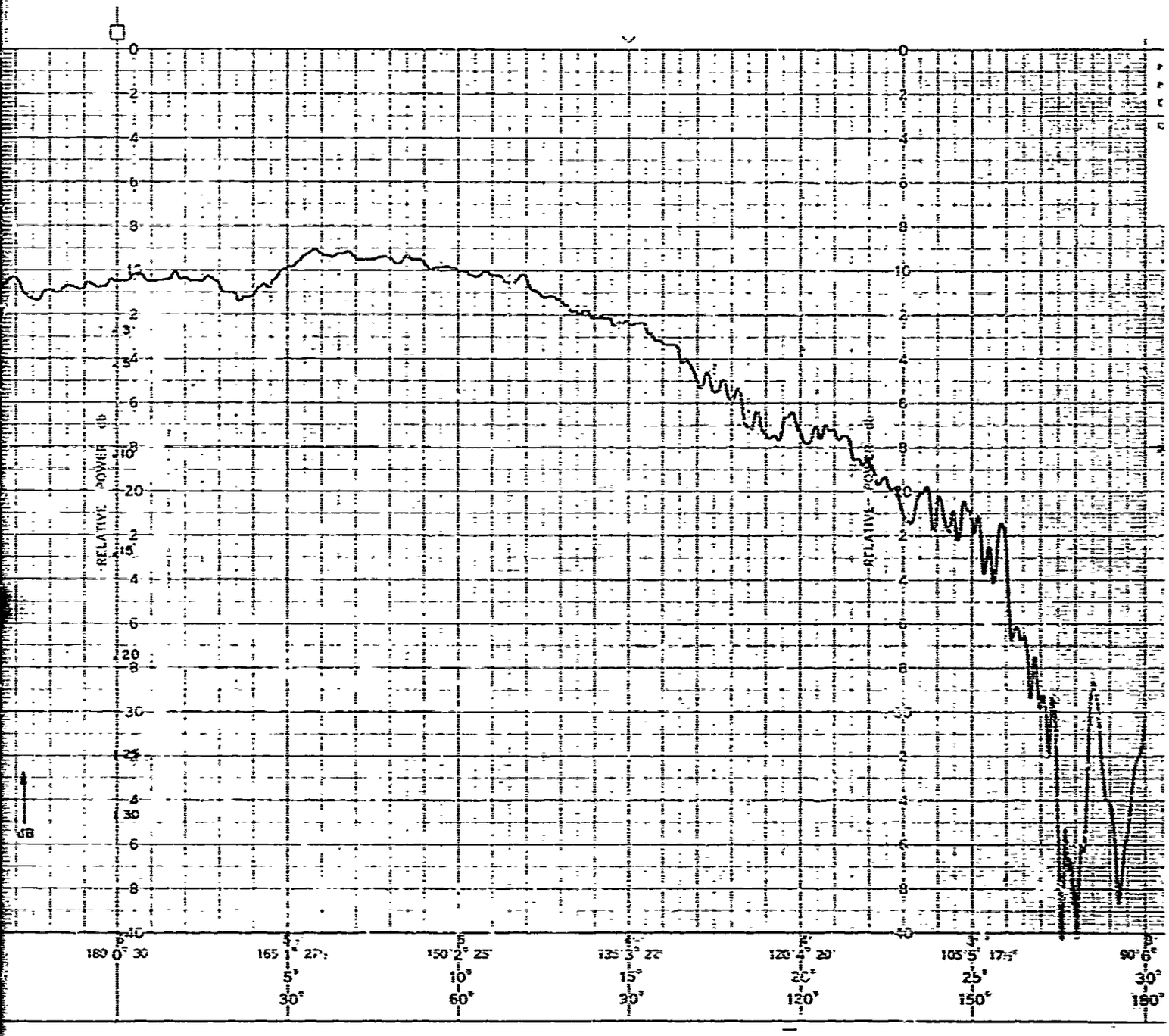
RELATIVE POWER db
RELATIVE POWER db
0
2
4
6
8
10
20
30
40
50
180° 0° 30
165° 1° 27½
150° 2° 25
135° 3° 22½
120° 4° 20
105° 5° 17½
90° 6°
5°
30°
10°
60°
15°
90°
20°
120°
25°
150°
30°
180°

B

Figure 76 illustrates the dimensions of the iris and its placement in the cells. Figure 77 is the center element pattern (H plane) with irises in place.

3-9 SUBREFLECTOR ARRAY, FIFTH SHORT SETTING, FIRST TYPE IRISES IN H-PLANE CELLS

After placing the irises in the subreflector array cells which principally influence H-plane performance, the subreflector array was remounted on the model antenna reflector for the optimum gain position. Figures 78 through 80 show the patterns. Results for the fifth short setting with 19.5-inch spacing from feed to subreflector array and first type irises are as follows:

Frequency (GHz)	Pattern Plane	Gain (dB)	Half Power Beamwidth (deg)	10-dB Beamwidth (deg)	20-dB Beamwidth (deg)	First Two Sidelobes (dB)	Other Sidelobes ($\pm 15^{\circ}$)(dB)
9.1	H	47.1	0.80	1.40	1.83	23	25
	E	--	0.7[illegible]	1.16	1.42	15	27
	45°	--	0.73	1.25	--	15	22

A slight improvement was noticed in the H-plane beamwidth when compared to that obtained with the fifth short setting (no irises) at 9.1 GHz. No increase of gain resulted, however, possibly due to the E-plane beamwidth broadening which also was noted. Since the best H-plane beamwidth previously obtained was with the second short setting (0.75°), those cells with irises were then reset to the second short setting and the H-plane pattern investigated. As before, the subreflector array was placed at the maximum gain position. Figures 81 and 82 are the resulting patterns.

Test results with the subreflector array, modified second short setting, first type irises in H-plane cells are summarized as follows for 20.2-inch spacing from feed to subreflector array:

Frequency (GHz)	Pattern Plane	Half Power Beamwidth (deg)	10-dB Beamwidth (deg)	20-dB Beamwidth (deg)	First Two Sidelobes (dB)	Other Sidelobes ($\pm 15^{\circ}$)(dB)
9.1	H	0.75	1.25	1.59	20	20
	E	0.76	1.80	--	(Shoulder)	25

The above data show no improvement in H-plane beamwidth over the second short setting with no irises. The E-plane pattern again shows an astigmatic condition, which indicates that this iris and short combination represents a poor choice. Since no improvement was anticipated, the gain was not measured for this configuration.

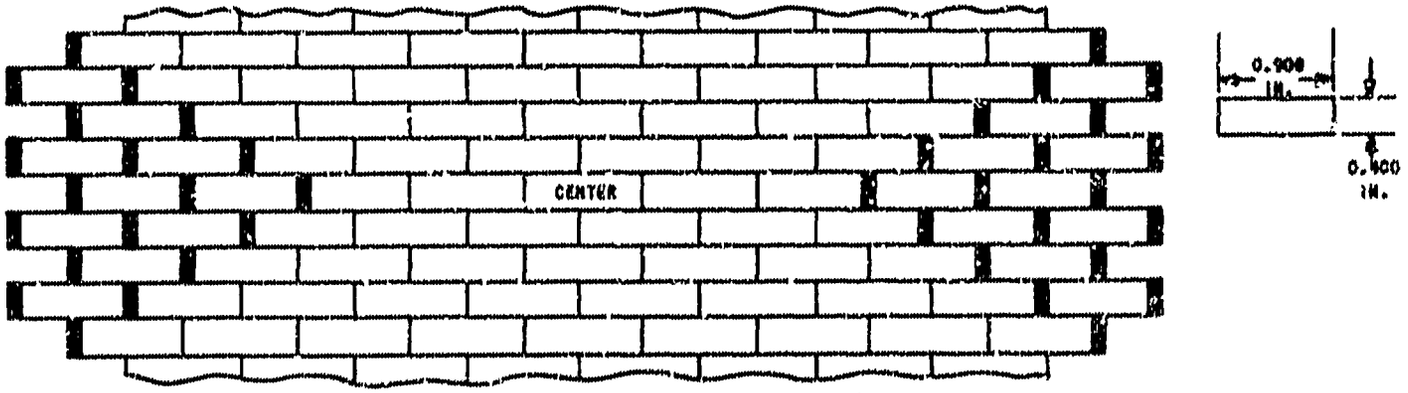

(a) IRIS PLACEMENT (CENTER AREA OF ENTRY SURFACE SHOWN)

(b) IRIS DIMENSIONS

FIGURE 76. TYPE I IRIS GEOMETRY

ANTLAB COLUMBUS, OHIO

CHART NO 26350-68

PRINTED IN U.S.A.

PATTERN NO. DATE

PROJECT

TAKEN

REMARKS

CENTER ELEMENT

FREQUENCY 9.1 GHz

PATTERN POLARIZATION H

RELATIVE POWER IN DECIBELS

0
-2
-4
-6
-10
-20
-30
-40

90 6° 10
30°
180°

75 5° 12
25°
150°

60 4° 10
20°
120°

45 3° 7
15°
90°

30 2° 5
10°
60°

15 2°
5°
30°

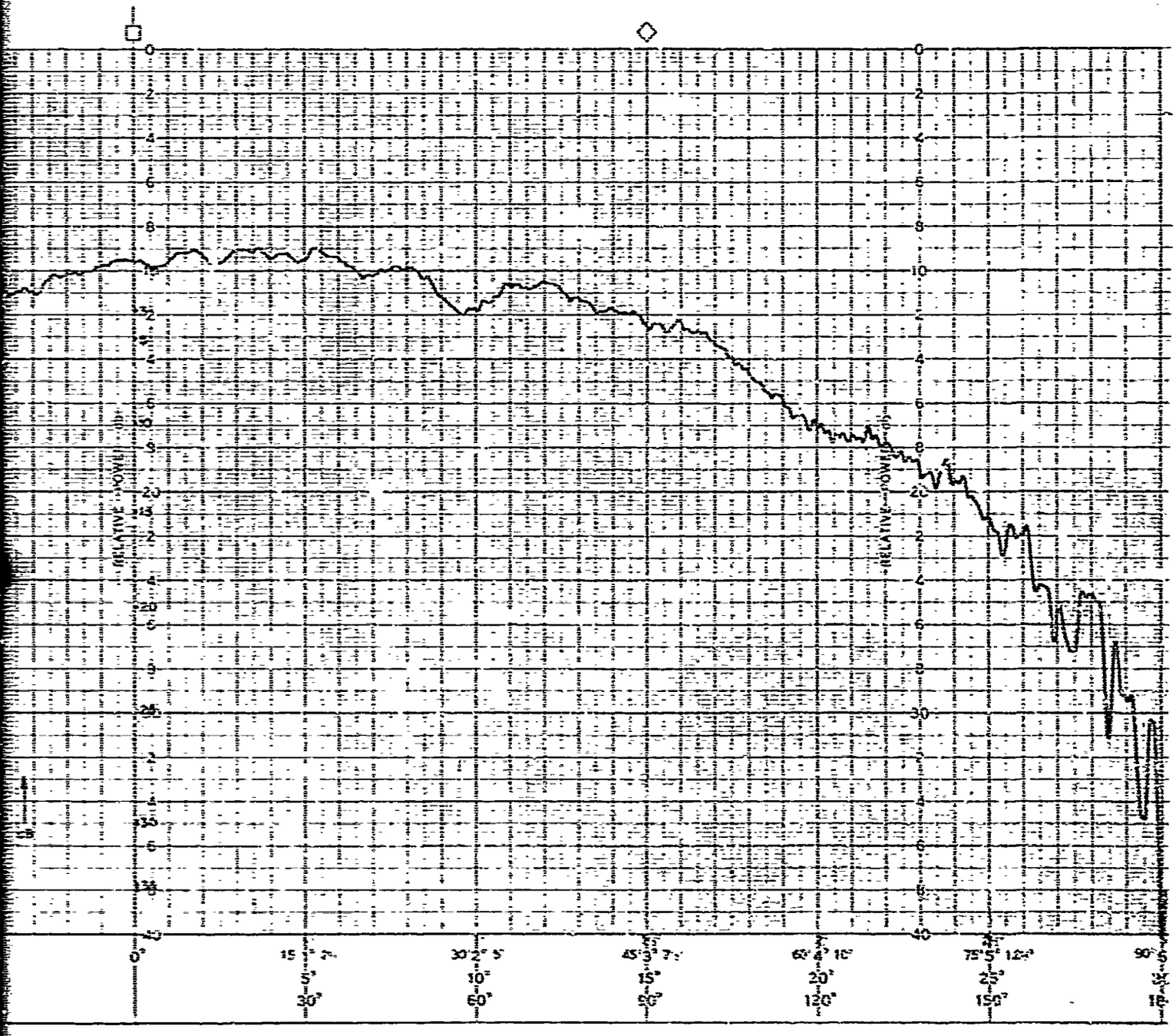

FIGURE 77. CENTER ELEMENT E-PLANE PATTERN WITH ASYMMETRICAL INDUCTIVE IRIS

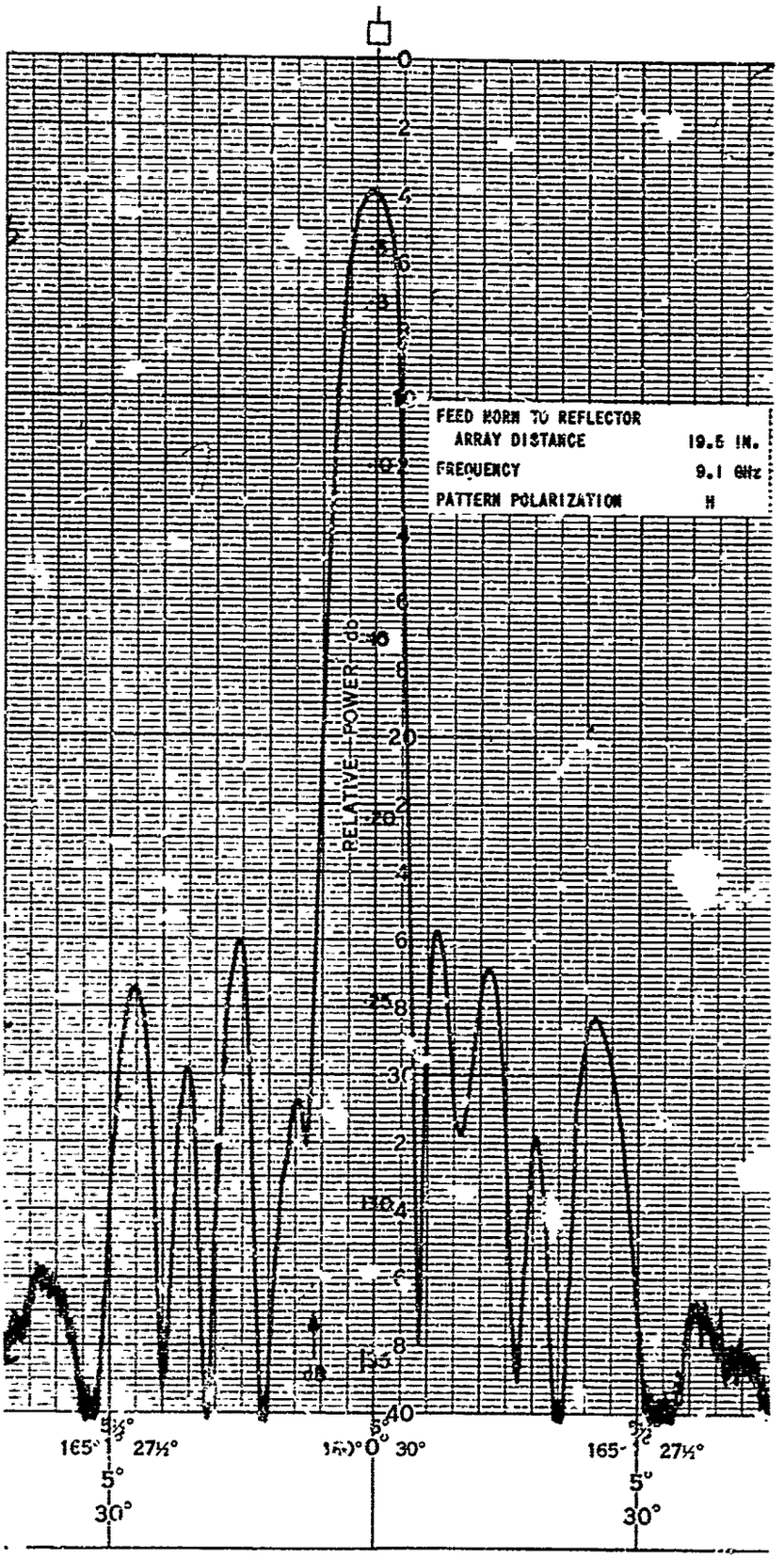

FIGURE 78. ANTENNA PATTERN PERFORMANCE WITH FIFTH SHORT SURFACE ADJUSTMENT AND ASYMMETRICAL INDUCTIVE IRIS MATCHING

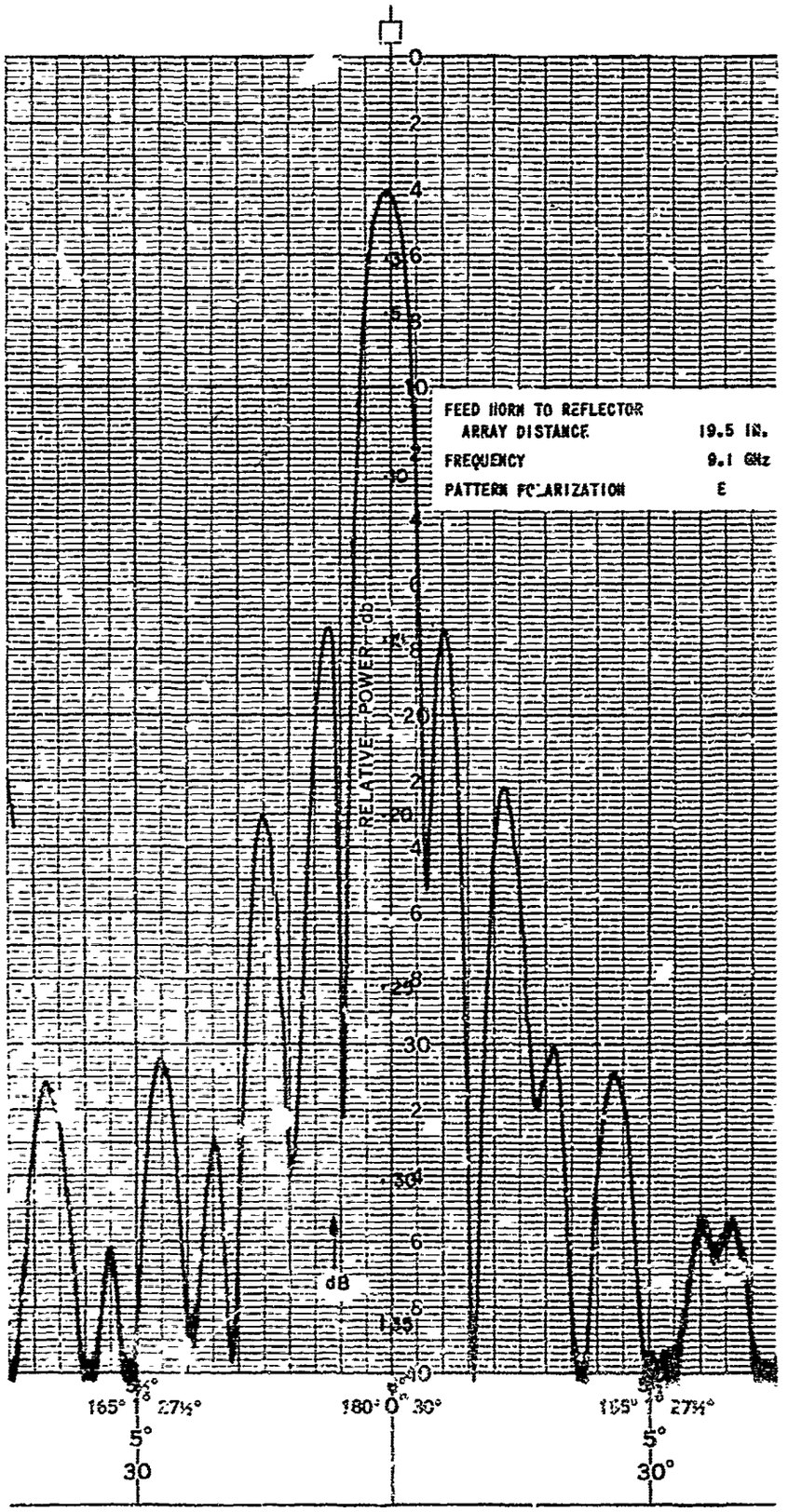

FIGURE 79. ANTENNA PATTERN PERFORMANCE WITH FIFTH SHORT SURFACE ADJUSTMENT AND ASYMMETRICAL INDUCTIVE IRIS MATCHING

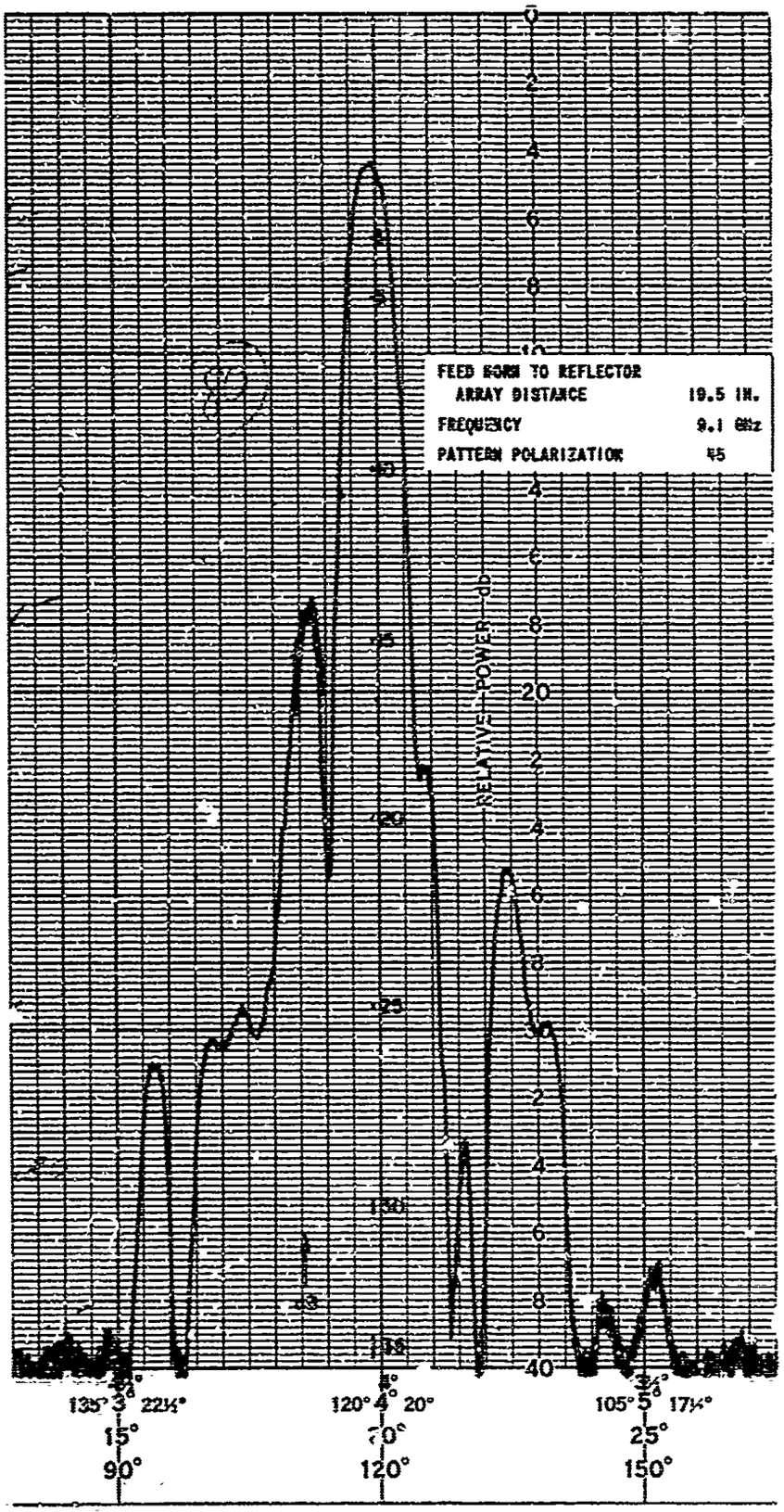

FIGURE 60. ANTENNA PATTERN PERFORMANCE WITH FIFTH SHORT SURFACE ADJUSTMENT AND ASYMMETRICAL INDUCTIVE IRIS MATCHING

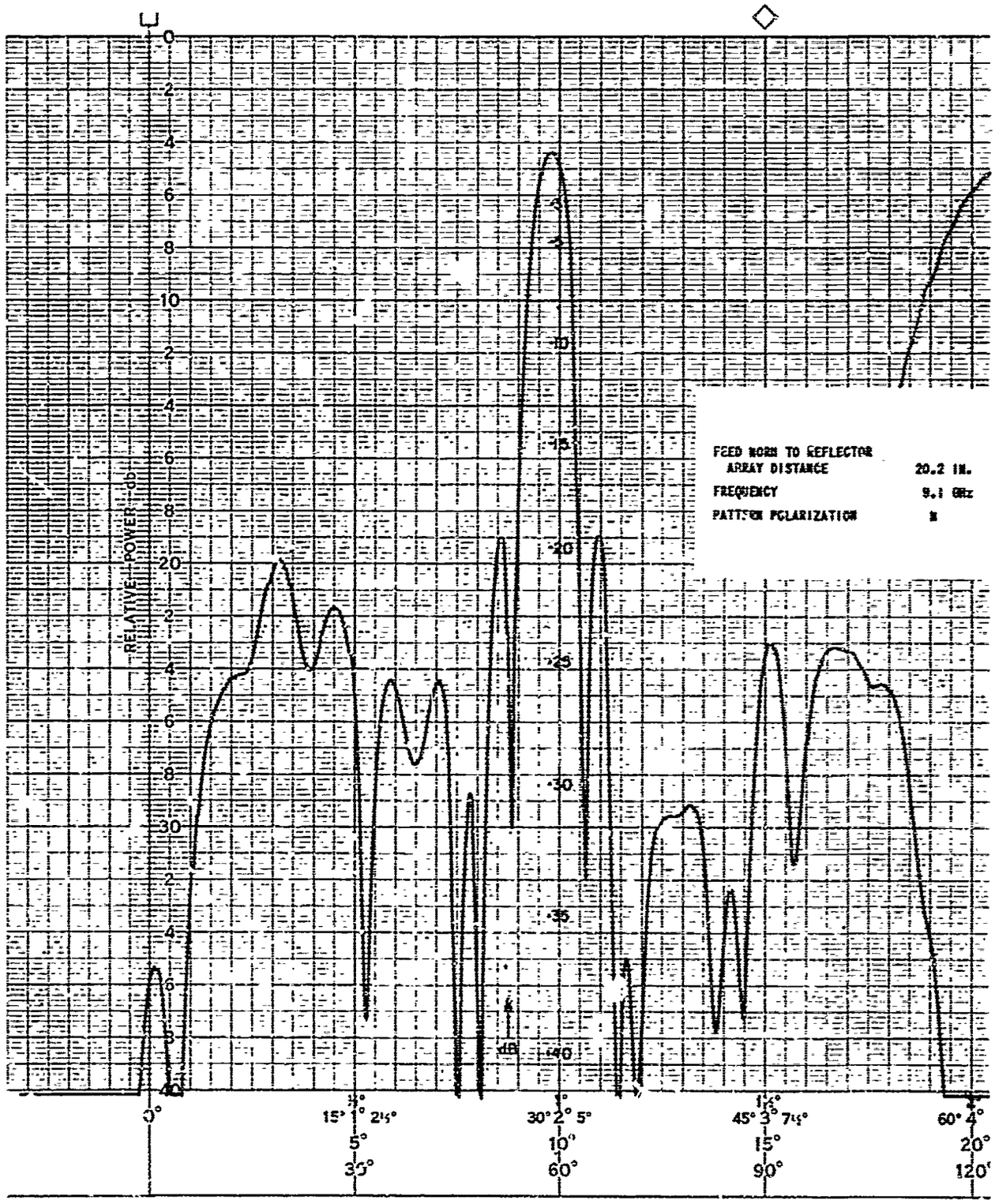

FIGURE 81. ANTENNA PATTERN PERFORMANCE WITH PARTIAL SECOND SHORT SURFACE ADJUSTMENT AND ASYMMETRICAL INDUCTIVE IRIS MATCHING

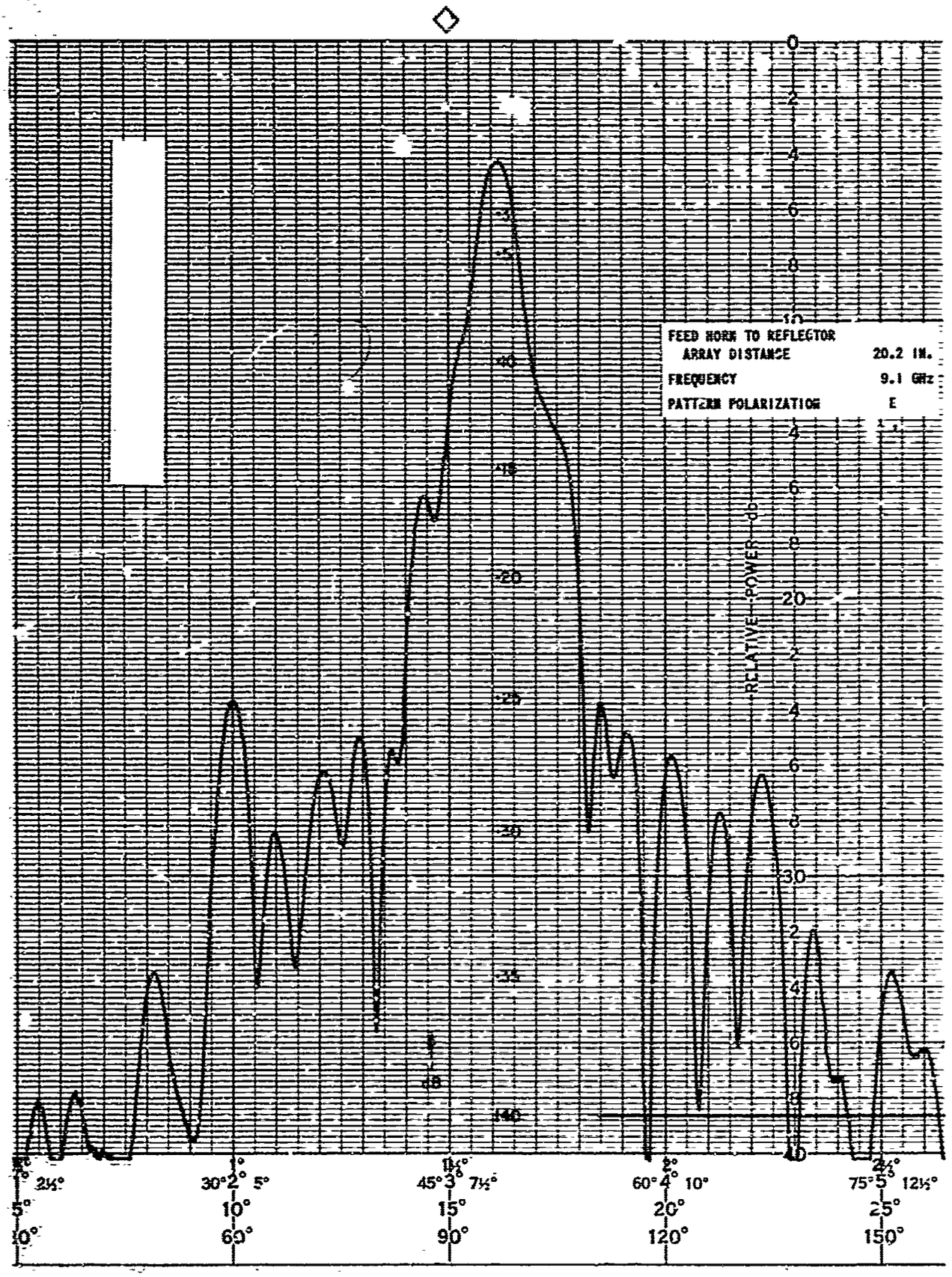

FIGURE 82. ANTENNA PATTERN PERFORMANCE WITH PARTIAL SECOND SHORT SURFACE ADJUSTMENT AND ASYMMETRICAL INDUCTIVE IRIS MATCHING

3-10 FEED-SUBREFLECTOR ARRAY PERFORMANCE

To obtain a better indication of main reflecting dish illumination by the use of feed-subreflector array patterns, the test arrangement shown in figure 83 was established. The subreflector array and feed were rotated about point P with the illumination being provided by a fixed transmitting horn. A bolometer was mounted on the feed and the output used to drive a pen recorder. Figures 84 through 100 show the resulting patterns for the parameters listed in table 1. A test frequency of 9.1 GHz was used throughout.

The feed-subreflector array patterns confirmed those taken on single elements with regard to H-plane element amplitude variations and nulls throughout the included scan angle of the subreflector array. Using this arrangement, another type of inductive iris was investigated with the goal of broadening the H-plane element pattern.

Table 1

FEED-SUBREFLECTOR ARRAY PATTERNS AT 9.1 GHz

Figure No.	Iris	Short Setting	Pattern Plane	Feed to Subreflector Array Distance (in.)
84	None	2	E	20.25
85	None	2	E	19.25
86	None	2	H	20.25
87	None	2	E	--
88	None	2	H	19.25
89	None	5	H	20.50
90	None	5	H	19.50
91	None	5	H	19.50
92	None	5	H	19.50
93	None	5	E	19.50
94	Type 2	5	H	19.50
95	None	5	H	19.50
96	None	5	H	19.50
97	Type 2	5	E	19.50
98	Type 2	5	H	19.50
99	Type 3	5	E	19.50
100	Type 3	5	H	19.50

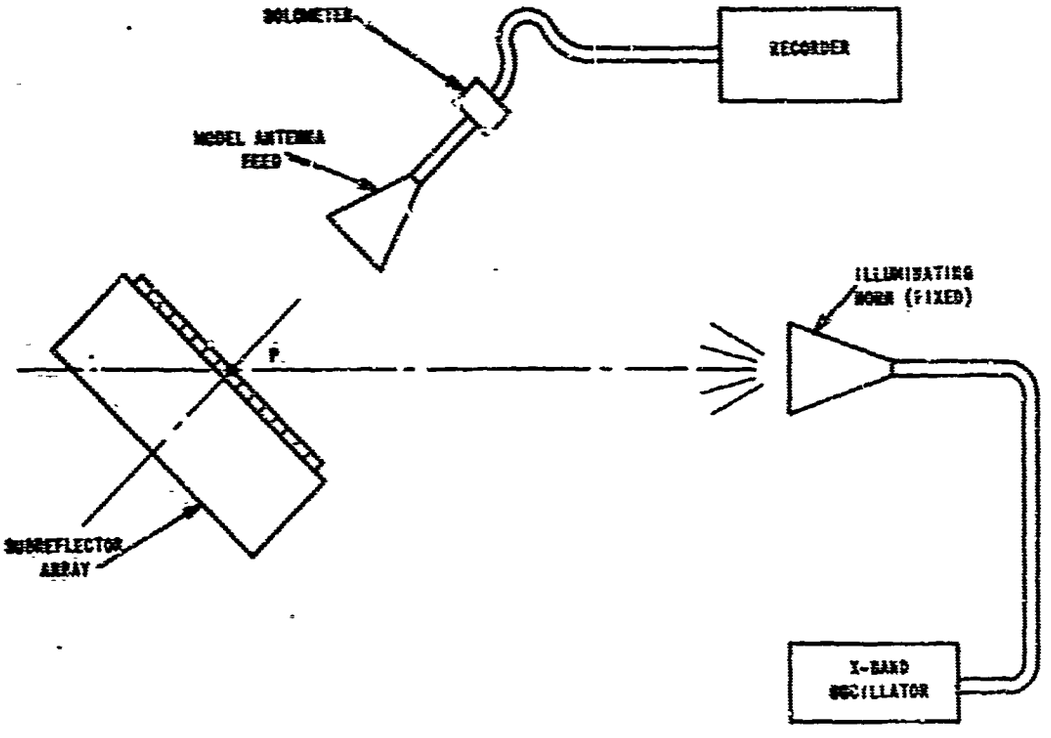

FIGURE 83. FEED-SUBREFLECTOR ARRAY PATTERN SET-UP

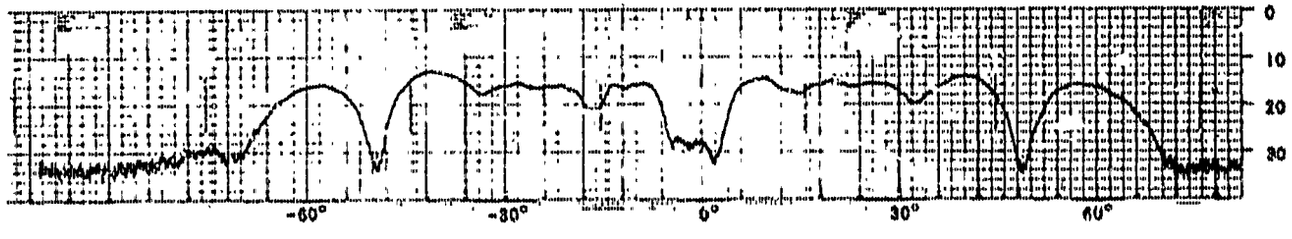

FIGURE 84. FEED-SUBREFLECTOR ARRAY PATTERN PERFORMANCE

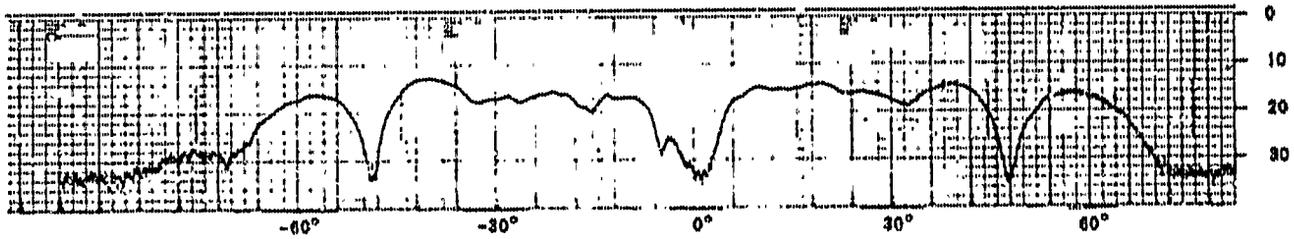

FIGURE 85. FEED-SUBREFLECTOR ARRAY PATTERN PERFORMANCE

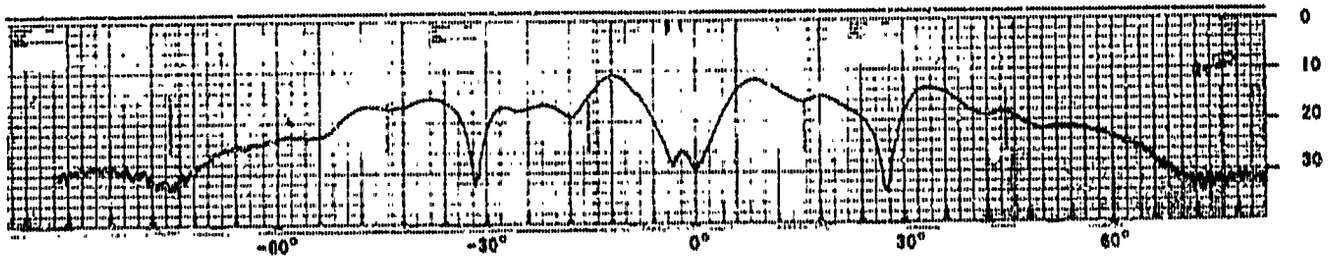

FIGURE 86. FEED-SUBREFLECTOR ARRAY PATTERN PERFORMANCE

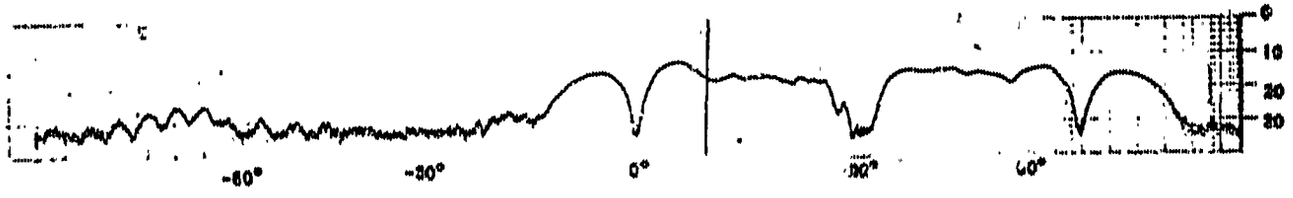

FIGURE 87. FEED-SUBREFLECTOR ARRAY PATTERN PERFORMANCE

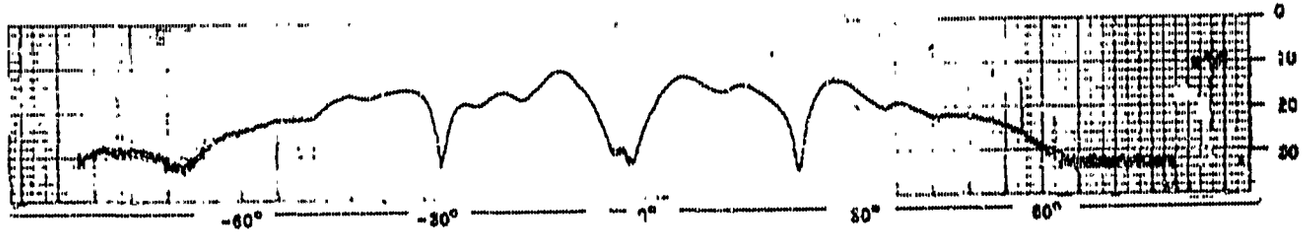

FIGURE 88. FEED-SUBREFLECTOR ARRAY PATTERN PERFORMANCE

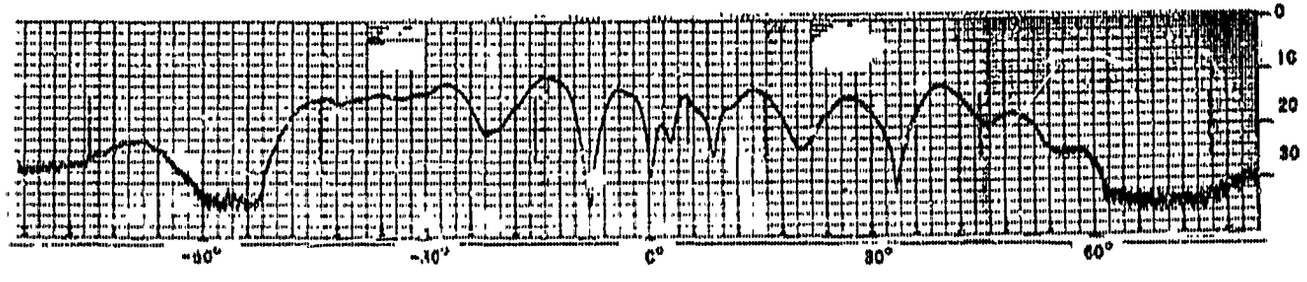

FIGURE 89. FEED-SUBREFLECTOR ARRAY PATTERN PERFORMANCE

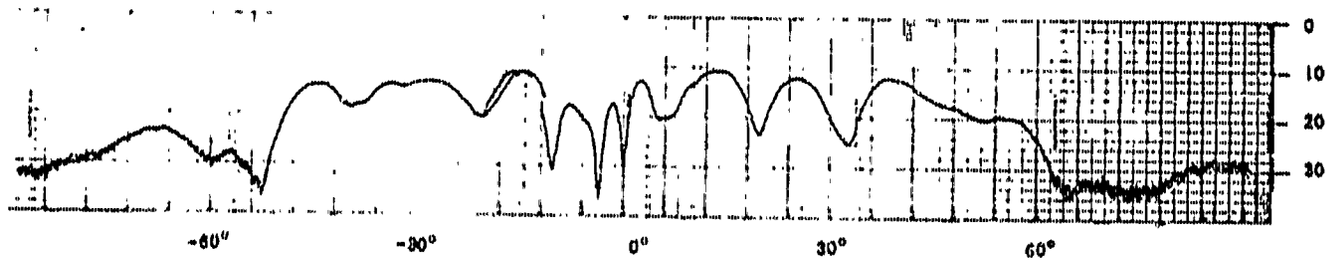

FIGURE 90. FEED-SUBREFLECTOR ARRAY PATTERN PERFORMANCE

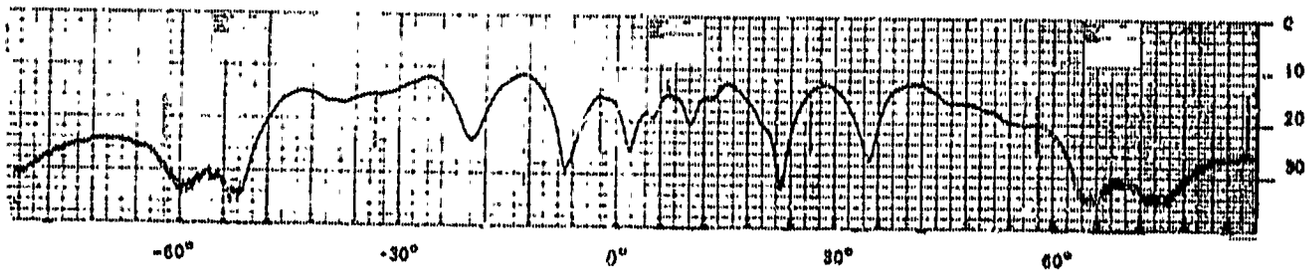

FIGURE 91. FEED-SUBREFLECTOR ARRAY PATTERN PERFORMANCE

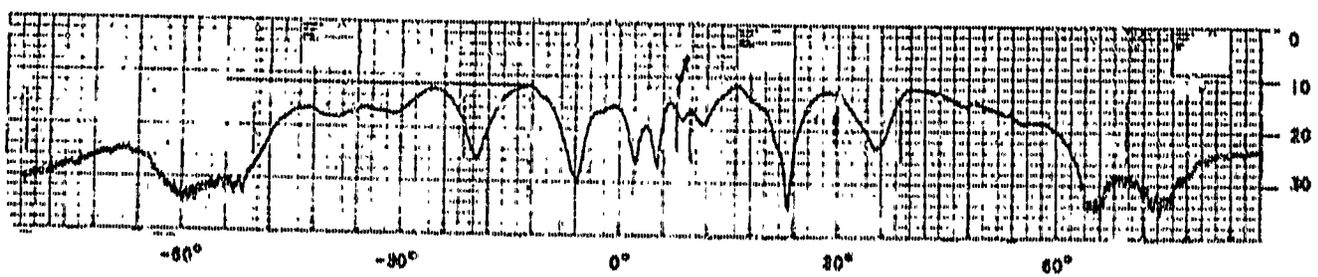

FIGURE 92. FEED-SUBREFLECTOR ARRAY PATTERN PERFORMANCE

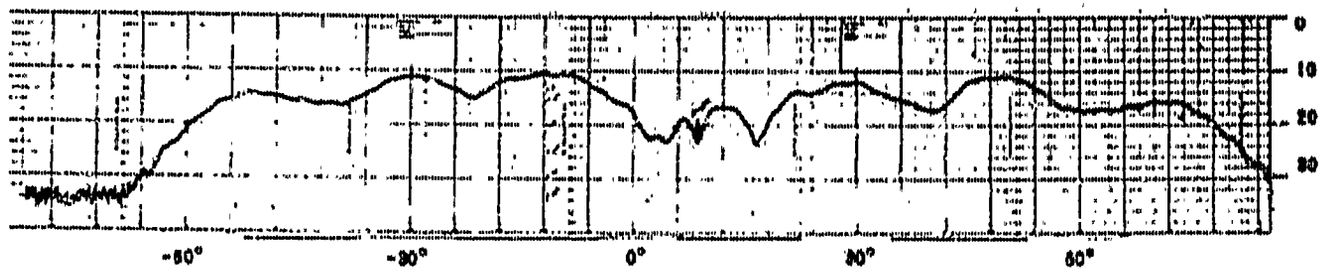

FIGURE 93. FEED-SUBREFLECTOR ARRAY PATTERN PERFORMANCE

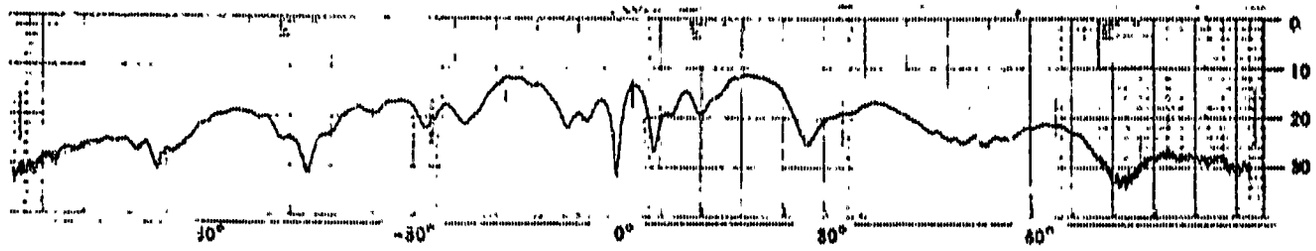

FIGURE 94. FEED-SUBREFLECTOR ARRAY PATTERN PERFORMANCE

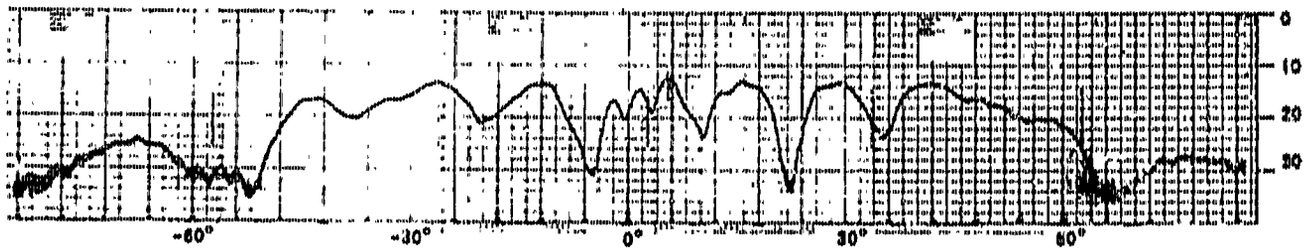

FIGURE 95. FEED-SUBREFLECTOR ARRAY PATTERN PERFORMANCE

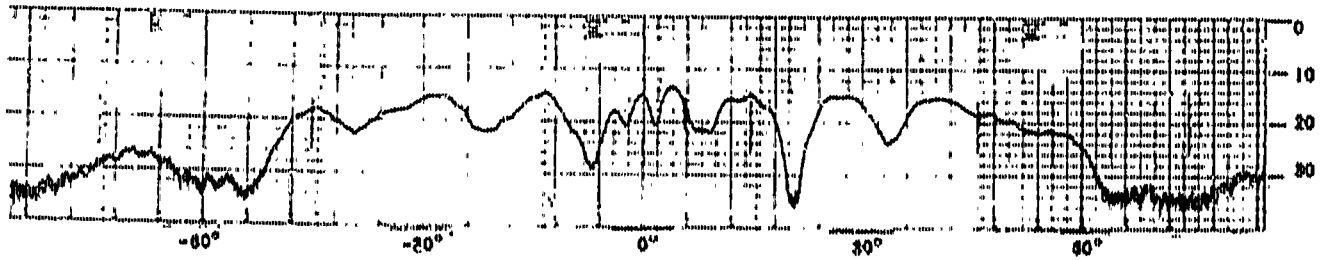

FIGURE 86. FEED-SUBREFLECTOR ARRAY PATTERN PERFORMANCE

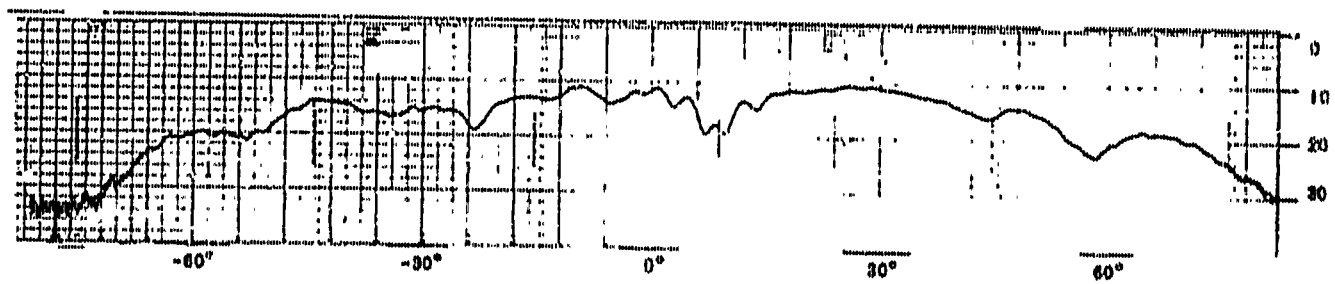

FIGURE 87. FEED-SUBREFLECTOR ARRAY PATTERN PERFORMANCE

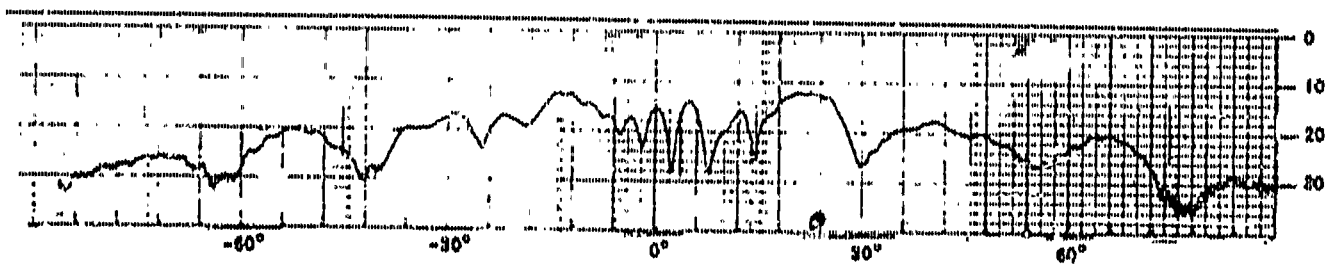

FIGURE 88. FEED-SUBREFLECTOR ARRAY PATTERN PERFORMANCE

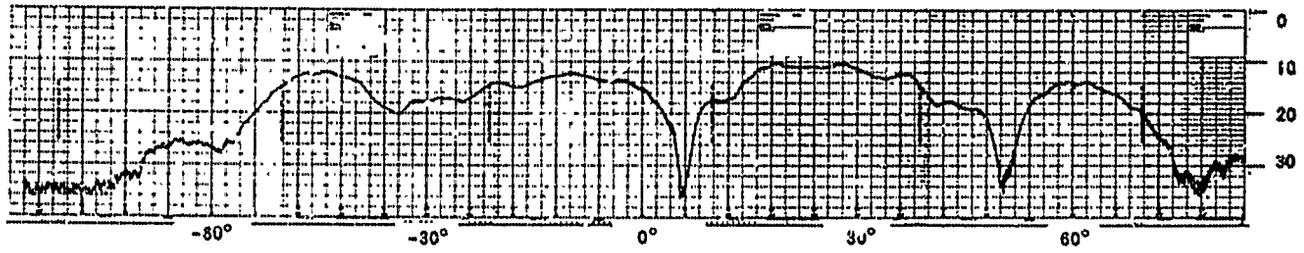

FIGURE 99. FEED-SUBREFLECTOR ARRAY PATTERN PERFORMANCE

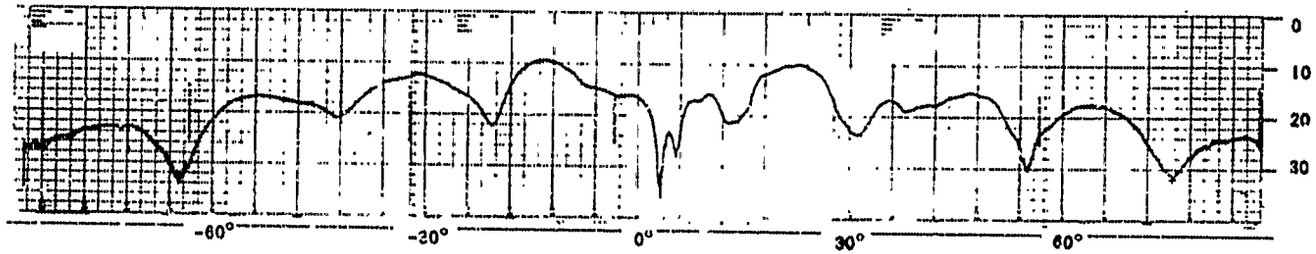

FIGURE 100. FEED-SUBREFLECTOR ARRAY PATTERN PERFORMANCE

The second and third type irises used for the feed-subreflector array patterns are illustrated in figures 101 and 102. As with the first type of irises, only those cells primarily responsible for H-plane performance had irises placed at their entry surface. The third type iris seemed to yield promising results based upon feed-subreflector array pattern performance. These irises gave the following secondary pattern results, with the subreflector array at the best focus H-plane position. The pattern is shown in figure 103 and is summarized below for the fifth short setting with 19.3-inch spacing from feed to subreflector array and type 3 irises:

Frequency (GHz)	Pattern Plane	Half Power Beamwidth (deg)	10-dB Beamwidth (deg)	20-dB Beamwidth (deg)	First Two Sidelobes (dB)	Other Sidelobes (dB)
9.1	H	1.08	1.94	-	15	17

The poor H-plane beamwidth obtained with these inductive irises can be attributed only to the fact that an incorrect short setting is being used. A phase error existed which may have been corrected by a shorting surface readjustment, but the exact formulation of the change is not easily determined.

3-11 SUBREFLECTOR ARRAY, FIFTH SHORT SETTING, MONOPULSE TYPE FEED HORN

The single-plane monopulse type feed horn shown in figure 1 was mounted in place of the conical pencil beam feed. Figures 105 through 111 are the H-plane sum and E-plane sum and difference patterns using the fifth short setting for the subreflector array (no irises). The gain of the model antenna is slightly lower using this type feed when compared to results with the conical feed at the fifth short setting. This is due to the somewhat higher feed spillover and to the fact that the feed illumination is only approximately that for which the subreflector array is designed. A summary of the performance for the fifth short setting with 19.4-inch spacing from feed to subreflector array and the monopulse type feed horn is as follows:

Frequency (GHz)	Pattern Plane	Gain (dB)	Half Power Beamwidth (deg)	10-dB Beamwidth (deg)	20-dB Beamwidth (deg)	First Two Sidelobes (dB)	Other Sidelobes ($\pm 15^{\circ}$)(dB)
8.6	H	46.7	0.78	1.26	1.71	19	20
	E	--	0.75	1.25	1.51	16	25
9.1	H	46.1	0.85	1.41	1.83	17	29
	E	--	0.67	1.00	1.37	15	26
9.6	H	46.4	0.80	1.40	1.90	17	24
	E	--	0.65	1.00	1.35	15	19

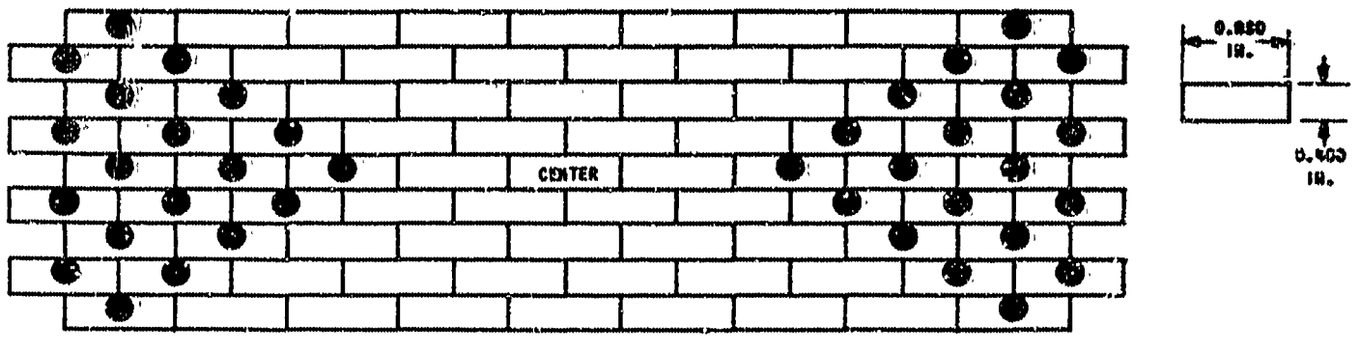

FIGURE 101. IRIS MOUNTING GEOMETRY

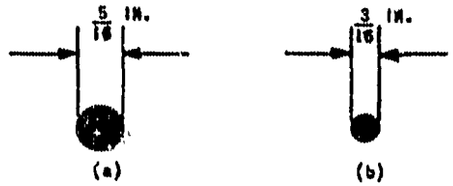

FIGURE 102. IRIS GEOMETRY

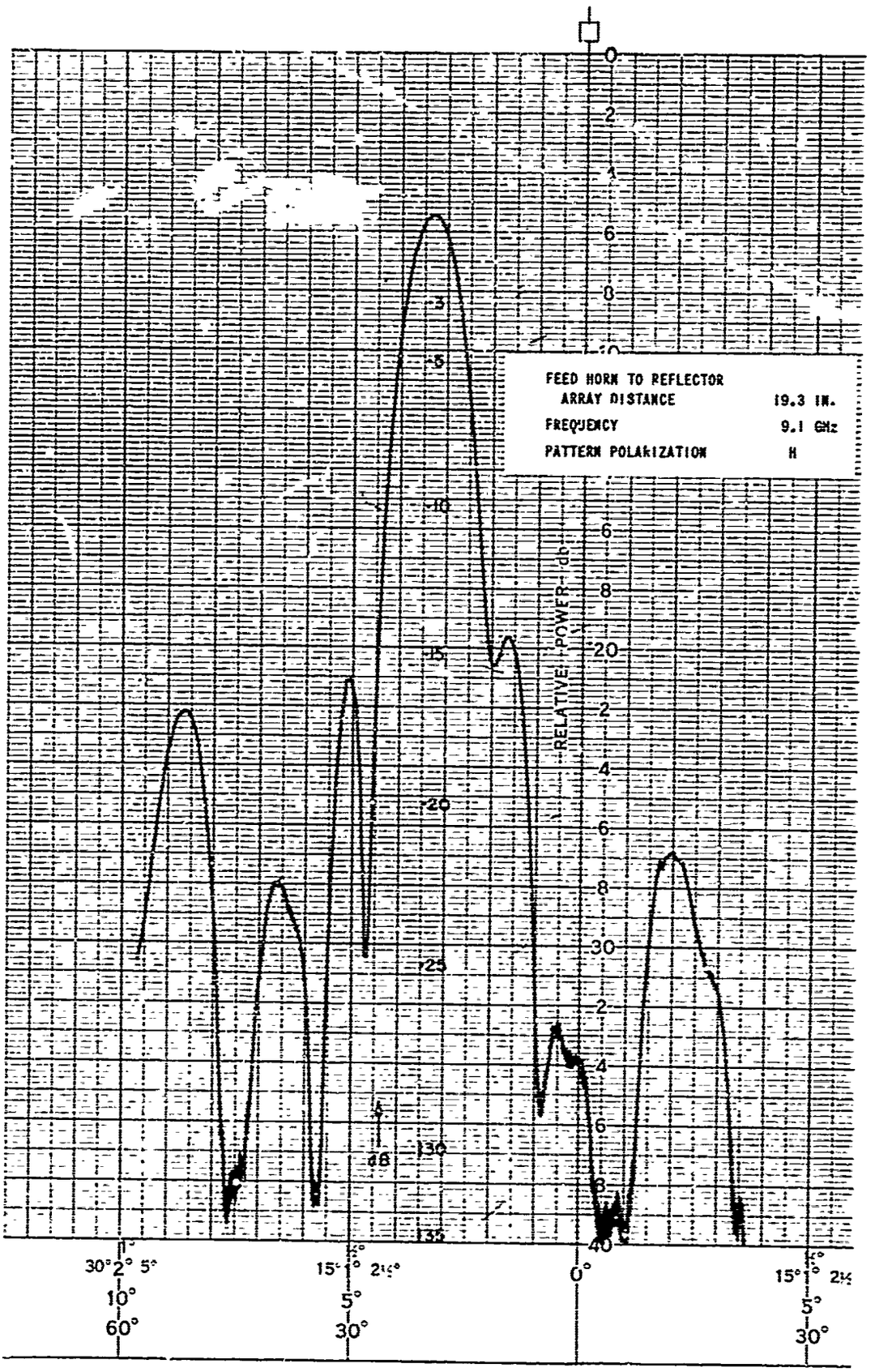

FIGURE 103. ANTENNA PATTERN PERFORMANCE WITH TYPE 3 IRIS MATCHING

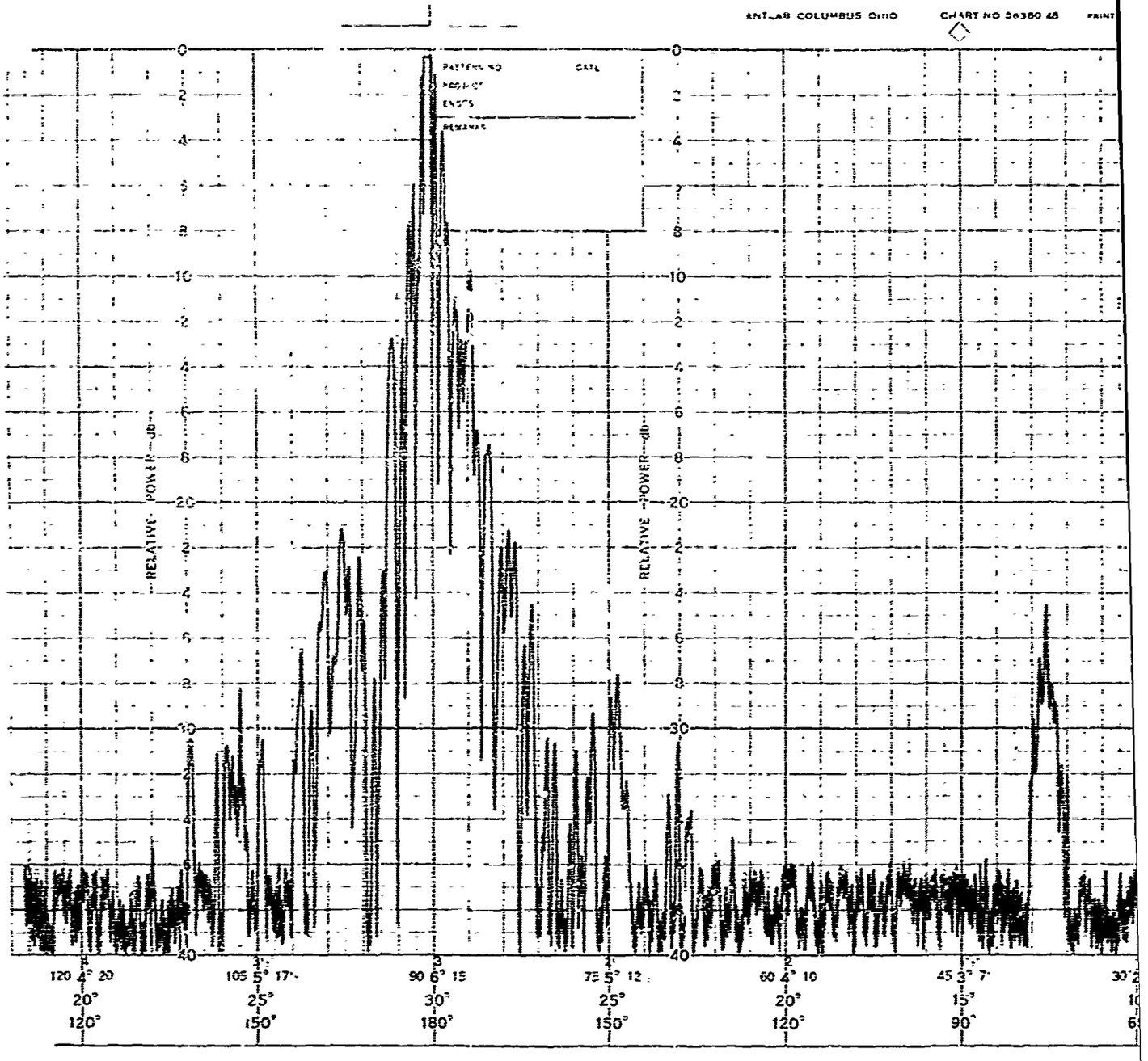

FIGURE 104. REPRESENTATIVE WIDE ANGLE PATTERN

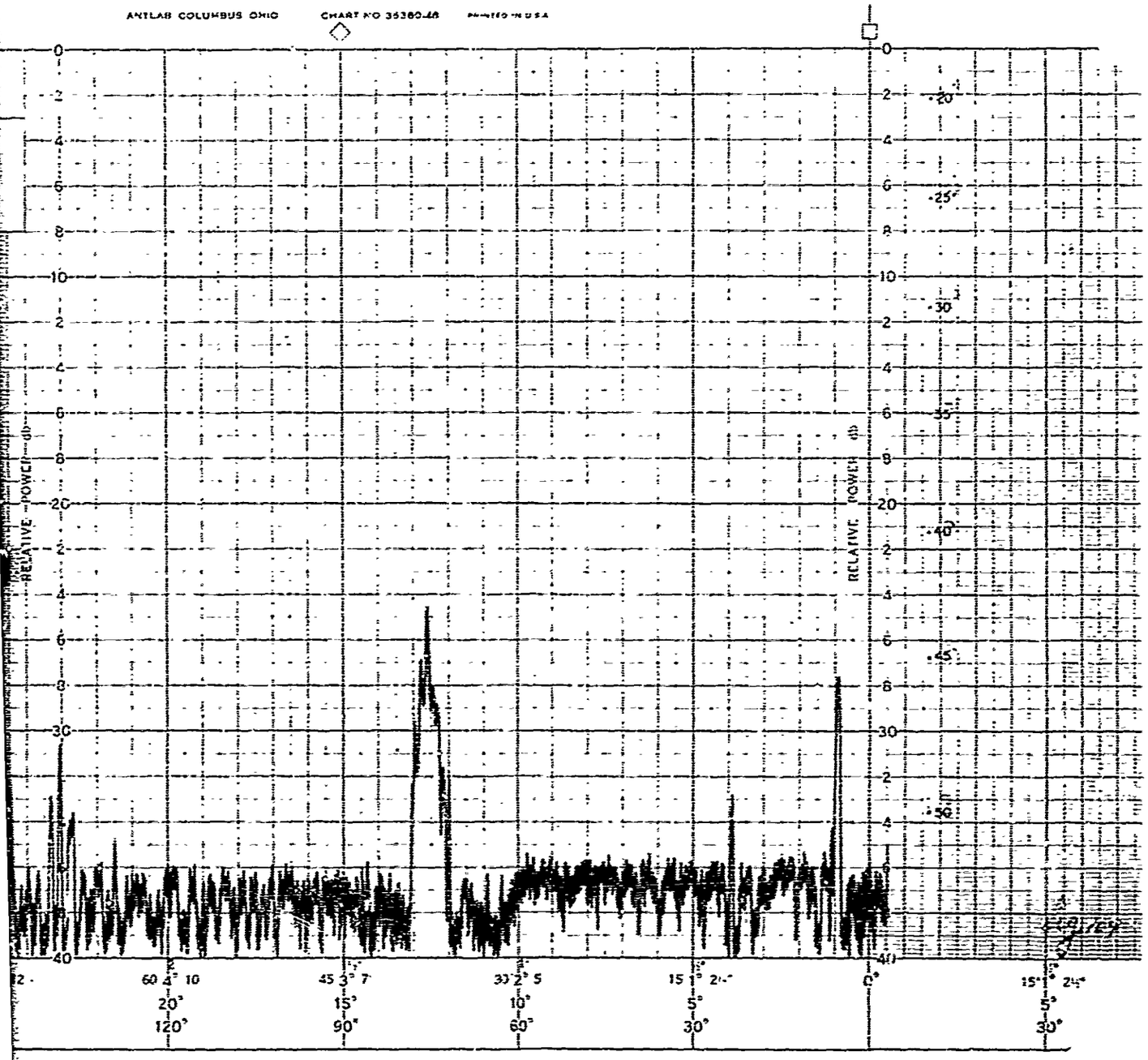
ANTLAB COLUMBUS OHIO
CHART NO 35360-46
RELATIVE POWER dB
RELATIVE POWER dB
0
2
4
6
8
10
20
30
40
-20
-25
-30
-35
-40
-45
-50
60 4° 10
45 3° 7
33 2° 5
15 1° 2½°
0°
15° 2½°
20°
15°
10°
5°
5°
120°
90°
60°
30°
30°

B

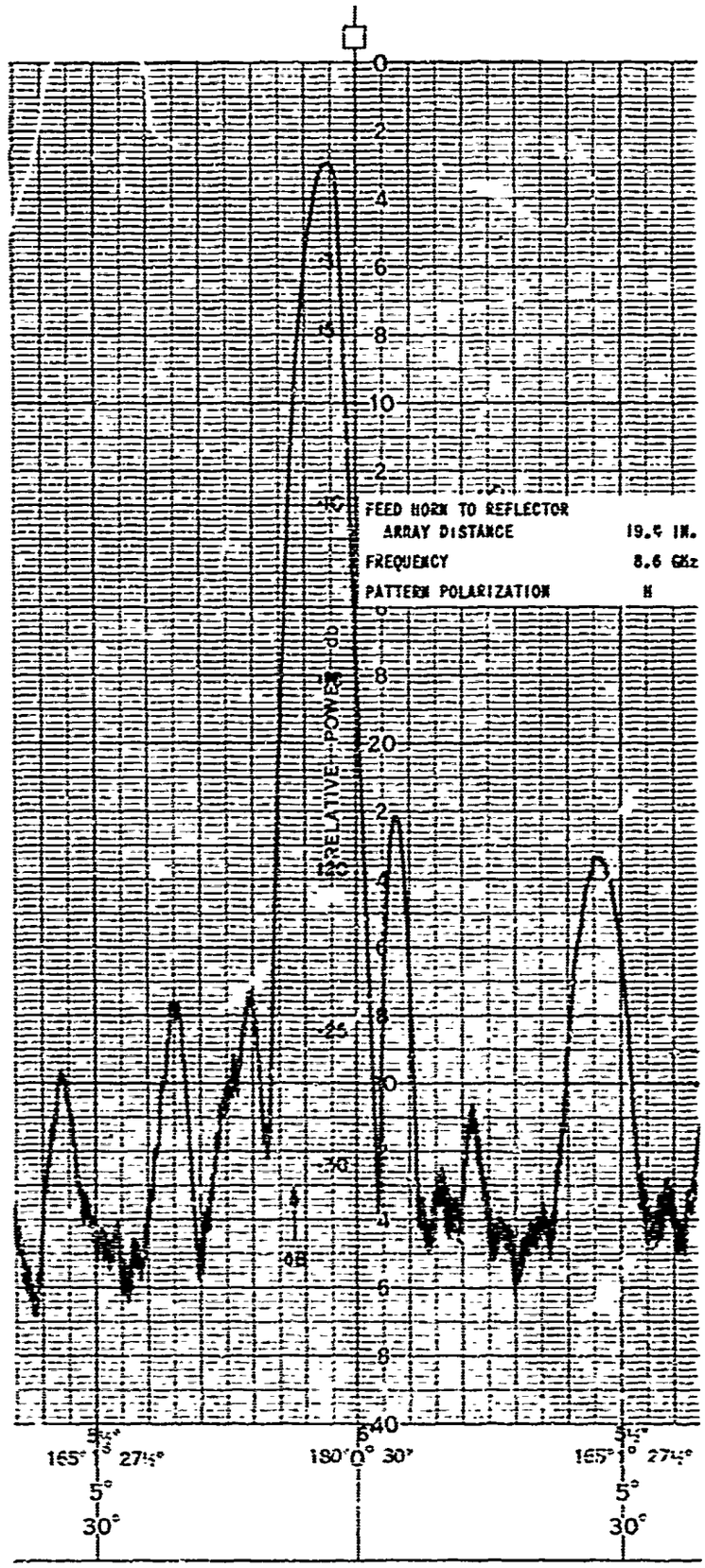

FIGURE 105. ANTENNA PATTERN PERFORMANCE WITH MONOPULSE FEED HORN

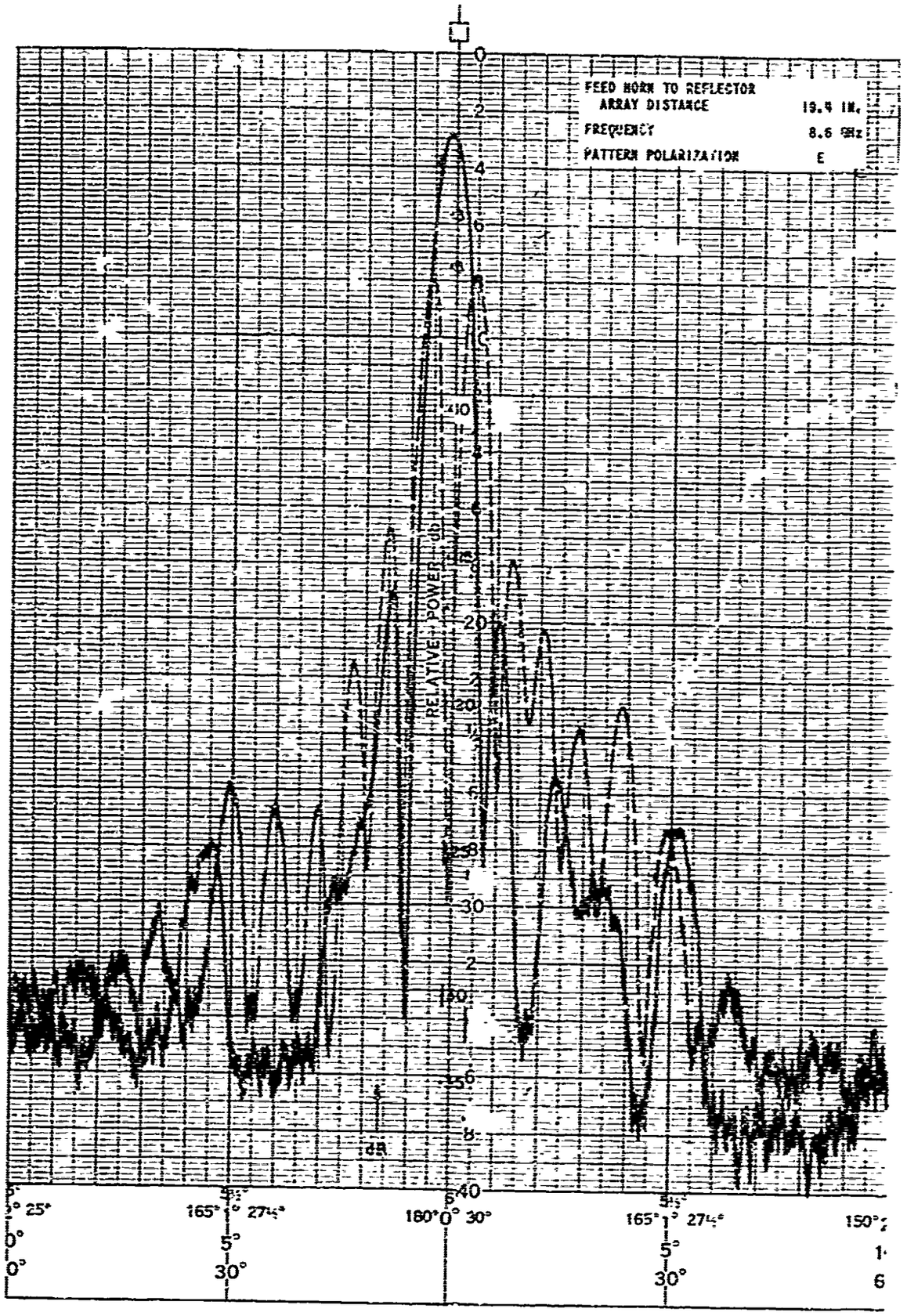

FIGURE 106. ANTENNA PATTERN PERFORMANCE WITH MONOPULSE FEED HORN

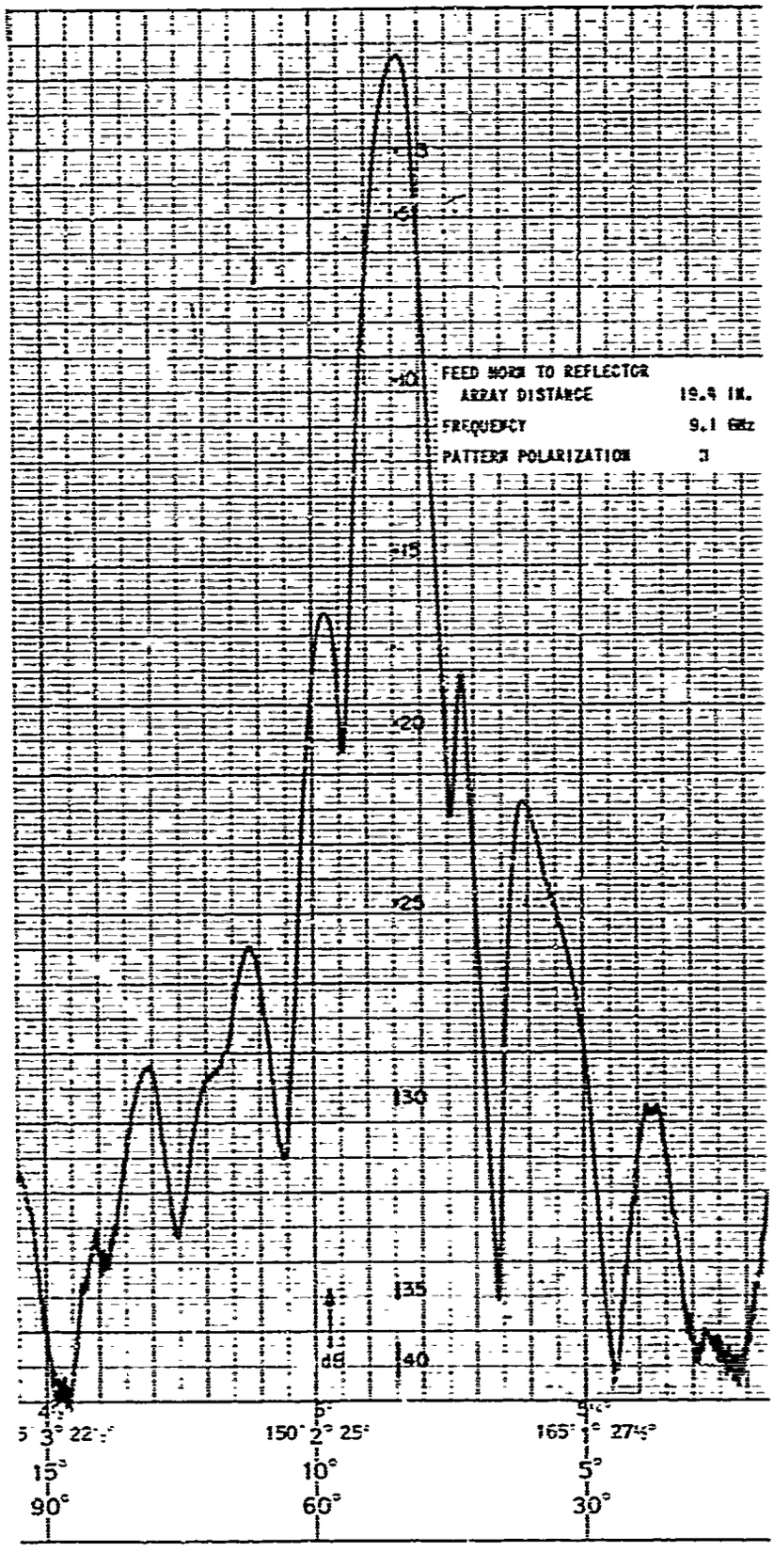

FIGURE 107. ANTENNA PATTERN PERFORMANCE WITH MONOPULSE FEED HORN

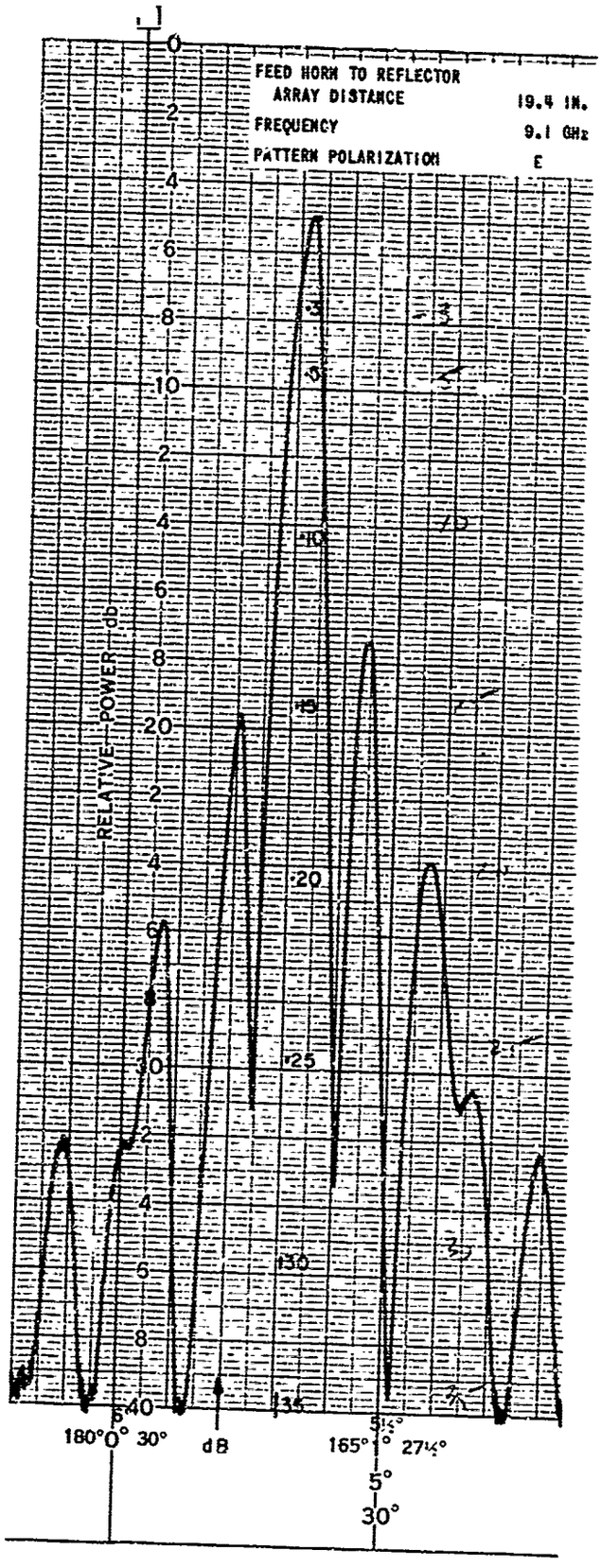

FIGURE 108. ANTENNA PATTERN PERFORMANCE WITH MONOPULSE FEED HORN

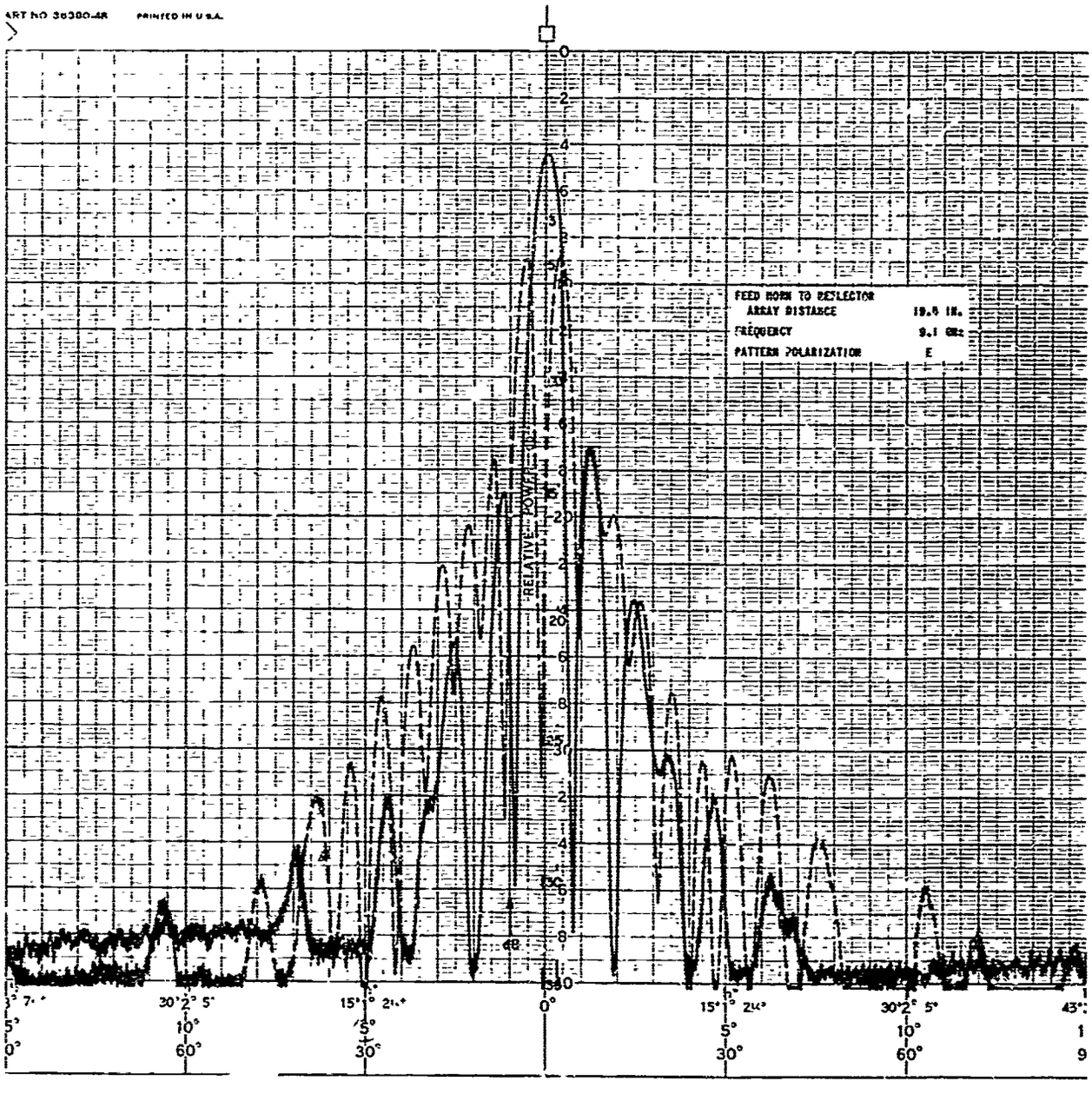

FIGURE 109. ANTENNA PATTERN PERFORMANCE WITH MONOPULSE FEED HORN

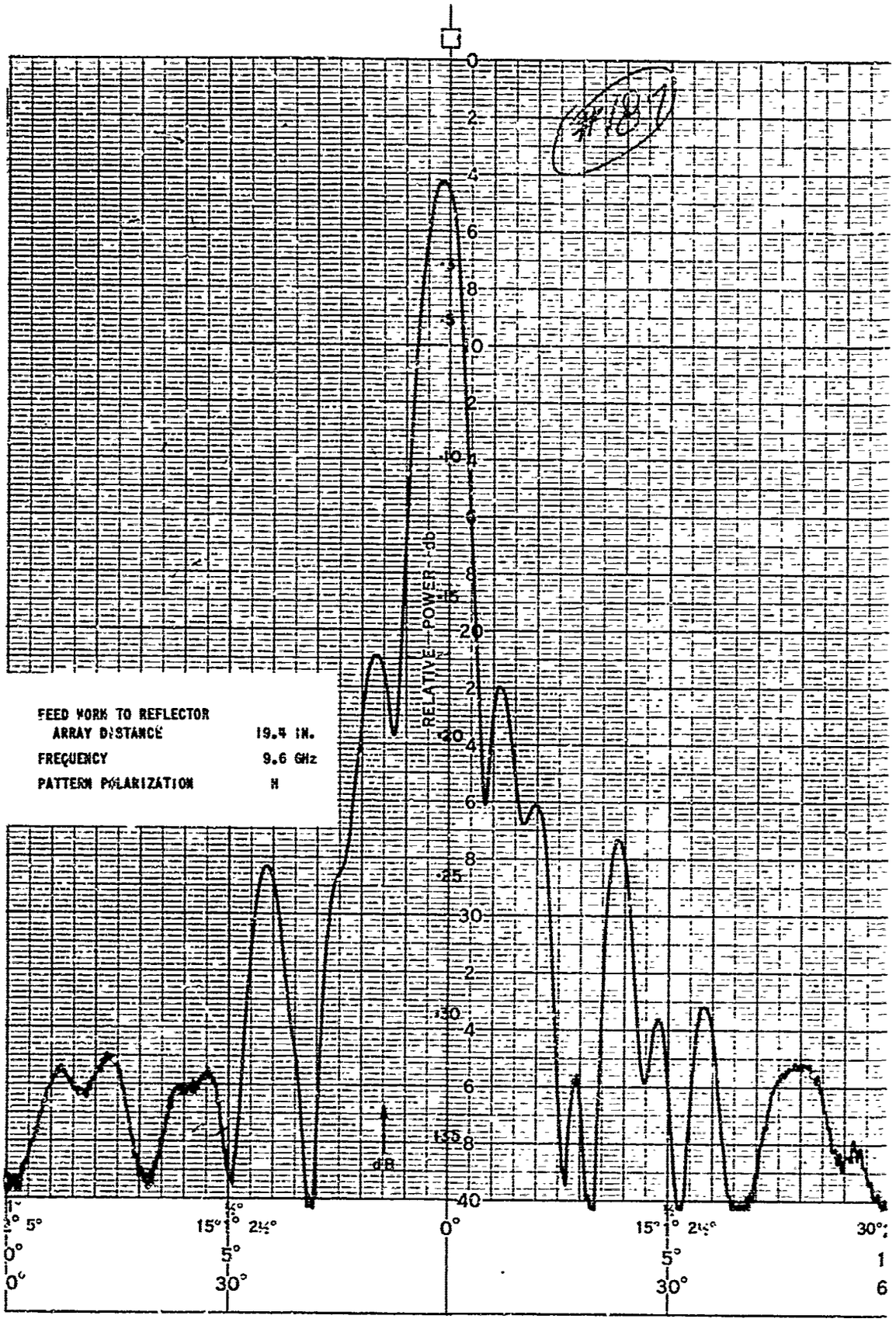

FIGURE 110. ANTENNA PATTERN PERFORMANCE WITH MONOPULSE FEED HORN

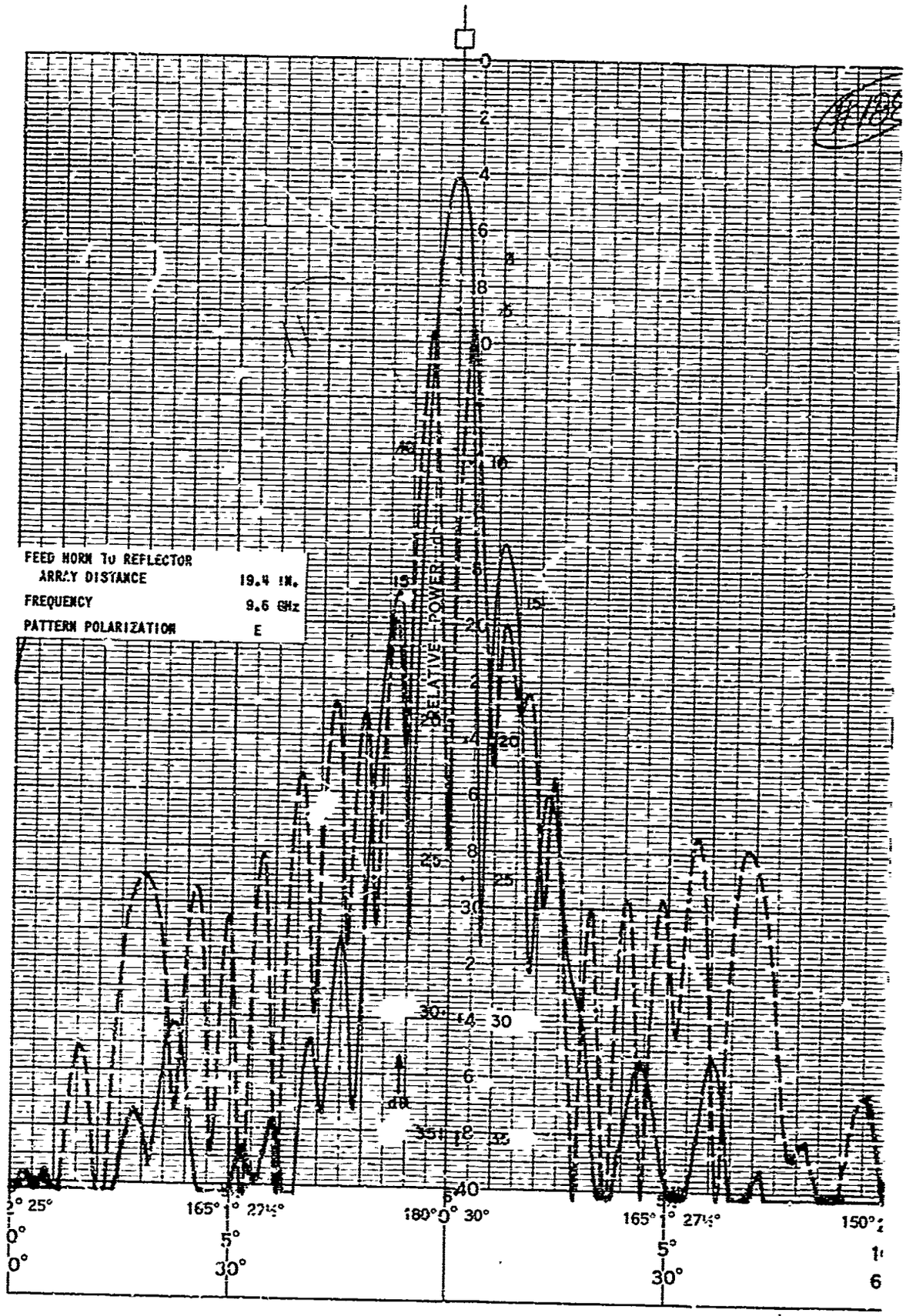

FIGURE III. ANTENNA PATTERN PERFORMANCE WITH MONOPULSE FEED HORN

The above results show that it is possible to use effectively a monopulse feed with the subreflector array.

3-12 VSWR OF MODEL ANTENNA

VSWR of the model antenna was measured with both the pencil beam and monopulse feed horns using the fifth short setting on the subreflector array. A somewhat higher mismatch at 9.1 GHz and 8.6 GHz accounts for some loss of gain at these frequencies. The results follow:

Feed Horn	Frequency (GHz)	VSWR
Pencil Beam	10	1.06:1
	9.6	1.14:1
	9.1	1.30:1
	8.6	1.30:1
	8.2	1.20:1
Monopulse Type	9.6	1.16:1
	9.1	1.21:1
	8.6	1.08:1

3-13 POLARIZATION INDEPENDENT SUBREFLECTOR ARRAY

At the time the dielectric-filled subreflector array was fabricated, the latest information available was the third set of computer-derived short settings. These settings were appropriately transformed to concur with the loaded square waveguide cells of the dielectric array. Once placed, the shorts can be changed by melting out the wax from the cells. Figures 112 and 113 are the pattern data for this subreflector array. Figure 114 is a photograph of the subreflector array. The tabulated results follow:

Frequency (GHz)	Pattern Plane	Gain (dB)	Half Power Beamwidth (deg)	10-dB Beamwidth (deg)	20-dB Beamwidth (deg)	First Two Sidelobes (dB)	Other Sidelobes (dB)
9.1	H	45.1	0.76	1.40	--	15	22
	E	--	0.73	1.23	--	15	20

The results indicate that optimization of the short positions for the polarization independent subreflector array has not been achieved.

3-14 NOISE TEMPERATURE MEASUREMENT

Measurement of antenna model noise temperature is made in accordance with IEEE standards [6]. This consists of a comparison of the antenna noise output with that of a standard noise temperature load. To minimize measurement error, the noise temperature of the standard is selected to be close to the

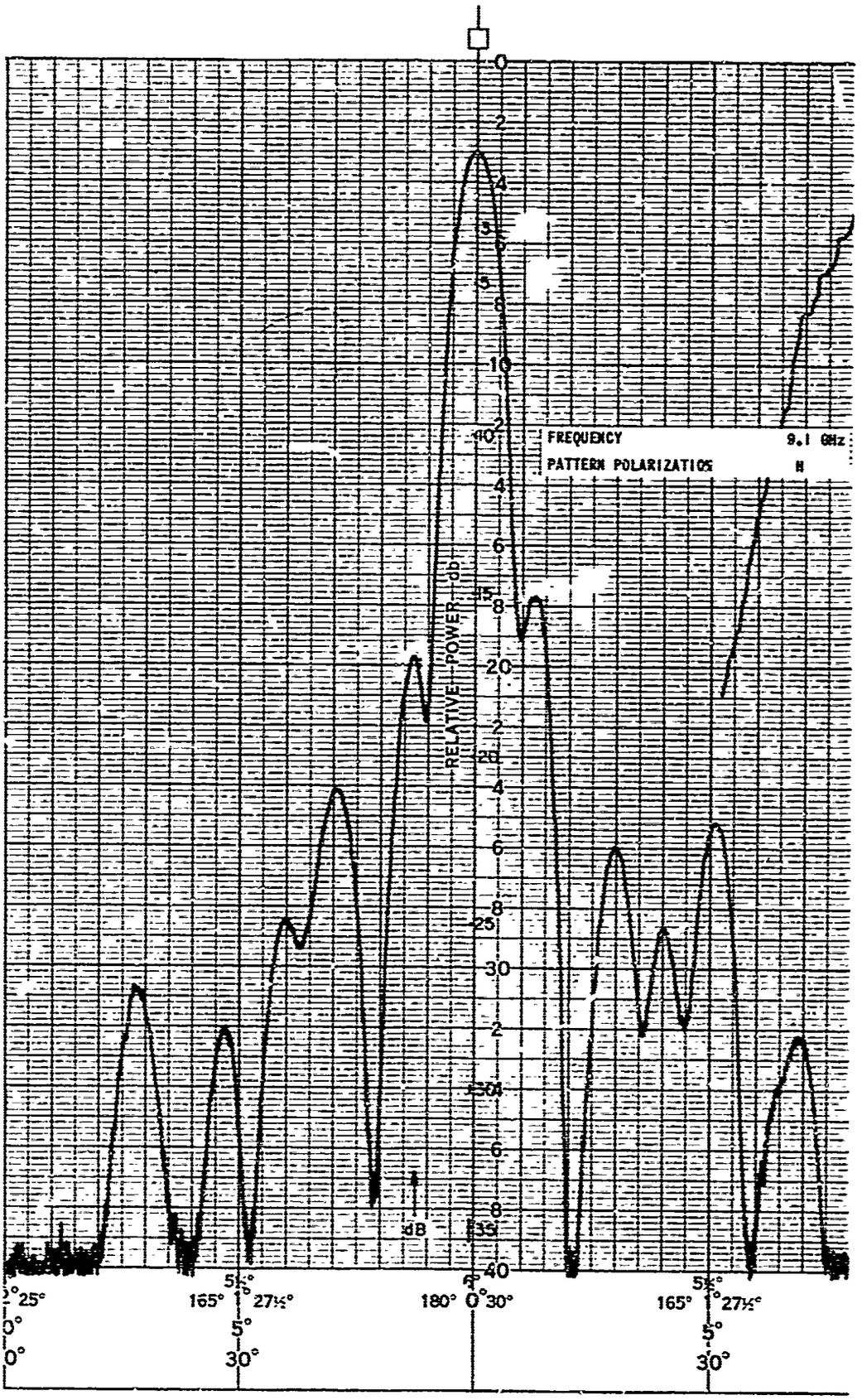

FIGURE 112. ANTENNA PATTERN PERFORMANCE WITH POLARIZATION INDEPENDENT SUBREFLECTOR ARRAY

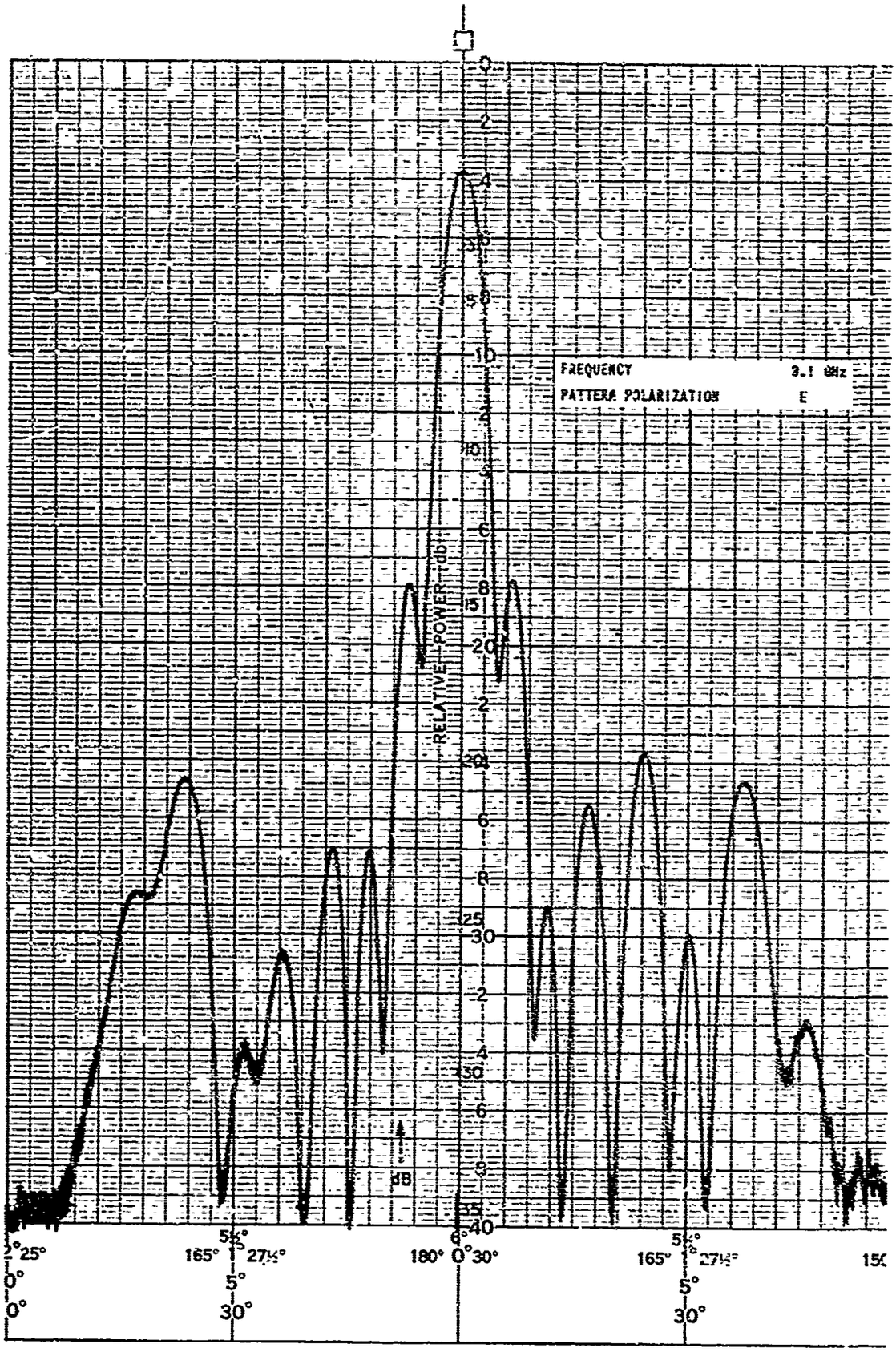

FIGURE 113. ANTENNA PATTERN PERFORMANCE WITH POLARIZATION INDEPENDENT SUBREFLECTOR ARRAY

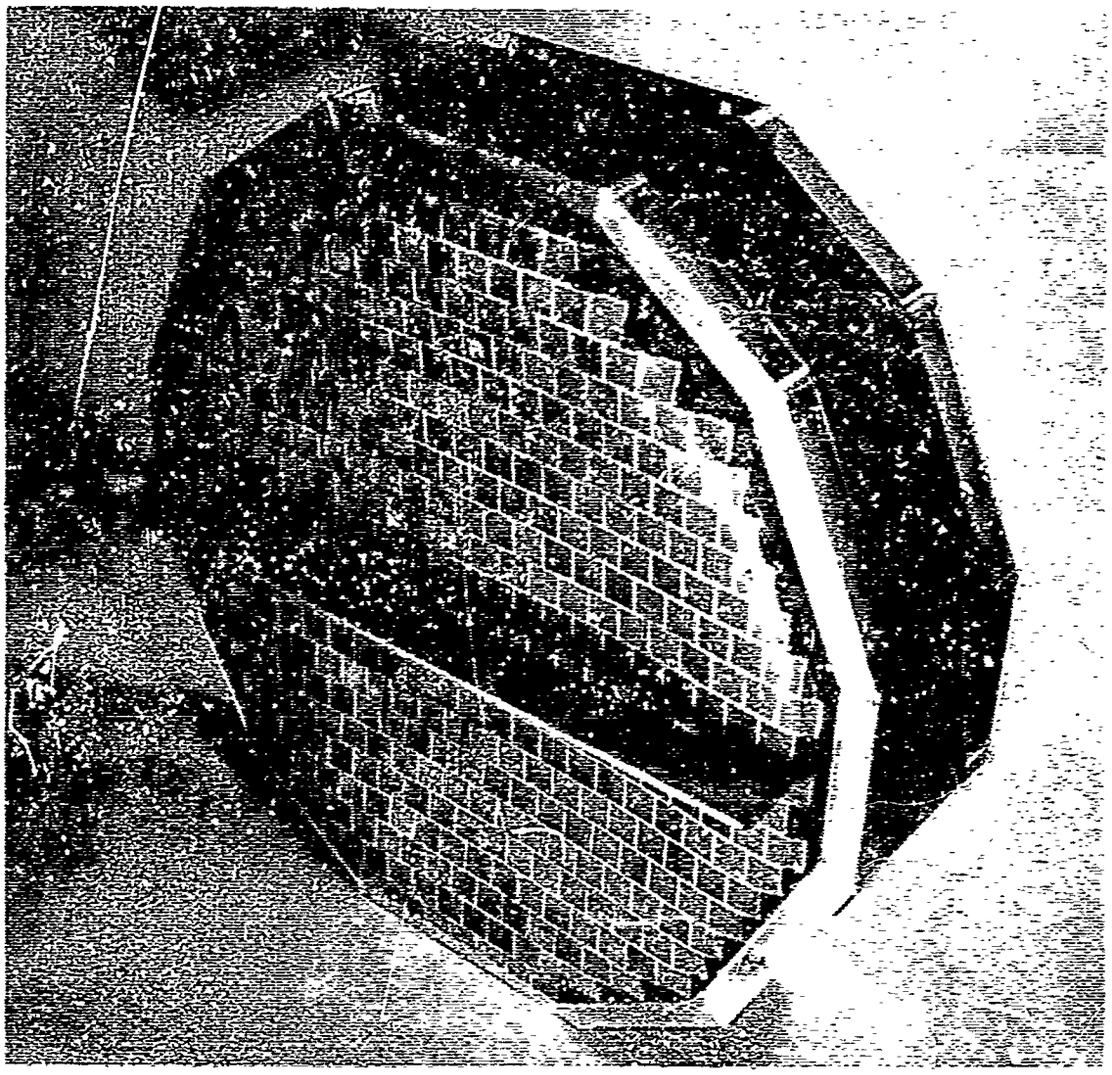

FIGURE 114. POLARIZATION INDEPENDENT SUBREFLECTOR ARRAY

anticipated antenna temperature. The standard load is a matched resistive termination of controlled physical temperature using liquid nitrogen (77.4°K) as a cooling agent. The standard is purchased from and calibrated by Maury Microwave Corporation. The load has a VSWR less than 1.05 over a 1-percent frequency band centered at 9.1 GHz, and is calibrated to a temperature accuracy of ±1°K. The quoted noise temperature of this load is 80°K. The noise temperature measurement circuit consists of single-pole double-throw waveguide switch connected alternately to the antenna under tests and the standard load. The noise output is connected through a precision waveguide attenuator to a microwave receiver that is pretuned to the test frequency. The precision attenuator is adjusted so that receiver noise power output is the same for alternate positions of the microwave switch. If L_a is the attenuator power loss ratio with the switch connected to the antenna, and L_s is the attenuator power loss ratio with the switch connected to the standard load, then the antenna temperature is given in terms of the ambient temperature and the standard load temperature by

$$T_{ant} = T_{amb} + \frac{L_a}{L_s} (T_{std} - T_{amb})$$

Measurements have been made for the antenna pointing within 15 degrees of zenith and during the evening to minimize external noise sources.

The measured noise temperature of the linearly polarized subreflector array with the pencil beam feed is 27°K. This represents the average of 150 measurements.

The measured noise temperature of the linearly polarized subreflector array with the monopulse feed is 32°K. This represents the average of 75 measurements.

In order to use the nitrogen cooled load at other than 9.1 GHz, the VSWR of the load was measured and used as a basis for recalibration. The following is a tabulation of the load VSWR, calibrated load temperature, and measured noise temperature of the pencil beam feed and the monopulse feed using the linearly polarized subreflector array.

MODEL ANTENNA NOISE TEMPERATURE

Frequency (GHz)	Load VSWR	Load Temp. (°K)	Pencil Beam Feed Temp. (°K)	Monopulse Feed Temp. (°K)
8.2	1.23	84	38	44
8.6	1.14	82	23	26
9.1	1.06	81	27	32
9.6	1.16	83	26	24
10.0	1.28	85.5	35	37

SECTION 4

DISCUSSION AND SUMMARY OF TEST RESULTS

The following is a discussion of the model antenna performance with respect to the established goals of the program. Established goals are as follows:

ANTENNA PERFORMANCE WITH PENCIL BEAM FEED

Parameter	Minimum	Objective
Noise temperature	50°K	35°K
Efficiency	68%	74%
Bandwidth	±5% at X band	±10% at X band
Gain	46 dB	46 dB
VSWR	Less than 1.3	Less than 1.3
Half power beamwidth	Less than 0.75°	Less than 0.70°
10-dB beamwidth	Less than 1.3°	Less than 1.2°
20-dB beamwidth	Less than 1.7°	Less than 1.7°
First two sidelobes	Less than -15 dB	Less than -15 dB
Other sidelobes within ±15°	Less than -25 dB	Less than -25 dB
Remaining sidelobes to ±180°	Less than -40 dB	Less than -40 dB
Polarization	Linear	Linear and circular

ANTENNA PERFORMANCE WITH MONOPULSE FEED

Parameter	Objective
Noise temperature	50^{o}K
Efficiency	60%
Bandwidth	±5% at X band
Gain	46 dB
VSWR	Less than 1.5
Half power beamwidth	Less than 0.8^{o}
10-dB beamwidth	Less than 1.4^{o}
20-dB beamwidth	Less than 1.9^{o}
First two sidelobes	Less than -15 dB
Other sidelobes within $\pm 15^{o}$	Less than -25 dB
Remaining sidelobes to $\pm 180^{o}$	Less than -40 dB
Polarization	Linear

The model tests reported in the previous section include performance using a linearly polarized subreflector array with both a pencil beam and monopulse feed and a polarization independent subreflector array using a pencil beam feed. The summarized results which follow represent the best model performance achieved, which generally corresponds to the fifth short setting for the linearly polarized subreflector array using both pencil beam and monopulse feeds.

4-1 NOISE TEMPERATURE

The noise temperature of the linearly polarized subreflector array with the pencil beam feed is less than 27^{o}K and with the monopulse feed is less than 32^{o}K over a ±5 percent X-Band frequency range. This satisfies the minimum pencil beam feed performance and the objective monopulse feed performance.

4-2 EFFICIENCY

Calculated efficiency for the linearly polarized subreflector array is shown in the tabulation below as a function of frequency:

	8.2 GHz	8.6 GHz	9.1 GHz	9.6 GHz	10.0 GHz
Measured gain (dB)	45.2	46.7	47.1	46.5	47.2
Mismatch loss (dB)	0.04	0.08	0.08	0.02	--
Excess transmission line loss (dB)	0.04	0.04	0.04	0.04	0.04
Excess blockage loss (dB)	0.08	0.08	0.08	0.08	0.08
Directive gain (dB)	45.4	46.9	47.3	46.6	47.3
Maximum gain (dB)	48.1	48.5	49.0	49.5	49.7
Gain loss (dB)	2.7	1.6	1.7	2.9	2.4
Calculated efficiency (percent)	54	69	68	52	58

The first line of the tabulation is the measured gain at the fifth short position for which the best results were obtained. Since no measurements were taken at the two ends of the band, however, the tabulation for this short position uses the third short setting data for these two columns.

The mismatch loss corresponds to the measured VSWR of the model antenna. The excess transmission line loss corresponds to length of waveguide between the feed and access flange.

The excess blockage loss corresponds to mounting and adjustment rings near the subreflector array which were required for model flexibility but which would be eliminated in a final design.

The directive gain of the antenna is the sum of the first four items in the above tabulation.

The maximum gain is that attainable by an ideal aperture of the model diameter (117 inches) at the indicated frequency.

The gain loss is the difference between the ideal maximum gain and the directive gain, and the efficiency, thus, is the gain loss converted to a percentage.

The calculated efficiency is in excess of 68 percent over a 5-percent frequency band and in excess of 52 percent over a ±10-percent frequency band for the linearly polarized subreflector array using the pencil beam feed.

A corresponding efficiency calculation for the monopulse feed is shown below.

	8.6 GHz	9.1 GHz	9.6 GHz
Measured gain (dB)	46.7	46.1	46.4
Mismatch loss (dB)	0.01	0.04	0.02
Excess transmission line loss (dB)	0.04	0.04	0.04
Excess blockage loss (dB)	0.08	0.08	0.08
Directive gain (dB)	46.8	46.3	46.5
Maximum gain (dB)	48.5	49.0	49.5
Gain loss (dB)	1.7	2.7	3.0
Calculated efficiency (percent)	68	54	50

The results indicate that the measurements were made at an adjustment position for the feed which favored the low end of the frequency band. At this end, an efficiency of 68 percent was achieved.

The measured gain of the polarization independent subreflector array of 45.1 dB corresponds to an efficiency of 43 percent. Additional work is required to optimize the performance of this unit.

4-3 BANDWIDTH

The model performance parameters were reported for as much as ±10-percent bandwidth at X band.

4-4 GAIN

The model gain with the linearly polarized subreflector array, and both pencil beam feed and monopulse feed, is more than 46 dB over a ±5-percent frequency band. The measured gain of the polarization independent subreflector array is 45.1 dB at the design frequency.

4-5 VSWR

Model measurements with the linearly polarized subreflector indicate a VSWR of less than 1.3:1 over ±10-percent frequency band for the pencil beam feed, and for ±5-percent frequency band for the monopulse feed.

4-6 HALF POWER BEAMWIDTH

The half power beamwidth for the linearly polarized subreflector array and pencil beam feed is found to be less than 0.70 degree in the E plane and less than 0.82 degree in the H and diagonal planes over a ±5-percent frequency band.

The larger H-plane and diagonal-plane beamwidth is attributed to poorer subreflector array element mismatch in these reflection planes.

The half power beamwidth with the monopulse feed is less than 0.75 degree in the E plane and less than 0.85 degree in the H plane over a ±5-percent frequency band.

4-7 10-dB BEAMWIDTH

The 10-dB beamwidth for linearly polarized subreflector array with pencil beam feed is less than 1.2 degrees in the E plane and less than 1.4 degrees in the H and diagonal planes over a ±5-percent frequency band.

The 10-dB beamwidth for the monopulse feed is less than 1.3 degrees in the E plane and less than 1.41 degrees in the H plane over a ±5-percent frequency band.

4-8 20-dB BEAMWIDTH

The 20-dB beamwidth for the pencil beam feed and linearly polarized subreflector array is less than 1.6 degrees in the E plane over a ±5-percent frequency band. Sidelobe shoulders in the H and diagonal planes smear the 20-dB beamwidth over the ±5-percent frequency band.

The 20-dB beamwidth for the monopulse feed and linearly polarized subreflector array is less than 1.6 degrees in the E plane and less than 1.9 degrees in the H plane over a ±5-percent frequency band.

4-9 FIRST TWO SIDELOBES

Measured first two sidelobes for the linear polarized subreflector array are in excess of 15 dB below the peak over a ±10-percent frequency band for the pencil beam feed and in excess of 15 dB below the peak over a ±5-percent frequency band for the monopulse feed.

4-10 OTHER SIDELOBES WITHIN ±15 DEGREES

Measured sidelobes within ±15 degrees of the beam peak are better than 26 dB below peak level over a 5-percent frequency band and better than 20 dB below peak level over a ±10-percent frequency band for the linearly polarized subreflector array and pencil beam feed.

Measurements with the monopulse feed indicate sidelobes better than 19 dB below peak level over a ±5-percent frequency band.

4-11 REMAINING SIDELOBES TO ±180 DEGREES

Far out sidelobe level measurements for the pencil beam and monopulse feed indicate sidelobe levels below 40 dB of the beam peak over a ±5-percent frequency band. Cross polarized sidelobes are below 40 dB of the beam peak. A representative wide angle pattern is shown in figure 104.

4-12 SUMMARY

A review of the measured performance indicates that significant gain-noise temperature performance improvements have been achieved over a 5-percent frequency band as compared to a conventional Cassegrain subreflector configuration. Despite these performance improvements, the pencil beam model results fall slightly short of the established goals in the following respects. Principally, the H-plane and diagonal-plane beamwidths exceed the established goals by up to 10 percent, which, for most applications, will not be significant. More important, the 68-percent efficiency is achieved over a 5-percent frequency band, rather than ±5 percent.

Although reasonably good performance has been achieved with the linearly polarized subreflector array using both the monopulse and pencil beam feeds, the performance is as yet somewhat less than the theoretically predicted ideal performance. This was found to be due to the poorer H-plane element match as a function of incidence and reflection angles. The measured array element pattern in the H plane possesses sharp dips which occur at angles closer to broadside than the angle corresponding to formation of the first grating lobe. These dips in the H-plane element pattern imply reduced element gain in these directions and reduced illumination efficiency for the parabolic reflector aperture. Further, it was found that changes occur in the element reflection coefficient at these angles which require significantly more shorting surface correction in the H plane as compared to the E plane. Adjustment of the shorting surface significantly reduced the mismatch phase error and eliminated the astigmatic behavior of the subreflector array. The shorting surface adjustment does not eliminate the amplitude error, however, which accounts for the broader H-plane versus E-plane pattern performance of the model antenna with its subreflector array.

The above-mentioned sharp dips in the array element pattern, for certain element configurations, have been reported in the literature. Until very recently, however, the explanation for and prediction of this type of performance was not possible. Recent reported results [8] indicate that the dips in the H-plane element pattern, which are dependent upon the array element and array lattice configuration, can be predicted by considering higher order modes in the aperture array interface. The implication is that further optimization of the subreflector array performance would require modification of the array element and array lattice.

SECTION 5

FOCAL FED LENS-ARRAY DESIGN

The purpose of the focal fed lens-array design is to improve the efficiency and noise temperature of a focal fed parabolic reflector. The mechanism for this improvement essentially is the same as for the subreflector array with a Cassegrain geometry. The lens-array will be placed between the feed and the parabolic reflector and will be designed to affect an aperture illumination transform. That is, the lens-array will transform a tapered feed radiation function into a nearly uniform parabolic reflector illumination function. In addition, the major part of the radiation pattern will be confined within the individual angle between the lens-array and the parabolic reflector to minimize spillover.

5-1 DESIGN EQUATIONS

Consider the geometry shown in figure 115. The cartesian coordinate system originates at the phased center of the feed. A second primed coordinate system is centered at the parabolic reflector focal point such that

$$x' = x,\ y' = y,\ z = z' + a \tag{1}$$

Assume a point on the entry surface of the lens-array, P_{1n}, with coordinates (x_{1n}, y_{1n}, z_{1n}), and a point on the exit surface of the lens-array, P_{2n}, with coordinates (x_{2n}, y_{2n}, z_{2n}). Assume a multicellular waveguide array which is constrained such that

$$x_{1n} = x_{2n}$$

$$y_{1n} = y_{2n} \tag{2}$$

To achieve a spherical phase front at the exit surface of the lens-array

$$\rho_{1n} + \frac{\lambda_o}{\lambda_g}(z_{2n} - z_{1n}) = \rho'_{2n} + C \tag{3}$$

where ρ_{1n} is the distance from the feed phase center to P_{1n}, and ρ'_{2n} is the distance from the parabolic reflector focal point to P_{2n}.

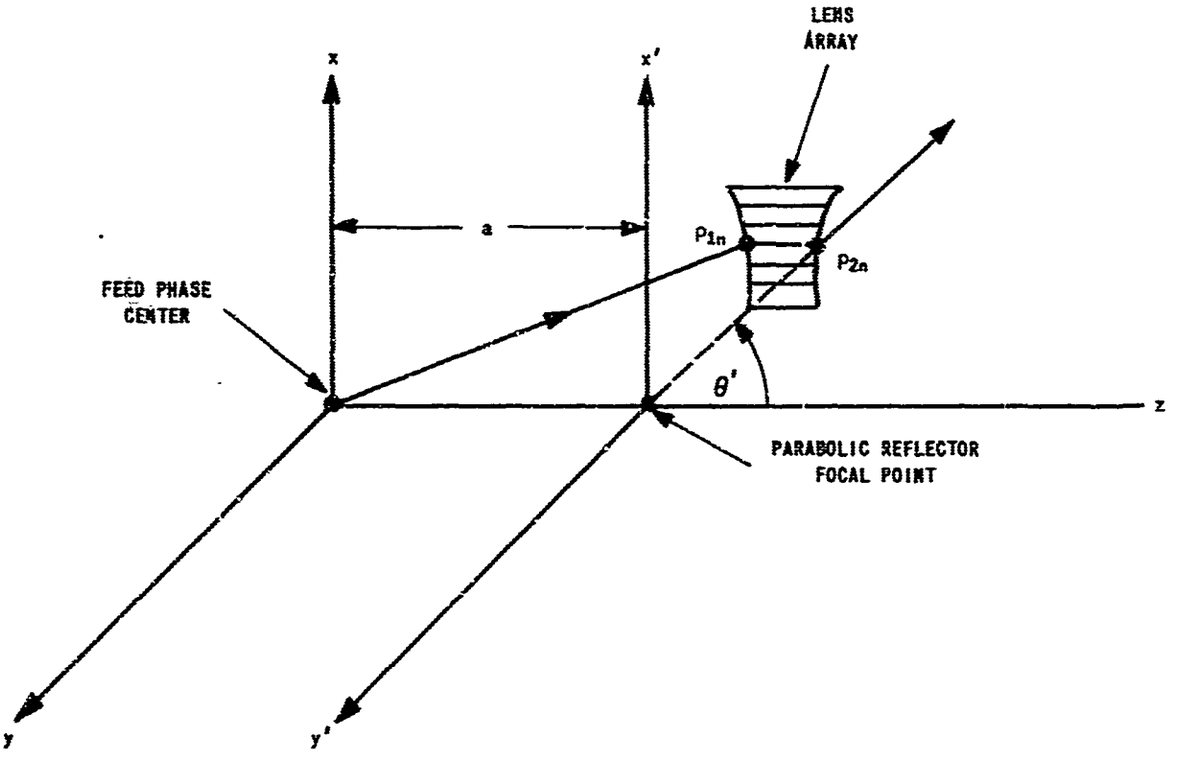

FIGURE 115. LENS ARRAY GEOMETRY

$$\rho_{1n} = \sqrt{x_{1n}^2 + y_{1n}^2 + z_{1n}^2} = \sqrt{r_{1n}^2 + z_{1n}^2}$$

$$\rho'_{2n} = \sqrt{x_{2n}^2 + y_{2n}^2 + (z_{2n} - a)^2} \tag{4}$$

$$\rho'_{2n} = \sqrt{r_{2n}^2 + (z_{2n} - a)^2}$$

$$\rho'_{2n} = \sqrt{r_{1n}^2 + (z_{2n} - a)^2} \tag{5}$$

The quantity, λ_o, in equation (3) is the free space wavelength, and λ_g is the guide wavelength for the lens-array. To evaluate the constant, C, we satisfy the path length requirements at the center of the lens-array

$$\rho_{10} + \frac{\lambda_o}{\lambda_g}(z_{20} - z_{10}) = \rho'_{20} + C \tag{6}$$

which reduces to

$$C = (z_{20} - z_{10})\left(\frac{\lambda_o}{\lambda_g} - 1\right) + a \tag{7}$$

This is in terms of the central thickness and propagation properties of the lens-array, and the distance between feed phase center and parabolic reflector focal point.

The above phase requirements provide one relationship between the exit and entry surface of the lens-array. In this form, the solution is still indeterminate. The specification of the desired amplitude transformation produces a deterministic solution.

Let the feed pattern function be described by $E(\theta)$, and the parabolic reflector aperture design amplitude by $F(r)$. Conservation of energy requires that

$$Q(\theta_m) = \int_0^{\theta_m} |E(\theta)|^2 \sin\theta d\theta = \int_0^{r_m} |F(r)|^2 \, r dr \tag{8}$$

where θ_m and r_m are dummy variables for the feed angle and the parabolic reflector radius, respectively. Also, we have assumed axial symmetry for both the feed pattern function and the parabolic reflector amplitude illumination function.

The function $F(r)$ is chosen with a normalization constant, K, so that the conservation of energy relationship is satisfied. As for the subreflector array design, (1) assume

$$F(r) = \left[\frac{1}{4f^2K}\right]^{1/2}\left[1 - k\left(\frac{r}{r_{max}}\right)^P\right] \tag{9}$$

where k and P are the illumination parameters which, respectively, determine the edge taper and the shape of the function. The quantity, f, is the parabolic reflector focal distance, and $r_{max} = d/2$ is the maximum radius of the parabolic reflector.

Equation (8) can then be written as

$$Q(\theta_m) = \frac{r_m^2}{4f^2K}\left[\frac{1}{2} - \frac{2k}{P+2}\left(\frac{r_m}{r_{max}}\right)^P + \frac{k^2}{2P+2}\left(\frac{r_m}{r_{max}}\right)^{2P}\right] \tag{10}$$

To evaluate the normalization constant, K, let $\theta_m \rightarrow \theta_{max}$ and $r_m \rightarrow r_{max}$. Then,

$$K = \frac{1}{\left(\frac{4f}{d}\right)^2 Q(\theta_{max})}\left[\frac{1}{2} - \frac{2k}{P+2} + \frac{k^2}{2P+2}\right] \tag{11}$$

and

$$Q(\theta_m) = \frac{Q(\theta_{max})\left(\frac{r_m}{r_{max}}\right)^2\left[\frac{1}{2} - \frac{2k}{P+2}\left(\frac{r_m}{r_{max}}\right)^P + \frac{k^2}{2P+2}\left(\frac{r_m}{r_{max}}\right)^{2P}\right]}{\left[\frac{1}{2} - \frac{2k}{2P+2} + \frac{k^2}{2P+2}\right]} \tag{12}$$

Now the aperture radius vector is related to the lens-array exit surface angle by

$$r_m^2 = 4f^2 \tan^2(\theta'_{2n}/2) \tag{13}$$

In terms of the exit surface coordinates

$$\frac{r_m}{r_{max}} = \frac{4f}{d}\left[\frac{\sqrt{r_{2n}^2 + (z_{2n} - a)^2} - (z_{2n} - a)}{\sqrt{r_{2n}^2 + (z_{2n} - a)^2} + (z_{2n} - a)}\right]^{1/2} \tag{14}$$

where

$$r_{2n}^2 = x_{2n}^2 + y_{2n}^2 \tag{15}$$

from equation (14)

$$z_{2n} - a = r_{2n}\left[1 - \left(\frac{r_m/r_{max}}{4f/d}\right)^2\right] \Big/ 2\left(\frac{r_m/r_{max}}{4f/d}\right) \tag{16}$$

To evaluate this expression at the center of the array, let $r_{2n} \to 0$ and $r_m \to 0$. Therefore,

$$z_{20} - a \to 2f/d \left(\frac{r_{2n}}{r_m/r_{max}} \right) \tag{17}$$

now also

$$r_{2n} = z_{10} \tan \theta_m \tag{18}$$

and for $\theta_m \to 0$

$$r_{2n} \to z_{10} \sin \theta_m \tag{19}$$

also from equation (12)

$$\frac{r_m}{r_{max}} \to \frac{\sqrt{Q(\theta_m)}}{\sqrt{Q(\theta_{max})}} \left[\frac{1}{2} - \frac{2k}{2P+2} + \frac{k^2}{2P+2} \right]^{1/2} \tag{20}$$

Therefore,

$$z_{20} - a \to (2f/d)\ z_{10} \frac{\sin \theta_m}{\sqrt{Q(\theta_m)}} \frac{\sqrt{2Q\ (\theta_{max})}}{\left[\frac{1}{2} - \frac{2k}{2P+2} + \frac{k^2}{2P+2} \right]^{1/2}} \tag{21}$$

But for

$$|E(\theta)|^2_{\text{at } \theta = 0} = 1 \tag{22}$$

then

$$\left[\frac{\sin \theta_m}{\sqrt{Q(\theta_m)}} \right]_{\theta_m = 0} = \sqrt{2} \tag{23}$$

and

$$z_{20} - a = (4f/d)\ z_{10} \sqrt{Q(\theta_{max})} \Big/ \left[\frac{1}{2} - \frac{2k}{2P+2} + \frac{k^2}{2P+2} \right]^{1/2} \tag{24}$$

Also

$$z_{20} = \frac{a \left[\frac{1}{2} - \frac{2k}{2P+2} + \frac{k^2}{2P+2} \right]^{1/2} - (4f/d)\ (z_{20} - z_{10}) \sqrt{Q(\theta_{max})}}{\left[\frac{1}{2} - \frac{2k}{2P+2} + \frac{k^2}{2P+2} \right]^{1/2} - (4f/d) \sqrt{Q/\theta_{max}}} \tag{24a}$$

To evaluate the expressions for the edge ray, let $r_m \rightarrow r_{max}$ and $r_{1n} = r_{2n} \rightarrow r_{1max}$. Therefore, from equation (14)

$$z_{2max} - a = r_{1max} \left[1 - d^2/16f^2\right] 2f/d \tag{25}$$

Using equations (3), (7) and

$$\rho_{1max} = r_{1max}/\sin(\theta_{max}) \tag{26}$$

$$\rho_{2max} = r_{1max} (1 + d^2/16f^2) 2f/d \tag{27}$$

$$z_{1max} = r_{1max} \cot(\theta_{1max}) \tag{28}$$

we find that

$$a = \left(\frac{1}{1 - \frac{\lambda_o}{\lambda_g}}\right)\left[\frac{\lambda_o}{\lambda_g} r_{1max} (1 - d^2/16f^2) 2f/d - \frac{\lambda_o}{\lambda_g} r_{1max} \cot(\theta_{max}) \right.$$

$$\left. + \frac{r_{imax}}{\sin\theta_{max}} - r_{1max} (1 + d^2/16f^2) 2f/d + (z_{20} - z_{10}) \left(1 - \frac{\lambda_o}{\lambda_g}\right)\right] \tag{29}$$

Now the lens-array solution will follow the same general procedure as for the subreflector array.[4] The input parameters are:

- Parabolic reflector focal length to diameter ratio (f/d).
- Maximum lens-array radius (r_{1max}).
- Feed pattern function, $E(\theta)$, and maximum feed angle, θ_{max}.
- Design illumination parameters, k and P.
- Free space to lens-array wavelength ratio, λ_o/λ_g.
- Center thickness of the lens-array, $(z_{20} - z_{10})$.
- Waveguide cell spacing and geometry.

The solution then proceeds as follows:

(1) Calculate $Q(\theta_{max})$ from equation (8)

(2) Calculate a from equation (29)

(3) Calculate z_{20} from equation (24a)

(4) Since $(z_{20} - z_{10})$ is known, calculate z_{10} from

$$z_{10} = z_{20} - (z_{20} - z_{10}) \tag{30}$$

(5) Increment r_{1n} in accordance with the number of lens-array radii for which solutions are desired.

(6) If $r_{1n}/r_{max} = 0$, then $z_{2n} = z_{20}$ and $z_{1n} = z_{10}$

(7) If $r_{1n}/r_{max} = 1$, then z_{2n} is obtained from equation (25) and z_{1n} is obtained from equation (28).

(8) If r_{1n}/r_{max} is not equal to zero and is not equal to 1, then solve using one of the following iterative procedures.

(9) Assume $(r_m/r_{max})_i = (r_{1n}/r_{1\,max})$

(10) Calculate $[Q(\theta_m)]_i$ from equation (12)

(11) Calculate $(\theta_m)_i$ from equation (8). The relative difficulty of this step will depend upon the form that is assumed for the feed pattern function. If we assume, for example,

$$E(\theta) = \cos^n \theta \tag{31}$$

then

$$\theta_m = \cos^{-1} \left[1 - (2n+1)\, Q(\theta_m)\right]^{1/(2n+1)} \tag{32}$$

(12) Solve for $(z_{2n})_i$ using equation (16)

(13) Solve for $(z_{1n})_i$ using equations (3), (4), (5), and (7)

(14) Calculate

$$(r_{1n})_i = (z_{1n})_i \tan \theta_m \tag{33}$$

(15) If

$$\left|\frac{r_{1n} - (r_{1n})_i}{r_{1max}}\right| \leq \epsilon \tag{34}$$

where ϵ is an arbitrarily small number, then a solution has been found and the calculation continues with step (18). Otherwise, let

$$(r_m/r_{max})_{i+1} = (r_m/r_{max})_i\, (r_{1n})_i/r_{1n} \tag{35}$$

and continue from step (10).

(16) Establish a limit on the maximum number of iterations. This number will be based upon experience with a particular set of calculation parameters. Subreflector array design calculations, for example, used 100 iterations as being sufficient.

(17) If the solution does not converge within the established maximum number of iterations, then replace equation (35) with

$$(r_m/r_{max})_{i+1} = \frac{r_{1n} - (r_{1n})_i}{r_{1max} - (r_{1n})_i} + \left(\frac{r_m}{r_{max}}\right)_i \left(\frac{r_{1max} - r_{1n}}{r_{1max} - (r_{1n})_i}\right) \tag{36}$$

and continue from step (9).

(18) Upon satisfying the convergence test described by equation (34), the solution is essentially complete. Let

$$z_{1n} = (z_{1n})_i \tag{37}$$

$$z_{2n} = (z_{2n})_i \tag{38}$$

This establishes the lens-array contour for the particular value of the radii r_{1n}. The solution then continues from step (5) until all desired radii values are complete.

5-2 LENS-ARRAY SUMMARY

Preceding has been a discussion of a detailed procedure for a lens-array design to improve the efficiency and noise temperature of a focal fed parabolic reflector. There are, in addition, other considerations for a complete evaluation of this technique.

The lens-array is visualized as a multicellular waveguide structure. A linearly polarized design would use rectangular waveguide, while a polarization independent design might use dielectrically or ridge loaded square waveguide. Other waveguide cross-sections also are possible; and the lens-array might be fabricated in light weight strip transmission line using compatible radiating elements.

For lightweight and/or broadband lens-array applications, consideration can be given to zoning the structure. Zoning techniques would be similar to those developed for the subreflector array.[4]

Surface mismatch effects for the lens-array must also be considered. In this case, it would be necessary to match both surfaces of the lens-array to minimize reflection losses and transmission phase errors. In this respect, the design of a lens-array would be more difficult than a subreflector array, which uses adjustment of the shorting surface to achieve partially the desired mismatch correction. Surface mismatch effects for a lens-array will be a function of incidence and reflection angles, as well as relative orientation of the electric field vector. This will generally require matching surfaces that are different for the two lens-array faces, and which vary over each face.

The design of a lens-array must also include diffraction pattern performance evaluation of the structure This is to insure that the lens-array element spacing and other design parameters are satisfactory, and that the design illumination function is achieved.

The applications for lens-array performance improvement would include both operational antenna systems and new designs. The lens-array will introduce additional support structure requirements, as well as additional blockage and loss. This will tend to minimize the efficiency and noise temperature improvement that can be achieved with this technique.

The decision between a focal fed or a Cassegrain reflector configuration is generally based upon allowable blockage for a particular design. The Cassegrain configuration is selected because the feed is near the vertex, is more accessible for transmission line connection, and represents reduced feed support problems. The focal fed configuration generally is selected when the subreflector represents excessive blockage, for a minimum, in the order of 10-wavelength diameter. If this is the case, lens-array blockage, for the focal fed configuration, would also represent excessive blockage. The minimum main parabolic reflector diameter for Cassegrain geometry is in the order of 80 to 100 wavelengths for a low aperture blockage, high efficiency design. Very similar minimum size limitations also apply for use of a lens-array. It is also likely that, for cases in which a focal fed and lens-array combination would provide improved antenna performance, that a vertex feed and subreflector-array would provide similar improvement. The vertex feed and subreflector array might then represent a better design choice.

SECTION 6

CONICAL SCANNING AND MONOPULSE SYSTEMS

This section considers the use of inverse taper transformation for conical scanning and monopulse antenna systems. Both the similarities and the differences between subreflector array design for the two tracking feeds, as compared to a pencil beam feed, are discussed.

Independent of feed type, subreflector array design, to achieve inverse taper transformation, depends upon specification of the feed horn pattern characteristics. The present design techniques require axially symmetrical feed pattern characteristics, low spillover power beyond the edge of the subreflector array, pattern polarization independence for a feed with arbitrary polarization capability, and non-astigmatic feed properties. The degree to which these properties are achieved, by either a tracking or pencil beam feed, will determine the antenna efficiency and noise temperature performance which can be achieved.

6-1 CONICAL SCANNING SYSTEMS

For the conical scanning feed system, the significant antenna parameters are the boresight gain, modulation sensitivity, and pattern symmetry. Boresight gain and modulation sensitivity are inversely related, so that a compromise must be made in terms of the beam squint angle. The use of subreflector array techniques, in conjunction with a conical scanning feed, can be expected to increase the gain of the squinted beam. This will provide the following design alternatives as compared to the use of a hyperbolic subreflector:

- Improved crossover gain for the same beamwidth separation and modulation sensitivity
- Improved modulation sensitivity for increased beamwidth separation and the same crossover gain
- A compromise improvement for both the crossover gain and modulation sensitivity.

In addition, the use of electronic phase shifters between the entry and shorting surfaces of the subreflector array provides a means for an inertia-less conical scanning system. Also one might consider design of the subreflector array to minimize the off-axis scanning aberrations of the conical scanning feed.

Subreflector array design is different for the conical scanning feed, as compared to a simple pencil beam feed, in terms of the off-axis feed requirements and the somewhat asymmetrical feed amplitude illumination. The effect of the small asymmetrical illumination will be insignificant. This is substantiated by calculated performance for various feed illumination functions with a given subreflector array.[4] These results indicate less than 1.5-percent efficiency change for as much as 3-dB change in the feed edge taper.

Subreflector array off-axis scan properties will be substantially the same as that for the replacement hyperbolic subreflector. The principal difference is in terms of the more nearly uniform amplitude illumination function which is characteristic of the subreflector array. This will produce a somewhat modified beam deviation factor and a somewhat larger coma error effect for a given beam scan angle. This is offset, however, by the reduced subreflector array beamwidth so that substantially the same aberrations will be evidenced in terms of beamwidths of scan.

6-2 MONOPULSE SYSTEMS

Monpulse systems, although similar to conical scan systems, obtain tracking information by use of fixed rather than scanned beams. Monopulse feed types include[7] (1) the four-horn feed, (2) the five-horn feed, (3) the twelve-horn feed, (4) the one-horn feed, (5) the two-horn dual mode feed, (6) the two horn triple mode feed, and (7) the four-horn triple mode feed. The essential differences between feed types are based upon polarization requirements and the desire to optimize the sum channel gain and the difference channel slope by providing difference feed aperture sizes for the various monopulse channels.

With respect to the sum channel illumination function, the transformation is the same as for a pencil beam feed. A sum channel gain improvement can be expected by transformation of the tapered feed pattern function into a more nearly uniform reflector aperture illumination function. This is indicated by the reported measurement results using a single plane monopulse feed. The above monopulse and conical scanning feed discussion pertains to both the cassegrain and focal fed antenna geometries. Substantially the same performance would be anticipated using either a subreflector array or a lens array to achieve the desired illumination taper transformation.

SECTION 7

CONCLUSIONS AND RECOMMENDATIONS

This report concludes a program of investigation concerned with the development and evaluation of an inverse taper transformation technique, used in conjunction with a parabolic reflector to achieve high efficiency and low noise temperature antenna performance.

The design equations for the subreflector array structure have been developed. This development is based upon achieving high aperture illumination, low noise temperature illumination functions which are within the diffraction limitations of the structure. The design includes calculation of the entry surface and shorting surface contours of the subreflector array and diffraction pattern performance calculation for the unit. Shorting surface calculations include the effect of input surface impedance parameters, propagation path length in the multicellular waveguide medium, and zoning to achieve either minimum depth or maximum bandwidth performance.

A demonstration model based on the above design has been built and tested at X band. This has utilized a 10-foot diameter parabolic reflector and a linearly polarized and a polarization independent subreflector array both of which are nominally 15 inches in diameter. Tests have been conducted using both a dual mode conical pencil beam feed horn and a single plane monopulse feed.

To optimize model performance, tests have been conducted using various shorting surface descriptions. Single element pattern characteristics have been examined in the array environment. Also, pattern measurements have been made using the feed-subreflector array combination, as well as the feed-subreflector array-parabolic reflector combination. Surface mismatch effects have been examined and various matching configurations have been investigated. Tests have been conducted to determine the necessary shorting surface modification to minimize the phase error due to surface mismatch.

Tests performed on the breadboard model antenna include principal plane and diagonal plane patterns. VSWR, gain, and antenna noise temperature.

Model tests using both type feed horns and the linearly polarized subreflector array indicate that antenna efficiencies of 68 percent can be achieved over a 5-percent frequency band. This represents a significant efficiency

improvement as compared to model measurements of 51.3-percent efficiency using a conventional hyperbolic subreflector. Model noise temperature measurements indicate 27°K and 32°K for the pencil beam and monopulse feeds, respectively over a ±5 percent frequency band.

Model tests using the polarization independent subreflector array indicate an antenna efficiency of 43 percent for this configuration. Optimization of the shorting surface has not been achieved and must await advances in the technology of subreflector array surface impedance matching techniques for dielectric loaded elements in this very special environment (curved surfaces, rapid amplitude variations, etc.).

The above model program has been based upon a parabolic reflector focal length-to-diameter ratio equal to 0.4. Increasing the focal length-to-diameter ratio to 0.5, for example, would improve the performance of the subreflector array since the range of incidence and reflection angles would be reduced for this geometry. The degree of improvement with increasing focal length to diameter ratio is not known at this time. An efficiency improvement from 68 percent to 75 percent represents an upper limit, however, for a 100 wavelength aperture as indicated by the theoretical subreflector array calculations in Reference 4. Also, due to increasing reflection angles some degradation in efficiency would be predicted by reduction of the focal length to diameter ratio 0.25.

The model antenna aperture size of approximately 92 wavelengths is found to be near minimum for a significant noise temperature efficiency improvement. This is based upon inverse taper structure blockage which places an upper limit on the size of the subreflector array. Diffraction limitations place a lower limit on the size of the subreflector array which is based upon the resulting aperture illumination efficiency that can be achieved. It is concluded, therefore, that designs for smaller parabolic reflector aperture sizes will show smaller efficiency improvement and that larger parabolic reflector aperture sizes will show larger efficiency improvements. Techniques for estimating efficiency variation with aperture have been established in Reference 4. Typically, it is estimated that an efficiency of 60 percent could be achieved with a 50 wavelength aperture and that an efficiency of 72 percent could be achieved with a 200 wavelength aperture over a 5 percent frequency band.

Inverse taper transformation techniques, for use with a focal fed parabolic reflector, have been examined. The design equations for a lens array to accomplish the above transformation have been established. The utility of this technique is limited, however, by lens array blockage. Typical efficiencies which might be anticipated for the focal fed geometry are the same as those for a cassegrain configuration. That is, 60, 68 and 72 percent for 50, 100, and 200 wavelength apertures, respectively. In all cases for which modification of an existing focal fed system is being evaluated, the use of a subreflector array and vertex feed should be considered as an alternate to a lens array and focal feed.

By virtue of the subreflector array and the lens array design the power densities on the structure will be considerably less than those at the feed. The structure is sufficiently simple so that no significant high power handling limitations are anticipated. A high power capability of up to 10 megawatts at X-Band should not represent a problem.

The model antenna and design calculations performed during the study program have been specifically concerned with X-Band operation. The design techniques are directly scalable with frequency. This would permit structure design and performance estimates for any operating frequency band within the range of frequencies from 0.40 to 10.0 GHz.

The results to date have demonstrated the present state-of-the-art capability of the inverse taper transformation subreflector array technique. All design areas have been investigated and analyzed in depth, particularly, aperture theory, measurement, and mutual coupling concepts.

Element pattern characteristics and impedance matching for very broad angles remains the only significant problem area, particularly in the H plane. With the present model, the incidence angle from the secondary subreflector array normal to the edge of the dish is much larger than 60 degrees. The problem is aggravated at the edge of the subreflector array since these cells are contoured backward. The reflecting cells at the edge are required to illuminate the dish at wider angles than they can "scan", in the H plane. Therefore the H-plane illumination inherently drops off much faster at the dish edge than is expected from simple ray optics or diffraction pattern reflection predictions. A number of techniques were unsuccessfully investigated during the above program to minimize this problem indicating that a basic technical breakthrough is necessary to effect further improvement.

The requirement for such a wide "scan" angle is beyond the state-of-the-art, 60 degrees being about the upper limit of H-plane scan. The problem is unique, too, because of the steep amplitude gradient and the spherical phase gradient which exists at the surface of the secondary subreflector array. Usually, arrays of elements work in concert to form a plane wave with only moderate amplitude gradients. Further theoretical and experimental investigation may lead to closer correlation to the theoretically predicted efficiency-noise temperature improvement, but the direction and basis of such an investigation is not defineable at this time.

SECTION 8

REFERENCES

1. "Low Noise Antenna Techniques", Technical Documentary Report No. RADC-TDR-64-423, November, 1964, prepared under Contract AF30(602)3382 by Radiation Division, Sperry Gyroscope Company.

2. "Low Noise Antenna Techniques", Technical Documentary Report No. RADC-TR-64-556, February 1965, prepared under Contract AF30(602)3382 by Radiation Division, Sperry Gyroscope Company.

3. "Low Noise Antenna Techniques - Final Report", Technical Report No. RADC-TR-65-166, July, 1965, prepared under Contract AF30(602)3382 by Radiation Division, Sperry Gyroscope Company.

4. "Low Noise Antenna Techniques", Technical Documentary Report No. RADC-TR-66-625, January, 1967, prepared under Contract AF30(602)4325 by Sperry Gyrsocope Company.

5. "Low Noise Antenna Techniques", Technical Documentary Report No. RADC-TR-67-42, March, 1967, prepared under Contract AF30(602)4325 by Sperry Gyroscope Company.

6. "Test Procedure for Antennas", Transactions on Antennas and Propagation, Volume AP-13, May 1965, pgs 461-462.

7. Hannan, P.W., "Optimum Feeds for All Three Modes of a Monopulse Antenna", IRE Trans. Antennas and Propagation, September, 1961, pgs. 444-460.

8. Farrell, G.F., Jr., and Kuhn, D.H., "Mutual Coupling Effects in Infinite Planar Arrays of Rectangular Waveguide Horns", IEEE International Antenna and Propagation Symposium, December, 1966.

UNCLASSIFIED

Security Classification

DOCUMENT CONTROL DATA - R & D

(Security classification of title, body of abstract and indexing annotation must be entered when the overall report is classified)

1. ORIGINATING ACTIVITY (Corporate author)	2a. REPORT SECURITY CLASSIFICATION
Sperry Gyroscope Co. Great Neck, NY 11020	Unclassified
	2b. GROUP

3. REPORT TITLE

LOW NOISE ANTENNA TECHNIQUES

4. DESCRIPTIVE NOTES (Type of report and inclusive dates)

Final Report - Dec 66 to Dec 67

5. AUTHOR(S) (First name, middle initial, last name)

R. W. Martin
C. Rothenberg
L. Zucker

6. REPORT DATE	7a. TOTAL NO. OF PAGES	7b. NO. OF REFS
April 1968	174	8

8a. CONTRACT OR GRANT NO.	9a. ORIGINATOR'S REPORT NUMBER(S)
AF30(602)4325 b. PROJECT NO. 4506 c. Task No. 450604 d.	SGD-5297-0020 9b. OTHER REPORT NO(S) (Any other numbers that may be assigned this report) RADC-TR-68-58

10. DISTRIBUTION STATEMENT

This document is subject to special export controls and each transmittal to foreign governments, foreign nationals or representatives thereto may be made only with prior approval of RADC (EMATA), GAFB, NY 13440.

11. SUPPLEMENTARY NOTES	12. SPONSORING MILITARY ACTIVITY
RADC Project Engineer: MARTIN JAEGER EMATA/AC 315 330-2443	Rome Air Development Center Techniques Branch (EMAT) Griffiss AFB, NY 13440

13. ABSTRACT

~~This final~~ report describes the progress made in analysis, development and evaluation of a subreflector array illumination control technique. The subreflector array technique is used in conjunction with a parabolic reflector and feed horn to reduce antenna noise temperature while providing increased antenna efficiency. This report includes the results of a model test program which indicates a model efficiency of 68 percent and a noise temperature of 27 degrees kelvin over a 5 percent S-band frequency range. Discussion also includes a focal fed lens array design and application to conical scanning and monopulse systems.

DD FORM 1 NOV 65 1473

UNCLASSIFIED

Security Classification